Influence of the intestinal microbiota composition on the individual susceptibility towards enteric infections in healthy individuals and hematological patients

Dissertation

zur Erlangung des akademischen Grades

doctor rerum naturalium (Dr. rer. nat.)

genehmigt durch die Fakultät für Naturwissenschaften
der Otto-von-Guericke-Universität Magdeburg

von M. Sc. Lisa Osbelt

geb. am 15.08.1992 in Dannenberg (Elbe)

Gutachter: Prof. Dr. Thomas Fischer
Prof. Dr. Bärbel Stecher

eingereicht am: 17.06.2020
verteidigt am: 14.12.2020

Die Wissenschaft nötigt uns,
den Glauben an einfache Kausalitäten aufzugeben.
~ Friedrich Nietzsche

Summary

Variations in the composition of the intestinal microbiota influence the susceptibility towards colonization and infection with multi-drug resistant (MDR) enterobacteria in human and mice. However, the role of specific members and their metabolites contributing to protection against initial colonization remains poorly understood. In this thesis, I aimed to identify factors derived from the microbiota that influence the individual infection susceptibility towards enteric pathogens. For this purpose, human feces samples from patients and healthy volunteers as well as isogenic mouse lines harboring distinct microbiota communities were used to identify potential factors in humans and to test these factors subsequently in relevant mouse models. By inoculation of feces samples of different healthy donors with MDR *K. pneumoniae,* I observed highly variable degrees of colonization resistance with up to 100,000-fold changes in pathogen growth between protected and susceptible individuals. Microbiome analysis revealed that low pH, high species richness and a high relative abundance of facultative anaerobic bacteria as well as high levels of short-chain fatty acid (SCFA) are key factors for colonization resistance during homeostasis. In line with these findings, I found a lower degree of colonization resistance in stool samples of patients' cohorts undergoing chemotherapy and after stem cell transplantation to be associated with higher pH, low species richness and low levels of SCFA. Strikingly, differences in colonization susceptibility could be transferred by humanization of germ-free (GF) animals with human stool samples as the animals showed the same response to colonization as their respective donors supporting the predictive value of the *in vitro* assay to anticipate colonization susceptibility. Similarly, treatment of mouse lines with chemotherapeutic drugs induced massive changes on the microbiome as previously observed in the human cohorts and the severity of mucositis was impacted by microbiota composition. In the second part of the thesis, the influence of natural variation in microbiota compositions on the individual infection susceptibility was explored using the enteric pathogen *C. rodentium*. Infection of genetically identical mouse lines with variable microbiota compositions led to highly variable colonization even in absence of antibiotic intervention. I found the same differences in formerly GF animals harboring the respective donors microbiota and also *in vitro* by co-culturing cecal bacteria from resistant and susceptible animals with *C. rodentium* showing that the phenotype is fully dependent on differences in the microbiota. Further microbiome and metabolome analysis revealed higher abundance of butyrate-producing bacteria and increased levels of butyrate in resistant mice. Supplementation of susceptible animals with butyrate significantly lowered the levels of colonization, highlighting that commensal-derived primary and secondary bacterial metabolites are potent modulators of host's susceptibility to *Enterobacteriaceae*. In the last part of the thesis, I assessed the probiotic properties of related commensal bacteria to reduce the susceptibility against MDR *K. pneumoniae* as initial screening of human feces samples associated the presence of commensal *Klebsiella* species with elevated protection. Strikingly, addition of commensal *K. oxytoca* strains significantly reduced the growth of MDR *K. pneumoniae* strains in *in vitro* and *in vivo* assays. By supplementation of susceptible animals with specific *K. oxytoca* strains, we could significantly lower luminal- and tissue-resident MDR *K. pneumoniae* and protected *K. oxytoca* treated animals from systemic spread of the pathogen. Mechanistically, commensal *K. oxytoca* induced faster restoration of anaerobic SCFA producing bacteria after antibiotic treatment and occupied a similar ecological niche acting as a potential new probiotic strain. Altogether, I identified in this thesis microbiome-derived factors contributing to differences in colonization resistance against enteropathogens in human and mice that may have therapeutic potential.

Zusammenfassung

Die Zusammensetzung der intestinalen Mikrobiota beeinflusst die individuelle Infektionsanfälligkeit mit multiresistenten (MDR) Enterobakterien im Menschen und dem Mausmodell. Allerdings ist die Identität der spezifischen Bakterien und die spezifische Funktion ihrer Stoffwechselprodukte beim Schutz gegen die initiale Besiedelung nicht hinreichend bekannt. In dieser Disputation sollten daher die komplexen Wechselwirkungen zwischen der Mikrobiota, dem Wirt und dem Krankheitserreger näher untersucht werden und diejenigen Faktoren identifiziert werden, welche für eine erhöhte Besiedelungsresistenz verantwortlich sind. Dafür sollten Stuhlproben von Patienten, gesunden Probanden und isogenetischen Mauslinien mit unterschiedlicher Mikrobiota verwendet werden, um mögliche Faktoren in humanen Proben zu identifizieren und daraus abgeleitete Hypothesen dann unter *in vivo* Bedingungen in Mausmodellen zu testen. Ein Besiedelungsassay mit einem MDR *K. pneumoniae* Stamm in humanen Stuhlproben gesunder Personen zeigte eine hohe Variabilität in der Besiedelungsfähigkeit mit dem Erreger. Vergleiche des Mikrobioms anfälliger und geschützter Probanden konnten einen niedrigeren pH-Wert, erhöhtes Artenreichtum insgesamt und bei fakultativen Anaerobiern im Speziellen sowie erhöhte Level an kurzkettigen Fettsäuren mit Besiedelungsresistenz gegenüber MDR *K. pneumoniae* assoziieren. Zusätzlich zeigten Stuhlproben von leukämischen Patienten unter Chemotherapie und nach Stammzelltransplantation eine höhere Besiedelunganfälligkeit mit dem Erreger und waren durch einen erhöhten pH-Wert, niedrige Artenvielfalt und niedrige Level an kurzkettigen Fettsäuren charakterisiert. Diese Unterschiede ließen sich durch die Humanisierung von keimfreien Mäusen *in vivo* nachstellen und unterstützen somit den prädiktiven Wert der Beobachtungen an Patientenproben. Die Behandlung von zwei Mauslinien in einem von Patienten abgeleiteten Chemotherapie-Modell, induzierte Änderungen in der Mikrobiomzusammensetzung und eine unterschiedlich starke Darmentzündung, welche auf Unterschiede im Mikrobiom zurückzuführen waren. Im zweiten Teil der Arbeit wurden unbehandelte isogenetische Mauslinien mit dem Erreger *C. rodentium* infiziert und zeigten eine hohe Variabilität in der Infektionsanfälligkeit. Die Unterschiede ließen sich durch Stuhltransplantation in keimfreie Mäuse und Kultivierungsversuche von isoliertem Darmmaterial reproduzieren und somit auf Unterschiede im Mikrobiom zurückführen. Detaillierte Analysen der Mikrobiota von anfälligen und geschützten Tieren identifizierten eine höhere Abundanz von Buttersäure-produzierenden Bakterien und erhöhte Buttersäurelevel als ursächliche Faktoren für den Schutz der resistenten Mauslinie. Supplementierung von anfälligen Tieren mit Buttersäure konnte die Anfälligkeit signifikant reduzieren und unterstreicht die Relevanz von primären und sekundären bakteriellen Metaboliten als potente Modulatoren bei der Wirtsanfälligkeit für Infektionen. Im letzten Teil der Arbeit wurde das probiotische Potenzial von artverwandten, kommensalen Bakterien gegen MDR Erreger näher untersucht. Ein initiales Screening von geschützten Spendern zeigte einen erhöhten Anteil an kommensalen *Klebsiellen*. Tatsächlich führten *K. oxytoca* Isolate bei unterschiedlichen *in vitro* und *in vivo* Versuchen zu einer signifikanten Reduktion von MDR *K. pneumoniae* Stämmen. Zusätzlich konnte die Anzahl luminaler und Gewebe-assoziierter MDR Bakterien und die daraus resultierende systemische Verteilung von MDR Bakterien durch die Supplementierung anfälliger Mäuse mit *K. oxytoca* verhindert werden. Mikrobiota-Analysen zeigten, dass kommensale *K. oxytoca* Isolate die Wiederherstellung der Besiedelungsresistenz nach Antibiotika-Gabe fördern und die metabolische Nische von *K. pneumoniae* effektiv blockieren können. Zusammenfassend konnten verschiedene Faktoren und Bakterienstämme in gesunden und medikamentös veränderten Mikrobiomen identifiziert werden, welche zu den Unterschieden in der Infektanfälligkeit zwischen Individuen beitragen könnten.

I. Table of contents

Summary **3**
Zusammenfassung **1**
II. List of abbreviations **9**
III. List of figures **12**
IV. List of tables **14**
1. General introduction **15**
1.1 The human gut microbiome **15**
1.1.1 Development of the human microbiota 16
1.1.2 Community structure of the healthy adult gut microbiome 16
1.1.3 Influencing factors shaping the community structure 19
1.2 Homeostasis – colonization resistance in the healthy gut **20**
1.2.1 Nutrient competition 21
1.2.2 Bile salts and short chain fatty acids 21
1.2.3 Bacteriocins, antimicrobial peptides, and type VI secretion systems 22
1.3 Loss of colonization resistance **24**
1.3.1 Strategies of pathogenic bacteria to establish during dysbiosis 25
1.4 In the spotlight: thy family of *Enterobacteriaceae* **27**
1.4.1 A/E pathogens: *Citrobacter rodentium* 27
1.4.2 The emergence of multi-drug resistance 29
1.4.3 *Klebsiella* spp. 31
1.5 The microbiome as a predictor for patient outcome **32**
1.6 Chances and limitations of microbiome studies **34**
1.6.1 Human microbiome studies 34
1.6.2 Mouse models 35
1.7 Aims of the thesis **38**
2. Material and methods **40**
2.1 Materials **40**
2.1.1 Instruments and equipment 40
2.1.2 Consumables 41
2.1.3 Kits and enzymes 41
2.1.4 Bacterial strains and mouse lines 42
2.1.5 Reagents 43
2.1.6 Buffers and solutions 44
2.1.7 Media and agar 47
2.1.8 Primers 48
2.1.9 Antibodies 49
2.1.10 Software and algorithms 50
2.2 Microbiological methods **50**
2.2.1 Sterilization and Disinfection 50
2.2.2 Cultivation of bacteria 50
2.2.3 Measurement of cell density and calculation of bacterial CFUs 51
2.2.4 Cryo-preservation of bacteria 51
2.2.5 Preparation of feces samples for determination of CFUs 51
2.2.6 Determination of colony forming units 51

2.2.7 Growth curves assay 52
2.2.8 *In vitro* competition-assay for human feces samples 52
2.3 Molecular biological methods 52
2.3.1 Polymerase-chain reaction 52
2.3.2 Agarose-gel-electrophoresis 53
2.3.3 Sanger sequencing of purified DNA 54
2.3.4 Microbial community DNA extraction 54
2.3.5 16S rRNA gene amplification and sequencing 54
2.3.6 Genomic DNA extraction 55
2.3.7 Library preparation for Illumina sequencing 55
2.3.8 RNA isolation 57
2.3.9 cDNA synthesis 58
2.3.10 Quantitative polymerase chain reaction 59
2.3.11 Tissue preparation for protein analysis 60
2.3.12 SDS – PAGE and Coomassie staining 60
2.3.13 Western Blotting 61
2.3.14 pH measurements 61
2.3.15 Measurements of short-chain fatty acids. 61
2.3.16 Metabolite derivatization 61
2.3.17 GC-MS analysis untargeted metabolome 62
2.4 Animal Experiments and human sample collection 62
2.4.1 Ethics statement 62
2.4.2 Mice 63
2.4.3 Cohousing and fecal microbiota transplant 63
2.4.4 *In vivo C. rodentium* infection 63
2.4.5 *In vivo* imaging (IVIS) 64
2.4.6 *In vivo Klebsiella pneumoniae* and enterobacterial colonization 64
2.4.7 *In vivo* competition experiments 64
2.4.8 *In vivo* decolonization experiments 65
2.4.9 *In vitro* competition assays for *K. pneumoniae* from cecal content 65
2.4.10 *In vitro* assays for *C. rodentium* in isolated cecal content 65
2.4.11 Quantification of fecal enterobacterial colonization. 66
2.4.12 Assessment of luminal and tissue colonization 66
2.4.13 Preparation of tissue sections for histopathological examination 66
2.4.14 Semi quantitative scoring of inflammation 67
2.5 Author contributions 68
3. Results 69
3.1 Individual infection susceptibility in healthy study populations is influences by multiple factors ..69
3.1.1 Stool samples of healthy volunteers show highly variable degree of colonization resistance against multi-drug resistant bacteria 69
3.1.2 Humanization of GF mice successfully transfer observed differences in CFUs in an *in vivo* colonization model 71
3.1.3 Actinobacteria-Akkermansia enterotype is correlated with higher ratios of susceptible samples 74
3.1.4 Resistant samples harbor significantly more SCFA producing bacteria in their microbiomes 75

3.1.5 Leukemic patients have an elevated risk for infection with MDR *K. pneumoniae* and show pronounced changes in their microbiomes 78
3.1.6 The microbiota composition of patients undergoing chemotherapy is extremely variable and displays a low degree of colonization resistance 81
3.1.7 The elevated risk of infection susceptibility decreases within the first two months after stem-cell transplantation 83
3.2 Cytarabine - driven mucositis severity is influenced by variations in microbiota composition of laboratory mice. 86
3.2.1 Induction chemotherapy leads to significant body weight loss and development of small intestinal mucositis without pronounced inflammation in the colon 86
3.2.2 Microbiota dynamically responses to induction chemotherapy with significant changes in the overall microbiome composition 90
3.2.3 Ara-C is sufficient to induce inflammation in SPF-H and SPF-J mouse lines 91
3.2.4 Each drug induces distinct changes in the microbiome composition 94
3.2.5 Chemotherapeutically-induced dysbiotic microbiome compositions likely elevate the risk for colonization with multi-drug resistant bacteria. 97
3.3 The variability of the microbiota composition influences the susceptibility towards the intestinal pathogen *Citrobacter rodentium* via short chain fatty acid production 99
3.3.1 Isogenic mouse lines feature distinct microbiota compositions and varying disease kinetics after *Citrobacter rodentium* infection 99
3.3.2 Variations in microbiota composition are correlated with lethal outcome of infections with Shiga toxin expressing *C. rodentium* strains 100
3.3.3 Delayed colonization in SPF-R mice is visible in all intestinal organs and tissues but most prominent in the cecum 101
3.3.4 Differences in colonization could be recovered *in vitro* indicating that mechanism mediated directly by resident microbes in the cecum 102
3.3.5 Cohousing and transfer of cultivable bacteria from resistant SPF-R mice leads to variable protective outcome in SPF-S mice 103
3.3.6 Resistance of SPF-R mice is associated with higher diversity and abundance of bacteria in the Firmicutes phylum 105
3.3.7 The metabolomics profile of resistant SPF-R is characterized by elevated SCFA levels, which strongly impair the growth of *C. rodentium in vitro* at pH 6.0 110
3.3.8 Supplementation of SPF-S mice with SCFA is sufficient to reduce *C. rodentium* growth *in vitro* as well as *in vivo* 114
3.4 Commensal *Klebsiella oxytoca* strains protect against colonization with multi-drug resistant *Klebsiella pneumoniae* 119
3.4.1 Pretreatment with ampicillin destroys natural colonization resistance in SPF-H mice and establishes a long term colonization of the pathogen 119
3.4.2 The ampicillin mouse model induces reproducible and robust colonization with different *Klebsiella pneumoniae* strains 121
3.4.3 Gnotobiotic Oligo-MM^{12} mice and GF mice are naturally susceptible to MDR *K. pneumoniae* and are unable to clear the pathogen. 122
3.4.4 Screening of human stool samples for commensal *Klebsiella* strains revealed high prevalence of *K. oxytoca* in protected stool samples. 123

3.4.5 Addition of *K. oxytoca* to amp treated cecal content efficiently reduces CFUs of recovered *K. pneumoniae* 126
3.4.6 Pretreatment of antibiotic-treated mice with probiotic *K. oxytoca* facilitates clearance of MDR *K. pneumoniae* from the feces 127
3.4.7 Protective effect is specific for human *K. oxytoca* strains and generally effective against another MDR *K. pneumoniae* strain 129
3.4.8 Probiotic *K. oxytoca* protects naturally susceptible Oligo-MM^{12} mice from colonization and is able to directly compete with MDR *K. pneumoniae* at the early phase of colonization in GF mice 131
3.4.9 Probiotic *K. oxytoca* protects susceptible animals from luminal and tissue invasion and systemic dissemination of the pathogen 133
3.4.10 The adaptive immune-system is dispensable for the observed phenotype supporting the hypothesis of a direct competitive effect 134
3.4.11 *K. oxytoca* helps anaerobic SCFA producers to recover faster after antibiotic dysbiosis thereby reestablishing colonization resistance. 135
3.4.12 *K. oxytoca* colonization reduces MDR K. pn in humanized SUS donor mice 137
3.4.13 *K. oxytoca* has the therapeutic potential to interfere with already established MDR *K. pneumoniae* colonization 138
4. General Discussion 140
4.1 Individual infection susceptibility in healthy study populations is influences by multiple factors 140
4.2 Cytarabine - driven mucositis severity is influenced by variations in microbiota composition in laboratory mice. 145
4.3 The variability of the microbiota composition influences the susceptibility towards the intestinal pathogen *Citrobacter rodentium* via short chain fatty acid production 149
4.4 Commensal *Klebsiella oxytoca* strains protect against colonization with multi-drug resistant *Klebsiella pneumoniae* 155
5. Outlook and future directions 162
6. References 164
Ehrenerklärung 178

II. List of abbreviations

3'	three prime
5'	five prime
5-FU	5-Fluorouracil
°C	degree Celsius
%	percentage
AAHC	antibiotic-associated hemorrhagic colitis
Abx	antibiotics
ADONIS	permutational multivariate analysis of variance
A/E	attaching and effacing
Act-Akk	Actinobacteria-Akkermansia cluster
ALL	acute lymphoblastic leukemia
AML	acute mylogenous leukemia
Amp	ampicillin
AMP	anti-microbial peptide
Ara-C	aracycline
ASF	Altered Schaedler Flora
BHI	brain-heart infusion broth
bp	base pair
BWL	body weight loss
cDNA	complementary DNA
C. difficile	*Clostridioides difficile*
chlor	chloramphenicol
CFU	colony forming unit
CRE	carbapenem resistant enterobacteria
CP	carbapenemase-producing
CP-CRE	carbapenemase-producing CRE
CR	Charles River laboratories
C. rodentium	*Citrobacter rodentium*
CS	Cesarean Section
ddH2O	double-distilled water
DNA	deoxyribonucleic acid
dNTP	deoxynucleotide triphosphates
dsDNA	double-stranded deoxyribonucleic acid
dsRNA	double-stranded ribonucleic acid
E. coli	*Escherichia coli*
EHEC	enterohaemorrhagic *E. coli*
EPEC	enteropathogenic *E. coli*
EDTA	ethylenediaminetetraacetic
ESBL	extended-spectrum ß-lactamases
FELASA	Federation of European Laboratory Animal Science Association
Fig	figure
FMT	fecal microbiota transplantation
GF	germ-free
FT	fecal transplant
GIT	gastrointestinal tract
h	hour
HAI	healthcare associated infection
HCl	hydrochloric acid

II. List of abbreviations

HGT	horizontal gene transfer
HIF	hypoxia inducible factor
HMP	human microbiome project
HSCT	hematopoietic stem-cell transplantation
HV	hypervirulent
HSP	heat-shock protein
HZI	Helmholtz-Centre for infection research
IBD	inflammatory bowel disease
IC	induction chemotherapy
ICU	intensive care unit
IFN	interferon
IgA	immunoglobulin A
IL-17	interleukin 17
IL-22	interleukin 22
i.p.	intraperitoneal
IMP	Imipenem-resistant *Pseudomonas*
INT	Intermediate
IVIS	*in vivo* imaging system
Kan	kanamycin
K. oxytoca	*Klebsiella oxytoca*
K. pneumoniae	*Klebsiella pneumoniae*
KPC	*Klebsiella pneumoniae* carbapenemase
LAVES	Lower Saxony State Office for Nature, Environment and Consumer Protection
LB	medium lysogeny broth medium
LCM	low complexity microbiota
LEfSE	Linear discriminant analysis Effect Size
MAIT	Mucosal-associated invariant T cells
MBL	Metallo β- lactamase
MDR	multi-drug resistant Gram-negative bacteria
µg	microgram
min	minute
µl	microliter
ml	milliliter
MLN	mesenteric lymph node
MLST	multilocus sequence typing
µM	micromolar
mRNA	messenger ribonucleic acid
MRSA	methicillin resistant *Staphylococcus aureus*
Muc-2	mucin 2
NaCl	sodium chloride
Na_2HPO_4	disodium phosphate
NaOH	sodium hydroxide
NCBI	National Center for Biotechnology Information
NCI	National Cancer Institute
NDM-1	New Delhi metallo-ß-lactamase 1
ng	nanogram
nm	nanometer
NMDS	non-metric multidimensional scaling
non-CP-CRE	non-carbapenemase-producing CRE
nt	nucleotide

II. List of abbreviations

OD	optical density
o.g.	oral gavage
Oligo-MM^{12}	Oligo 12 mouse microbiota
OSF	Original Schaedler Flora
OTU	operational taxonomic unit
OXA	oxacillinase
P. aeruginosa	*Pseudomonas aeruginosa*
PBS	phosphate buffered saline
PcoA	principal coordinates analysis
PCR	polymerase chain reaction
p.c.	post colonization
p.i.	post infection
qPCR	quantitative PCR
Reg3γ	regenerating islet-derived 3
RES	resistant
Ripp	ribosomally synthesized and post-translationally modified peptide
PPI	proton pump inhibitor
RNA	ribonucleic acid
ROS	reactive oxygen species
rpm	revolutions per minute
RPMI	Roswell Park Memorial Institute medium
rRNA	ribosomal ribonucleic acid
RT	room temperature
s	second
S. aureus	*Staphylococcus aureus*
SCFA	short-chain fatty acid
SI	small intestine
SFB	segmented filamentous bacteria
SPF	specific pathogen free
ST	sequence type
S. Tm	*Salmonella* Typhimurium
strep	streptomycin
Stx	shiga toxin
SUS	susceptible
T6SS	Type VI secretion systems
TAE	tris-acetate-EDTA
TierSchG	national animal protection law (Tierschutzgesetz)
TLR	toll-like receptor
Tx	stem cell transplantation
UV	ultraviolet
VIM	Verona integron-encoded metallo-ß-lactamases
VRE	vancomycin resistant *Enterococcus*
WHO	World Health Organization

III. List of figures

Figure 1: Indigenous microbiota of the human gastrointestinal tract. 17
Figure 2: Factors shaping the gut microbiome. 20
Figure 3: Direct colonization resistance mechanisms. 24
Figure 4: Expansion and engraftment strategies of invading species. 26
Figure 5: Different disease kinetics in isogenic mouse lines infected with *C. rodentium* 28
Figure 6: Classification of the different mechanisms of drug resistance in CRE. 30
Figure 7: Factors shaping colonization resistance in healthy adult individuals. 70
Figure 8: Humanization of GF mice transfers phenotype from donors. 74
Figure 9: Enterotypes in the healthy human microbiome. 76
Figure 10: Resistant samples harbor more SCFA producing bacteria in their microbiome. 77
Figure 11: Colonization resistance and microbiome composition in different human cohorts. 80
Figure 12: Patients microbiota composition during chemotherapy is highly variable. 82
Figure 13: Susceptibility towards K.pn MDR1 after HSCT. 84
Figure 14: Loss of body weight is a direct effect of chemotherapy in different mouse lines. 87
Figure 15: Small intestinal mucositis is a direct effect of chemotherapy in different mouse lines. 89
Figure 16: Microbiota dynamically responds to induction chemotherapy. 91
Figure 17: Ara-C induces small intestinal inflammation in SPF-H mice. 92
Figure 18: Ara-C induces small intestinal inflammation in SPF-J mice. 93
Figure 19: Each drug induces distinct changes on the microbiome of SPF-H mice. 95
Figure 20: Each drug induces distinct changes on the microbiome of SPF-J mice. 96
Figure 21: Induction chemotheraoy-induced changes in the microbiome promote colonization with MDR-E. 98
Figure 22: Microbiome differences between SPF-S and SPF-R mice.. 99
Figure 23: Variations in microbiota composition are correlated with lethal outcome of infections with a Shiga toxin-expressing *C. rodentium* strains. 100
Figure 24: Delayed colonization in SPF-R mice is visible in all intestinal organs and tissues but most prominent in the cecum. 101
Figure 25: Different *in vitro* approaches could recover the observed phenotype. 103
Figure 26: Cohousing and transfer of cultivable bacteria from resistant mice leads to variable protective outcome in SPF-S mice. 104
Figure 27: Resistance of SPF-R mice is associated with higher diversity and abundance of bacteria in the Firmicutes phylum. 106
Figure 28: Cohousing experiments lead to various outcome in the phenotype with high abundance of SCFA producing bacteria in resistant mice. 107
Figure 29: Isolated facultative anaerobic bacterial species do not contribute to inhibition of *C. rodentium in vivo*. 109
Figure 30: The metabolome of resistant SPF-R is characterized by elevated SCFA levels 110
Figure 31: Untargeted metabolomics data of SPF-S and SPF-R mice before and after infection reveal strong differences between isogenic mouse lines. 111
Figure 32: SPF-R SCFA levels strongly impair the growth of *C. rodentium in vitro* at pH 6.0. 112

Figure 33: The metabolomics profile of resistant SPF-R is characterized by elevated SCFA levels, which strongly impair the growth of *C. rodentium in vitro* at pH 6.0. 114
Figure 34: Supplementation of susceptible SPF-S mice with SCFA lead to reduced *C. rodentium* burden *in vitro* and *in vivo*..... 116
Figure 35: Short-term butyrate supplementation did not lead to major differences in the microbiome of SPF-S mice. 117
Figure 36: Supplementation of GF and antibiotic treated SPF-S mice significantly reduces *C. rodentium* CFUs.. 118
Figure 37: Ampicillin treatment renders SPF-H mice long-term susceptible to *K. pneumoniae* colonization 120
Figure 38: Colonization of SPF-H mice with different pathogenic *K. pneumoniae* strains.. 121
Figure 39: Oligo-MM^{12} mice and GF mice are naturally susceptible to *K. pneumoniae*.. 123
Figure 40: Occurrence of *Klebsiella* species in healthy human cohorts. 124
Figure 41: Addition of *K. oxytoca* to susceptible cecal content reduces CFUs of MDR *K. pneumoniae.* .. 127
Figure 42: *K. oxytoca* increases clearance rates after antibiotic intervention in susceptible SPF-H mice. 128
Figure 43: Protective effect of *K. oxytoca* is common for different isolates but species specific.. 129
Figure 44: *K. oxytoca* protects against another common MDR *K. pneumoniae* strain. 130
Figure 45: *K. oxytoca* protects Oligo-MM^{12} mice against MDR *K. pneumoniae*..... 131
Figure 46: *K. oxytoca* partially protects GF mice against MDR *K. pneumoniae*.. 132
Figure 47: Probiotic *K. oxytoca* strain protects susceptible animals from luminal and tissue invasion and systemic spread. 133
Figure 48: Organ burden results in *Rag2*$^{-/-}$ SPF-H mice show the same phenotype..... 134
Figure 49: *K. oxytoca* reestablishes colonization resistance after antibiotic intervention..... 136
Figure 50: Humanization of GF mice transfers phenotype from donors. 137
Figure 51: Decolonisation of MDR *K. pneumoniae* trough *K. oxytoca* treatment. 139
Figure 52: Factors influencing individual colonization susceptibility in this thesis. 143
Figure 53: Potential pathways of the resident microbiota interfering in the development of mucositis. 148
Figure 54: Microbiota related differences between SPF-S and SPF-R mice.. 154
Figure 55: Potential mechanisms of K. oxytoca mediated protection..... 160

IV. List of tables

Table 1: Common bacterial constituents of the human gastrointestinal tract microbiota 18
Table 2: Bacterial composition of frequently used defined mouse microbiota models 36
Table 3: List of equipment used in this thesis. 40
Table 4: List of consumables used in this study 41
Table 5: List of kits used in this thesis. 41
Table 6: List of bacterial strains used in this thesis. 42
Table 7: List of mouse lines used in this thesis. 42
Table 8: Reagents and drugs used in this thesis. 43
Table 9: List of buffer and solutions used in this thesis. 44
Table 10: List of media and agar used in this thesis. 47
Table 11: List of primers used in this thesis. 48
Table 12: List of antibodies used in this thesis 49
Table 13: List of software and algorithms used in this thesis. 50
Table 14: Components for 16S gene colony PCR 53
Table 15: Touchdown PCR program 53
Table 16: 16S gene PCR program 55
Table 17: Reaction for genomic DNA fragmentation. 56
Table 18: Reaction for adaptor ligation. 56
Table 19: Reaction for enrichment of adaptor-ligated DNA. 57
Table 20: PCR program for enrichment of adaptor-ligated DNA. 57
Table 21: Reaction for primer annealing. 58
Table 22: Master mix for cDNA generation. 58
Table 23: qPCR Master mix. 59
Table 24: qPCR program SYBR. 59
Table 25: Histological scoring. 67
Table 26: Meta-data of MikroResist cohort. 74
Table 27: Meta data of patient cohorts recruited in this study. 79
Table 28: Commensal *Klebsiella* strain isolated from healthy volunteers 125

1. General introduction

1.1 The human gut microbiome

Each individuals gut is colonized with more than 100 trillion of microorganisms belonging to several hundreds of different species collectively termed the microbiome (Wang et al., 2017). These complex and dense microbial communities consist mainly of bacteria, but also archaea, fungi, protozoa and viruses are part of the human microbiome (Buffie and Pamer, 2013). Important advances in culture- independent approaches and sequencing techniques including DNA sequencing, metabolomics and proteomics have led to more sophisticated and comprehensive results. As a result, numerous studies in humans and other mammals highlighted the tremendous impact of these microbes on the host physiology, both in health and disease (Wang et al., 2017). The microbial genome exceeds human genes by the factor of 150 conferring metabolic capabilities exceeding those of the host organism alone (Kim, Covington and Pamer, 2017). The microbiome thereby contributes to metabolic functioning, protects against pathogens, is involved in development of the immune system and through these basic functions, affect directly or indirectly most of our physiologic functions (Shreiner, Kao and Yang, 2015; Sommer and Bäckhed, 2013).

The crucial role of the human microbiota in health and disease occurs via several mechanisms. First, an essential function is to maintain proper digestive function of the gut. The microbiota increases energy extraction from food (Turnbaugh et al., 2006) as well as nutrient harvest and provides the host with unique and specific enzymes (Gill et al., 2006). The large metabolic potential of the microbiota encodes for essential biochemical pathways, which are involved in digestion of carbohydrates, biosynthesis of essential vitamins (Lozupone et al., 2012) and production of microbial derived metabolites such as short-chain fatty acids (SCFA) (Morrison and Preston 2016), choline and secondary bile acids (Nicholson et al., 2012). Another important role of the microbiota is the prevention of pathogen colonization and host entry via direct and indirect microbiota-pathogen interactions, collectively termed colonization resistance (Buffie and Pamer, 2013). Overall, the microbiota is essential for development of a proper immune system and intestinal mucosa (Bouskra et al., 2008; Macpherson and Harris, 2004). Taken together, a well-balanced and symbiotic microbiota is crucial to ensure proper development of the immune system and to maintain a healthy status of the host.

1.1.1 Development of the human microbiota

Immediately after birth simple microbial communities colonize the sterile infant consequently stimulating the prior naïve immune system to adapt and develop (Lozupone et al., 2012). However, studies exist suggesting that initial contact with microbes might occur already in the uterus as the placenta, amniotic fluid and meconium may not be completely sterile (Perez-Munoz et al., 2017). The neonatal microbiome composition is strongly determined by the mode of delivery and the local environment (Lawley and Walker 2013; Moore and Townsend, 2019). While naturally born children come into contact with the vaginal flora of the mother containing *Bacteroides*, *Bifidobacteria* or *Escherichia*, C-section infants are firstly colonized by species frequently found on the skin, in the oral cavity or the surrounding environment such as Staphylococci, Streptococci or *Propionibacterium* (Bäckhed et al., 2015; Dominguez-Bello, 2010). This altered, less beneficial initial colonization is maintained over long time and may ultimately explain why Cesarean Section (CS) is associated with numerous long-term health changes such as risks of developing immune-associated and allergic diseases, as well as hard to treat infections, inflammatory bowel disease, coeliac disease, childhood asthma and obesity (Jakobsson et al., 2014; Sevelsted et al., 2015). After parturition, the infantile microbiome experiences rapid changes and is mainly shaped by the way of feeding. Breastfeeding ensures proper development of the child having multiple health promoting properties including transfer of probiotic microbes, anti-adhesive antimicrobial agents, maternal antibodies and anti-biofilm compounds having bacteriostatic effects against selected pathogens (Moore and Townsend, 2019). With introduction of solid food, the microbiome begins to maturate and stabilize from a simple *Actinobacteria* and *Proteobacteria* dominated to a diverse adult-like microbiota that can metabolize starches present in more complex diet (Sekirov et al., 2010).

1.1.2 Community structure of the healthy adult gut microbiome

Even though the composition of the microbiome depends on multiple influencing factors and varies within and between each individual, a “core community structure” consisting of genes encoding for the same basic functions is shared among humans resulting in a high functional redundancy between microbiomes (Human Microbiome Consortium, 2012). Overall, most of the microbes predominantly belong to four different phyla, namely Bacteroidetes, Firmicutes, Actinobacteria and Proteobacteria (Buffie and Pamer, 2013) (Fig 1A, Table 1).

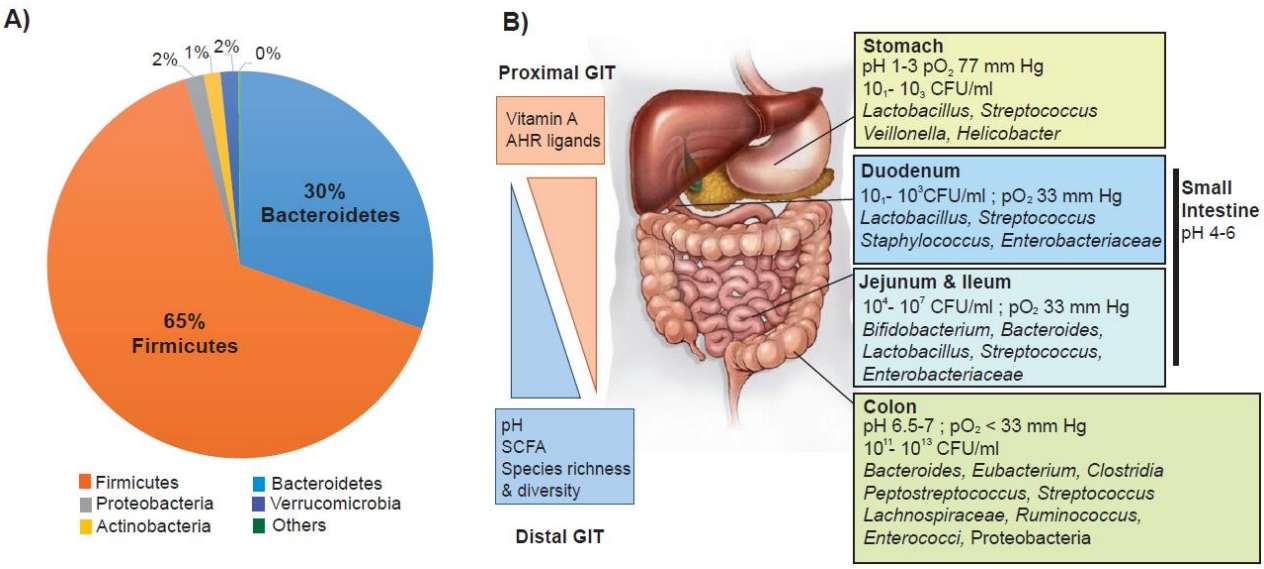

Figure 1: Indigenous microbiota of the human gastrointestinal tract. A) Main bacterial phyla and their overall abundance in the gastrointestinal tract (GIT). B) The indigenous microbiota and produced metabolites vary along the length of the human GIT. The densities of colonizing microbes, as well as SCFAs and the pH increases towards the distal GIT, whereas other environmental factors like vitamin A and oxygen decrease towards the distal end. For each distinct part of the gut, some main species present are highlighted (modified from Sartor, 2008).

The majority, with more than 90 % of the bacterial population is made up by gram positive Firmicutes and gram negative Bacteroidetes. Furthermore, in the homeostatic state Actinobacteria and Proteobacteria are regularly present in lower abundance (Lawley and Walker, 2013).

The GIT consists of a broad range of physiological conditions creating distinct niches for specific microbial communities (Fig 1B). In contrast to the neutral pH of the saliva, which contains up to 10^9 microbial cells/m, the extremely acidic milieu of the stomach serves as a valid barrier against microbial entry into the lower intestinal tract. As a result of the decreased peristalsis and acidity, the upper part of the small intestine is colonized with relatively low and simple microbial communities containing mostly facultative anaerobic and acidic tolerant species like Lactobacilli, Streptococci and Enterococci (Hayashi et al., 2005). Along with an increasing pH and decreasing transit time in the distal SI, microbial abundances and species diversity increases significantly up to 10^7 CFU/ml in the Ileum. However, the main part of bacteria, especially obligate anaerobic species resides in the colon, which supplies a neutral pH, low oxygen, slow transit time and a plethora of different nutrients that escaped enzymatic digestion in the small intestine (Lawley and Walker, 2013). In total, bacterial levels may reach up to 10^{13} CFU/ml in the feces making the mammalian intestine one of the densely colonized microbial habitats in nature (Whitman, Coleman and Wiebe, 1998).

Table 1: Common bacterial constituents of the human gastrointestinal tract microbiota (adapted from Lawley and Walker, 2012)

Phylum	Brief description	Commonly detected genera
Actinobacteria	Gram-positive, typically obligate anaerobic or microaerophilic, high GC-content, secondary metabolite production. Some genera most abundant in infants	*Atopobium*, *Bifidobacterium*, *Collinsella*, *Eggerthella*
Bacteroidetes	Gram-negative, typically obligate anaerobic, rod-shaped, non-spore forming bacilli. Often abundant in the gut microbiota. Degradation of complex carbohydrates	*Alistipes*, *Bacteroides*, *Barnesiella*, *Parabacteroides, Prevotella*
Firmicutes	Gram-positive, typically obligate anaerobic, low GC- content, ability to form endospores. Often highest abundance in the gut microbiota, and typically highly diverse. Majority of constituent species have yet to be cultured in the laboratory	Lachnospiraceae family: *Anaerostipes*, *Blautia*, *Butyrivibrio, Coprococcus*, *Dorea*, *Lachnospira*, *Roseburia* Ruminococcaceae family: *Anaerotruncus*, *Coprobacillus*, *Faecalibacterium*, *Ruminococcus*, *Subdoligranulum* Other *Firmicutes Acidaminococcus*, *Dialister*, *Enterococcus*, *Finegoldia*, *Holdemania*, *Lactobacillus*, *Megasphaera*, *Phascolarctobacterium*, *Streptococcus*, *Veillonell*a *Segmented filamentous bacteria (only in mice, not part of the human microbiota)
Proteobacteria	Gram-negative, mainly facultative anaerobic species. Includes many pathogenic species	*Alcaligenes*, *Bilophila*, *Campylobacter*, *Desulfovibrio*, *Enterobacter*, *Escherichia*, *Hafnia*, *Helicobacter*, *Klebsiella*, *Oxalobacter*, *Parasutterella*, *Proteus*, *Sutterella*
Others	Typically less abundant members of the gut microbiota	*Akkermansia*, *Fusobacterium*, *Victivallis*

From the main bacterial lineages, the bulk of bacteria belongs to the phylum of Firmicutes (65 %) which is composed of Gram- positive, mostly spore-forming, obligate and facultative anaerobic bacteria (Table 1). The class Clostridia is highly heterogeneous and is further divided into clusters. Members of *Clostridium* cluster *XIVa* and *IV* represents most organisms residing in the intestinal tract, which are implicated with several beneficial roles including production of SCFA and promotion of host immune homeostasis (Kim, Covington and Pamer, 2017). The second big lineage of bacteria is the Bacteroidetes phylum, which is composed of Gram-negative, non- spore forming and rod-shaped bacteria colonizing different regions of the intestinal tract.

One of the most predominant groups in the intestine is the genus *Bacteroides*, which are well known to digest complex polysaccharides yielding in the release of SCFA serving as an energy source of gut epithelial cells (Rajilić-Stojanović and de Vos, 2014). Taken together, most of the bacteria belonging to the main phyla contribute to important metabolic functions and maintain a beneficial relationship with the host.

Actinobacteria represent a minor phylum in the microbiome, consisting of Gram-positive, obligate anaerobic or microaerophilic bacteria, which have a higher GC content in their DNA compared to Firmicutes (Buffie and Pamer, 2013). The most abundant bacteria within this phylum are Bifidobacteria, which are considered having pronounces probiotic effects such as competitive exclusion of pathogens through bile salt hydrolase activity, immune modulation, and the ability to adhere to the mucus or intestinal epithelium (Picard et al., 2005; Tojo et al., 2014; Vlasova et al., 2016). In the healthy gut, Proteobacteria are normally present in low abundances. This phylum consist of Gram-negative, mainly facultative anaerobic bacteria including many pathogenic species as well as normal non-pathogenic gut members.

1.1.3 Influencing factors shaping the community structure

Several intrinsic and extrinsic factors can shape the human microbiota leading to unique community structures in each individual. As multiple factors have been identified one can start to analyze which factors such as age (Claesson et al., 2012; Yatsunenko et al., 2012), birth mode (Dominguez-Bello et al., 2010; Marques et al., 2010), diet (Sonnenburg and Sonnenburg, 2014; Subramanian et al., 2015; David et al., 2014), geography (Yatsunenko et al., 2012) , lifestyle (Clarke et al., 2014), hygiene level (Gupta et al., 2020), presence of infections and diseases (Bäumler and Sperandio, 2016) as well as intake of medications (Maier et al., 2018) can affect the “normal” gut microbiota to which extend (Fig 2). Interestingly, the differences between individuals are larger than changes in a person over time, suggesting that genetics have a minor role compared to environmental factors. Nevertheless, large human cohorts including twins showed that some taxa like *Christensenella* are highly heritable (Goodrich et al., 2014). Buy far more important is the intake of medications. It is known that antibiotics have profound effects on the gut microbiome that can even be persistent, especially when exposed in early childhood (Cho et al., 2012; Gough et al., 2014; Kozyrskyj et al., 2007). In addition, there is increasing evidence that also many non-antibiotic drugs impact the gut microbiota such as cyclophosphamides (Xu et al., 2015), proton pump inhibitors (Imhann et al., 2016) and multiple other prescription drugs (Maier et al., 2018; Devkota et al., 2016).

Another important factor in shaping the gut community structure is diet and food-ingested bacteria. Numerous studies showed that dietary changes result in substantial and rapid changes in the gut microbiota composition (David et al., 2014; Wu et al., 2011). Mouse and human studies showed that a high fat-low fiber diet decreases the number of bacterial species (alpha-diversity), whereas fiber-rich diet has been linked with health promoting properties because it modulates the gut microbiome in a beneficial way (Koh et al., 2016). 16S ribosomal RNA (rRNA) gene sequencing have distinguished three different enterotypes in humans based on the types of bacteria present, namely *Bacteroides*, *Prevotella* and *Ruminococcus* (Arumugam et al., 2011). These enterotypes were strongly associated with long-term diet habits showing that protein and animal fat were associated with *Bacteroides* enterotype, whereas carbohydrates were associated with the *Prevotella* enterotype (Wu et al., 2011). Interestingly, also drastic short-term changes in diet are sufficient to alter the gut microbiota (Bonder et al., 2016; David et al., 2014; Heinritz et al., 2016). The question arises whether long-term dietary interventions can create stable alteration in the bacterial enterotype and higher or lower incidence of diseases.

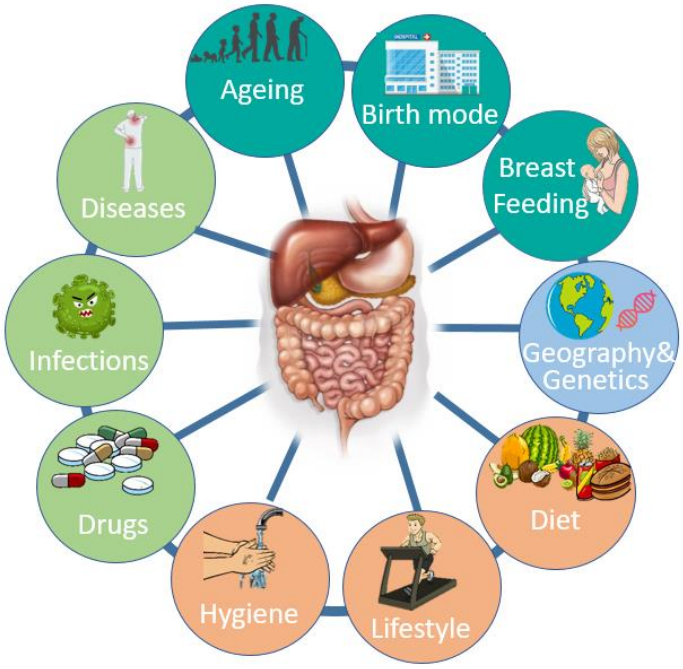

Figure 2: Factors shaping the gut microbiome. Multiple factors are known to influence the composition of the human microbiome. Clockwise from top right: Way of delivery at childbirth; breast or bottle feeding during childhood; geographic origin and genetics; fiber rich or fiber low diet, exercises and other personal habits; hygiene; intake of antibiotics and other medications; presence of infections; presence of diseases (e.g. inflammatory or autoimmune diseases) or ageing. (Modified from Quigley, 2017).

1.2 Homeostasis – colonization resistance in the healthy gut

Homeostasis defines the undisturbed and well-balanced status of the gut, in which the microbiota is stable and capable to protect the host against invading pathogens, via a mechanism called “colonization resistance”. Protection can either occur via direct competition strategies of present bacteria in the gut microbiota (Fig 3) or indirectly via immune- mediated mechanisms like proper induction of immune cells or enhancement of antibacterial pathways (Caballero and Pamer, 2015).

1.2.1 Nutrient competition

Competition for essential nutrients and environmental niches in the gut is the result of cross-feeding patterns and redundant substrate preferences between different bacteria to maximize utilization of the available substrates (Pereira and Berry, 2017). As a result, it is rather unlikely for exogenous species to find an unoccupied niche thereby being forced to compete with established species for limited carbon sources, trace minerals or spatial habitats (Stecher, Berry and Loy, 2013). In general, this competition for resources is considered as exploitative because species compete for one or more limited resources (Little et al., 2008). Food sources like simple sugars have been demonstrated to be subject of competition between the endogenous microbiota and invading pathogens like *Escherichia coli* (*E. coli*) or *Citrobacter rodentium* (*C. rodentium*) (Fabich et al., 2008; Kamada et al., 2012). Overlapping sugar utilization patterns between commensal and pathogenic *E. coli* or unrelated species such as *C. rodentium* and *Bacteroides thetaiotaomicron* highlight the importance of carbon and energy source availability. However, the impact of nutrient limitation influencing colonization resistance in the context of a balanced diet and an undisturbed, complex microbiota still needs to be determined (Sorbara and Pamer, 2019). Besides carbon and energy sources, invading bacteria compete with the resident microbiota trace minerals such as iron and zinc (Deriu et al., 2013; Gielda and DiRira, 2012). For example, probiotic *E. coli* Nissle protects mice from *Salmonella* infection by competition for iron (Deriu et al., 2013). In addition, immunization of mice to generate antibodies against iron-scavenging siderophores reduces the burden of *Salmonella* infection (Sassone-Corsi et al., 2016).

Also spartial niches such as crypts or mucosal surfaces can be subjects for competition (Stecher, Berry and Loy, 2013). For example, Pédron and colleagues identified specific communities of aerobic bacteria inhabiting cecal and colonic crypts of different mouse lines regardless of the line and breeding origin, reflecting a coevolutionary process under selective conditions (Pédron et al., 2012). It is likely, that numerous commensal and compound interactions as parts of nutritional competition will be identified in the future.

1.2.2 Bile salts and short chain fatty acids

Production of toxic or inhibitory compounds directly antagonizing other species is another main mechanism of direct colonization resistance. This process is known as interference competition (Little et al., 2008). Unabsorbed bile salts initially generated in the liver to increase fat solubilization and digestion are metabolized by specific members of the microbiota such as *C. scindens* into secondary bile salts (Fig

3). These secondary bile salts have been shown to induce germination of pathogenic *C. difficile* spores and inhibit the replication of vegetative cells (Urdaneta and Casadesus, 2017). Other dominant phyla like *Bacteroidetes* and *Firmicutes* are able to metabolize diverse substrates like complex polysaccharides, simple sugars and glycans by fermentation of ingested fibers and generate SCFA (Flint et al., 2015). The three main SCFA in the gut are acetate, butyrate and propionate reaching highest total concentrations in the proximal colon with 70-140 mM (Topping and Clifton, 2001). High levels of SCFA contribute to acidification of the lumen, which ranges between a pH of 6 and 7 in healthy individuals (Farmer et al., 2004). Numerous studies showed that SCFA can inhibit the replication of multiple enterobacterial pathogens at an acidic pH including *E. coli* (Roe et al., 2002)*, Salmonella* Typhimurium (S. Tm) (Jacobson et al., 2018) and *Citrobacter rodentium* (*C. rodentium*) (Osbelt et al., 2020) and loss of SCFA producing bacteria and acidic pH correlated with *in vivo* susceptibility to S. Tm (Bohnhoff and Miller, 1964) and *Klebsiella* (Sorbara et al., 2019). Higher SCFA concentrations also help to maintain low levels of oxygen and nitrate in the gut lumen, as loss of butyrate production triggers increased oxygen and nitrate release into the lumen of the gut favoring the outgrowth of *Enterobacteriaceae* (Kelly et al., 2015; Rivera-Chavez et al., 2016). Additionally, SCFAs trigger a complex modulation of virulence factors expression in S. Tm (Durant et al., 2000; Gantois et al., 2006; Hung et al., 2013; Lawhon et al., 2002), highlighting that SCFAs may influence colonization resistance in multiple direct and indirect ways.

1.2.3 Bacteriocins, antimicrobial peptides, and type VI secretion systems

Some species of the resident microbiota are also able to inhibit invading pathogens or other related bacteria through active antagonism, like production of bacteriocins, antimicrobial peptides or TypeVI Secretion systems (T6SS) (Fig 3). These antimicrobials have activity against both Gram-negative and Gram-positive pathogens and are produced through complex and diverse biosynthetic pathways (Sorbara and Pamer, 2019). The most frequently microbiota-produced antimicrobials include ribosomally synthesized and post-translationally modified peptides (RiPP) that either kill or inhibit the growth of closely related species, so called bacteriocins. Members of the order *Lactobacillales* such as *Lactococcus lactis* are known to produce some of the best-characterized bacteriocins, such as the lactibiotic Nisin, inhibiting a broad range of potentially pathogenic Gram-positive bacteria like *Staphylococcus aureus* and *Listeria monocytogenes* (Asaduzzaman and Sonomoto, 2009). Other potent bacteriocins include Abp118 produced by *Lactococcus salivarius*, which is able to protect mice from *L. monocytogenes* infection (Corr et al., 2007). Some bacteriocins like Thuricin CD produced by commensal *Clostridium thuringiensis* only target specific pathogens like *C. difficile* without targeting other members of the resident microbiota (Rea

et al., 2010). Systematic bioinformatics approaches revealed that biosynthetis gene clusters to produce inhibitory substances are widely distributed in the human microbiota and include Lantibiotics, thiazole/oxazole modified microcins and thiopeptides (Donia et al., 2014). Other bacteriocin producing strains include commensal *Enterococcus* species that are able to selectively kill multi-drug resistant vancomycin- resistant enterococci (VRE) (Kommineni et al., 2015) or nasal *Staphylococcus lugdunensis,* which can directly inhibit the growth of methicilline resistant *S. aureus* (MRSA) and VRE (Zipperer et al., 2016).

As a counterpart, also Gram-negative members of the microbiota, especially family members of the *Enterobacteriaceae* can produce potent short peptide bacteriocins, so called microcins, which are active against closely related species (Duquesne et al., 2007). Common producers of microcins are commensal *E. coli* including the probiotic *E. coli* Nissle strain, which compete with both *E. coli* and *Salmonella* only under inflamed conditions but not in mice treated with streptomycin alone (Sassone-Corsi et al., 2016). The reason is the competition for iron, which becomes limited under inflamed conditions and is critical for *Enterobacteriaceae* expansion (Deriu et al., 2013). In contrast to the numerous short peptides, some members such as *Bacteroides* species and *Escherichia* strains are able to produce larger proteins with antimicrobial activities (AMP). These AMPs act against surface molecules in the cell wall or encode colicins that can target related species lacking appropriate immunity proteins and increase competitiveness in the gut (Cascales et al., 2007; Roelofs et al., 2016).

In contrast to secreted peptides, some commensal Gram-negative species have developed complex structures so called T6SS that allow injection of effector molecules into adjacent bacteria or eukaryotic cells via cell-to-cell contact (Silverman et al., 2012) (Fig 3). Antagonism against neighboring cells occurs via various mechanisms of action, including degradation of NAD(P)+ and peptidoglycan hydrolysis (Russell et al., 2011; Silverman et al., 2012). T6SS are expressed by pathogenic γ-proteobacteria such as *P. aeruginosa* and commensal *Bacteroides* species. Crucially, T6SS+ strains must encode an immunity protein that negates the activity of the effector to avoid self-targeting (Russell et al., 2011).

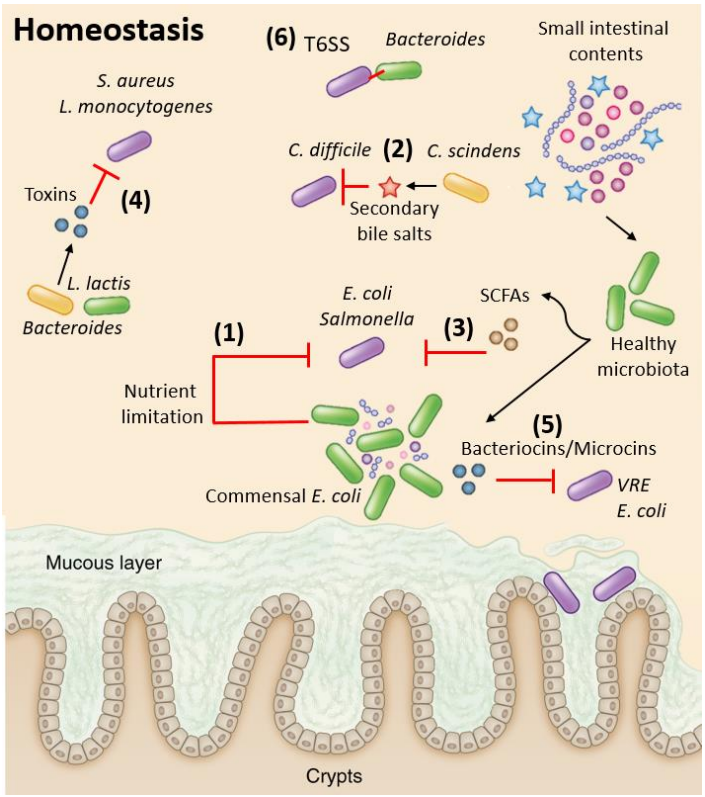

Figure 3: Direct colonization resistance mechanisms. The resident microbiota metabolism contributes to colonization resistance. 1) Resident microbiota members occupy niches and limit nutrients from pathogenic species. 2) Members of the microbiota, such as *C. scindens*, convert primary bile salts (blue stars) into secondary bile salts (red stars) that inhibit the vegetative growth of *C. difficile*. 3) The healthy microbiota ferments diet-derived simple sugars (purple/pink circles), complex polysaccharides (blue lines), and microbiota-liberated metabolites from the mucous layer to produce inhibitory SCFA. 4-5) Specific members produce toxic substances and bacteriocins to inhibit the growth of various pathogenic species 6) Commensal *Bacteroides* strains express T6SS to inject effector molecules in adjacent cells (modified from Sorbara and Pamer, 2019).

Under homeostatic conditions the complex communities in the microbiota can provide colonization resistance via multiple direct and indirect ways and can be used to restore recurrent *C. difficile* infections in disturbed conditions using fecal microbiota transplantation (FMT) (Kelly et al., 2016). Current research is spent on designing defined minimal consortia that provide colonization resistance or specifically eradicate pathogens from the microbiota. Several papers have already identified defined consortia that provide full or partial colonization resistance against *C. difficile* (Buffie et al., 2015) VRE (Caballero et al., 2017), *L. monocytogenes* (Becattini et al., 2017) or *Salmonella* (Brugiroux et al., 2016) in animal models.

1.3 Loss of colonization resistance

Alterations of the homeostatic composition of the microbiota through perturbations lead to an imbalanced status often referred to as dysbiosis. Dysbiosis or more general speaking disturbances in the microbiome are associated with various diseases in humans and animals including inflammatory bowel disease (Degruttola et al., 2016), asthma (Sokolowska et al., 2018), obesity (Arslan, 2014), metabolic syndrome (Tilg and Moschen, 2014), cardiovascular disease (Jin et al., 2019), immune-mediated conditions (Sandhya et al., 2016), cancer (Schulz et al., 2014), and neurodevelopmental conditions such as autism spectrum disorder (Mayer et al., 2011).

An imbalanced microbiome harbors higher levels of potentially harmful bacteria such as Proteobacteria, which are normally present in low abundance, leading to a shift in relative abundances of species which

is mostly accompanied with a slight or pronounced loss of beneficial, mostly strictly anaerobe species ultimately leading to loss of colonization resistance. Factors inducing or promoting imbalance are versatile. A high fat- low fiber diet has been shown to be linked with altered fecal bile acid profiles and growth of microbes promoting inflammatory bowel disease (Turnbaugh et al., 2009).

Another well-known factor for microbial imbalance are medications especially antibiotics, which are highly successful in treating bacterial infections but also exhibit severe and long-lasting effects on the microbiome (Sekirov et al., 2008). Especially antibiotic exposure in early life has been linked with an elevated risk for the development of numerous diseases and conditions including asthma, allergies and obesity (Kim and Covington, 2017).

1.3.1 Strategies of pathogenic bacteria to establish during dysbiosis

Antibiotic perturbation creates an opportunity for expansion of common nosocomial pathogens including members of the *Enterobacteriaceae*, VRE, and *C. difficile,* which are able to exhibit their own forms of colonization resistance and competition in imbalanced gut niches leading to persistent and recurrent infections (Lam and Monack, 2014). Pathogens have developed several antagonistic strategies to exploit gaps in the colonization resistance (Fig 4). Pathogenic bacteria such as *Salmonella* or pathogenic *E. coli* use the inflamed gut environment to upregulate expression of their own antimicrobial proteins and frequently those pathogenic strains carry a greater number of microcin genes than their non-pathogenic counterparts (Nedialkova et al., 2014; Smajs et al., 2010). Furthermore, intestinal pathogens frequently express tightly regulated T6SS during colonization and deliver a wide range of effectors to inhibit the commensal microbiota in response to specific cues as stress (Sana et al., 2016).

Enterobacteriaceae can rapidly expand upon inflammation or microbial imbalance due to their ability to utilize nutrients uniquely present in these conditions (Fig 4). In contrast to most strictly anaerobic members of the healthy gut microbiota, *Enterobacteriaceae* are able to perform aerobic and anaerobic respiration using oxygen or other molecules as terminal electron acceptors.

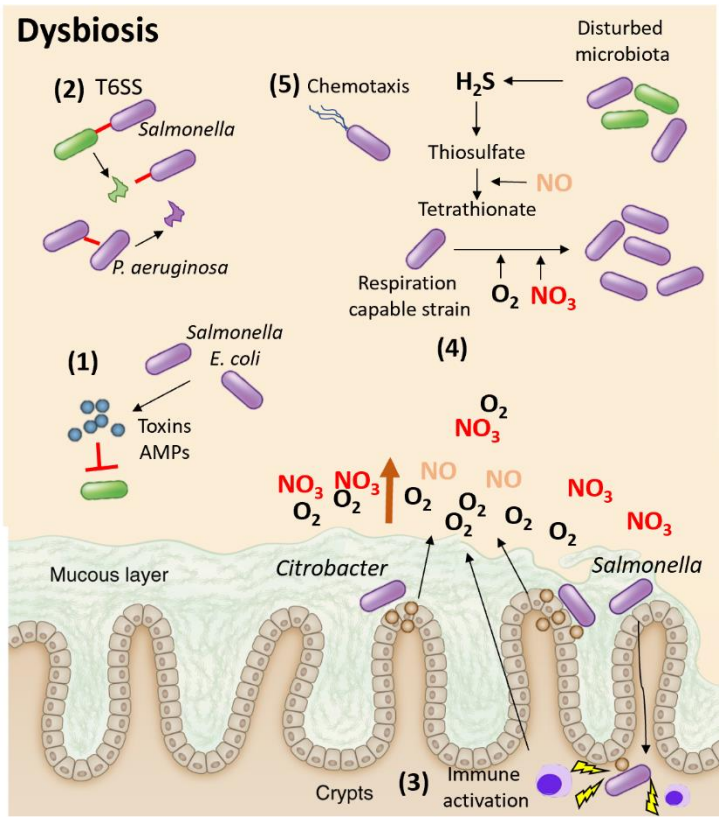

Figure 4: Expansion and engraftment strategies of invading species. 1) Pathogenic bacteria such as *Salmonella* or pathogenic *E. coli* upregulate expression of antimicrobial proteins and microcins in inflamed environments. 2) Some pathogens, such as *Salmonella* and *P. aeruginosa*, target either the microbiota or other opportunistic species through T6SS. 3) Pathogens can drive host inflammatory responses (yellow blizzards) in order to trigger the release of nitrates or oxygen into the lumen of the gut, and the formation of an oxidative environment. 4) Novel metabolites formed by oxidation, such as tetrathionate, O2 and NO3 are used in anaerobic and aerobic respiration pathways by pathogens able to use these electron acceptors resulting in blooming of pathogenic enterobacteria (5). Chemotactic attraction of pathogen through generation of alternate carbon sources (modified from Sorbara and Pamer, 2019).

In response to inflammation, reactive oxygen and nitrogen species are generated creating an oxidative environment, which can be exploited by oxygen and nitrogen reactive species (Sorbara and Pamer, 2019). Increased oxygen availability in the gut also leads to oxidation of carbon sources in the gut and generation of carbon sources normally absent during homeostasis such as generation of galactarate and glucarate from galactose and glucose (Faber et al, 2016) or usage of alternate carbon sources as ethanaloamine (Thiennimitr et al., 2011) or 1,2-propanediol (Faber et al., 2017).

Lastly, disruption of homeostasis can trigger a transient increase of typically low abundant metabolites, which can be efficiently used by pathogenic species. Well known examples include mucus- derived sialic acid, which can be utilized by *Salmonella* and *C. difficile* or microbiota-derived succinate, additionally utilized by *C. rodentium* (Ferreyra et al., 2014; Ng et al., 2013; Spiga et al., 2017; Vimr et al., 2004). Furthermore, *Salmonella* is able to use microbiota generated H_2 as an electron donor in the anaerobic gut to drive anaerobic respiration and utilize host-derived fucose (Maier et al., 2013; Pickard et al., 2014). Taken together, pathogenic bacteria are well adapted to take advantage of transient increases in microbiota-derived metabolites to create a growth advantage over commensal bacteria.

1.4 In the spotlight: thy family of *Enterobacteriaceae*

In the healthy adult gut, the phylum of Proteobacteria shares in only minor parts of all gut bacteria and encompasses a wide range of Gram- negative, facultative anaerobic bacteria (Janda, 2006). Even though members of this phylum are normal colonizers of the healthy gut, the phylum itself has the most known influence regarding human gastrointestinal diseases. Increased prevalence of Proteobacteria serve as a potential diagnostic marker of microbial imbalance and risk of diseases (Shin, Whon and Bae, 2015). Especially the family of *Enterobacteriaceae* within the class of γ-proteobacteria contains multiple bacteria with pathogenic potential like *Citrobacter, Enterobacter, Escherichia, Proteus, Shigella*, *Proteus,* and *Klebsiella,* which are normally present in low abundance, but can easily bloom and dominate the gut after pertubations. It is known that the intestinal microbiota affects the susceptibility to infections with *Enterobacteriaceae* such as *Citrobacter* or *Klebsiella*, but it remains still poorly understood which specific commensal bacteria and which pathogen-microbiota interactions contribute to protection against enteric pathogens.

1.4.1 A/E pathogens: *Citrobacter rodentium*

Infectious diarrhea, especially caused by enteric pathogens such as enterohemorrhagic and enteropathogenic *Escherichia coli* (EHEC) and (EPEC), is still a major health problem worldwide contributing to significant morbidity and mortality (WHO, 2020). EHEC, EPEC and *Citrobacter rodentium* are members of the *Enterobacteriaceae* and belong to the family of attaching and effacing (A/E) lesion-forming bacteria. Importantly, EHEC and EPEC can cause severe intestinal inflammation and diarrhea, with some EHEC strains expressing a highly potent Shiga toxin (Stx) causing nephrotoxicity resulting in severe cases in the death of infected individuals (Collins et al., 2014). *C. rodentium* is frequently used to mimic EHEC and EPEC infections in mice as these human pathogens only induce modest pathogenicity in rodents (Bhinder et al., 2013; Collins et al., 2014; Mallick et al., 2012). Several studies highlighted the impact of the microbiota regarding the intestinal colonization with *C. rodentium*. For instance, treatment with certain antibiotics such as metronidazole has been shown to increase susceptibility by eradication of specific microbes, whereas other antibiotics such as streptomycin did not affect severity of infection indicating that specific, but yet unknown, bacteria confer resistance to *C. rodentium* (Wlodarska et al., 2011). Furthermore, transfer of fecal microbiota from resistant to susceptible mice could delay colonization and reduce mortality of the susceptible mice indicating the importance of the microbiota to protect against *C. rodentium* (Willing et al., 2011). Upon fecal transplantation increased levels of interleukin (IL)-22 coupled with augmented antimicrobial peptides regenerating islet-derived 3 (Reg3)γ

and Reg3β were measured showing that yet unknown bacteria are able to promote resistance via indirect, immune-mediated pathways (Willing et al. 2011). Transfer of segmented filamentous bacteria (SFB) reduces *C. rodentium* colonization of the epithelium but not the lumen via increased expression of genes associated with inflammation and anti-microbial defenses (Ivanov et al., 2009).

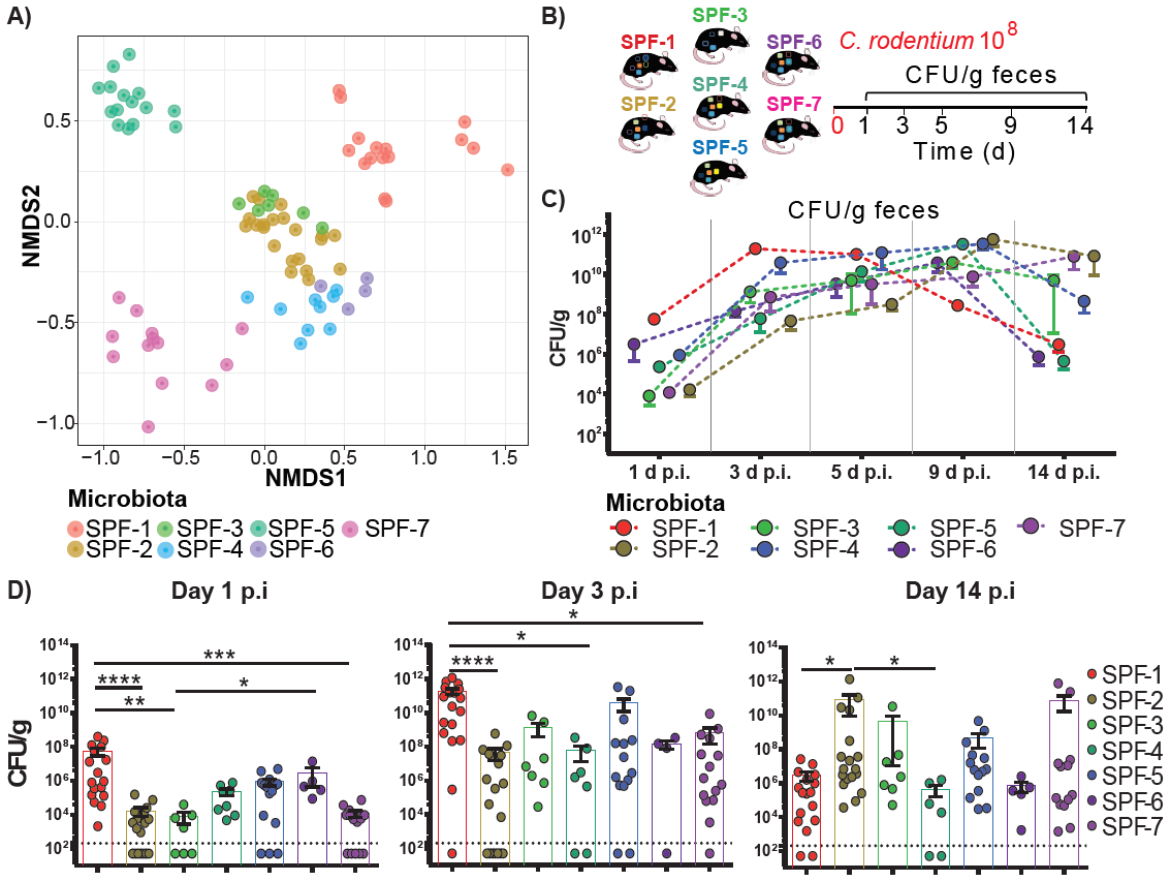

Figure 5: Different disease kinetics in isogenic mouse lines infected with *C. rodentium*. (A) Fecal bacterial microbiota composition of different specific pathogen free (SPF) mouse lines including SPF-1 (n = 17), SPF-2 (n = 18), SPF-3 (n = 7), SPF-4 (n = 9), SPF-5 (n = 15), SPF-6 (n = 4) and SPF-7 (n = 12) were evaluated using 16S rRNA gene sequencing. β-diversity was analyzed using Bray-Curtis dissimilarity matrix and non-metric multidimensional scaling (NMDS). (B) Mice with different microbiota settings were orally infected with 10^8 CFU *C. rodentium*. (C) CFU of *C. rodentium* was determined in the feces of each mouse line at day 1, 3, 5, 9 and 14 post infection (p.i.). (D) Fecal colonization of each individual mouse is indicated after day 1, 3 and 14 p.i. Dashed line indicates detection limit. Results represent one representative experiment with n = 4-17 mice/group as mean ± SEM. P values indicated represent a nonparametric Kruskal-Wallis test with multiple comparisons (one-way ANOVA). *p<0.05, **p<0.01, ***p<0.001, ****p<0.0001 (Adapted from Osbelt et al., 2020).

Moreover, higher ratios of Clostridia species were considered to influence the epithelial barrier, specifically mucus secretion, therefore, indirectly affecting luminal colonization of *C. rodentium* (Wlodarska et al., 2015). Within the lumen, the expansion of commensal *E. coli* has been shown to inhibit *C. rodentium* colonization by competition for monosaccharides as nutrient (Kamada et al., 2012).

Even though multiple mechanisms have been demonstrated how the microbiota can affect susceptibility, it is still unknown which specific members are able to confer resistance against infection with *C. rodentium*. Previous work from our group demonstrated that isogenic mouse lines feature different microbiota compositions on a standardized diet and observed highly variable colonization with the enteric pathogen *C. rodentium* without antibiotics intervention. We found the same differences in formerly GF animals harboring the respective donors' microbiota showing that the phenotype is fully dependent on differences in the microbiota (Osbelt et al.2020). The underlying reason for this phenotype remained elusive.

1.4.2 The emergence of multi-drug resistance

Antibiotic resistance occurs if a bacterium survives after being exposed to a drug that, under normal conditions, would inhibit its growth or kill it (Centre for disease control, 2018). Consequently, resistant strains multiply and spread due to reduced selective pressure, as other bacteria are sensitive to the same drug. Due to inappropriate use of antibiotics during the last decades, colonization and infection with multi-drug resistant bacteria have become one of the greatest health concerns worldwide. In 2017, the WHO ranked the development of new antibiotics against carbapenem- and 3rd generation cephalosporin resistant *Enterobacteriaceae* as a critical priority (WHO, 2020). Initially, *Enterobacteriaceae* became resistant to extended-spectrum ß-lactamases (ESBLs) turning the first-line empirical treatments to carbapenems, resulting in the emergence of carbapenem-resistant *Enterobacteriaceae* (CRE) such as *K. pneumoniae* (Sheu et al., 2018). During the last 15 years, the incidence of infections as well as the numbers of death linked to cabapenem- resistant *K. pneumoniae* has been rising to an alarming rate in European hospitals. The estimated median number for infections rose from 2,535 in 2007 to 15,910 in 2015, while attributable deaths increased from 341 to 2,094 (Cassini et al., 2019).

Three major mechanisms exist by which *Enterobacteriaceae* become resistant to carbapenems including enzyme production, efflux pumps and porin mutations (Fig 6) (Haidar et al., 2017). Generally, CRE can be divided into two main subgroups: carbapenemase-producing CRE (CP-CRE) and non-carbapenemase-producing CRE (non-CP-CRE). Enzyme production is by far the most prominent mechanism, initially through the production of ß-lactam-hydrolyzing enzymes extending to cephalosporinases, ESBLs, metallo-ß-lactamases (MBLs) and other carbapenemases with the introduction of new antibiotics (Suay-Garcia and Perez-Gracia, 2019). CP-CRE can produce a large variety of carbapenemases classified as class A, B and D ß-lactamases (Fig 6).

The *Klebsiella pneumoniae* carbapenemase (KPC) is most prevalent and globally spread resulting in high clinical relevance due to the limited treatment options of bacteria acquiring this resistance (Caballero et al., 2015). KPC-producing *Enterobacteriaceae* are endemic in the United States, Colombia, Argentina, Greece and Italy (Suay-Garcia and Perez-Gracia, 2019).

The second major class are Metallo-β lactamases (MBLs), which are specifically problematic as they have a high potential for horizontal gene transfer (HGT), lack useful inhibitors and have broad hydrolytic activities expect for monobactams (van Duin and Doi, 2017). The most common families include New Delhi metallo-ß-lactamase 1 (NDM-1) which are mainly expressed in *K. pneumoniae* and *E. coli;* Imipenem-resistant *Pseudomonas* (IMP)-type carbapenemases and the Verona integron-encoded metallo-ß-lactamases (VIM) (Codjoe and Donkor, 2017). MBL resistance is frequently found in India, Pakistan and Sri-Lanka and is usually associated with multi-drug resistance encoding different ß-lactamases, quinolone resistance and 16S rRNA methylases which confer resistance to aminoglycosides (Suay-Garcia and Perez-Gracia, 2019).

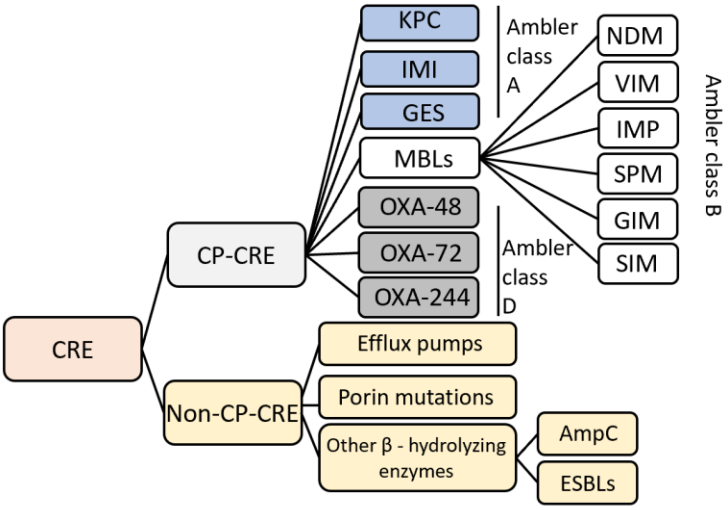

Figure 6: Classification of the different mechanisms of drug resistance in CRE. (Light grey: Ambler class A, White: Ambler class B, Dark grey: Ambler class D) (CRE: Carbapenem-resistant *Enterobacteriaceae*; CP: carbapenemase producing; KPC: *Klebsiella pneumoniae* carbapenemase; IMI: Imipenem-hydrolyzing ß-lactamase; GES: Guiana extended-spectrum ß-lactamase; MBLs: Metallo-ß-lactamase; OXA: oxacillinase; NDM: New Delhi metallo-ß-lactamase; VIM: Verona integron-borne metallo-ß-lactamase; IMP: Imipenem-resistant *Pseudomonas* carbapenemase; SMP: Sao Paulo metallo-ß-lactamase; GIM: German imipenemase; SIM: Seoul imipenemase; AmpC: Type C ampicillinase; ESBLs: Extended-spectrum ß-lactamase). (Adapted from Suay-Garcia and Perez-Gracia, 2019)

The third group of carbapenemases with high clinical relevance are Oxacillinase -48-like (OXA-48) within the Ambler class D which mainly occurs in Turkey, Malta, the Middle East and North-Africa. From six variants, OXA-48 is among the most widespread found in *K. pneumoniae, E. coli, C. freundii* and *E. cloacae* (Poirel, Potron and Nordmann, 2012). These plasmid mediated enzymes have a high ability to mutate, no existing inhibitors work against them and they easily expand their activity spectrum. They show high activity against penicillins, intermediate activity against broad-spectrum cephalosporins and low activity against carbapenems.

Taken together, all three groups of enzymes are plasmid encoded facilitating a fast spread of carbapenem-resistance worldwide. The development of new treatment options if therefore an urgent need.

1.4.3 *Klebsiella* spp.

The genus *Klebsiella* currently includes 18 species with five of them frequently found in the gut environment including *K. pneumoniae, K. quasipneumoniae, K. variicola, K. michiganensis* and *K. oxytoca* (Holt et al., 2015). *Klebsiella* sp. are ubiquitously found in nature and are characterized as rod-shaped, non-motile, encapsulated bacteria. The species *K. oxytoca* is genetically heterogeneous and is currently subdivided into seven phylogroups (Ko1 to Ko4 and Ko6 to Ko8) forming closely related subspecies (Merla et al., 2019). Even though *Klebsiella* species are common asymptomatic colonizers in the gut, *K. pneumoniae* is among the most problematic species associated with healthcare-associated infections (HAI) including respiratory tract infections, bloodstream infections and urinary tract infections in immunocompromised hosts (Bengochea and Sa Pessoa, 2018). More recently, the emergence of community acquired infections by multi-drug resistance (MDR) and hypervirulence in *K. pneumoniae* isolates has become a major health concern worldwide (Caballero et al., 2015). Hypervirulent (HV) strains exhibit unique features as hypermucoviscosity and specific virulence genes such as aerobactin leading to higher virulence compared to classical *K. pneumoniae* strains. Normally, HV *K. pneumoniae* are sensitive to common antibiotics, whereas MDR strains show lower virulence. Additionally, HV and MDR *K. pneumoniae* show different genotypes with different clonal groups (Shen et al., 2019). However, recent studies showed emerging of MDR-HV strains through acquisition of multidrug-resistant or hypervirulent plasmids (Dong et al., 2018; Feng et al., 2018; Gu et al., 2018; Shen et al., 2019; Zhang et al., 2016). The genetic basis of *K. pneumoniae* strains can be determined through multilocus sequence typing (MLST) dividing strains into distinct allelic profiles, called sequence types (ST) (Diancourt et al., 2005). Some of these sequence types are especially associated with antibiotic resistance or hypervirulence (Fasciana et al., 2019). For example, ST395 is associated with multi-drug resistance in Europe (Muggeo et al., 2018).

Modulation of *K. pneumoniae* is modulated through different virulence factors, which can be encoded in the core or the accessory genome. Virulence factors include various siderophores, lipopolysaccharide, pili, specific polysaccharide capsule serotypes, and *rmpA* genes that are associated with hypermucoidity (Broberg et al., 2014). Furthermore, efflux pumps efficiently shuffle antibiotics out of the bacterial cell thereby mediating antibiotic resistance and expression of T6SS enables injection of effector molecules and toxins into other cells (Journet and Cascales, 2016).

Gastrointestinal colonization rates range from 6 % among healthy individuals up to 19% in hospitalized persons (Gorrie et al., 2017), supporting that a direct link between colonization and infection of *K. pneumoniae* exists. Genomic analyzing techniques confirmed 80 % concordance between colonizing and infecting isolates of *K. pneumoniae* (Gorrie et al., 2017; Martin et al., 2016; Martin and Bachman, 2018). However, the link from colonization to infection is currently not know. Risk factors for colonization and infection include broad-spectrum antibiotic usage, immune suppression and intravascular devices (Kang et al., 2013). While colonization itself does not directly lead to inflammation, in case of injury of the mucosal surface, present bacteria may translocate beyond the intestinal tract, leading to subsequent deep tissue and systemic bloodstream infections (Sorbara et al., 2018). In line with these findings, several studies highlighted that intestinal colonization and expansion with *K*. *pneumoniae* after loss of colonization resistance due to antibiotics represents an early step in the progression of these infections (Taur et al., 2012).

1.5 The microbiome as a predictor for patient outcome

Individual variations in microbiota composition impact the host's degree of colonization resistance. This has been extensively shown in different diseases settings in dysbiotic conditions of the microbiota rendering the host susceptible to infections as well as in undisturbed conditions associating inter-individual microbiota compositions with different outcome of susceptibility to enteric infections (Human Microbiom Consortium, 2012, Pop et al., 2014, Tacket et al., 2010). A very critical risk group for intestinal inflammation and life-threatening infectious diseases are hematologic cancer patients due to their disease itself and the treatment with broad-spectrum antibiotics and strongly immunosuppressive drugs.

Immunosuppressive cancer treatments based on chemotherapy commonly cause inflammatory conditions in the oral cavity and the gastrointestinal tract known as mucositis (Carvalho et al., 2018; Viaud et al., 2015). Mucositis is highly prevalent in hematologic cancer patients, reaching incidences up to 80 % for intensive chemotherapy to treat neoplasms and affecting all patients receiving myeloablative-conditioning regimens prior to hematopoietic stem cell transplantation (Niscola et al., 2007). Since mucositis has been identified as a critical risk factor for infections it is still considered as one of the most serious complications in cancer treatment worsening the patient's outcome and increasing health care costs (Al-Dasooqi et al., 2013; Peterson, Bensadoun and Roila, 2011). The cytotoxic effects of chemotherapy broadly affect various mucosal tissue such as the oral cavity as well as the gastrointestinal tract including esophagus, stomach and intestines facilitating invasion of bacteria causing infections (Al-Dasooqi et al., 2013).

Different studies highlighted the impact of the microbiota to influence the development and course of cancer and mucositis (Galloway-Peña et al., 2016, Panebianco, Andriulli and Pezienza, 2018; Zwielehner et al., 2011). Of note, microbial dysbiosis can not only contribute to cancer pathogenesis and mucosal inflammation but also influences the therapeutic outcome due to microbial abilities to metabolize drugs thereby affecting the drug efficacy (Kang et al., 2013; Yoo et al., 2014) and to modulate host inflammation and immune responses (Alexander et al., 2017; Pouncey, Scott and Alexander, 2018).

Growing interest to understand the interaction between microbiota and chemotherapeutic effects has led to numerous publications with various outcomes, aiming to investigate the interplay between different chemotherapeutic drugs and the resident microbiota. DNA topoisomerase inhibitors like Irinotecan hydrochloride exhibited microbiota dependent intestinal cytotoxicity leading to diarrhea in treated rats, which could be ameliorated at least partially by administration of antibiotics (Takasuna et al., 1998). Stringer and colleagues (2009) reported changes in the microbiota and mucin and gene expression profiles of rats including reduction of glucuronidase-producing *Bacteroides spp*. as well as probiotic Bifidobacteria and Lactobacilli and increase of *Staphylococcus spp*., *Clostridium spp*. and *E.coli*, accompanied by overwhelming upregulation of the toll-like receptor (TLR) signaling pathway. The pyrimidine antagonist 5- Fluorouracil (5-FU) frequently causes leukopenia, thrombocytopenia and diarrhea and number of paper suggested that changes in the microbiota play a role in mechanistically underlying pathophysiology of these side-effects (Stinger et al., 2009). Interestingly, GF mice are more resistant to 5-FU and Irinotecan-induced mucositis, supporting the hypothesis that the microbiota is essential for development of mucositis (Brandi et al., 2006; Generoso et al., 2015). The alkylating agent Chlorambucil allowed the proliferation of pathogenic bacteria facilitating the development of *C. difficile*-associated diarrhea, which in turn has been shown to exacerbate mucositis in those patients (Gifford and Kirkland, 2006; Yamazawa et al., 2001). Various other chemotherapeutic agents including etoposide, carmustine and melphanan (Montassier et a., 2015), cyclophosphamide (Xu and Zhang, 2015), cytarabine (Galloway-Peña et al., 2016), or doxorubicin (Rigby et al., 2016) have been shown to reduce the richness of the microbiome and shift the composition to a dysbiotic state favoring outgrowth of bacteria with pathogenic potential. The majority of the literature available concerning mucositis is based on clinical observations, with very little basic research existing. If and how inter-individual differences in undisturbed microbiota compositions might already predetermine the patient outcome, course and success of cancer therapy and risk for infection needs still to be elucidated.

1.6 Chances and limitations of microbiome studies

1.6.1 Human microbiome studies

A big problem researcher facing in studies of the human microbiome is the resulting associations are most often correlative rather than clearly causal. With advances in metagenomics and high-throughput sequencing in the early 2000s projects aimed to capture the human microbiome diversity in large populations. Through the completion of the "Human microbiome project" (HMP) in 2012 which included a total of 242 screened and phenotyped adults at 18 body sites, we gained detailed knowledge about the basic composition of the "healthy" microbiome regarding species abundances, strains, and biomolecular functional elements; and statistically associating changes in those features with population phenotypes or exposures (Human Microbiome Project Consortium, 2012). However, the functionality of specific bacteria as well as the metabolic potential and redundancy of different species remains still poorly understood. In diseases populations or after antibiotic-driven changes many human studies observe a links between overgrowths of single species or defined consortia, but the pathological mechanisms remain largely elusive (Bäckhed et al., 2012; Hsaio et al., 2013; Garrett, 2015; Peterson and Round, 2014; Stecher, Maier and Hardt, 2013; Trompette et al., 2014). These studies demonstrate a clear limitation of human population studies to establish causality. Further limitations are high costs and difficulties to control human studies at each stage including sample collection, data generation, and data analysis. However, in contrast to *in vitro* assays and animal models which often lacks translational value, direct measurements of exposures and health risks in the desired organism are possible (Chung et al., 2012). The gut microbiota is most commonly sampled from stool since it is easy to obtain and assayed. Stool greatly represents microbial community from the colonic lumen, but only to a smaller degree more proximal parts of the GIT or gut mucosal sites (Yasuda et al., 2015). Clinically, mucosal biopsies provide a more precise biogeographically resolved snapshot of the mucosal-associated microbial community but are more challenging to obtain and assayed (Morgan et al., 2012). Alternative sampling types like mucosal brushing or rectal swabs are less well studied regarding protocol consistency and accurate community representation (Tong et al., 2014).

1.6.2 Mouse models

To overcome the limitations faced in human studies, mouse models are a suitable tool to assess the impact of the microbiome on different infection diseases. Mice harbor extensive similarities in anatomy physiology and genetics and are therefore widely used in biomedical research. Further advantages include the availability of numerous genetically modified mouse lines, low maintenance costs, high reproductive rates and short life cycles (Nguyen et al., 2015).

In gut microbiota research mouse models are being used to study the role and functioning of specific members of the microbiome and its association with diseases. Essential manipulations techniques include host genetic background manipulation (gene knock-outs and knock-ins), controlled inoculation with species into GF mice, ecosystem interventions including diet interventions, antibiotic treatment and FMT (Nguyen et al., 2015). One milestone in standardization of animal models was the development of isogenic mouse lines, a result of selective inbreeding over decades leading to mice with nearly identical genetic backgrounds (Beck et al., 2000). Commercially available mice are raised “specific- pathogen free” (SPF), meaning they are devoid of specific pathobionts like *Helicobacter* or viruses, which are common colonizers of wild mice or conventionally housed mice (Dobson et al., 2019). Even if one specific mouse line is genetically identical, SPF mouse lines originating from different breeding facilities harbor diverse microbiota compositions. This variation in the microbiota is one major reason for variable and inconsistent results in multiple disease and infection experiments e.g. DSS-induced colitis (Roy et al., 2017), *Salmonella* Typhimurium (Thiemann et al., 2017; Velazquez et al., 2019), malaria (Villarino et al., 2016) and stroke (Sadler et al., 2017) highlighting the enormous impact of the microbiota in altering disease susceptibility. Other potential influencing factors for microbiota mediated phenotypes include genetic variabilities, gender, age and vertical transmission from parents as well as environmental factors, i.e. housing conditions, diet and handling. Detailed knowledge about the used mouse models, use of littermate controls and cohousing is therefore crucial to reduce and explain observed variability in performed experiments.

To assess the impact of specific microorganisms and to reduce the complexity of mice with undefined microbiota compositions researchers have developed GF mice, raised completely sterile and gnotobiotic animals, harboring only a selected set of bacteria (Kennedy, King and Baldridge, 2018). In contrast to conventionally raised animals, GF mice show several anomalies in their immune system including abnormal numbers of several immune cell types, deficits in local and systemic lymphoid structures including spleen and lymph nodes and perturbed cytokine levels (Macpherson and Harris, 2004; Round and Mazmanian, 2009). Nevertheless, these are valuable tools to study the impact of specific species and can be used as a starting point for experiments studying defined microbes.

Table 2: Bacterial composition of frequently used defined mouse microbiota models

Taxanomy	strain No.	OSF	ASF	CRASF®	Oligo-MM^{12}
Escherichia coli	–	+	–	–	–
***N Streptococcus* group**	–	+	–	–	–
***Clostridium* sp.**	356	+	+	+	–
***Lactobacillus* sp.**	360	+	+	+	–
Lactobacillus murinus	361	+	+	+	–
***Flexistipes* group**	457	–	+	+	–
Eubacterium plexicaudatum	492	+	+	+	–
Low GC content Gram + group	500	–	+	+	–
***Clostridium* sp.**	502	–	+	+	–
***Bacteroides* sp.**	519	+	+	+	–
Enterococcus faecalis	KB1	+	–	–	+
Akkermansia muciniphila	YL44	–	–	–	+
Bacteroides caecimuris	I48	–	–	–	+
Muribaculum intestinalis	YL27	–	–	–	+
Turicimonas muris	YL45	–	–	–	+
Bifidobacterium longum* subsp. *animalis	YL2	–	–	–	+
Acutalibacter muris	KB18	–	–	–	+
Clostridium clostridioforme	YL32	–	–	–	+
Clostridium innocuum	I46	–	–	–	+
Blautia coccoides	YL58	–	–	–	+
Flavonifractor plautii	YL31	–	–	–	+
Lactobacillus reuteri	I49	–	–	–	+

Development of defined mouse microbiotas started with the introduction of eight bacterial strains into GF mice named as Original Schaedler Flora (OSF) (Schaedler, Dubs and Costello, 1965). Later, the OSF was further modified for better standardization by the National Cancer Institute (NCI) and renamed as Altered Schaedler Flora (ASF) containing eight murine strains as well, four from OSF and four new ensuring normal growth and development of gnotobiotic mice (Wannemuehler et al., 2014).

Mice in the animal facility of the HZI contain a defined microbiota from Charles River Laboratories, containing the same strains as the ASF, but sequencing revealed that over several years of in-house breeding additional strains invaded into the HZI flora, including *Lachnospiraceae*, *Rikenellaceae*, *Erysipelotrichaceae* and *Ruminococcacae* leading to the term undefined low complexity microbiota (LCM).

More recently, another valuable gnotobiotic mouse model was developed: The Oligo 12 mouse microbiota (Oligo-MM^{12}) contains bacterial isolates from the mouse intestine representing members from the main phyla of bacteria (Table 2). Compared to GF mice, which are highly susceptible to infections, this consortium of 12 bacteria provides partial colonization resistance against *Salmonella* Typhimurium (Brugiroux et al., 2016).

To enhance translational value from mouse work to humans, researches started to develop humanized mouse model. It has been demonstrated that mice humanized with stool from different human donors result in similar microbiota composition and metabolic profiles with preservation of individual-specific features (Daharsh, Ramer-Tait and Li, 2019). Recent effort is spent on development of functional minimal human microbial consortia that are easy to maintain and manipulate. Taken together human studies, *in vitro* techniques and mouse models have individual strengths and limitations. Combination of all three approaches will likely lead to the best possible read-outs

1.7 Aims of the thesis

The fight against multi-drug resistant *Enterobacteriaceae* (MDR-E) has intensified in the last years as it is increasingly recognized as a global health threat. Initially, these pathogens were considered a healthcare-associated problem, but evidence of digestive carriage of MDR-E in the general population has started to raise concerns on the potential dissemination among the global human population and the associated risks during unrelated medical treatments and hospitalizations. Especially infections during the therapy of hematological-oncological patients are highly problematic prolonging hospital stays and increasing mortality rates. Leukemic patients are highly susceptible towards not only infections, but also the development of mucositis, colitis and graft-versus-host diseases (GvHD). This susceptibility is caused due to their illness itself as well as the combination with prophylactic and therapeutic treatment with broad-spectrum antibiotics and immune-suppressive drugs. There is evidence that the development of mucositis and individual infection susceptibility is associated with changes in the microbiome but detailed knowledge about the impact of specific members in the patient's microbiome influencing individual infection susceptibility is still poorly understood. Since susceptibility to infection is influenced by multiple factors, I aimed to study using a combination of human samples and mouse models three questions: i) how chemotherapy together with adjunct therapies influences microbiota composition and *ex vivo* colonization with MDR *K. pneumoniae*, ii) how difference in microbiota composition influence infection with enteropathogens *in vivo* and iii) how members of the microbiota can be utilized to prevent colonization with MDR *K. pneumoniae* strains.

In the first part of the thesis, I aimed to investigate the role of the microbiome in different patient cohorts regarding the infection susceptibility and development of mucositis. To unravel the complex network of microbiome composition and susceptibility towards infections, an *in vitro* assay of human fecal samples was utilized to investigate basic questions regarding the microbiome variability and parameters on the ability of MDR *K. pneumoniae* to expand or not in these samples. To do so, stool samples of different groups of individuals including leukemic patients undergoing chemotherapy and patients after stem cell transplantation as well as healthy individuals were compared regarding different parameters including species richness, species composition, amount and diversity of facultative anaerobic bacteria, pH-value and SCFA concentrations. In addition, to test the degree of colonization resistance in healthy individuals compared to risk group of patients, feces samples were inoculated with a MDR *K. pneumoniae* strain and growth was monitored.

1. Aims of the thesis

Based on the observations from the human cohorts, different parameters were identified comparing highly susceptible and protected individuals and were subsequently tested using mouse models. In order to test how the microbiota responds to repetitive cycles of chemotherapy, isogenic mouse lines with different microbiota compositions were utilized. In detail, I aimed to understand which species were specifically affected by drugs frequently used during chemotherapy such as chemotherapeutics, antibiotics and proton-pump-inhibitor and if specific changes in the microbiome would in turn lead to differing severity of intestinal mucositis. As infection susceptibility may be already predetermined by variations in the microbiome even in absence of drug-induced changes, I evaluated how differences in undisturbed microbiota compositions influences infection susceptibility with enteropathogens. Previous findings demonstrated that isogenic C57BL/6N mouse lines feature distinct microbiota profiles and significantly differ in their infection susceptibility towards *C. rodentium.* It was the major goal of this part to unravel the underlying mechanism and to identify bacteria or microbiota related factors explaining the observed phenotype. To unravel the underlying mechanism and to discriminate between a direct mechanism and an immune-mediated mechanism, different approaches were performed. These experiments included *in vitro* assays in isolated cecum content, cohousing and microbiome analysis of the mouse lines, isolation and transfer of specific groups of bacteria in susceptible animals, measurements of cytokine levels, pH and SCFA, analysis of mucus architecture and metabolic landscape and comparison of the oxygen levels in both mouse lines. These analysis revealed higher levels of SCFA in resistant mice and inspired by multiple studies highlighting the importance of SCFA levels during infections I aimed to further investigate the inhibitory properties of SCFA in the *C. rodentium* model using different *in vitro* and *in vivo* approaches.

Decolonization of MDR-Es by antibiotics have been shown to be ineffective, to disturb the microbiota and causing major side effects such as diarrhea. As FMT is considered as innovative tool to eradicate MDR colonization without causing severe side effects but remains largely undefined and uncontrollable, we aimed to identify specific members of the healthy microbiota that can compete with MDR *K. pneumoniae* strains in the last part of the thesis. As niche competition of MDR with commensal strains might be a likely mechanism of how the microbiota could protect against MDR colonization, fecal samples of resistant individuals were screened for commensal *Klebsiella* species and subsequently tested for their protective and decolonizing potential against MDR *K. pneumoniae.* To do so, different *in vitro* and *in vivo* approaches were performed using susceptible antibiotic treated SPF-mice or gnotobiotic animals. Taken together, it was the major goal of this thesis to broaden the understanding and to identify the underlying mechanisms by which the microbiota is able to modulate individual infection susceptibility against pathogens.

2. Material and methods

2.1 Materials

2.1.1 Instruments and equipment

Table 3: List of equipment used in this thesis.

Instruments	Model	Providers
Anaerobic chamber	Anaerobic chamber	Coy Laboratory
Autoclave	VX-65	Syntec
	Tuttnauer	Biomedis
Bead-Beater	Mini-Beadbeater-96	Bio Spec
Blotting System	Trans-Blot Turbo Transfer System	Biorad
Centrifuge	Centrifuge 5424 R	Eppendorf
	Centrifuge 5430 R	
	MULTIFUGE1 S-R Heraeus	Heraeus
	Savant DNA SpeedVac	Thermo Scientific
Chemiluminescense Imager	ChemiDoc XRS	Biorad
Colony counter	Protocol3	Synbiosis
Gel electrophoresis	Mupid-One	Advance
Gel documentation	Gel jet imager	INTAS
Rotor-Stator Homogenizer	PT 2500 E	POLYTRON
Incubator	HERATHERM Incubator	Thermo Fisher Scientific
Incubator shaker	Multitron	INFORS HT
In vivo imager	IVIS System	PerkinElmer
Magnetic stand	Magnetic rack	BioRad
Magnetic stirrer	MH15	Roth
PCR-cycler	FlexCycler^2	Analytik Jena
pH Meter	827 pH Lab	Metrohm
Photometer	Biophotometer plus	Eppendorf
	Varioskan Flash	Thermo Scientific
	Synergy 2 Multi-Mode Reader	Biotek
Pipettes	Research	Eppendorf

	Biohit	Sartorius AG
Power Supply	PowerPac HC power supply	BioRad
qPCR cycler	Light Cycler 480	Roche Diagnostics
Scale	Entris	Sartorius AG
	Precision scale CA214	VWR
Thermomixer	ThermoMixerF1.5	Eppendorf
	ThermoMixer comfort	Eppendorf
Spectrophotometer	NanoDrop1000	Thermo Fisher Scientific
Sterile bench	SAFE 2020	Thermo Fisher Scientific
Vortex - shaker	Vortex Genie 2	Bender & Hobein AG
Western Blot System	Mini-Trans Blot Cell and Criterion Blotter	Biorad

2.1.2 Consumables

Table 4: List of consumables used in this study

Name	Providers
96 Well Lightcycler Platte	Sarstedt
AMPureX beads	Bioz
Anaero Gen 3.5 L	Thermo Fisher Scientific
Any kD™ Mini-PROTEAN® TGX™ Precast Protein Gels	BioRad
Corning™ 96-Well Half-Area Plates	Fisher Scientific
Sterican 26 G disposable needles	B|Braun
Omnifix Syringes 1 mL	B|Braun
Pehanon pH 6.0-8.1	Macherey Nagel
pH Fix 0-14	Macherey Nagel
Plastic Ware	Sarstedt
Trans-Blot® Turbo™ Mini PVDF Transfer Packs	BioRad
Water for molecular biology	Panreac AppliChem
Zirconium/glass-Beads 0.,1 mm	Carl Roth
Zirconium/glass-Beads 1 mm	Carl Roth

2.1.3 Kits and enzymes

Table 5: List of kits used in this thesis.

Name	Providers
ECL reagent	Advansta
EZ-10 Spin Column PCR Products Purification KIT	BioBasic Inc.
DNAse I	Roche
DNeasy Blood & Tissue Kit	Qiagen
GeneRuler™ DNA Ladder Mix #SM0331/2/3	Thermo Fisher Scientific
Gel loading Dye, Orange 6 X	NewEngland BioLabs inc.
KAPA SYBR FAST qPCR Kit	Kapa Biosystems

Mix2Seq kit	Eurofins Genomics
NEBNext® Ultra™ DNA Library Prep Kit for Illumina®	NewEngland BioLabs inc.
Page Ruler™ Prestained Protein Ladder	Thermo Fisher Scientific
Polymerase Q5 High Fidelity	NewEngland BioLabs inc.
Polymerase TSG	BioBasic
Proteinase K (7528.2)	Carl Roth
RevertAid Reverse Transcriptase	Thermo Fisher Scientific
RNA later solution (R0901)	Sigma
RNAse	AppliChem
Roth poly d(T)12-18 Primer	Carl Roth
Spin Column PCR Product Purification Kit	BioBasic
StainIN™ GREEN Nucleic Acid Stain	highQU

2.1.4 Bacterial strains and mouse lines

Table 6: List of bacterial strains used in this thesis.

Bacterial strain	origin
Citrobacter rodentium ICC180	(Wiles et al., 2004)
Citrobacter rodentium DBS770	(Mallick et al., 2012)
Escherichia coli isolate 103	This thesis
Klebsiella pneumoniae YA21621 (ST395)	University hospital Magdeburg
Klebsiella pneumoniae SB4551 (ST285)	Pasteur Institute France
Klebsiella pneumoniae SB3341 (ST66)	Pasteur Institute France
Klebsiella oxytoca isolate 5	This thesis
Klebsiella oxytoca isolate 9	This thesis
Klebsiella oxytoca isolate 17	This thesis
Klebsiella oxytoca isolate 21	This thesis
Klebsiella oxytoca isolate 22	This thesis
Klebsiella oxytoca isolate 35	This thesis
Klebsiella oxytoca isolate 36	This thesis

Table 7: List of mouse lines used in this thesis.

Mouse line	Description	origin / flora	Genetic
C57BL/6N	SPF-S (SPF-1) SPF-R (SPF-2) SPF-H (SPF-5) SPF-J (SPF-6)	NCI (In-house flora) Charles River Barrier 11 HZI (In-house flora) Janvier	Wildtype
Germ-free C57BL/6NTac	GF	HZI	Wildtype
Oligo-MM^{12} C57BL/6NTac	Oligo-MM^{12}	MHH (Bugiroux et al., 2016)	Wildtype
Rag2$^{-/-}$ C57BL/6N	SPF-H *Rag2*$^{-/-}$	HZI	Total knock-out

2.1.5 Reagents

Table 8: Reagents and drugs used in this thesis.

Name	Producer
Acetic Acid (CH_3COOH)	J.T.Baker
Agarose	Carl Roth
Ampicillin sodium salt	Sigma
Amino acid solution (MEM non-essential amino acids 100X)	Thermo Fisher Scientific
Ara-C (Ara-Cell) 5g (100mg/ml)	Stada
Apramycin	Sigma
Bromophenol blue	Sigma
Calcium-chloride ($CaCl_2$)	Sigma
Chloramphenicol	Sigma
Chloroform	Avantor Performance Materials B.V
Ciprofloxacine	Sigma
cOmplete Protease Inhibitor Cocktail Tablets	Roche Diagnostics
EDTA	Carl Roth
Ethanol (EtOH)	J.T.Baker
Fetal bovine serum (FBS)	Sigma
Gentamycin	Sigma
Glucose	Sigma
Glycine	Carl Roth
Glycerol	Carl Roth
Hydrochloric acid (HCl)	Carl Roth
Isopropanol	J.T.Baker
Isoflurane	Ecuphar
Kalium-chloride (KCl) (KH_2PO_4)	Carl Roth
Kalium-di-hydrogen-phosphate	Carl Roth
Kanamycin sulfate	Carl Roth
L-cystein	Carl Roth
Levofloxacin 100 ml (5 mg/ml)	Fresenius Kabi
Magnesium-chloride ($MgCl_{2)}$	Carl Roth
Magnesium-sulfate ($MgSO_4$)	Sigma
Malate	Carl Roth
Methanol	J.T.Baker
Metronidazole	Sigma
Milk powder	Sigma
Mineral solution	Thermo Fisher Scientific
Natrium-chloride (NaCl)	Carl Roth
Natrium-deoxycholate	Carl Roth
Natrium-di-hydrogen-phosphate (Na_2HPO)	Carl Roth
Natrium-hydroxid (NaOH)	Carl Roth
Neomycin	Sigma
NP-40	Sigma
Pantoprazole Amneal 40 mg	Amneal

Resazurin	Sigma
Roti-Phenol/Chloroform/Isoamyl alcohol	Carl Roth
Sheep blood (defibrinated)	Thermo Fisher Scientific
Sodium acetate (3 M)	AppliChem
Sodium acetate	Sigma
Sodium butyrate	Sigma
Sodium dodecyl sulfate (SDS)	Sigma
SDS (20%) solution	AppliChem
Sodium propionate	Sigma
Streptomycin	Sigma
Succinate	Carl Roth
TE buffer	AppliChem
Trace Minerals	Thermo Fisher Scientific
TriReagent	Zymo Research
Tris	Carl Roth
Tris-base (TrisOH)	Sigma
Triton-X-100	Carl Roth
Tween20	Sigma
Vitamin K	Carl Roth
Vancomycin	Carl Roth

2.1.6 Buffers and solutions

Table 9: List of buffer and solutions used in this thesis.

Ingredient	Amount
10 x PBS	500 ml
NaCl (1370 mM) KCL (27 mM) $Na_2HPO_4X2H_2O$ (100 mM) KH_2PO_4 (20 mM) dH_2O	160.12 g 4.0 g 35.6 g 5.44 g 500 ml
2 x Buffer A	200 ml
NaCl (200 mM) Tris (200 mM) EDTA Na (20 mM) → pH 8 dH_2O →filter sterilize with V25 250 ml 0.22 µm	2.32 g 4.84 g 1.48 g Fill up to 200 ml
NP-40 lysis buffer	**200 ml**

NaCl (200 mM) Tris-HCl (500 mM) pH 8 NP-40 dH_2O → sterile filtrate and add protease inhibitor right before use	1.753 g 20 ml 2 ml Fill up to 200 ml
Tris-HCl	**200 ml**
Tris dH_2O → pH to 8 with HCl	12.11 g 200 ml
RIPA buffer	**100 ml**
NaCl SDS Na-deoxycholat Tris Triton-x 100 → pH 8 (use concentrated HCl) dH_2O	0.877 g 0.1 g 0.5 g 0.606 g 1 ml Fill up to 100 ml
6 x sample buffer	
2M Tris/HCL (pH6,8) SDS 100% Glycerol Bromophenol blue 2-Mercaptoethanol dH_2O aliquot in 1ml epis and store in -20°C	2.4 ml 1.2 g 4.5 ml 0.6 g 1.2 ml 8.8 ml
10 x Running buffer	**2 l**
TrisOH SDS Glycine dH_2O	60 g 5 g 72 g Fill up to 2 l
10 x Transfer buffer	**1 l**
250mM Tris 1,92M Glycine dH_2O	30.3 g 144 g Fill up to 1 l
1 x Transfer buffer	**100 ml**
10 x Transfer buffer Methanol dH_2O	10 ml 20 ml Fill up to 100 ml
10 x TBS	**1 l**
1M Tris-Base NaCl 25mM $MgCl_2$ → pH 7,3 (with concentrated aq. 37% HCl) dH_2O	121.14 g 58.44 g 5.08 g Fill up to 1 l

1x TBS-T	**1 l**
10 x TBS Tween20 dH_2O	100 ml 0.5 ml Fill up to 1 l
1x Blocking solution (3%)	**100 ml**
Milk powder 1 x TBS-T	3 g 100 ml
Stripping buffer	**250 ml**
Glycine SDS Tween20 → pH to 2.2 dH_2O	3.75 g 0.25 g 2.5 ml Fill up to 250 ml
50 x TAE	**10 ml**
Tris (c=242 g/l) Acetic Acid (c=57.1 g/l) EDTA (0,5 M or 100 ml/L) → pH 8 dH_2O	121 g 27.19 ml 50 ml Fill up to 500 ml
Apramycin	**10 ml**
Apramycin dH_2O filter sterilize with non-pyrogenic 0.2 µm sterile-R dilute 1:100 in media	0.25 g 10 ml
Ampicillin	**10 ml**
Ampicillin sodium salt dH_2O filter sterilize with non-pyrogenic 0.2 µm sterile-R dilute 1:100 in media	0.5 g 10 ml
Ampicillin for infection experiments	**1 l**
Ampicillin sodium salt Tap water filter sterilize with V25 500 ml 0.22 µm	0.5 g 1 l
Chloramphenicol	**10 ml**
Chloramphenicol 100 % EtOH filter sterilize with non-pyrogenic 0.2 0.2 µm sterile-R dilute 1:100 in media	0.25 g 10 ml
Ciprofloxacin	**10 ml**
Ciprofloxacin 0.1 M HCl filter sterilize with non-pyrogenic 0.2 µm sterile-R dilute 1:100 in media	0.1 g 10 ml

Gentamycin	**10 ml**
Gentamycin dH_2O filter sterilize with non-pyrogenic 0.2 µm sterile-R dilute 1:100 in media	0.25 g 10 ml
Kanamycin	**10 ml**
Kanamycin sulfate dH_2O filter sterilize with non-pyrogenic 0.2 0.2 µm sterile-R dilute 1:100 in media	0.5 g 10 ml
Levofloxacin	**10 ml**
Levofloxacin Dilute to 12 µg/ ml in media	5 mg/ ml
Neomycin	**10 ml**
Neomycin dH_2O filter sterilize with non-pyrogenic 0.2 µm sterile-R dilute 1:100 in media	0.1 g 10 ml
Streptomycin	**10 ml**
Streptomycin dH_2O filter sterilize with non-pyrogenic 0.2 0.2 µm sterile-R dilute 1:100 in media	1 g 10 ml

2.1.7 Media and agar

Table 10: List of media and agar used in this thesis.

Ingredient	**Amount**
BBL Thioglycollate Medium	BD bioscience
BHI broth	**500 ml**
Brain-Heart Infusion Broth (Fluka) dH_2O	18.5 g Fill up to 500 ml
BHI – blood agar	**500 ml**
BHI (Oxoid) Bacto agar (BD) dH_2O → autoclave Sheep blood	18.5 g 9 g 25 ml
LB-Agar	**500 ml**
LB-Agar Lennox (Roth) dH_2O	17.5 g Fill up to 500 ml
LB broth	**500 ml**
LB-Media (Roth) dH_2O	10 g Fill up to 500 ml

MacConkey-Agar	**500 ml**
MacConkey agar (Roth)	17.5 g
dH_2O	Fill up to 500 ml
M9 Salts (5x)	**1 l**
Na_2HPO_4 x $7H_2O$	37.6 g
KH_2PO_4	15 g
NaCl	2.5 g
NH_4Cl	5 g
dH_2O	Fill up to 1 l
M9-Media	**100 ml**
M9 salts (5x)	20 ml
20 % Glucose	2 ml
1M $MgSO_4$	200 µl
1M $CaCl_2$	10 µl
dH_2O	Fill up to 100 ml
MRS agar	
MRS agar (Sigma)	31 g
dH_2O	500 ml
Supermedium agar	**500 ml**
BactoAgar (BD)	9 g
dH_2O	250 ml
→ Autoclave	
BHI	18.5 g
Vitamins	5 ml
Minerals	5 ml
Amino acids	5 ml
Vitamin K	0.5 ml
Resazurin	0.25 g
dH_2O	210 ml
→Filter sterilize	
→ add sheep blood	25 ml
→ add mixture to agar	

2.1.8 Primers

Table 11: List of primers used in this thesis.

Description	**Sequence**
16S_27F (#1)	5' AGAGTTTGATCMTGGCTCAG
16S_1492R (#7)	5' TACGGYTACCTTGTTACGACTT
16S_V4Seq_515F	5´AATGATACGGCGACCACCGAGATCTACACTATGGTAATTG TGTGCCAGCMGCCGCGGTAA
16S_V4Seq_806R	5' GGACTACNNGGGTATCTAAT
16S_qPCR_334F	5´ ACTCCTACGGGAGGCAGCAGT
16S_qPCR_514R	5´ATTACCGCGGCTGCTGGC
Akkermansia F	5' CAGCACGTGAAGGTGGGGAC
Akkermansia R	5' CCTTGCGGTTGGCTTCAGAT
Klebsiella oxytoca F PEH-C	5'GATACGGAGTATGCCTTTACGGTG

Klebsiella oxytoca R PEH-D	5‘ TAGCCTTTATCAAGCGGATACTGG
Klebsiella pneumoniae F Pf	5’ ATTTGAAGAGGTTGCAAACGAT
Klebsiella pneumoniae R Pf/Pr2	5‘CCGAAGATGTTTCACTTCTGATT
SFB F	5’ GACGCTGAGGCATGAGAGAGCAT
SFB R	5’ GACGGCACG GATTGTTATTCA
NEBNext Adaptor for Illumina	5’ GAT CGG AAG AGC ACA CGT CTG AAC TCC AGT CUA CAC TCT TTC CCT ACA CGA CGC TCT TCC GAT
NEBNext Universal PCR Primer for Illumina	5’ AAT GAT ACG GCG ACC ACC GAG ATC TAC ACT CTT TCC CTA CAC GAC GCT CTT CCG ATC
NEBNext Index 1 Primer for Illumina	5’ CAAGCAGAAGACGGCATACGAGATCGTGATGTGACTG GAGTTCAGACGTGTGCTCTTCCGATC
NEBNext Index 2 Primer for Illumina	5’ CAAGCAGAAGACGGCATACGAGATACATCGGTGACTG GAGTTCAGACGTGTGCTCTTCCGATC
NEBNext Index 3 Primer for Illumina	5’ CAAGCAGAAGACGGCATACGAGATGCCTAAGTGACTG GAGTTCAGACGTGTGCTCTTCCGATC
NEBNext Index 4 Primer for Illumina	5’ CAAGCAGAAGACGGCATACGAGATTGGTCAGTGACTG GAGTTCAGACGTGTGCTCTTCCGATC
NEBNext Index 5 Primer for Illumina	5’CAAGCAGAAGACGGCATACGAGATCACTGTGTGACTG GAGTTCAGACGTGTGCTCTTCCGATC
NEBNext Index 6 Primer for Illumina	5’CAAGCAGAAGACGGCATACGAGATATTGGCGTGACTG GAGTTCAGACGTGTGCTCTTCCGATC
NEBNext Index 7 Primer for Illumina	5’CAAGCAGAAGACGGCATACGAGATGATCTGGTGACTG GAGTTCAGACGTGTGCTCTTCCGATC
NEBNext Index 8 Primer for Illumina	5’CAAGCAGAAGACGGCATACGAGATTCAAGTGTGACTG GAGTTCAGACGTGTGCTCTTCCGATC
NEBNext Index 9 Primer for Illumina	5’CAAGCAGAAGACGGCATACGAGATCTGATCGTGACTG GAGTTCAGACGTGTGCTCTTCCGATC
NEBNext Index 10 Primer for Illumina	5’CAAGCAGAAGACGGCATACGAGATAAGCTAGTGACTG GAGTTCAGACGTGTGCTCTTCCGATC
NEBNext Index 11 Primer for Illumina	5’CAAGCAGAAGACGGCATACGAGATGTAGCCGTGACTG GAGTTCAGACGTGTGCTCTTCCGATC
NEBNext Index 12 Primer for Illumina	5’CAAGCAGAAGACGGCATACGAGATTACAAGGTGACTG GAGTTCAGACGTGTGCTCTTCCGATC

2.1.9 Antibodies

Table 12: List of antibodies used in this thesis

Name	Providers	Dilution
Primary Rabbit Anti-HIF-1 alpha antibody (16897)	Abcam	1:500
Primary Mouse Anti-actin-beta antibody (8226)	Abcam	1:1000
Secondary - Goat Anti-Rabbit IgG H&L (HRP)	Abcam	1:10000
Secondary - Goat Anti-Mouse IgG H&L (HRP)	Abcam	1:10000

2.1.10 Software and algorithms

Table 13: List of software and algorithms used in this thesis.

Name	Application
Adobe Illustrator CS5	Figures
Excel 2016	Data analysis
Geneious prime R11	Blasting Sequences
GraphPad Prism 8.02	Data analysis
Image Lab	Western blot imaging
Image J	Western blot quantification
LefSe	16S data analysis
Living Image Software V 4.3.1	IVIS data analysis
Mendeley	Reference managing
Pubmed NCBI	Literature sources
R Studio - FastTree Price - Greengenes reference database; gg_otus-13_8-release - MEGA6 - OTU picking with UCLUST - Phyloseq - PyNAST alignment - QIIME v.1.8.0 (Quantitative Insights into microbial ecology) - R statistical programming environment - Ribosomal Database Project (RDP) classifier - Usearch 8.1 software package - Silva Ref NR database version 123.1	16S data analysis

2.2 Microbiological methods

2.2.1 Sterilization and Disinfection

All instruments, solution and media used for growth of bacteria were vapor sterilized at 121 °C and 2 bar. Heat-sensitive solutions, like antibiotics, vitamins and trace minerals were sterilized by filtration (0.2 µm).

2.2.2 Cultivation of bacteria

Bacteria were cultivated in liquid media or an agar plate. To prepare an overnight-culture, single colonies were picked and suspended in 5 ml sterile LB broth or BHI medium with or without appropriate antibiotics and incubated at 37°C. The next day, 1 ml of overnight culture was suspended in 24 ml of fresh media and incubated for approximately 4 hours at 37°C. Then the culture was adjusted to a desired OD_{600} of 0.2 for subsequent *in vitro* assays or $5*10^8$ CFUs/ml for *in vivo* experiments.

2.2.3 Measurement of cell density and calculation of bacterial CFUs

Optical density of bacterial cultures were measured using a photometer in a cuvette at 600 nm. Resulting OD_{600} was used to calculate required CFUs/ml of enterobacteria using following equitation:

$$\frac{1x10^9}{0.942}\ x\ OD_{600} = x\frac{CFU}{ml} \qquad \frac{5x10^8}{x\ CFU/ml}\ x\ 1000\ \mu l = x\ \mu l\ \frac{bacteria}{ml}$$

2.2.4 Cryo-preservation of bacteria

For cryo-preservation, 1 ml of an overnight culture was suspended in 24 ml fresh medium. The culture was incubated for 24 h at 37 °C and centrifuged at 800 *xg* for 15 min. The pellet was resuspended in 2 ml of BHI media. Afterwards duplicates were prepared by mixing 1 ml of bacterial solution with 210 µl of 89 % Glycerol (v/v), by pipetting up and down. Glycerol stocks were stored at -80 °C.

2.2.5 Preparation of feces samples for determination of CFUs

For determine CFUs, feces samples of mice and humans were collected in feces tubes, weighted and prepared by adding 1 mm Zirconia beads and 1 ml of PBS. Feces were homogenized for 2 times 25 sec with 1 min resting using a Mini-BeadBeater-96. Afterwards, 100 µl were transferred into 96 well plates, serial diluted and streaked out on agar plates. Remaining solution was centrifuged for 10 min at 15000 x*g.* The resulting pellet was stored at -20 °C for subsequent DNA extraction and 16S rRNA gene sequencing.

2.2.6 Determination of colony forming units

For determination of CFUs from bacterial cultures or fecal samples, serial dilutions on agar plates were prepared. To do so, homogenized samples or cultures was transferred to the first row of a 96-well plate. Remaining rows were filled with 225 µl of PBS and 25 µl of samples were transferred from top to the bottom and mixed after each transfer step by pipetting up and down several times. Next, two agar plates with respective antibiotics, were quartered and 25 µl were plated in each quarter starting with the highest dilution. Plates were incubated for 24 h at 37 °C. Afterwards, colonies were counted on the two highest countable dilutions and CFUs/ ml and CFUs/ g were calculated using the following equitation:

$$\frac{(CFU\ Dilution\ 1 + CFU\ Dilution\ 2\ )}{2} x\ 40 = \frac{CFU}{ml} \qquad \frac{\left(\frac{CFU}{ml}\right)}{weight\ in\ g\ of\ samples} = \frac{CFU}{g}$$

2.2.7 Growth curves assay

Bacterial culture was grown overnight at 37°C in LB broth with or without respective antibiotics. Subsequently, the culture was diluted 1:100 in fresh medium, and subcultured for 4 hours at 37°C in appropriate medium. A 96-well plate was equipped with 190 µl of appropriate medium with or without supplements (e.g. specific carbon sources or SCFA) and normalized to pH 6.0 or 7.0. Bacterial culture was normalized to 10^6 CFUs/ml and 10 µl were added per well. Each condition was performed in duplicates or triplicates. The plate was incubated in an automated plate reader under aerobic or anaerobic conditions at 37°C. The OD_{600} was measured every 30- or 60-min with 5 sec shaking before each measurement. Blank values were deducted manually and the average of two or three samples was calculated and plotted using GraphPad Prism.

2.2.8 *In vitro* competition-assay for human feces samples

Human feces samples were homogenized in 1 ml PBS or BHI (with or without SCFA) using a mini bead-beater as described in 2.7.5. 10 µl of bacterial solutions with an OD_{600} of 0.2 were added to the tubes and mixtures were incubated for 24 h at 37 °C under aerobic or anaerobic conditions. For anaerobic culturing, an airtight plastic box was equipped with Anaero Gen 3.5 L (Thermo Scientific). After 24 h of incubation, cultures were serial diluted and plated on appropriate agar plates to recover viable CFUs of desired bacteria as described in 2.7.6.

2.3 Molecular biological methods

2.3.1 Polymerase-chain reaction

Polymerase chain reaction (PCR) was used to amplify 16S gene DNA-sequences of unknown bacteria in order to identify species identity. The underlying concept of this method is exponential increase of the desired DNA through cyclic repeats of a three- step process consisting of denaturation at high temperatures, annealing of specific primers to the template DNA and synthesizes the complementary strand of the template. The 16S gene is highly conserved in all bacteria, but has variable regions which are distinct for different species allowing species discrimination via sequencing.

Table 14: Components for 16S gene colony PCR

Component	Volume / Amount [µl]
DNA template (colony in water)	2 µl
Forward primer (10 µM)	1 µl
Reverse primer (10 µM)	1 µl
dNTPs (10 µM)	1 µl
20 mM $MgSO_4$	5 µl
TSG buffer (10x)	5 µl
TSG polymerase	0.2 µl
ddH_2O	35.8 µl
	Final volume of 50 µl

For 16S gene colony PCR, grown colonies were picked and resuspended in 10, 20 or 30 µl of dH_2O depending on the size of the colony and used as template DNA. To amplify the 16S gene the forward primer: 16S_27F (#1) and the reverse primer: 16S_1492R (#7) (see chapter 2.1.8 Primers) generating a product of 1456 bp length, were used. PCR reactions were prepared as shown in Tab 14 and PCR program was conducted using conditions shown in Tab 15.

Table 15: Touchdown PCR program

Temperature (°C)	Time	Cycles
94	2 min	1
94	20 s	11
61→57 (Δ-0.3°C)	20 s	11
72	90 s	1
94	20 s	26
56	20 s	26
72	90 s	26
72	5 min	1
4	∞	1

2.3.2 Agarose-gel-electrophoresis

To separate generated PCR products, agarose gel electrophoresis was used. This technique utilizes a gel matrix and an electric field to separate the negatively charged DNA fragments by size. Migration speed of the DNA to the anode only depends on the length of the fragments, leading to slower migration of larger PCR products and fast migration of small products.

DNA samples were mixed with 1 µl of Orange G, loaded on 1% stained agarose (w/v) gel, buffered with 0.5 x TAE buffer and ran for 20 min and 135 V. For staining, 3 µl of stain green (Roth) was used per 40 ml gel. Afterwards, PCR products were visualized under UV light at 312 nm wavelength.

2.3.3 Sanger sequencing of purified DNA

After visualization PCR products were purified using EZ-10 Spin Column PCR Products Purification KIT (BioBasic) according to the manufacturers protocol and resulting DNA concentration and purity was measured using Nanodrop. Pure DNA should range between 1.8 to 2.0. DNA was normalized to required concentration. For sequencing, templates had to consist of 10 µl purified DNA with minimum 10 ng/µl. 1-2 µl of 16S_27F (#1) Primer per sample was added to a separate 1.5 ml tube. All samples were either send to the in-house sequencing platform "GMAK" or send to Eurofins sequencing over-night service. Resulting sequences were blasted in NCBI or analyzed using the program Geneious to determine species of bacteria.

2.3.4 Microbial community DNA extraction

Feces samples were collected and stored at – 20°C until processing for DNA based 16S rRNA gene sequencing. DNA was extracted using a phenol-chloroform-based method as described by (Turnbaugh et al., 2009). In brief, 500 µl of extraction buffer (200 mM Tris, 20 mM EDTA, 200 mM NaCl, pH 8.0), 200 µl of 20% SDS , 500 µl of phenol:chloroform:isoamyl alcohol (PCI) (24:24:1) and 100 µl of zirconia/silica beads (0.1 mm diameter) were added per feces sample. Lysis of bacteria was performed by mechanical disruption using a Mini-BeadBeater-96 for two times 2 min with 1 min chilling on ice in between. After centrifugation for 3 min at 8000 rpm, aqueous phase was passed for another phenol:chloroform:isoamyl alcohol extraction before precipitation of DNA using 500 µl isopropanol and 0.1 volume of 3 M sodium acetate. Samples were incubated at - 20°C for at least several hours or overnight and centrifuged at 4°C at maximum speed for 20 min. Resulting DNA pellet was washed with ethanol, dried using a speed vacuum and resuspended in TE Buffer with 100 µg/ml RNase I. Crude DNA was column purified using the Spin Column PCR Product Purification Kit from BioBasic Inc. to remove PCR inhibitors.

2.3.5 16S rRNA gene amplification and sequencing

16S rRNA gene amplification of the V4 region (F515/R806) was performed according to an established protocol described by Caporaso et al., 2011. Briefly, DNA was normalized to 25 ng/µl and used for sequencing PCR with unique 12-base Golary barcodes incorporated via specific primers (obtained from Sigma). PCR was performed using Q5 polymerase in triplicates for each sample, using following PCR conditions

Table 16: 16S gene PCR program

Temperature (°C)	Time	Cycles
98	30 s	1
98	10 s	25
55	20 s	25
72	20 s	25
72	5 min	1
4	∞	1

After pooling and normalization to 10 nM, PCR amplicons were sequenced on an Illumina MiSeq platform via 250 bp paired-end sequencing (PE250). Using Usearch8.1 software package (http://www.drive5.com/usearch/) the resulting reads were assembled, filtered and clustered. Sequences were filtered for low quality reads and binned based on sample-specific barcodes using QIIME v1.8.0 (Caporaso et al. 2010). Merging was performed using -fastq_mergepairs – with fastq_maxdiffs 30. Quality filtering was conducted with fastq_filter (-fastq_maxee 1), using a minimum read length of 250 bp and a minimum number of reads per sample = 1000. Reads were clustered into 97% ID OTUs by open-reference OTU picking and representative sequences were determined by use of UPARSE algorithm (Edgar, 2010). Abundance filtering (OTUs cluster > 0.5%) and taxonomic classification were performed using the RDP Classifier executed at 80% bootstrap confidence cut off (Wang, Garrity, Tiedje, & Cole, 2007). Sequences without matching reference dataset, were assembled as *de novo* using UCLUST. Phylogenetic relationships between OTUs were determined using FastTree to the PyNAST alignment (Price, Dehal, & Arkin, 2010). Resulting OTU absolute abundance table and mapping file were used for statistical analyses and data visualization in the R statistical programming environment package phyloseq (McMurdie & Holmes, 2013).

2.3.6 Genomic DNA extraction

For genomic DNA extraction 5 ml of a bacterial culture grown until OD_{600} of 1 was centrifuged for 15 min at 800 x*g*. DNA was extracted using the DNeasy Blood & Tissue Kit (Quiagen) according to the manufacturer's protocol. Additional 10 µl of 10 µg/ µl RNAse was added when adding Proteinase K.

2.3.7 Library preparation for Illumina sequencing

For library preparation the NEBNext® Ultra™ DNA Library Prep Kit for Illumina® (NewEngland BioLabs inc.) was used according to the manufacturer's protocol. The genomic DNA was extracted as described in 2.3.6

For the fragmentation of the genomic DNA following mixture was prepared:

Table 17: Reaction for genomic DNA fragmentation.

Component	Volume / Amount [µl]
DNA template (100 ng)	5.2 µl
NEBNext Ultra II FS Reaction Buffer	1.4 µl
NEBNext Ultra II FS Enzyme Mix	0.4 µl
	Final volume of 7 µl

The reaction was vortexed for 5 s, briefly spanned down and run to following program with a lid preheated to 75°C: 5 min at 37°C, followed by 30 min at 65 °C. For the following adaptor ligation, the following mixture was prepared.

Table 18: Reaction for adaptor ligation.

Component	Volume [µl] per one library
FS Reaction mixture	7 µl
NEBNext Ultra II Ligation Master Mix	6 µl
NEBNext Ligation Enhancer	0.2 µl
NEBNext Adaptor for Illumina	0.5 µl
	Final volume of 13.7 µl

The reaction was incubated at 20 °C for 15 min in a thermocycler with the heated lid off and afterwards 0.6 µl of USER®Enzyme was added to the ligation mixture. Reaction was mixed and incubated for 15 min with the heated lid set to ≥ 47 °C. To perform the size selection of Adaptor-ligated DNA for the final Library size distribution, AMPure XP beads were vortexed and warmed up for at least 30 min at RT before use. First 5.7 µl of 0.1 x TE were added to bring up the volume of the reaction to 20 µl. Afterwards, 8 µl of resuspended AMPure XP beads were added to the mixture and equally distributed by pipetting up and down. Samples were incubated for at least 5 min at RT, before they were transferred to a magnetic stand. As soon as the solution was clear, the supernatant was removed and the pellet was washed by adding 40 µl of 80 % freshly prepared ethanol for 30 s. This washing step was repeated once. After removing all visible liquid, the beads were air dried under the clean bench for up to 5 min. Afterwards, the samples were removed from the magnetic stand, DNA was eluted adding 21 µl 0.1 x TE-buffer and mixed by vortexing. Then, the tubes were placed again on a magnetic stand. When the solution was clear, 20 µl were transferred to a new tube and 10 µl of resuspended beads were added. The solution was mixed by vortexing and incubated for 5 min at RT. Samples were placed again on the magnetic stand and the washing step and elution of DNA was repeated as previously described.

To enrich the adaptor-ligated DNA the following mixture was prepared and the following PCR program was performed:

Table 19: Reaction for enrichment of adaptor-ligated DNA.

component	Volume [µl] per one library
Adaptor Ligated DNA Fragments	9 µl
NEBNext Ultra II Q5 Master Mix	15 µl
Index Primer	3 µl
Universal PCR Primer/i5 Primer	3 µl
	Final volume of 30 µl

Table 20: PCR program for enrichment of adaptor-ligated DNA.

Temperature (°C)	Time	Cycles
98	30 s	1
98	10 s	7
65	75 s	7
65	5 min	1
4	∞	1

To clean up the PCR reaction, 10 µl of resuspended AMPureX beads were added to the PCR reaction and mixed by pipetting up and down. Samples were incubated at RT for at least 5 min before they were placed on a magnetic stand. When the solution was clear, the supernatant was removed and the beads were washed with 120 µl ethanol and dried as described. To elute the DNA target from the beads, 21 µl 0.1 x TE was added and pipetted up and down. The samples were incubated for 2 min at RT before they were placed on a magnetic stand. As soon as the solution became clear, 20 µl of the supernatant were transferred to a new tube. The DNA was stored at -20 °C until the library was assessed on a Bioanalyzer subsequently followed by Illumina sequencing.

2.3.8 RNA isolation

Tissue samples were harvested and washed in ice cold PBS or transferred into RNA-later solution if not processed immediately. For RNA isolation, 200µl of 1mm beads and 1 ml of Tri-Reagent were added to an empty microfuge tube. Approximately 2 cm tissue was added per tube and homogenize using a Mini-BeadBeater96 for 1 min followed by 2 min resting on ice. Homogenization step was repeated 4-5 times until tissue was sufficiently disrupted. Afterwards, samples were incubated for 5 min at RT to permit the complete dissociation of nucleoprotein complexes followed by centrifugation at 300 *xg* for 3min at 4°C to pellet remaining fat and tissue debris. The supernatant was transferred to a new tube and mixed with 200 µl of chloroform per 1ml TRI-reagent vigorously for 15 sec and incubated at RT for 2-3min. Next, samples were centrifuged at 12,000 *xg* for 15min at 4°C to separate phases into lower red (chloroform) phase, interphase and colorless upper aqueous phase with RNA.

The upper aqueous phase was carefully transferred into a new tube without disturbing the interphase. To precipitate RNA, Use 500 µl of isopropanol were added per sample and incubated overnight at -20 °C. The next day, samples were centrifuged at 12,000 *xg* for 30 min at 4°C. Resulting gel-like RNA pellet was washed once with 1ml 75% ethanol and mixed by vortexing followed by centrifugation at 7,500 *xg* for 5min at 4°C. Ethanol was carefully removed and RNA pellet was air dried for 5min on ice. Resulting RNA was dissolved in 40 µl of fresh pure water by passing solution a few times through a pipette tip. RNA was stored at -80°C for storage or used to generate cDNA.

2.3.9 cDNA synthesis

To generate complementary DNA (cDNA) from isolated RNA, following reaction was added in a nuclease free tube on ice:

Table 21: Reaction for primer annealing.

component	Volume [µl] per sample
Total RNA (2 µg) or mRNA (1 µg)	2 µl
Oligo (dT) Primer (0.5 µg/µl)	1 µl
DEPC-treated water	7 µl
	Final volume of 10 µl

Reaction was gently mixed, briefly centrifuged and incubated for 5 min at 65°C, followed by cooling down on ice and brief centrifugation. Next, the following master-mix was prepared:

Table 22: Master mix for cDNA generation.

component	Volume [µl] per sample
Reaction buffer (5x) for reverse transcriptase	4 µl
dNTP mix (10 mM)	2 µl
RevertAid™ H minus reverse transcriptase	1 µl
DEPC-treated water	3 µl
	Final volume of 10 µl

10 µl of master mix was added to the RNA, mixed and briefly centrifuged. Mixture was incubated for 60 min at 42°C and then terminated by heating up to 85°C for 5 min. Resulting cDNA was subsequently used for qPCR or stored at -80°C for long-term storage.

2.3.10 Quantitative polymerase chain reaction

cDNA was diluted 1:10 in fresh water and mixed with appropriate primers and SybrFast gene expression master-mix. Quantitative PCR (qPCR) reactions were performed using a Lightcycler480 system. Relative gene expression was normalized to total 16S genes as a house-keeping gene.

The before described PCR technique only allows a qualitative result, which means weather the desired bacterium or gene is present or not. Especially for the detection of specific bacteria or cytokines which modulate immune responses a simultaneous amplification and quantification of the desired products are desired therefore using so-called quantitative PCR or real-time PCR technique. The amount of product is detected via a fluorescing reporter dye directly after each cycle so a continuously detection of the amplification is given (Chang, Chen and Yang 2009). cDNA was diluted 1:10 in fresh water and mixed with appropriate primers and SybrFast gene expression master-mix. For expression of bacteria such as *Akkermansia* or SFB, relative gene expression was normalized to total 16S genes as a house-keeping gene. PCR reaction were prepared as listed below (Table 23) in a 96 well-plate sealed with plastic foil and shortly centrifuged at 300 rpm. PCR run was performed using a Lightcycler480 system (BioRad) with the conditions listed in the following (Table 24). Annealing temperature differed between 53°C for 16S gene total bacteria primer, 55°C for cytokine primers and 57°C for *Akkermansia* and SFB primers.

Table 23: qPCR Master mix.

component	Volume [µl] per sample
cDNA	0.5 µl
Forward Primer (10µM)	1 µl
Reverse Primer (10µM)	1 µl
Master Mix SYBR FAST	5 µl
DEPC-treated water	2.5 µl
	Final volume of 10 µl

Table 24: qPCR program SYBR.

Temperature (°C)	Time	Cycles
94	2 min	1
94	20 s	39
53-55-57	10 s	39
72	20 s	39
Melting curve until 95°C	5s/°C	1
Cooling until 37°C	1°C/min	1

CT values were analyzed using Excel and GraphPad Prism. The CT value is defined as the number of cycles, which are required for the fluorescence signal to cross the background level. The relative abundance of the bacteria of interest or gene of interest was sustained by using following equation.

$$relative\ abundance\ of\ gene\ of\ interest = \frac{2CT\ (house\ keeping\ gene)}{CT\ (gene\ of\ interest)}$$

The applied equitation is a based on the delta-delta-CT (ΔΔCt) method for analysis of qPCR data. This algorithms is appropriate to analyze differences in relative gene expression under specific conditions (Chang, Chen and Yang, 2009).

2.3.11 Tissue preparation for protein analysis

Tissue was harvested, weighted for normalization and immediately transferred into ice-cold PBS for washing. Next, tissues were transferred into tubes filled with 200 µl of 1mm beads and 1 ml RIPA buffer freshly prepared with protease inhibitor. Tissues were homogenized using a Mini-BeadBeater96 for 1 min followed by 2 min resting on ice. Bead-beating step was repeated 6-7 times until tissue was sufficiently homogenized. Afterwards, samples were centrifuged for 10 min at 10,000 rpm at 4°C and the resulting supernatant was transferred into a new Eppendorf tube. Samples were either immediately prepared for SDS-Page or stored at -80°C.

2.3.12 SDS – PAGE and Coomassie staining

To separate proteins by mass sodium dodecyl sulfate polyacrylamide gel-electrophoresis (SDS-Page) was used. 100 µl of tissue lysates were mixed with 20 µl of sample buffer (6x) and boiled for 5 min at 95°C to denature the proteins and to cover the charge of all proteins. Next, samples were centrifuged for 5 min at max speed at 4°C. 20 µl of samples were loaded onto 10% SDS- polyacrylamide gels next to 5 µl of prestained marker and run for 20 min at 80 V followed by 1.5 h at 110 V. Subsequently the gel was used for Coomassie staining or transferred on a membrane by western blot. For staining, gel was fixed for 30 min followed by staining in Coomassie Blue R-250 solution for 30 min. The gel was subsequently destained in 10% Acetic for 2 h and more until the background became clear. Stained gels were imaged using the Chemidoc XRS system.

2.3.13 Western Blotting

For western blot, PDVF membrane (Amersham / GE Healthcare Life Science) was quickly soaked in methanol until membrane became transparent. Membrane and transfer paper were soaked in transfer buffer for 3 min and subsequently assembled with the gel for blotting at 25V and 2.5 A for 7 min using the BIO-RAD Trans-Blot Transfer System. After blocking with 3% skimmed milk for 1 h at RT, membranes were incubated with the appropriate primary antibody overnight, followed by 1 h incubation with HRP-conjugated secondary antibodies at RT. In between membranes were washed with 1 x TBS-T 3 times for 5 min. HIF-1α and β-actin (loading control) were detected using rabbit anti-HIF-1α (Abcam 82832) and mouse anti- β-actin (Abcam 8226) at 1: 500 and 1:1000 respectively and an anti-rabbit or anti mouse secondary antibody using 1: 10000 dilution. Protein bands were visualized using ECL reagent (Advansta) using a western blot imaging system (BioRad) and quantified using Image J software.

2.3.14 pH measurements

For pH measurements of buffer and solutions a pH meter was used and pH was normalized using HCl and NaOH. For pH determination in human feces and mouse intestinal contents, samples were diluted in 1ml of NaCl and pH was determined using sensitive pH paper (Macherey Nagel) by dipping the paper into the solution and waiting for 2-3 minutes for color changes.

2.3.15 Measurements of short-chain fatty acids.

Approximately 50-100 mg of cecal content was collected, weighted and immediately snap-frozen in liquid nitrogen and stored at - 80°C until further processing. For extraction of SCFAs, samples were resuspended in 600 µl water spiked with internal standard (2 µl o-cresol/250 ml) and 60 µl 65% HPLC-grade sulfuric acid per 50 mg fresh weight and mixed vigorously for 5 min. Next, 400 µl of the mixture were extracted with 200 µl of tert-butyl methyl ether, and the ether phase was analyzed by GC-MS as described previously (Neumann-Schaal, Hofmann, Will, & Schomburg, 2015). Standard curves of organic acids were used for external calibration.

2.3.16 Metabolite derivatization

Online metabolite derivatization was performed using an Axel Semrau Autosampler. Dried polar metabolites were dissolved in 15 µl of 2% methoxyamine hydrochloride in pyridine at 40°C under shaking.

After 90 min, an equal volume of N-methyl-N-(trimethylsilyl)-trifluoracetamide (MSTFA) was added and held for 30 min at 40°C.

2.3.17 GC-MS analysis untargeted metabolome

Sample (1 µl) was injected into an SSL injector at 270°C in split mode (1:5). GC-MS analysis was performed using an Agilent 7890A GC equipped with a 30m VF-35MS + 5m Duraguard capillary column (0.25 mm inner diameter, 0.25 µm film thickness). Helium was used as carrier gas at a flow rate of 1.0 mL/min. The GC oven temperature was held at 80°C for 6 min and increased to 300°C at a rate of 6°C/min and held at that temperature for 10 min. Subsequently, the temperature was increased to 325°C at a rate of 10°C/min and held at that temperature for 4 min, resulting in a total run time of 60 min per sample. The GC was connected to an Agilent 5975C MS operating under electron impact ionization at 70 eV. The transfer line temperature was set to 280°C. The MS source was held at 230°C and the quadrupole at 150°C. The detector was operated in scan mode. Full scan mass spectra were acquired from *m/z* 70 to *m/z* 800 at a scan rate of 2 scans/s. Tuning and maintenance of the GC-MS was done according to the supplier´s instructions, an automated tuning routine was applied every 150 injections. Data processing was done using the MetaboliteDetector software (Hiller et al., 2009).

2.4 Animal Experiments and human sample collection

2.4.1 Ethics statement

All animal experiments have been performed in agreement with the guidelines of the Helmholtz-Zentrum für Infektionsforschung, Braunschweig, Germany, the national animal protection law (Tierschutzgesetz (TierSchG)) and animal experiment regulations (Tierschutz-Versuchstierverordnung (TierSchVersV)), and the recommendations of the Federation of European Laboratory Animal Science Association (FELASA). The study was approved by the Lower Saxony State Office for Nature, Environment and Consumer Protection (LAVES), Oldenburg, Lower Saxony, Germany; permit No. 33.4-42502-04-14/1415, No. 33.19-42502-04-16/2124, No. 33.19-42502-04-17/2573, No. 33.19-42502-04-17/2445 and No. 33.19-42502-04-19/3293. Human sample and data collections have been perfomed in agreement with the guidelines of the Helmholtz-Zentrum für Infektionsforschung, Braunschweig, Germany, the Otto-von Guericke University in Magdeburg Germany, the ethics committeesin Lowes Saxony and Saxony Anhalt (permit No. 8629_BO_K_2019; No. 8750_BO_K_2019; No. 168/16_2016) and the European data protection laws (Europäische Datenschutz-Grundverordnung DSGVO). All human donors have signed a letter of informed consent in accordance with the World Medical Association Declaration of Helsinki.

2.4.2 Mice

C57BL/6N SPF-S mice were purchased from NCI and were maintained (including breeding and housing) at the animal facilities of the Helmholtz Centre for Infection Research (HZI) under enhanced specific pathogen-free (SPF) conditions. C57BL/6N SPF-R, and SPF-J mice were purchased from different vendors and housed under enhanced SPF conditions at the HZI for at least two weeks before the start of the experiment: Charles River (SPF-R), Janvier (SPF-J). Wildtype (WT) SPF-H mice and *Rag2*$^{-/-}$ SPF-H mice were generated, bred and housed under enhanced SPF conditions at the HZI (Stehr et al., 2009). Germ-free (GF) C57BL/6NTac mice were bred in isolators (Getinge) in the GF facility at the HZI. Animals used in experiments were gender and age matched. Female and male mice with an age of 8-12 weeks were used for experiments if not indicated otherwise. Mice received sterilized food and water *ad libitum* and were kept under strict 12-hour light cycle (lights on at 7:00 am and off at 7:00 pm). Depending on the experimental setup mice were housed in groups of up to five mice per cage. All mice were euthanized by asphyxiation with CO_2 and cervical dislocation.

2.4.3 Cohousing and fecal microbiota transplant

For cohousing experiments with conventional raised mice, age- and gender-matched C57BL/6N mice were housed together in cages at 1:1 ratios for three to four weeks before infection experiments. For cohousing experiments with GF mice, mice were cohoused at 1:1 ratio in specific ventilated isocages equipped with individual HEPA filters (Techniplast).

For fecal microbiota transplantation intestinal content of donor mice was transferred to BBC Thioglycollate media tubes and cycled into an anaerobic chamber. Mixture was filtrated (Corning ® Cell Stainer 100 µm), diluted in 7 ml of BHI and centrifuged for 10 min at 520 *xg*. Pellet was suspended in 1 ml BHI. Mice received 200 µl of fecal microbiota transplant per oral gavage.

2.4.4 *In vivo C. rodentium* infection

Bioluminescence expressing *C. rodentium* strain ICC180 was used for all infection experiments (Wiles et al., 2004) except for two infection experiments under BSL3 conditions were a Shiga toxin-producing *C. rodentium* strain DBS770 (Mallick et al., 2012) was used. *C. rodentium* inoculi were prepared by culturing bacteria overnight at 37°C in LB broth with 50 µg/ml kanamycin. Subsequently, the culture was diluted 1:100 in fresh medium, and subcultured for 4 hours at 37°C in LB broth. Bacteria were washed twice in phosphate-buffered saline (PBS) and spent down for 15 min at 500 *xg*.

Mice were orally inoculated with $5x10^8$ CFU (see chapter 2.7.3) of *C. rodentium* diluted in 200 µl PBS. Weight of the mice was monitored, and feces were collected at different time points (1, 3, 5, 9 and 14 days) after infection for measuring pathogen burden and 16S rRNA gene sequencing.

2.4.5 *In vivo* imaging (IVIS)

Mice were infected with bioluminescence expressing *C. rodentium* strain ICC180 as described in 2.4.4 and 2.7.3. After different time points of the infection (d1, 3, 5, 8, 11, 15, 21) mice were anesthetized using isoflurane (4 Vol %) and transferred into the in vitro imaging system (IVIS). Before the first imaging, mice were shaved on the belly to enhance detection of the bioluminescence signal. Images were taken after different exposure times (1 s, 30 s, 1 min, 3 min) and luminescence was quantified as average radiance ($p/s/cm^3/sr$). After termination of the experiment luminescence intensities of all pictures were normalized and quantified using the Live Image software.

2.4.6 *In vivo Klebsiella pneumoniae* and enterobacterial colonization

SPF mice with HZI microbiota were treated with ampicillin (0.5 g/l) for 5 consecutive days before start of the experiment to deplete competitive microbiota. Oligo-MM^{12} and GF mice did not receive any antibiotics. *Klebsiella pneumoniae* inoculi were prepared by culturing bacteria overnight at 37°C in LB broth with 50 µg/ml ampicillin and/or 50 µg/ml chloramphenicol. Subsequently, the culture was diluted 1:100 in fresh medium, and subcultured for 4 hours at 37°C in LB broth. Bacteria were washed twice in phosphate-buffered saline (PBS) and spent down for 15 min at 500 *xg*. Mice were orally inoculated with $5x10^8$ CFU of *Klebsiella pneumoniae* diluted in 200 µl PBS (see chapter 2.7.3). Weight of the mice was monitored, and feces were collected at different time points (1, 3, 6, 9, 14, 21, 28 and 42 days) after colonization for measuring pathogen burden and 16S rRNA gene sequencing.

2.4.7 *In vivo* competition experiments

For *in vivo* competition experiments, SPF-H mice (WT or *Rag2*$^{-/-}$ deficient) received ampicillin (0.5 g/l) for 5 consecutive days before they were precolonized with $5x10^8$ CFUs/ml of isolated enterobacteria diluted in 200 µl PBS per oral gavage. Oligo-MM^{12} and GF mice did not receive any antibiotics during the whole experiment and were immediately colonized with the same amount of bacteria. Inoculi of bacteria were prepared as described in 2.9.4. Fecal colonization and weight was monitored for two weeks before mice were challenged with *K. pneumoniae* as decribed in 2.9.4.

Fecal colonization was either monitored for 6 weeks at different time points (1, 3, 6, 9, 14, 21, 28 and 42 days) or mice were sacrificed at day 6 for assessment of CFUs in the intestinal organs and tissues.

2.4.8 *In vivo* decolonization experiments

SPF mice with HZI microbiota were treated with ampicillin (0.5 g/l) for 5 consecutive days before start of the experiment to deplete competitive microbiota. Oligo-MM[12] and GF mice did not receive any antibiotics during the whole experiment. *Klebsiella pneumoniae* inoculi were prepared as described in 2.4.5 and were orally inoculated with $5x10^8$ CFU of *Klebsiella pneumoniae* diluted in 200 µl PBS (see chapter 2.7.3). Three days after colonization, mice received $5x10^8$ CFU of *Klebsiella oxytoca or E.coli* diluted in 200 µl PBS per oral gavage. Weight of the mice was monitored, and feces were collected at different time points (1, 3, 6, 9, 14, 21, 28 and 42 days) after colonization for measuring pathogen burden and 16S rRNA gene sequencing.

2.4.9 *In vitro* competition assays for *K. pneumoniae* from cecal content

For *in vivo* competition assays, mice received ampicillin via drinking water for 5 days before the start of the experiment. At day 4 of ampicillin treatment mice were precolonized with $5x10^8$ CFUs/ml isolated *K. oxytoca*. Mice received 200 µl of 5×10^8 CFUs bacterial suspension per oral gavage. The next day, mice were euthanized by asphyxiation with CO_2 and cervical dislocation and cecal content was isolated, weighted and diluted in a 1:1 ratio with PBS. Subsequently, content was homogenized for two times 25 seconds using a Mini-BeadBeater-96 (BioSpec) and spiked with 10 µl of *K. pneumoniae* (OD= 0.2) and incubated at 37°C under aerobic or anaerobic conditions for 24 hours. Twenty-five µl of each sample were serial-diluted in 96 well plates and plated on selective agar plates with 25 µg/ml chloramphenicol to recover viable amounts of *K. pneumoniae*.

2.4.10 *In vitro* assays for *C. rodentium* in isolated cecal content

Mice were sacrificed and cecal content was isolated, weighted and diluted in a 1:1 ratio with PBS or BHI (with or without SCFAs added) and homogenized for two times 25 seconds using a Mini-BeadBeater-96 (BioSpec). Samples were either prepared aerobically or anaerobically in an anaerobic chamber. If required SCFA were added in different concentrations and pH was adjusted to pH 6.0 or 7.0 using HCl or NaOH. *C. rodentium* was grown in LB media with kanamycin and normalized to 10^6 CFUs. Tubes were inoculated with 10 µl of *C. rodentium* and cultivated at 37°C under aerobic or anaerobic conditions for 6 or 24 hours.

Twenty-five µl of each sample were serial-diluted in 96 well plates and plated on selective agar plates with 50 µg/ml kanamycin to recover viable amounts of C. rodentium.

2.4.11 Quantification of fecal enterobacterial colonization.

Fresh fecal samples were collected, and weight was recorded. Subsequently, fecal samples were diluted in 1 ml LB medium and homogenized by bead-beating with 1 mm zirconia/silica beads for two times 25 seconds using a Mini-Beadbeater-96 (BioSpec). To determine CFUs, serial dilutions of homogenized samples were plated on LB and MacConkey plates with appropriate antibiotics (50 µg/ml kanamycin for *C. rodentium*, 50 µg/ml ampicillin for *E. coli* and *K. oxytoca* strains and 25 µg/ml chloramphenicol for MDR *K. pneumoniae* strains). Plates were cultured at 37°C over night before counting. CFUs of enterobacteria were calculated after normalization to the weight of feces.

2.4.12 Assessment of luminal and tissue colonization

Mice were sacrificed after different time points after infection using asphyxiation with CO_2 and cervical dislocation. Intestinal organs and other required organs such as liver, spleen, gall bladder or mesenteric lymph nodes (MLN) were extracted. Intestinal organ content was squeezed out in a tube, weighted and tissues were diluted in 5 ml PBS. Afterwards, tissues were flushed, washed with PBS, weighted and diluted in 3 (spleen, MLN, gall bladder) or 5 ml (cecum, colon, small intestine (SI), liver) PBS. All samples were homogenized using Rotor-Stator Homogenizer. CFUs were determined as described in chapter 2.7.6.

2.4.13 Preparation of tissue sections for histopathological examination

Cecum, colon and SI samples were rolled up to “swiss roles”, fixed in 4% neutrally buffered formaldehyde and embedded in paraffin according to standard histological procedures. Sections of 3µm thickness were stained with hematoxylin-eosin (HE) for standard scorings and evaluated by a specialist blinded to the experimental groups using light microscopy. For mucus staining a combined Periodic-Acid-Schiff (PAS)/ Alcian-blue staining was performed according to standard laboratory procedures and also scored by a blinded specialist.

2.4.14 Semi quantitative scoring of inflammation

The histological scoring used to evaluate the severity of inflammation was modified from the TJL-score developed by The Jackson Laboratory (Mähler et al., 1998). The alteration of the score has been previously described (Pils et al., 2010). The colon was divided into a proximal and distal section, each of about the same size. The small intestine was divided into proximal duodenum, middle ileum and distal jejunum. The cecum was not further divided. All sections were scored from 0-3 for the general criteria severity, inflammatory infiltrate, villous atrophy, crypt damage and percentage of area involved as listed in the following leading to a maximum score of 15 for very severe inflammation.

Table 25: Histological scoring.

Category	Score	Degree	Description
Severity	0	none	no symptoms
	1	mild	mild lesion, normal structure of organ, mild invasion of inflammatory cells, no damage to the epithelium
	2	moderate	clearly visible lesion, but normal structure of organ mostly present, moderate change in the epithelium, moderate invasion of inflammatory cells
	3	severe	normal structure of organ destroyed, transmural invasion of inflammatory cells, severe damage to the epithelium
Inflammatory infiltrate:	0	none	no symptoms
	1	mild	mild infiltrate restricted to the lamina propria
	2	moderate	moderate infiltrate reaching the submucosa or focal transmural infiltrate
	3	severe	diffuse or multifocal transmural infiltrate
Villous atrophy:	0	none	no symptoms
	1	mild	25-50% reduction in villi length, normal morphology
	2	moderate	50% -75% reduction in villi length, normal morphology
	3	severe	more than 75% reduction in villi length, or disturbed morphology
Crypt damage:	0	none	no symptoms
	1	mild	single cell apoptosis, reduced depth of crypts, normal morphology
	2	moderate	degeneration of Paneth cells, increased rate of apoptosis
	3	severe	crypt abscesses (inflammatory cells in cypts)
Area involved:	0	none	no symptoms
	1	mild	up to 30% length of the SI
	2	moderate	until 30-70% length of the SI
	3	severe	more than 70% length of the SI is involved into the inflammation

2.5 Author contributions

L. Osbelt and T. Strowig designed the experiments. L. Osbelt performed all experiments and analysis if not indicated otherwise. Genome libraries were prepared by M. Wende and specific bioinformatics analysis (writing of R scripts, KEGG and Pricrust analysis) was conducted by Dr. T. R. Lesker and Dr. U. Muthukumarasamy. Histological samples were prepared and scored by M Pils and metabolomics samples were measured by K. Hohagen-Schmidt and M Neumann-Schaal.

3. Results

3.1 Individual infection susceptibility in healthy study populations is influences by multiple factors

3.1.1 Stool samples of healthy volunteers show highly variable degree of colonization resistance against multi-drug resistant bacteria

To investigate the influence of variations in microbiota composition and linked changes in the intestinal milieu towards the susceptibility to colonization with MDR-E in healthy individuals, fecal samples of 59 healthy adult volunteers were characterized in an integrated approach. Volunteers in this cohort (MikroResist) were defined as healthy when they did not take antibiotics for at least four weeks and did not have any chronic disease. The MikroResist cohort had an average age of 32.2, an average BMI of 22.62 and did not include vegan or vegetarian individuals (Table 26). To test whether samples showed variable degrees of colonization resistance *in vitro*, fecal samples were inoculated with a clinical isolate of a MDR *K. pneumoniae* (K. pn MDR1, ST395). The tested strain produced the enzyme carbapenemase (New Delhi metallo-beta-lactamase, *bla*NDM-1) and encoded multiple other resistance genes thereby being resistant against four different classes of antibiotics representing the emerging group of highly antibiotic-resistant strains (Fig 6). Aliquots of fecal samples were preserved to later measure levels of SCFA, for microbiota analysis and fresh aliquots were used to measure pH or were homogenized in 1 ml dH_2O and freshly spiked in with 10^6 CFUs of the K.pn strain (Fig 7A). These factors were chosen based on recent literature highlighting SCFA, pH and presence of commensal Enterobacteria as potential key-factors in mouse models influencing colonization susceptibility (Jacobson et al 2018; Litvak et al., 2019; Sorbara et al., 2018). Interestingly, human samples showed highly variable degrees of colonization resistance with more than 100,000- fold differences in the *in situ* growth of the pathogen (Fig 7B). The majority (39 out of 59 or 66.1%) of the samples showed medium high numbers of colonization between 10^8 to 10^{10} CFUs and were considered as “intermediate” (INT). Only 13.6 % (8 out of 59) of the samples displayed CFUs lower than 10^8 and were considered as “resistant” (RES). From the remaining samples (12 out of 59 or 20.3 %) more than 10^{10} CFUs could be recovered. These samples were considered as “susceptible” (SUS). To explain the variability within the samples I tried to correlate the outcome of the growth assay to variations in pH value (Fig 7C), abundance of other facultative anaerobes (Fig 7D) or variations in SCFA levels (Fig 7E-G). Protected samples were characterized by significantly lower pH values in the feces, compared to INT and SUS samples (Fig 7C). Also higher levels of facultative anaerobic species (Fig 7D) as well as higher levels of

SCFA including propionate, butyrate and acetate (Fig 7E) were associated with reduced CFUs of the MDR-E. To validate if the results from the *in vitro* growth assay and the subsequent grouping in RES, INT and are reproducible for different individuals I tested selected donors from the different groups multiple times (Fig 7H).

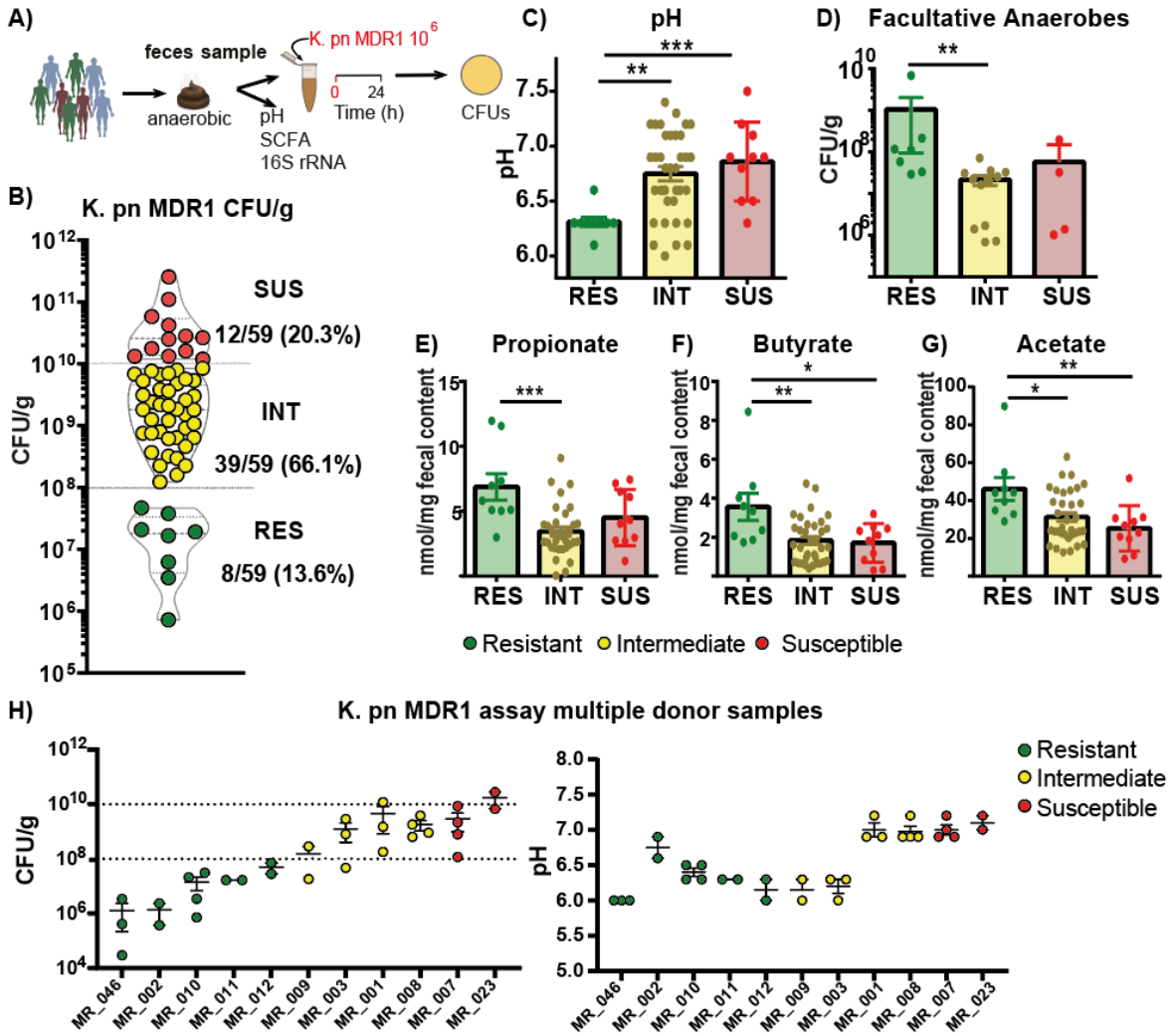

Figure 7: Factors shaping colonization resistance in healthy adult individuals. (A) Stool samples of healthy individuals were spiked in with 10^6 CFUs K.pn MDR1 and incubated anaerobically for 24h. pH, SCFA, levels of facultative anaerobes and 16S rRNA gene profiles were determined from each sample and CFUs of K.pn MDR1 were recovered on selective agar plates. (B) Samples grouped into susceptible (SUS), intermediate (INT) and resistant (RES) individuals based on the recovered CFUs K.pn MDR1. Each dot represents one individual. In total 12/59 (20.3%) belong to the SUS group, 39/59 (66.1%) belong to the INT group and 8/59 (13.6%) belong to the RES group. (C) pH value in stool samples of healthy individuals. (D) Levels of facultative anaerobic bacteria in stool samples of healthy individuals recovered after 24h of aerobic growth on BHI-blood agar. (E-G) Levels of fecal SCFA propionate, butyrate and acetate. (H) Several repeats of growth assay and pH measurement described above for selected samples from RES, INT and SUS group. Results are represented as mean ± SEM. P values indicated represent a nonparametric Kruskal-Wallis test *p<0.05, **p<0.01, ***p<0.001.

Stool samples were collected at least one week after the previous sampling and treated the same way as before. Resulting CFUs and pH value showed some degree of variability but the phenotype of low and medium grade colonization remained stable over different repeats. One of the SUS individuals showed large variability over the different repeats, whereas the other individual showed low variability between the repeats, indicating that the SUS phenotype is less stable but the overall trend of high CFUs is reproducible. The previously described data of the two susceptible samples were generated from the highest CFUs values in the first repeat. SCFA and microbiome data from the repeat samples have not yet been investigated, it therefore remains to be tested to which degree intra-individual changes in the microbiome compositions lead to lower CFUs in these two individuals. In the future, data points from more individuals would be beneficial to increase the reproducibility of the phenotypes. Nevertheless, certain trends were reproducible over different repeats suggesting that defined factors remained relatively stable over time if the microbiome is not disturbed by environmental factors such as major change in diet or drug intake.

3.1.2 Humanization of GF mice successfully transfer observed differences in CFUs in an *in vivo* colonization model

Next, I aimed to investigate if the observed differences in colonization *in vitro* could be reproduced *in vivo* by transferring human donor microbiota into germ-free (GF) mice. To do so, GF mice were gavaged once with feces of one SUS (donor ID: MR007) and one RES (MR011) donor. After 11 days of precolonization, mice received ampicillin for 3 consecutive days to reduce species richness and transiently lower the colonization resistance against K. pn MDR1 as 98% of all *Klebsiella* strains encode a chromosomal beta-lactamase making them resistant against Ampicillin/Amoxicillin (Livermore, 1995). On day 3 of amp treatment, mice were colonized with K. pn MDR1 and colonization kinetics were assessed after different time points after colonization. After three days, mice received normal drinking water to evaluate the protective effects of the different donor microbiotas (Fig 8A). Indeed, mice receiving feces from the RES donor cleared the colonization significantly faster compared to mice receiving feces from a SUS donor sample (Fig 8C). Specifically, on day 21 all RES animals (4/4) cleared the colonization, whereas none of the SUS animals (0/5) as K. pn MDR1 remained detectable in their feces (Fig 8C-D). This pilot experiment provides support that the observed differences in the *in vitro* assay are reproducible in a simplified *in vivo* colonization model.

Hence, I wanted to verify if the phenotypes can be consistently transferred if more donors are used. In addition to repeating the experiment with the susceptible donor MR007, an additional susceptible donor (MR023) and four intermediate donors (MR001, MR003, MR004 and MR043) were included. Mice (1 mouse / donor) were precolonized for two weeks and subsequently treated with ampicillin and colonized with K. pn MDR1 (Fig 8E). The resulting pathogen burden was assessed at multiple time points after colonization. Similar to the first experiment, the second experiment showed a good transferability of the human *in vitro* assay to the *in vivo* colonization model. Mice receiving different INT donor feces could clear the colonization significantly faster than the two mice harboring a SUS donor microbiota (Fig 8F).

To verify how accurate humanized mice reflect the donor microbiome, fecal samples from the first experiment were analyzed using 16S rRNA gene sequencing at various time points before and after colonization. On the beta diversity plot, three global clusters could be observed including the human donors and the mice with RES or SUS donor microbiome. Of note, mice clustered more closely to their respective donors than to the other donor, indicating that differences of the respective donor microbiota could at least partially be transferred to the mice (Fig 8G). Significant portion of the data variability could be attributed according to an ADONIS test to the donor (29.3 %) and the different time points of sampling (37.4 %) with significant differences between the groups. The remaining portion (33.3%) could not be explained. Regarding the alpha diversity, we could observe differences between the two groups of mice with a lower diversity in the SUS donor mice compared to the mice harboring the RES donor microbiota (Fig 8 H). The differences were maintained until the end of the experiment after 21 days post colonization. Analysis of the average microbiota composition on family levels revealed differences between the human and resulting mouse microbiota in terms of relations of species but transferability of the respective donor enterotype was achieved (Fig 8I). The RES donor belonged to the *Prevotella* enterotype which could be transferred into the humanized mice, whereas the SUS donor microbiota was characterized by high abundances of *Bifidobacterium* and presence of *Erysipleotrichaceae* or *Christenellaceae*. *Akkermansia* expanded to high amounts in all mice, whereas some taxa including *Erysipleotrichaceae* or *Christenellaceae* were not able to establish themselves in the mouse gut.

In summary, these pilot experiments provide support for the *in vitro* observations and are a promising starting point for the further development of human-related models to better reflect human microbiota situations and potentially facilitate the evaluation of new probiotics against MDR-E colonization (see 3.4).

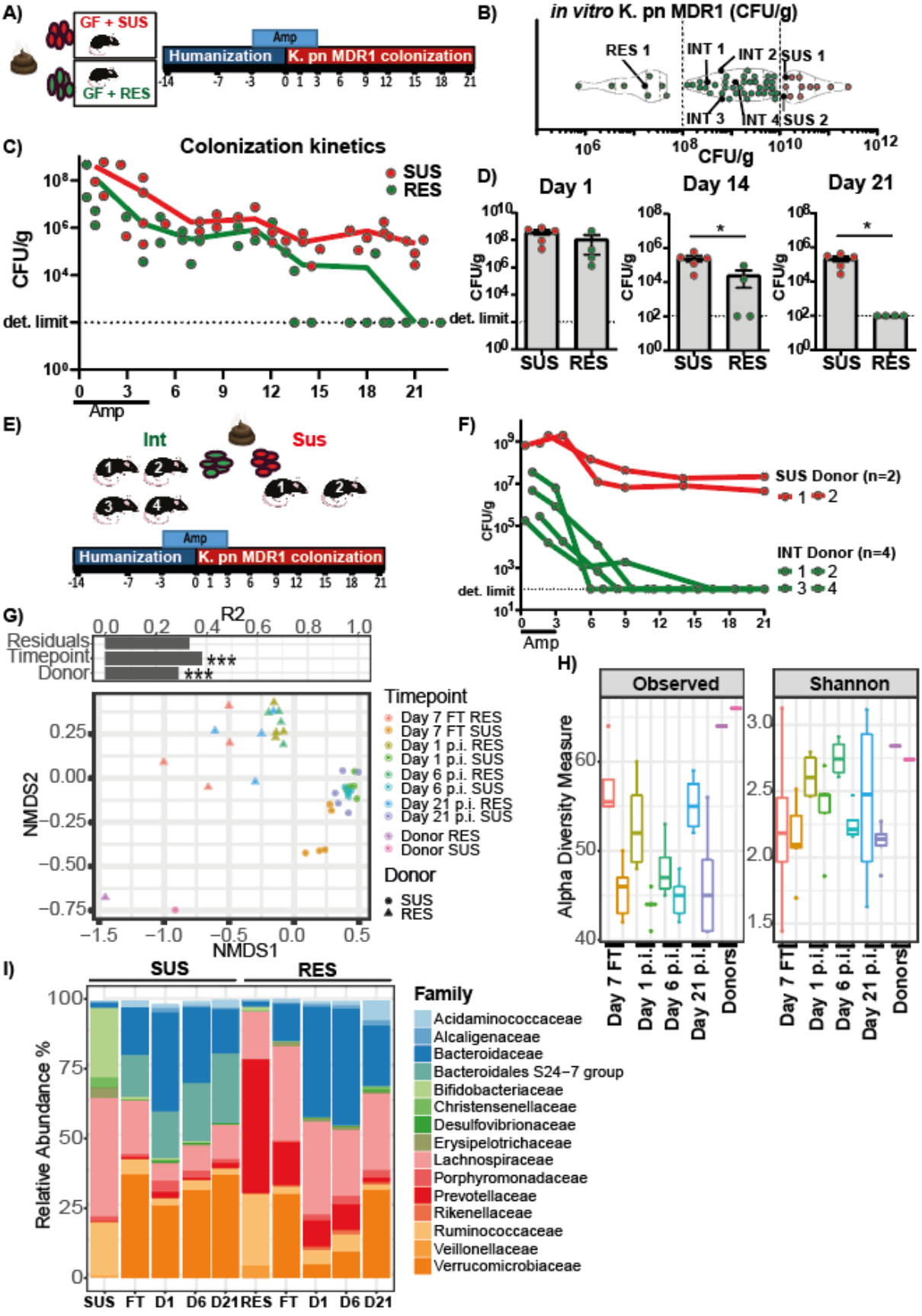
A)
GF + SUS
GF + RES
Amp
Humanization
K. pn MDR1 colonization
B)
in vitro K. pn MDR1 (CFU/g)
RES 1
INT 1
INT 2
SUS 1
INT 3
INT 4
SUS 2
CFU/g
C)
Colonization kinetics
SUS
RES
CFU/g
det. limit
Amp
D)
Day 1
Day 14
Day 21
SUS
RES
E)
Int
Sus
F)
SUS Donor (n=2)
INT Donor (n=4)
G)
R2
Residuals
Timepoint
Donor
NMDS1
NMDS2
Timepoint
Donor
H)
Observed
Shannon
Alpha Diversity Measure
Day 7 FT
Day 1 p.i.
Day 6 p.i.
Day 21 p.i.
Donors
I)
SUS
RES
Relative Abundance %
Family
Acidaminococcaceae
Alcaligenaceae
Bacteroidaceae
Bacteroidales S24−7 group
Bifidobacteriaceae
Christensenellaceae
Desulfovibrionaceae
Erysipelotrichaceae
Lachnospiraceae
Porphyromonadaceae
Prevotellaceae
Rikenellaceae
Ruminococcaceae
Veillonellaceae
Verrucomicrobiaceae

Figure 8: Humanization of GF mice transfers phenotype from donors. (A) 4-5 GF animals received fecal transplants (FT) from a RES or SUS donor. After 11 days of precolonization mice were treated with amp for 6 consecutive days and colonized with K. pn MDR1 after three days of amp treatment. Fecal burden of K. pn MDR1 was assessed after different time points. (B) *In vitro* colonization of different human donors and their corresponding assembly to RES, INT or SUS phenotype. Donors selected for the humanization of GF mice are highlighted as black dots. (C) Colonization kinetics with K. pn MDR1 of GF mice receiving FT from a RES and SUS donor. (D) Fecal burden of K. pn MDR1 after 1, 14 and 21 days p.c.. Mean and SEM of one independent experiments with n=5-6 mice per group. P values indicated represent a nonparametric Kruskal-Wallis test *p<0.05. (E) Single GF mice received FT from different SUS or INT donors and were subsequently colonized with K. pn MDR1 as described before. (F) Resulting colonization kinetics of K. pn MDR1 in single GF mice receiving FT from different human donors. Means of one independent experiment with n=1 mouse per group. P values indicated represent a nonparametric Kruskal-Wallis test p>0.05. (G) β-diversity was analyzed using non-metric multidimensional scaling (NMDS). Individual effect size of tested covariates is indicated. To calculate the variance explained by individual factors such as donor and time point a permutational multivariate analysis of variance (ADONIS) was used. A significant effect was dedicated when $p < 0.05$ and $R^2 > 0.10$ (equivalent to 10% of explained variance) ***p < 0.001. (H) α-diversity in mice and donors was determined using Chao1 and Shannon index. (I) Average microbiome level in different clusters are displayed on family level.

3.1.3 Actinobacteria-Akkermansia enterotype is correlated with higher ratios of susceptible samples

SCFA, pH and low abundant commensal facultative anaerobic bacteria were identified as markers for higher colonization resistance, yet, if a specific microbiota composition is observed in RES, INT and SUS individuals was not explored initially. To do so, fecal samples of each donor were analyzed using 16S rRNA gene sequencing and subsequently evaluated regarding specific clustering, occurrence of index species in different groups of individuals, alpha diversity and impact of other factors such as age or gender. In general, three enterotypes were identified in the healthy cohort being reflected in three distinct clusters in the beta-diversity plot (Fig 9A). Out of 59 sequenced samples 25 individuals (42.4 %) had a *Bacteroides* dominated microbiota. The second group was shaped by the presence of *Prevotella* with a total number of 21 samples (35.6 %). The third group was characterized by absence of *Prevotella* indicating that this signature is a subgroup of the *Bacteroides* enterotype but harbored higher amounts of Actinobacteria especially the genus *Bifidobacterium* and also members of the phylum Verrucomicrobia (Genus *Akkermansia*) (Fig 9C).

Table 26: Meta-data of MikroResist cohort.

Population	Healthy (adult)
N	59 (100)
Female	33 (55.9%)
Male	26 (44.1%)
Average age	32.2
Average BMI	22.62
Diet	omnivorous
Diseases	no chronic diseases
Medication	no Abx for 4 wks

In total, 13 individuals (22%) belonged to this cluster. Interestingly, larger human studies describe another human enterotype which is characterized by high levels of *Ruminococcus* (Arumugam et al., 2011). This group was not evident in our cohort as *Ruminococcus* was similar abundant in all three clusters. In terms of species richness, no major differences occurred between the enterotypes, but the

donors belonging to the group of Actinobacteria- Akkermansia (Act-Akk) tended to have lower numbers of observed species compared to *Prevotella* and *Bacteroides* enterotype (Fig 9B). While a distinct clustering for the RES, INT and SUS groups individuals according to enterotype was not observed, the Act-Akk enterotype was linked with higher CFUs when comparing the upper quartile (n=15 donors (25%) HIGH) and the lower quartile (n=15 donors (25%) LOW) samples regarding their enterotype affiliations (Fig 9D). Out of 13 samples belonging to this cluster, 6 individuals belonged to the HIGH group (46.2 %), whereas only 1 sample was associated with a resistant phenotype (7.7 %). The remaining samples belong to the INT group. In contrast, ratios of susceptible samples were much lower in the *Bacteroides* and *Prevotella* enterotype with 4/25 (16%) and 5/21 (23.8 %) individuals. In total, 7 individuals of both enterotypes belong to the resistant groups indicating that no clear prevalence exist regarding resistance in *Bacteroides* and *Prevotella* enterotype.

3.1.4 Resistant samples harbor significantly more SCFA producing bacteria in their microbiomes

To test whether specific bacterial groups were elevated in the most resistant samples independent of enterotype affiliation, the microbiome composition between the heterogeneous group of the LOW and HIGH quartile (n=15) were compared regarding significantly different taxa in the microbiome as well as specific SCFA producing taxa and resulting SCFA levels (Fig 9D). Linear discriminant analysis Effect Size analysis (LEfSE) and analysis of relative abundances revealed significantly higher levels of the family *Ruminococcaceae* and the genera *Ruminococcus* and *Coprococcus* in the LOW microbiomes (Fig 10A-D). These genera are known SCFA producers (Vital, Karch and Pieper, 2017) linked with the production of butyrate and propionate partially explaining observed differences in SCFA levels and pH values between RES and SUS samples. Comparing the LOW and HIGH quartiles, significantly elevated level of propionate and acetate and a trend towards higher butyrate levels could be associated with LOW quartile samples further supporting the protective role of SCFA and SCFA producing bacteria against MDR-E colonization in healthy individuals. To test, whether the abundance of SCFA producing bacteria directly correlates with resulting CFUs of K. pn MDR1 recovered from the *in vitro* assay, abundances of the respective bacteria were plotted against the CFUs (Fig 10H-I). I could not find a direct correlation between the abundance of *Ruminococcaceae*, *Ruminococcus* and *Coprococcus* singly or in combination. The resulting correlation coefficients ranged between R^2 = 0.00012 for *Ruminococcus* vs CFUs of K. pn MDR1 and 0.048 for combined abundance of *Ruminococcus* and *Coprococcus* against resulting CFUs of K. pn MDR1.

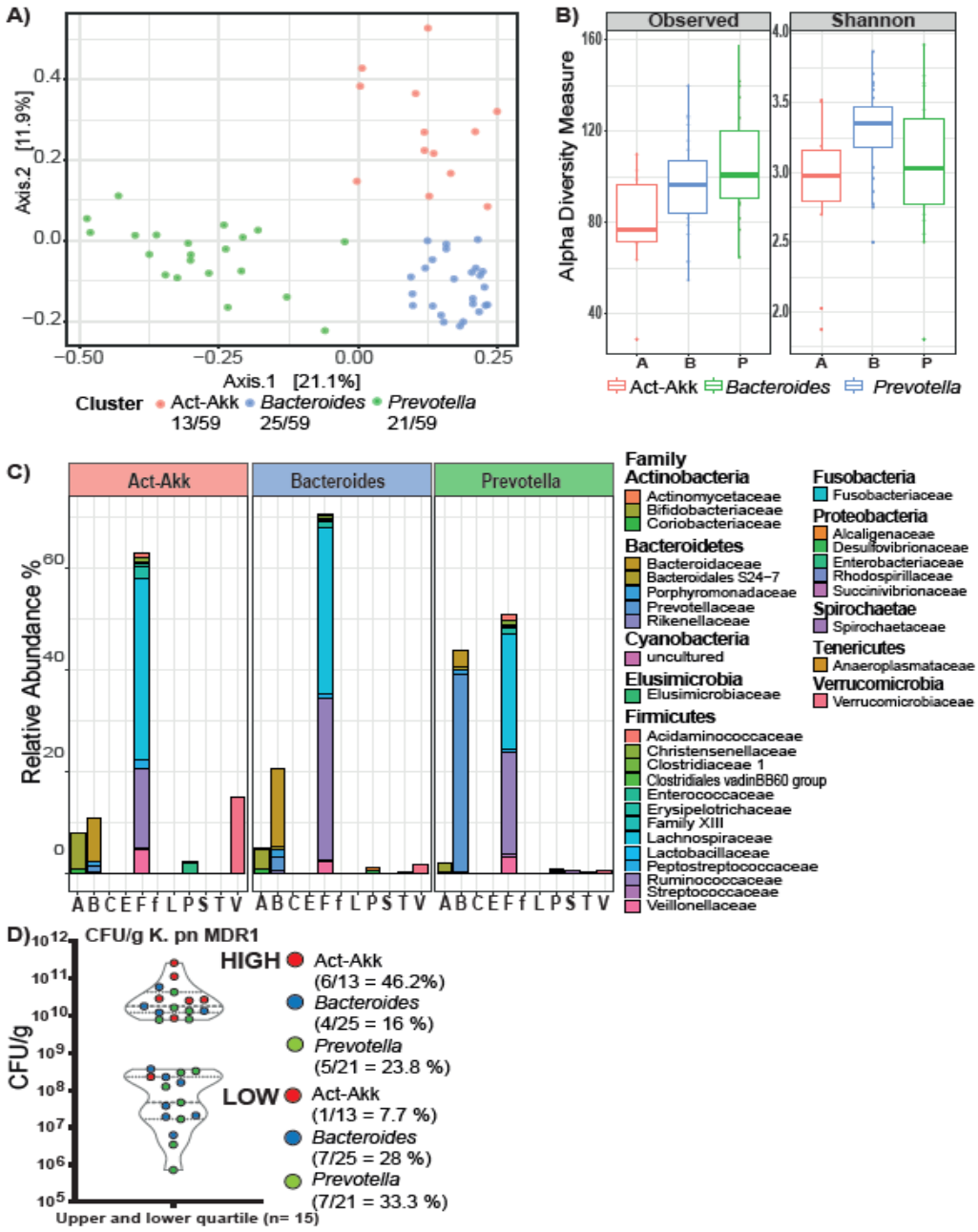

Figure 9: Enterotypes in the healthy human microbiome. (A) Fecal bacterial microbiota composition of healthy volunteers were evaluated using 16S rRNA gene sequencing and grouped by their enterotype. β-diversity was analyzed using principal coordinates analysis (PCoA). Three distinct microbiome signatures were defined as *Actinobacteria-Akkermansia* (Act-Akk), *Bacteroides* and *Prevotella* dominated microbiomes. 25/59 (42.4 %) belonged to the *Bacteroides* enterotype, 21/59 (35.6 %) belonged to the Prevotella enterotype and 13/59 (20%) belonged to Act-Akk. (B) α-diversity measures are displayed as observed species richness and Shannon diversity index in the enterotypes (C) Fecal microbiome composition in Act-Akk, *Bacteroides* and *Prevotella* enteotype displayed at family level. (D) LOW and HIGH quartile of the most resistant (n=15) and susceptible (n=15) microbiomes in response to K. pn MDR1 grouped according to the underlying enterotype of each sample.

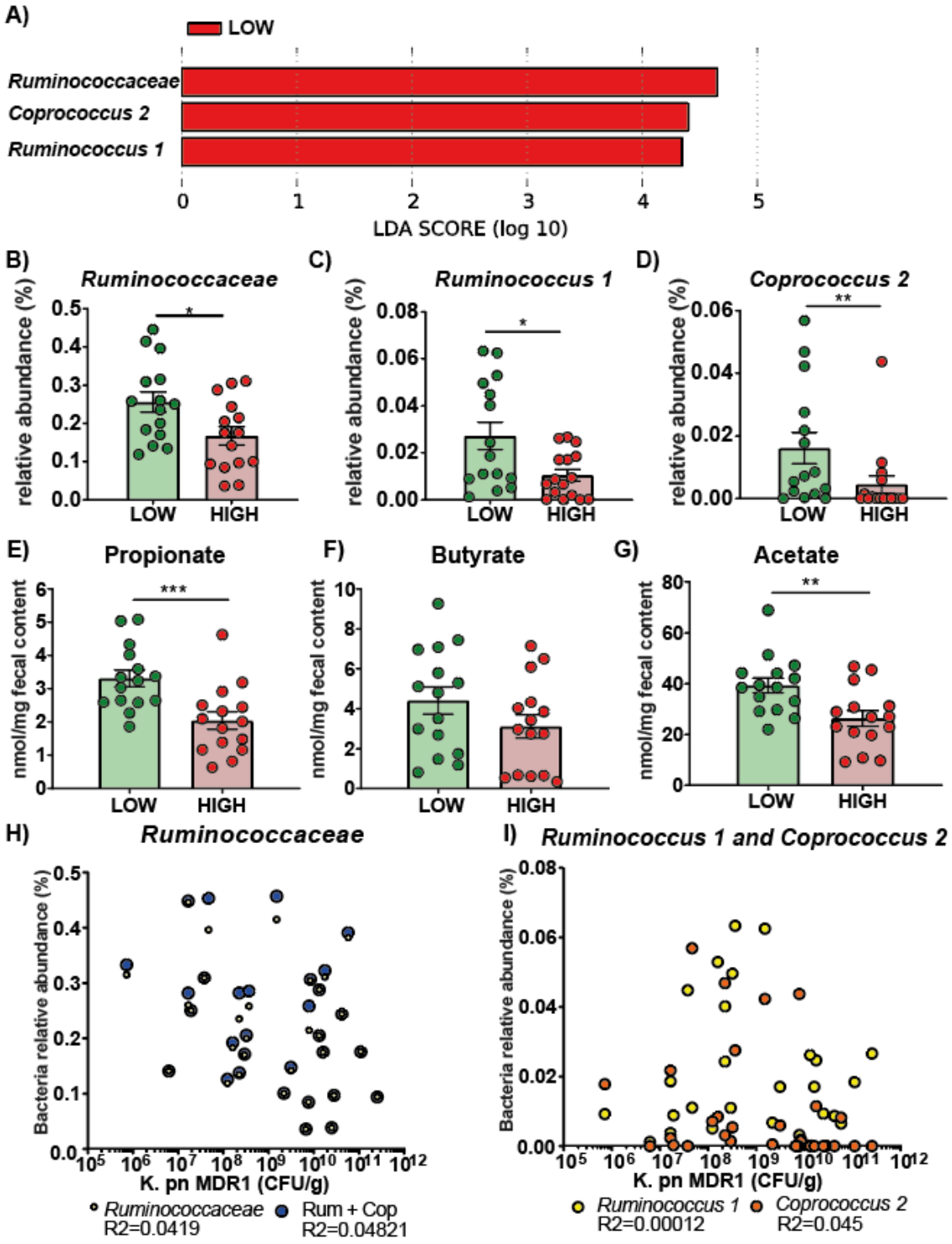

Figure 10: Resistant samples harbor more SCFA producing bacteria in their microbiome. (A) Statistically different taxa between top 15 LOW and HIGH samples were analyzed using LEfSe (Kruskal-Wallis test $p<0.05$, LCA 4.0). (B-D) Relative abundances of statistically different taxa in the group of LOW and HIGH samples. (E-G) Fecal SCFA level of the LOW and HIGH of samples. Results are represented as mean of n=15 samples ± SEM. P values indicated represent a nonparametric Kruskal-Wallis test *$p<0.05$, **$p<0.01$, ***$p<0.001$. (H-I) Correlation of significantly different bacteria in LOW and HIGH samples plotted against resulting CFUs of K. pn MDR1 in the *in vitro* assay. Correlation coefficient R describes direct correlation between both variables.

Hence, a combination of key factors including pH, SCFA levels, richness, enterotype and abundance of specific commensals contribute to creating an individual niche which is more or less likely to favor outgrowth with MDR-E in healthy adults.

3.1.5 Leukemic patients have an elevated risk for infection with MDR *K. pneumoniae* and show pronounced changes in their microbiomes

Leukemic patients receiving chemotherapy or hematopoietic stem cell transplantation (HSCT) are at high risk to colonization and eventual infection with MDR-E due to their immunocompromised status caused by the disease itself and treatment with different drugs (Galloway-Peña et al., 2016; Taur et al., 2014). To observe how the microbiota changes during anti-leukemia therapy and if the colonization ability is as variable as observed in healthy individuals, stool samples of hematological patient's undergoing induction chemotherapy (IC) and HSCT were collected. HSCT patients did not receive chemotherapeutics anymore. In total, 15 HSCT patients and 24 patients undergoing IC could be recruited in this cohort (MikroIntest). Patients were diagnosed with acute myelogenous leukemia (AML), acute lymphoblastic leukemia (ALL) and other hematological malignancies. HSCT patients and patients receiving IC of the MikroIntest cohort had an average age of 46.4 and of 51.9 years, respectively. Samples were collected 24-66 days after transplantation and within or after the first or second cycle of induction chemotherapy. Both "diseased" groups were compared against healthy control samples (Tab 27).

All samples were spiked with 10^6 CFUs K. pn MDR1 and incubated for 24 h under anaerobic conditions before plating on selective agar plates (Fig 11A). Significantly more K. pn MDR1 were recovered from patients stool samples compared to the healthy control samples (Fig 11B) indicating that colonization resistance is reduced due to drug intake impacting the microbiota composition. In terms of beta diversity, three clusters were distinguished within the healthy control samples and four clusters in the patients (Fig 17D-E). The microbiome of the diseased cluster 1, which contained samples of HSCT patients scattered largely and did not cluster closely together indicating a high inter-individual microbiota diversity (dark-green triangles). Within the patients undergoing IC, I found samples with variable and imbalanced microbiota compositions characterized by elevated levels of Proteobacteria, *Akkermansia* and Bifidobacteria (cluster 2 = light-blue dots) as well as samples dominated by *E. coli* (cluster 3 = purple dots) or *Enterococcus* (cluster 4 = pink dots). Overall, the status (healthy or diseased) could explain 20.2 % of sample variability and the different clusters could explain 21.1%, whereas gender only had a minor impact on the observed variability (2.5 %). The majority of variability could not be explained (56.2 %).

Alpha diversity did not differ between the healthy clusters and was significantly higher compared to the patient samples. The strongest reduction was observed in all patient groups undergoing IC, but most strongly in those samples facing a bloom of *E. coli* (cluster 3) or *Enterococcus* (cluster 4) (Fig 11C).

All patient groups showed significantly elevated relative abundances within the phylum of Proteobacteria and strong reduction of the relative abundances and diversities in the Firmicutes and Bacteroidetes phylum, except for the genus *Enterococcus* (Fig 11F). Overall, HSCT patient samples showed less pronounced changes in the microbiome, but still harbored significantly more Lactobacilli and Proteobacteria in their microbiotas than observed in any of the healthy clusters (Fig 11F).

Based on these findings it is a likely hypothesis that antibiotic naive-microbiota suppresses the growth of antibiotic- resistant clinical isolates of *K. pneumoniae* by acidification of the proximal colon and triggering SFCA mediated intracellular acidification as reported recently (Jacobson et al., 2018, Sorbara et al., 2018). An alternative hypothesis is that level of infection susceptibility is influences by commensal related *Enterobacteriaceae* that block the niche for incoming pathogens and compete for essential nutrients, O2 and NO3 which would facilitate outgrowth of these pathogens as demonstrated by Velazquez, Litvak and colleagues (Litvak et al., 2019; Velazquez et al., 2019).

Table 27: Meta data of patient cohorts recruited in this study.

Population	Healthy (adult)	Hematopoietic stem cell transplantation (HSCT)	Induction Chemotherapy (IC)
Cohort name	**MikroResist**	**MikroIntest**	**MikroIntest**
N	59 (100)	15 (100%)	24 (100%)
Female	33 (55.9%)	4 (27%)	13 (54.1%)
Male	26 (44.1%)	11 (73 %)	11 (45.9%)
Average age	32.2	46.4	51.9
Average BMI	22.62	21.65	-
Diet	omnivorous	omnivorous	omnivorous
Diseases	no chronic diseases	AML, ALL, other	AML, ALL, other
Days after Tx Cycle	-	24-66	Within or after induction chemotherapy cycle I or II
Medication	no Abx for 4 wks	Abx, PPI	Abx, PPI, Chemotherapy

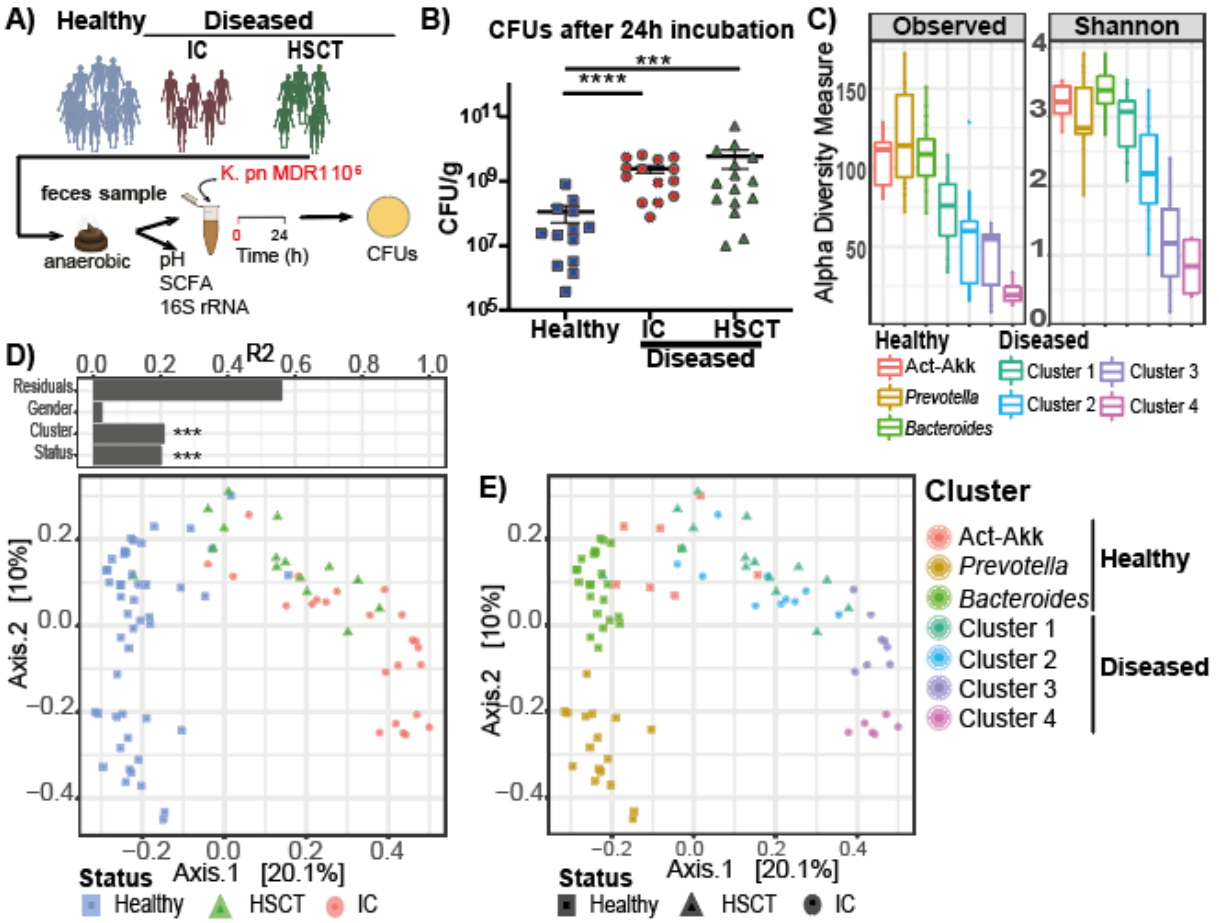
A)
Healthy
Diseased
IC
HSCT
feces sample
K. pn MDR1 10⁶
anaerobic
pH
SCFA
16S rRNA
0
24
Time (h)
CFUs
B)
CFUs after 24h incubation
***
****
CFU/g
Healthy
IC
HSCT
Diseased
C)
Observed
Shannon
Alpha Diversity Measure
Healthy
Diseased
Act-Akk
Prevotella
Bacteroides
Cluster 1
Cluster 2
Cluster 3
Cluster 4
D)
R2
Residuals
Gender
Cluster
Status
***
***
Axis.2 [10%]
Axis.1 [20.1%]
Status
Healthy
HSCT
IC
E)
Axis.2 [10%]
Axis.1 [20.1%]
Status
Healthy
HSCT
IC
Cluster
Act-Akk
Prevotella
Bacteroides
Cluster 1
Cluster 2
Cluster 3
Cluster 4
Healthy
Diseased
F)
Healthy
Diseased
Act-Akk
Prevotella
Bacteroides
Cluster 1
Cluster 2
Cluster 3
Cluster 4
Relative Abundance %
A B C E F f P S T V
Actinobacteria
Actinomycetaceae
Bifidobacteriaceae
Coriobacteriaceae
Corynebacteriaceae
Bacteroidetes
Bacteroidaceae
Bacteroidales S24−7
Chitinophagaceae
Porphyromonadaceae
Prevotellaceae
Rikenellaceae
Cyanobacteria
uncultured
Elusimicrobia
Elusimicrobiaceae
Firmicutes
Acidaminococcaceae
Christensenellaceae
Clostridiaceae 1
Clostridiales vadinBB60
Defluviitaleaceae
Enterococcaceae
Erysipelotrichaceae
Firmicutes
Family XI
Family XIII
Lachnospiraceae
Lactobacillaceae
Leuconostocaceae
Peptococcaceae
Peptostreptococcaceae
Ruminococcaceae
Staphylococcaceae
Streptococcaceae
Veillonellaceae
Fusobacteria
Fusobacteriaceae
Proteobacteria
Alcaligenaceae
Desulfovibrionaceae
Enterobacteriaceae
Oxalobacteraceae
Rhodospirillaceae
Succinivibrionaceae
Spirochaetae
Spirochaetaceae
Tenericutes
Anaeroplasmataceae
Verrucomicrobia
Verrucomicrobiaceae

Figure 11: Colonization resistance and microbiome composition in different human cohorts. (A) Stool samples of healthy individuals (MikroResist), patients undergoing IC and after HSCT (MikroIntest) were spiked in with 10^6 CFUs K. pn MDR1 and incubated anaerobically for 24h. CFUs of K. pn MDR1 were recovered on selective agar plates. (B) Resulting CFUs of selected healthy individuals and patient samples. Each dot represents one individual. Results are represented as mean ± SEM. P values indicated represent a nonparametric Kruskal-Wallis test ***p<0.001; ****p<0.0001 (C) α-diversity in different patient groups and healthy individuals was determined using Chao1 and Shannon index. (D-E) β-diversity was analyzed using a PCoA plot. Individual effect size of tested covariates is indicated. To calculate the variance explained by individual factors such as status, cluster, and gender an ADONIS test was used. A significant effect was dedicated when $p < 0.05$ and $R^2 > 0.10$ (equivalent to 10% of explained variance) ***$p < 0.001$. (F) Average microbiome level in different clusters are displayed on family level.

3.1.6 The microbiota composition of patients undergoing chemotherapy is extremely variable and displays a low degree of colonization resistance

Overall, stool samples from patients undergoing IC (cluster 2-4) displayed a low level of colonization resistance against K. pn MDR1 (Fig 11B). Detailed analysis of the microbiota composition revealed that these three clusters did not directly correlate with the duration of chemotherapy treatment but are rather defined by blooming of specific species such as *E. coli* or *Enterococcus* (Fig 12A). Patients which did not face a bloom *E. coli* or *Enterococcus* (Fig 12D-E) defined a third cluster with extremely variable microbiotas between each individual (Fig 12A and C). Overall, more than 85.4% percent of the observed variability could be attributed to the patient's microbiome and only 5.8% could be attributed to the factor "cycle". 8.8% of sample variability could not be explained. Global analysis of the alpha diversity over the duration of chemotherapy showed a tendency of increasing species loss over time (Fig 12B). The microbiota plots of each patients in the Cluster 2 further emphasize the variability between each individual (Fig 11C). Of note, two patients donated two fecal samples during different cycles of chemotherapy. These samples were also characterized by extreme changes in the microbiota composition (Fig 12F). Overall, the data set only reflect a limited amount of samples but the analyzed data indicate that the microbiota composition is extremely unstable during the course of chemotherapy and is prone for infection, which is supported by the fact that high portions of samples were dominated by *Enterobacteriaceae* (13/24 = 54.2%) or *Enterococcus* (6/24 = 25%) which fit to ratios reported in other studies (Galloway-Peña et al., 2016; Taur et al., 2012). Of not, *Enterobacteriaceae* and *Enterococcus* clusters were confirmed by classical cultivation approaches to contain VRE or multi-resistant *Enterobacteriaceae*.

The recovered CFUs in the *in vitro* assay for K. pn MDR1 were overall high but did not directly correlated with the cycle in which the used samples were taken or the clusters to which each sample belonged (Fig 12G-H). It is difficult to draw further conclusions as the data set reflects only a limited number of patients and the observed microbiota plots are highly variable between and within the patients.

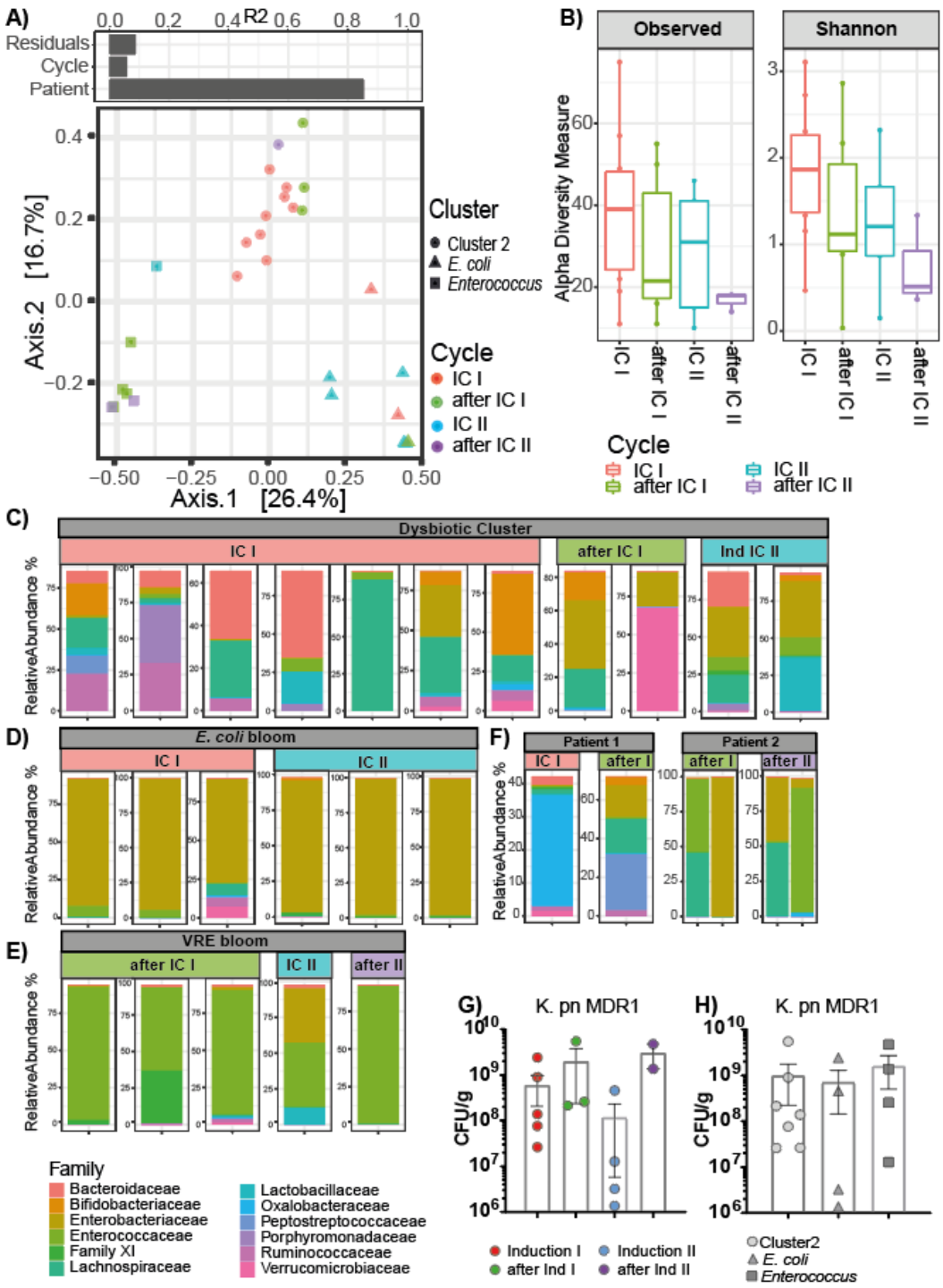

Figure 12: Patients microbiota composition during chemotherapy is highly variable. (A) β-diversity of patients microbiota compositions grouped according to the phase of chemotherapy and occurrence of index species was analyzed using a PCoA plot. (C) α-diversity at different phases of chemotherapy determined using Chao1 and Shannon index. (C-F) Individual microbiota composition in each patient displayed on family level and grouped according to the phase of chemotherapy and the cluster. (G-H) Resulting CFU/g K. pn MDR1 recovered after 24 h of anaerobic incubation grouped by the phase of chemotherapy and cluster affiliation of each sample. Results are displayed as mean ± SEM. P values indicated represent a nonparametric Kruskal-Wallis test with p>0.05.

3.1.7 The elevated risk of infection susceptibility decreases within the first two months after stem-cell transplantation

Interestingly, patient samples after HSCT showed highly variable susceptibility towards K. pn MDR1 colonization *in vitro*, with more than 1000 fold different levels in colonization (Fig 11B and Fig 13A). Based on the findings of different studies longitudinally assessing the microbiota composition within the first month after HSCT (Taur et al., 2012; Taur et al., 2014) and the fact that the microbiome resilience after perturbation is a known effect after antibiotic intervention (Dethlefsen et al., 2008) I hypothesized that samples obtained after a longer period of time after stem cell transplantation might be more resistant than those taken shortly after chemotherapy and transplantation. Indeed, reduced CFUs of K. pn MDR1 strongly correlated with increasing time post transplantation (Fig 13A) indicating that the first 2 months after transplantation might be associated with increased risk for colonization with MDR-E. Further analysis of the microbiome revealed that the two most susceptible samples clustered apart from all other samples (Fig 13B). These samples were associated with strongly decreased alpha diversity (Fig 13C), absence of specific groups of bacteria such as Bacteroidetes and increase of specific families such as *Veillonellaceae, Enterococcaceae* and *Fusobacteriaceae* (Fig 13D).

All these observations support the finding that chemotherapy induces severe compositional and functional imbalance in the gut microbiome which are still present in the first month after HSCT explaining reduced colonization resistance in these samples. Furthermore, SCFA were significantly reduced in those samples which are known to have inhibitory potential against outgrowth of enterobacterial pathogens (Sorbara et al., 2018, Jacobson et al., 2018) and promote regulatory T cells and intestinal homeostasis (Arpaia et al., 2013; Smith et al., 2013). This recovery of colonization resistance after chemotherapy likely takes up to two months since samples taken after this time period showed lower CFUs accompanied by increase of SCFA and symbiotic bacterial families defining a critical period of elevated risk for bacterial infection for hematological patients.

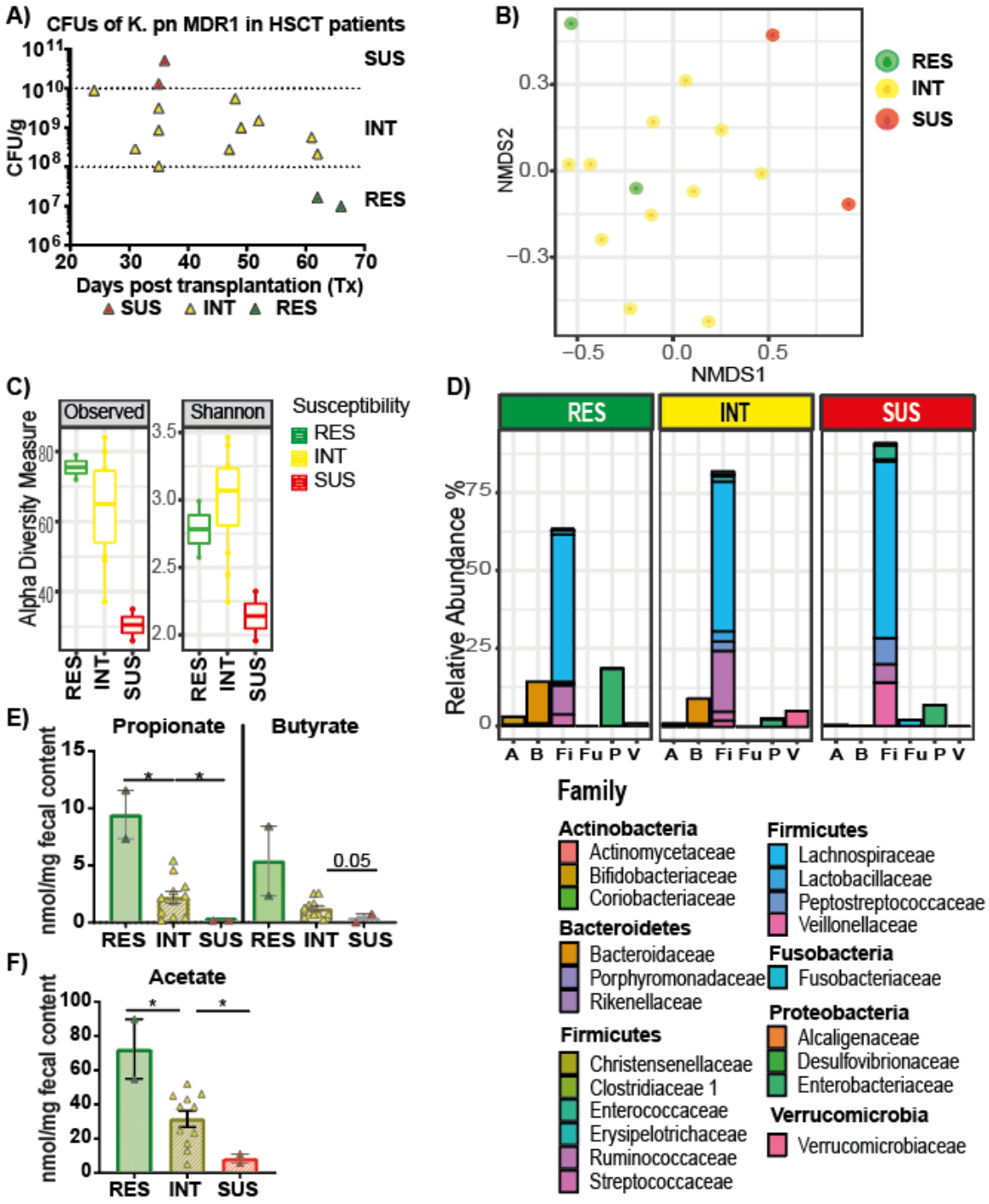

Figure 13: Susceptibility towards K.pn MDR1 after HSCT. (A) Recovered CFUs of K. pn MDR2 in patient stool samples plotted against the time after SCR when the sample was taken. Based on the CFUs samples were grouped as RES, INT or SUS. (B) β-diversity in RES, INT and SUS samples was analyzed using a PCoA plot. (C) α-diversity in RES, INT and SUS determined using Chao1 and Shannon index. (D) Average microbiome level in RES, INT and SUS samples are displayed on family level. (E-F) SCFA levels in the feces of RES, INT and SUS samples. Results are displayed as mean ± SEM. P values indicated represent a nonparametric Kruskal-Wallis test with *p<0.05.

In summary, in this chapter I was able to identify that healthy volunteers display large inter-individual differences regarding the colonization resistance against a MDR K.pn strain *in vitro*. Several factors including low pH value, higher levels of SCFA and presence of specific bacterial species such as low abundant facultative anaerobes, SCFA producing genera *Ruminococcus* and *Coprococcus* and higher species richness were associated with colonization resistance. Of note, some individuals who seem to have lower protection levels against outgrowth of MDR K.pn were enriched in a distinct cluster named Act-Akk characterized by high levels of *Akkermansia* and *Bifidobacteria*, lower species richness, higher pH and lower SCFA levels. In pilot experiments, these differences could successfully be transferred in humanized GF animals further supporting the predictive value of the *in vitro* assay. Analyzing colonization resistance in stool samples from leukemia patients undergoing IC and after HSCT revealed enhanced susceptibility towards K. pn MDR1 colonization *in vitro* not only in the acute phase of treatment but also up to two month after chemotherapy. Similar to susceptible healthy individuals, these patients displayed reduced species richness, disturbed microbiota compositions with elevated levels of potentially harmful bacteria and decrease in SCFA producing bacteria and other probiotic anaerobes, higher pH value and reduced levels of SCFA. Thus, multiple independent and dependent mechanisms are likely to contribute together to colonization resistance against MDR K.pn.

To analyze these observations in more detail and to functionally explore mechanisms of infection-susceptibility in homeostatic and disturbed microbiota situations in the whole organism, isogenic and gnotobiotic mouse models can be utilized to globally investigate the influence of microbiota composition to infection susceptibility with *Enterobacteriaceae*. In the next chapter, the impact of chemotherapy on a complex and less complex microbiome and the development of intestinal inflammation will be assessed. In the following chapter I will study the impact of specific microbes and SCFA in two undisturbed microbiota settings regarding the natural susceptibility against the pathogen C*. rodentium*. In the last part I will focus on the intervention against infection with MDR *K. pneumoniae* in antibiotic-treated mice and mice with defined microbiota settings using specific commensal *K. oxytoca*.

3.2 Cytarabine - driven mucositis severity is influenced by variations in microbiota composition of laboratory mice.

3.2.1 Induction chemotherapy leads to significant body weight loss and development of small intestinal mucositis without pronounced inflammation in the colon

Mucositis is a frequent complication during the treatment of hematological-oncological patients (van Vliet et al., 2010). To test how the microbiome responds to chemotherapy and if mice develop intestinal mucositis, isogenic mouse lines on a highly related genetic background (C57Bl6/N sublines sublines HZI in house and RJ) were treated with two repetitive cycles of chemotherapy for 7 days with a recovery phase of 5 days in between the two cycles to model IC in humans. Mice received high-dose aracycline (Ara-C) as intraperitoneal (i.p) injection (100 mg/kg) combined with an oral gavage consisting of levofloxacin (40 mg/kg) as a prophylactic antibiotic (Abx) and pantoprazole (40 mg/kg) as a proton pump inhibitor (PPI) similar to regular IC patients. Mice were weighted every day during chemotherapy cycles to assess body weight loss (BWL) and feces were taken at different time points to analyze the microbiome composition before and after each cycle. At the end of the experiment, colon and small intestine were assessed for signs of inflammation by histology (Fig 14A).

As likely direct consequence of chemotherapy, both mouse lines started to lose weight during the first cycle reaching statistical significance at day 4 (SPF-J) or day 5 (SPF-H) and reached lowest levels after the end of the first cycle at day 7-8 (Fig 14B-C and 14E). Body weight started to increase during the recovery phase at (day 9-13) and decreased again during the second cycle of chemotherapy (day 14-18) with less pronounced effects on total body weight compared to the first cycle (Fig 14B-C and E). Interestingly, SPF-H lost significantly more body weight compared to SPF-J with a total BWL of 10-15% compared to 5-10% in SPF-J mice (Fig 14D -E). Overall, BWL was a measurable but rather mild to medium severe side effect of the chemotherapy model in mice with a 100 % survival rate of all treated animals.

Next, I assessed the development of inflammation and mucositis in the gastrointestinal organs in response to the chemotherapy. Colon length and histological scoring of the small intestine (SI) and colon were used to determine severity of inflammation in both mouse lines. Even though, significant colon shortening could be observed in both mouse lines (Fig 15A), there was no pronounced inflammation found in the histological scorings of the colon. In turn, inflammation was mainly located in the SI of both mouse lines with changes most visible in the last third of the SI (Fig 15B-F). In addition, SPF-J mice had significantly higher inflammation scores compared to SPF-H mice in the SI (Fig 15B).

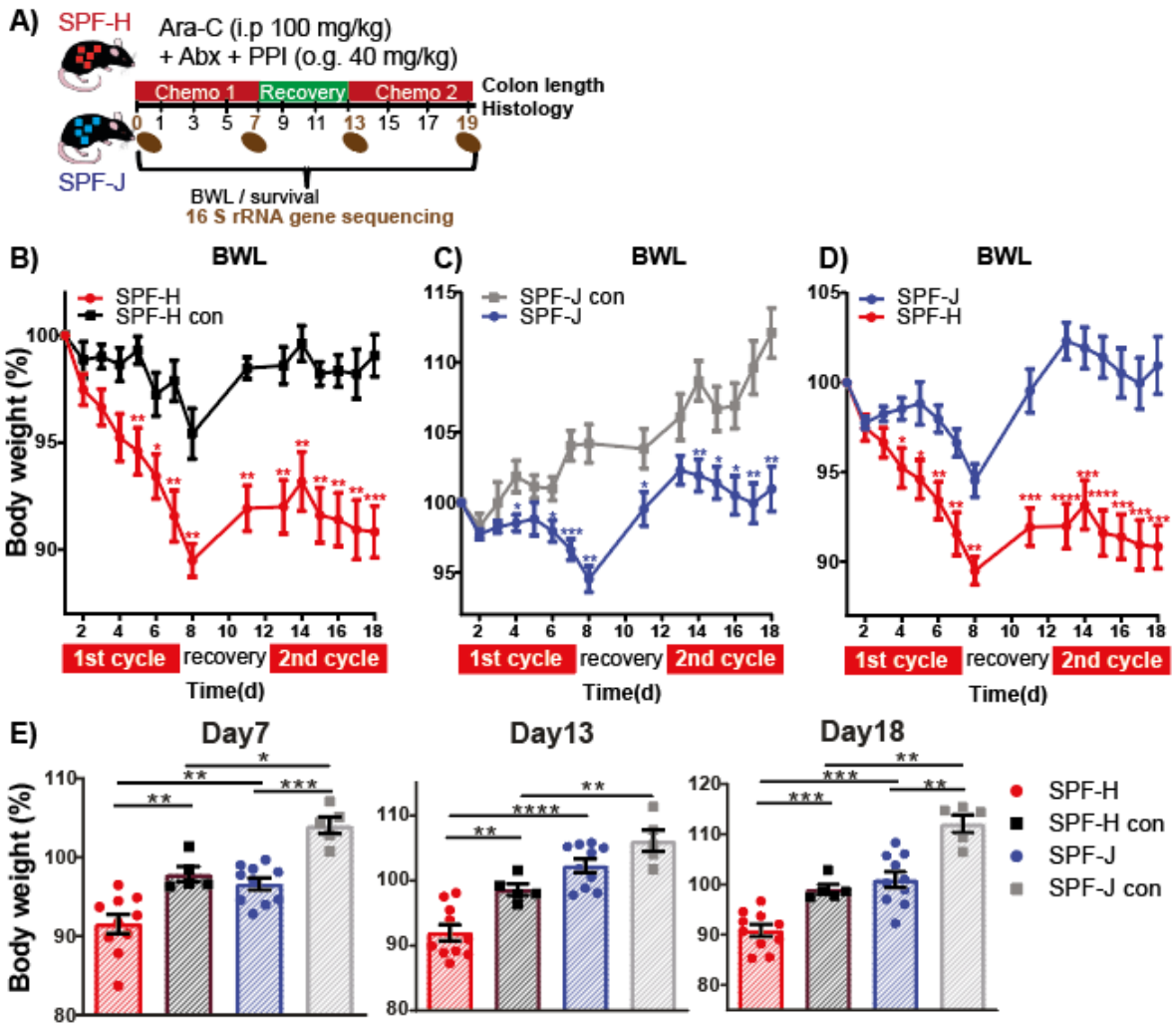

Figure 14: Loss of body weight is a direct effect of chemotherapy in different mouse lines. (A) SPF-H and SPF-J mice were treated with two consecutive cycles of chemotherapy consisting of seven daily doses with 100 mg/kg Ara-C per i.p., 40 mg/kg Abx per i.p and 40 mg/kg PPi per o.g. In between both cycles mice were left untreated for five consecutive days. (B-D) Resulting BWL curves of SPF-H and SPF-J mice compared to their untreated control groups or compared to each other. (E) Representative body weight plotted at day 7, 13 and 18 of the experiment. Results represent two independent experiments with n = 4-5 mice/group as mean ± SEM. P values indicated represent a nonparametric Kruskal-Wallis test *p<0.05, **p<0.01, ***p<0.001, ****p<0.0001.

SPF-J mice showed some macroscopic signs of elevated inflammation including swollen intestinal tissues especially in the cecum and very dark and dried out feces which may be a hint for intestinal bleeding. Overall, intestinal inflammation score could reach a maximum of 15 with five different categories scoring from (0-3) including severity, area involved, villus atrophy/dysplasia, inflammatory cell infiltrates and crypt damage (see 2.4.14 for detailed description of each score). Control slides showed normal intestinal structure with regard to length of villi and amount of immune cells. Nevertheless, numbers of immune cells seem to appear slightly increased in SPF-J mice compared to SPF-H (Fig 15E-F left panels of pictures).

The most prominent effect of chemotherapy was villi shortening in both treated groups, which has also been reported in other studies in humans as well as in animals (Viana et al., 2013; Logan et al., 2007). Villi shortening was more pronounced in SPF-J mice overall and best visible in the distal part of the SI (Fig 15D). Most treated animals in the SPF-J reached a score of 2 in this category indicating that 50% -75% reduction in villi length compared to normal morphology could be observed. Especially in the Ileum some mice scored as high as 3 with more than 75% reduction of villi length compared to control animals (Fig 15E-F, lower right pictures). Furthermore, SPF-J mice showed larger areas involved in inflammation especially in the proximal part with up to 70% of the SI inflamed (score 3) (Fig 15C) and a medium-grade influx of inflammatory cells and a higher rate of apoptosis of enterocytes (Fig 15E lower right picture, arrow head). For some animals small abscesses were visible in crypts of the duodenum, as well as degeneration of paneth cells (Fig 15E-F lower right picture, arrows) and increased influx of lymphocytic cells into the lamina propria.

SPF-H mice only showed pronounced shortening of intestinal villi due to increased amounts of apoptotic/necrotic epithelial cells (Fig 15E-F upper right picture, arrow head) but no degeneration of paneth cells (Fig 15E upper right picture, arrows). Taken together, SPF-J mice developed more severe SI inflammation characterized by stronger influx of inflammatory cells, degeneration of paneth cells and higher grades of damage to the morphology of the intestinal epithelium with regard to villi shortening apoptosis of intestinal epithelial.

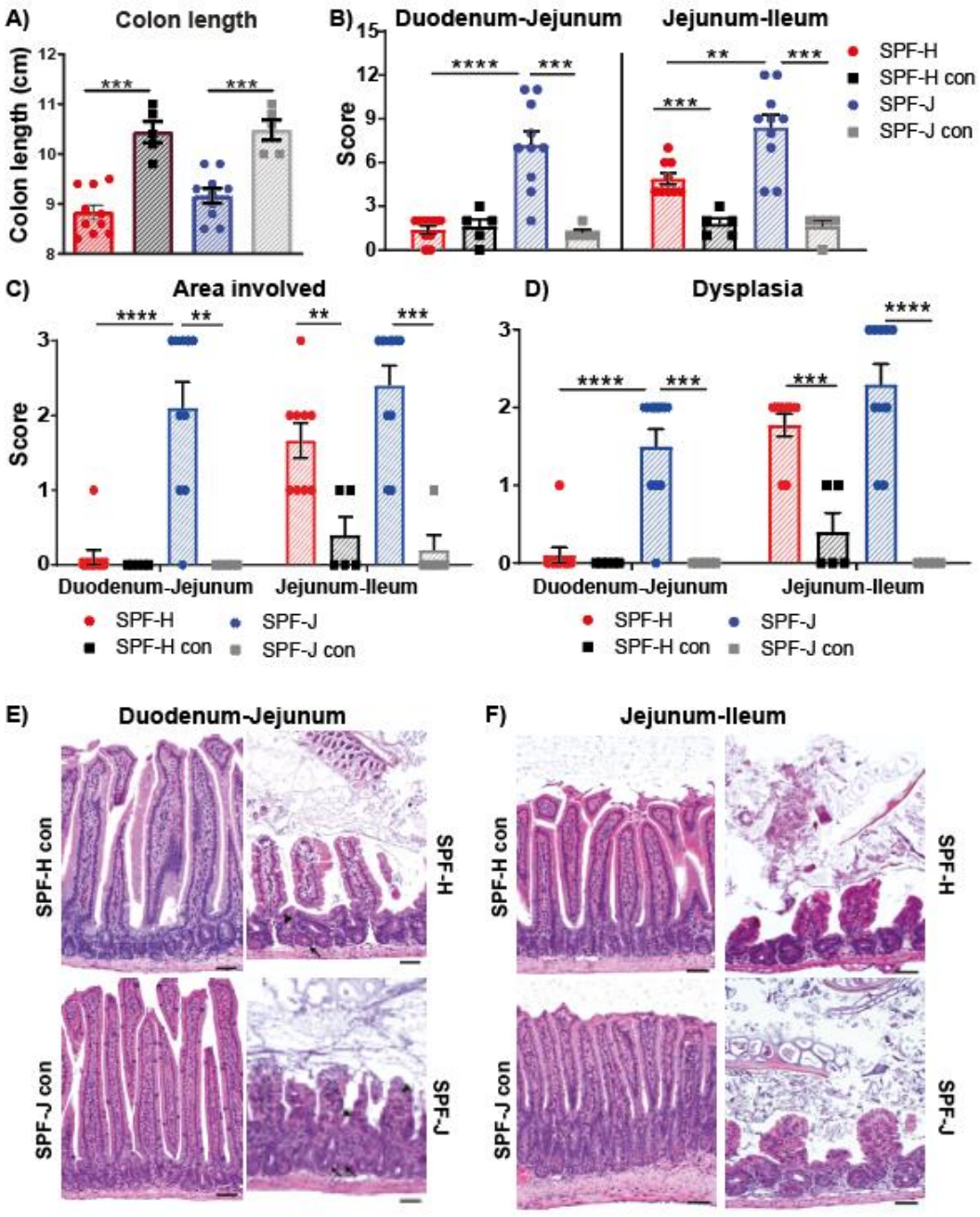

Figure 15: Small intestinal mucositis is a direct effect of chemotherapy in different mouse lines. (A) Colon length of SPF-H and SPF-J mice is displayed after two consecutive cycles of chemotherapy. (B) SI inflammation score of SPF-H and SPF-J after two consecutive cycles of chemotherapy is displayed for the proximal part (duodenum-jejunum) and the distal part (jejunum-ileum) of the SI. The maximum score is 15 resulting from the sum of 5 single parameters including severity, crypt damage, area involved, dysplasia and inflammatory cell infiltrate which can reach a maximum score of 3. C-D) Histological parameters "area involved" and "dysplasia" are shown individually. (E-F) Representative pictures of HE stained sections of the duodenum-jejunum and jejunum-ileum are shown for each group. Bar represents approx. 50 µm. Results represent two independent experiments with n = 4-5 mice/group as mean ± SEM. P values indicated represent a nonparametric Kruskal-Wallis test **p<0.01, ***p<0.001, ****p<0.0001.

3.2.2 Microbiota dynamically responses to induction chemotherapy with significant changes in the overall microbiome composition

To study the impact of the chemotherapy on the microbiome, fecal samples were analyzed using 16S rRNA gene sequencing before and after each chemotherapy cycle and the overall microbiota composition and dynamics (beta-diversity), species richness (alpha-diversity) and species composition was analyzed (Fig 16A). Similar pattern could be observed regarding beta-diversity changes in both mouse lines. Compared to steady state, composition changed rapidly on day 7, was moving closer to the initial composision after day 12 during the recovery phase, before the microbiota exhibited another strong shift on day 18 due to the second chemotherapy cycle (Fig 16B and E). This fluctuating pattern was also visible in terms of species richness. Observed species and shannon diversity index decreased significantly after the first chemotherapy cycle, recovered partially or completely in the recovery phase and decreased again after the second cycle (Fig 16C and F). In contrast to SPF-H mice, which showed less dramatic decreases in alpha- diversity, SPF-J mice exhibited a constant and strong decrease after the second cycle of chemotherapy compared to the steady state condition with nearly 50% of observed species lost (Fig 16E). Especially obligate anaerobic bacterial families were affected upon chemotherapy including *Lachnospiraceae* and *Rikenellaceae* in both mouse lines (Fig 16D and G). In contrast, ratios of *Lactobacillaceae* increased during the course of chemotherapy. In SPF-J mice, an additional increase of the genus *Akkermansia* within the family of *Verrucomicrobiaceae* and decrease of *Muribaculaceae* which are not present in the less complex microbiome of SPF-H mice could be observed. Taken together, this experiment could show that chemotherapy leads to pronounces and unique microbiota shifts in both communities with fluctuating response patterns and moderate to severe species loss in response to the single phases of IC.

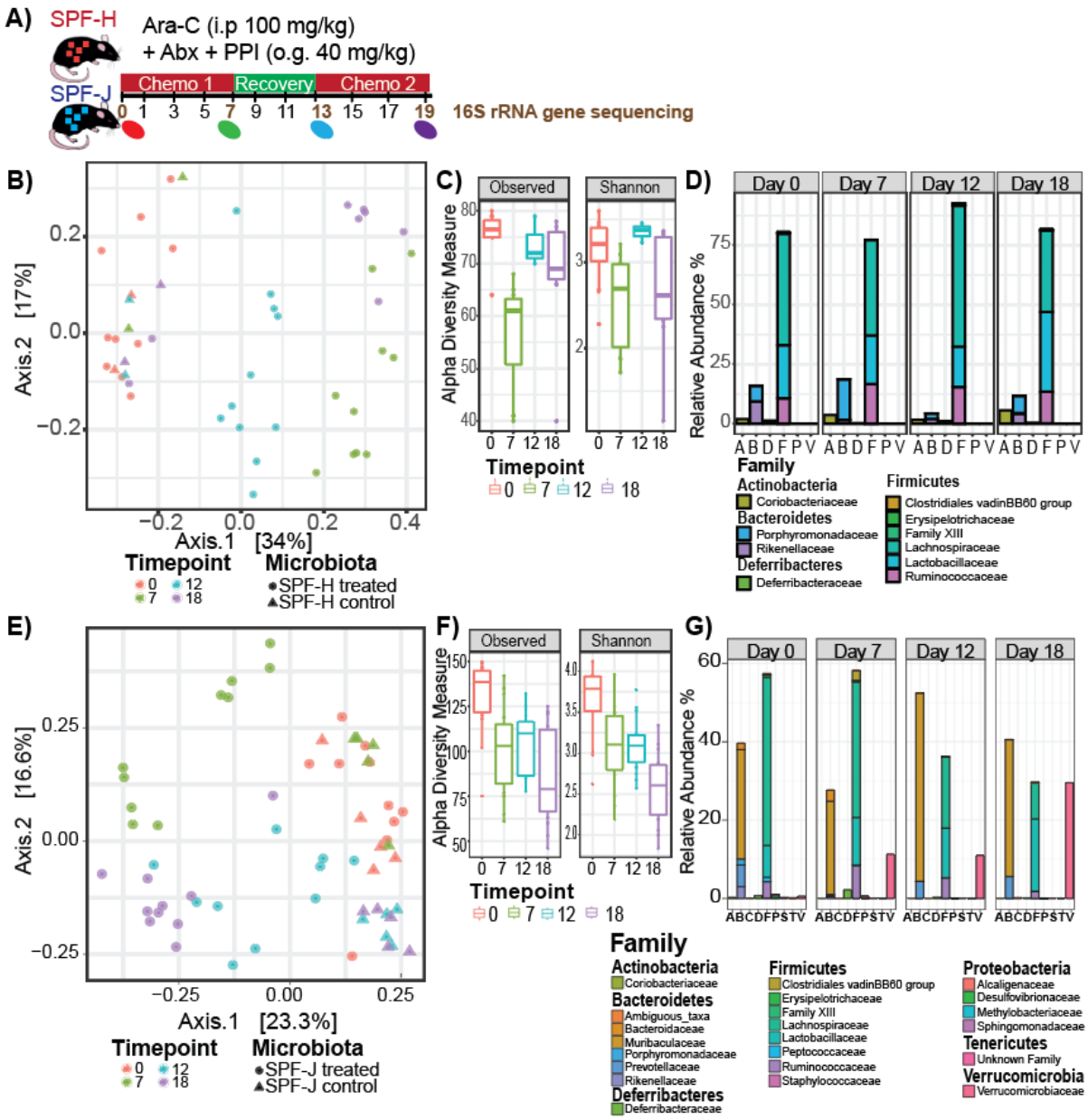

Figure 16: Microbiota dynamically responds to induction chemotherapy. (A) Fecal bacterial microbiota composition of SPF-H and SPF-J mice were evaluated using 16S rRNA gene sequencing on different timepoints. (B) β-diversity of SPF-H mice was analyzed using a PCoA plot. (C) α-diversity measures of SPF-H mice are displayed as observed species richness and Shannon diversity index on different time points. (D) SPF-H fecal microbiome composition on day 0, 7, 12 and 18 is displayed at family level. (E) β-diversity of SPF-J mice was analyzed using a PCoA plot. (F) α-diversity measures of SPF-J mice are displayed as observed species richness and Shannon diversity index on different time points. (G) SPF-J fecal microbiome composition on day 0, 7, 12 and 18 is displayed at family level.

3.2.3 Ara-C is sufficient to induce inflammation in SPF-H and SPF-J mouse lines

To evaluate the impact of each single drug on the development of mucositis and their influences on the microbiome composition, the same chemotherapy model in SPF-H and SPF-J mice as initially established, but including groups of mice receiving only Ara-C, Abx, PPI or PBS as a control was assessed (Fig 17A).

Again, no severe BWL could be observed in SPF-H mice during the course of chemotherapy, but mice treated with chemotherapy or Ara-C alone lost significantly more body weight compared to mice treated with PPI, Abx or PBS indicating that Ara-C has a major influence on SI mucositis (Fig 17B-D). Colon shortening was visible in all groups treated with chemotherapy mixture or single drugs compared to the PBS control group (Fig 17E). Histology of the SI revealed that Ara-C is indeed the main factor for inflammation development, as mice treated with Ara-C alone exhibited the same scores as mice receiving all drugs in combination (Fig 17F). To evaluate if Ara-C alone is sufficient to explain observed differences in severity of inflammation between SPF-H and SPF-J mice, the same experiment was performed with SPF-J mice and one group of Ara-C single treated SPF-H mice was included as a control. Again, I observed that all mouse lines treated with Ara-C singly or in combination lost more body weight as the groups treated with PPI or Abx alone (Fig 17A-B).

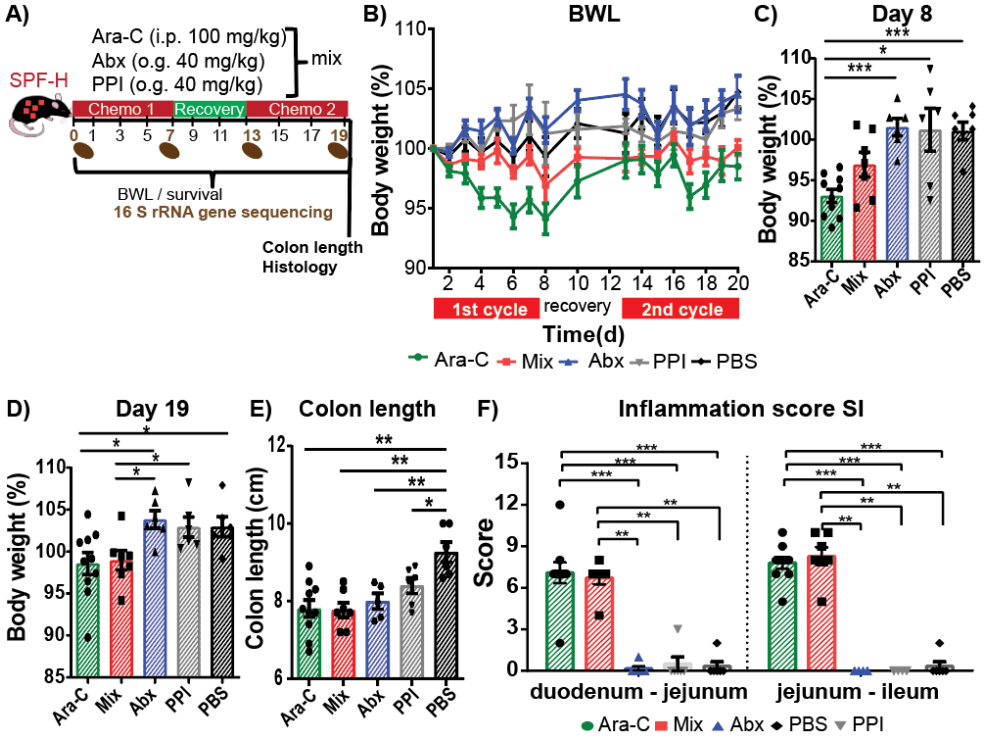

Figure 17: Ara-C induces small intestinal inflammation in SPF-H mice. (A) SPF-H mice were treated with two consecutive cycles of chemotherapy consisting of seven daily doses with 100 mg/kg Ara-C per i.p., 40 mg/kg Abx per i.p and 40 mg/kg PPI per o.g singly or in combination. In between both cycles mice were left untreated for five consecutive days. (B) Resulting BWL curves of SPF-H mice treated with different drugs. (C-D) Representative body weight plotted at day 7 and 19. (E) Colon length of SPF-H mice after two consecutive cycles of chemotherapy is displayed. (F) SI inflammation score of SPF-H mice after two consecutive cycles of chemotherapy is displayed for the proximal part (duodenum-jejunum) and the distal part (jejunum-ileum) of the SI. The maximum score is 15 resulting as the sum of 5 single parameters including severity, crypt damage, area involved, dysplasia and inflammatory cell infiltrate which can reach a maximum score of 3. Results represent one representative experiment with n = 6-9 mice/group as mean ± SEM. P values indicated represent a nonparametric Kruskal-Wallis test *p<0.05, **p<0.01, ***p<0.001, ****p<0.0001.

No differences in BWL could be observed between SPF-H and SPF-J Ara-C treated mice (Fig 18A). Colon shortening was absent in all groups except those treated with Ara-C alone. Of note, SPF-J mice tend to have shorter colon length compared to SPF-H mice indicating higher levels of inflammation in this mouse line (Fig 18B). As a confirmation, histological analysis revealed significant higher scores in all groups of mice treated with Ara-C alone or in combination (Fig 18C-D). This effect was visible in the proximal and also in the distal part of the SI. In addition, SPF-J Ara-C treated mice revealed again higher scores as the samples from SPF-H mice in the ileum-jejunum indicating that Ara-C is the main driver for inflammation in both mouse lines and differently influences the severity of inflammation in isogenic mouse lines.

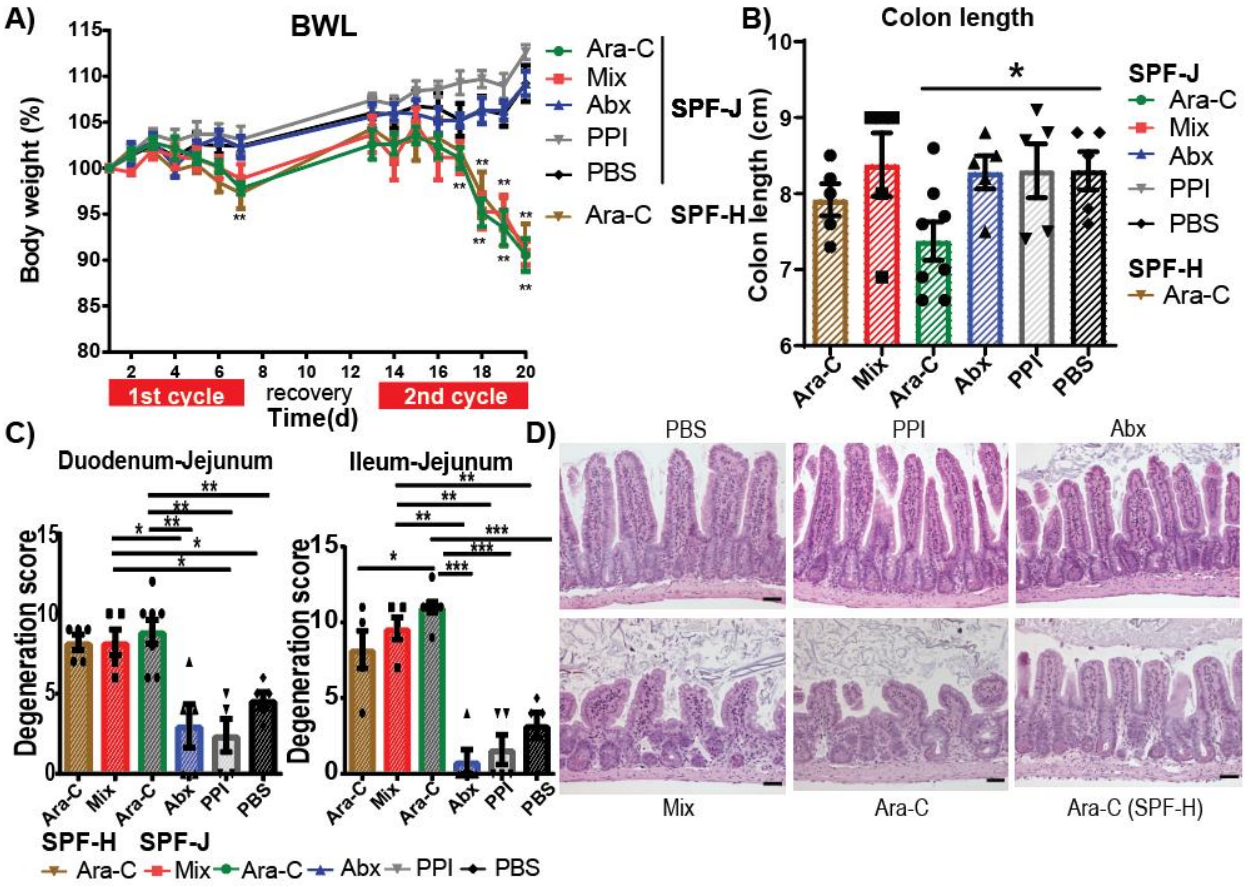

Figure 18: Ara-C induced small intestinal inflammation in SPF-J mice. (A) BWL curve of SPF-J mice, which were treated with two consecutive cycles of chemotherapy consisting of seven daily doses with 100 mg/kg Ara-C per i.p., 40 mg/kg Abx per i.p and 40 mg/kg PPI per o.g singly or in combination. In between both cycles mice were left untreated for five consecutive days. One group of SPF-H mice was treated with Ara-C as a control. (B) Colon length of SPF-J and SPF-H mice after two consecutive cycles of chemotherapy are displayed. (C) SI inflammation score of SPF-J mice after two consecutive cycles of chemotherapy is displayed for the proximal part (duodenum-jejunum) and the distal part (jejunum-ileum) of the SI. The maximum score is 15 resulting as the sum of 5 single parameters including severity, crypt damage, area involved, dysplasia and inflammatory cell infiltrate which can reach a maximum score of 3. (D) Representative pictures of HE stained sections of the jejunum-ileum are shown for each group. Bar represents approx. 50 µm. Results represent one representative experiment with n = 5-8 mice/group as mean ± SEM. P values indicated represent a nonparametric Kruskal-Wallis test *p<0.05, **p<0.01, ***p<0.001.

3.2.4 Each drug induces distinct changes in the microbiome composition

One major difference between both mouse lines is the composition and complexity of their gut microbiota. SPF-H mice harbor a less complex in-house microbiota without any Enterobacteria or known immunomodulatory bacteria such as *Akkermansia* (Kang et al., 2013), segmented filamentous bacteria (SFB) (Ivanov et al. 2009). To analyze the impact of Ara-C, levofloxacin and Pantoprazole on the microbiome individually, fecal samples of each treated group before and after each chemotherapy cycle were sequenced. The overall composition was most strongly affected by levofloxacin and Ara-C (Fig 19A), while samples of PPI treated SPF-H mice clustered relatively close to the PBS control samples after two consecutive cycles of chemotherapy. Levofloxacin treated samples clustered closely to the mice that received a combination of all three drugs indicating that the antibiotics effect was also pronounced in the mixture samples. In contrast, most Ara-C treated animals built a unique cluster apart from all other groups indicating that Ara-C alone induced specific changes to the overall community structure. In terms of species richness, levofloxacin and the combined therapy most strongly reduced the observed species, while Ara-C alone showed only a minor reduction in species richness. Compared to PBS, PPI did not significantly reduced observed species amount and evenness (Fig 19B). Interestingly, Ara-C alone lead to strong reduction of Shannon diversity index, indicating that Ara-C did not eradicate many species but shifts the relative amounts to an imbalanced status. Relative abundances on family level reveal that *Erysipelotrichaceae*, especially the genus *Turicibacter* increased massively due to Ara-C treatment accompanied with a relative reduction of *Lachnospiraceae* Family XIII in the Firmicutes phylum (Fig 19C). The other families were almost not affected. In contrast, Pantoprazole eradicated *Rikenellaceae* and *Erysipelotrichaceae* from the microbiome. In the antibiotics treated group, Bacteroidetes phylum was completely eradicated from the microbiome and also *Erysipelotrichaceae* were not present in the Firmicutes phylum. Taken together, Ara-C treatment alone seems to be a main driver for bacterial dysbiosis with significant outgrowth of some specific bacterial families resulting in the remarkable fluctuations described for the combined therapy before (Fig 19D-E).

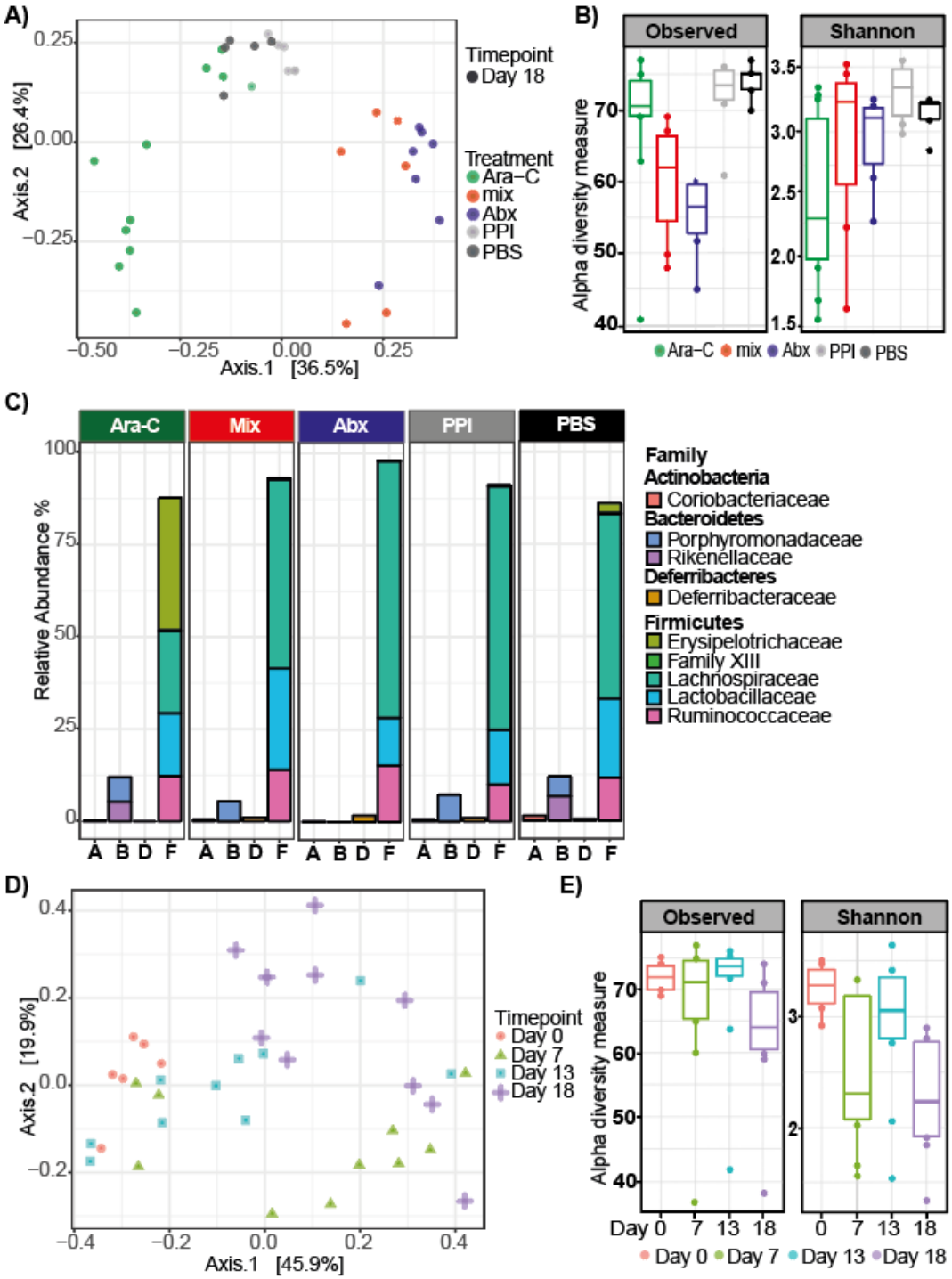

Figure 19: Each drug induces distinct changes on the microbiome of SPF-H mice. (A) Fecal bacterial microbiota composition on day 18 of SPF-H mice treated with Ara-C, Abx, PPI a combination of all drugs or PBS as a control were evaluated using 16S rRNA gene sequencing. β-diversity was analyzed using a PCoA plot. (B) α-diversity after two consecutive cycles of chemotherapy in different groups of SPF-H mice was determined using Chao1 and Shannon index. (C) Average microbiome level from treated SPF-H mice displayed on family level. (D) β-diversity of fecal bacterial microbiota composition at day 0, 7, 13 and 18 of Ara-C treated SPF-H mice using PCoA. (E) α-diversity in Ara-C treated SPF-H mice was determined at day 0, 7, 13 and 18 using Chao1 and Shannon index.

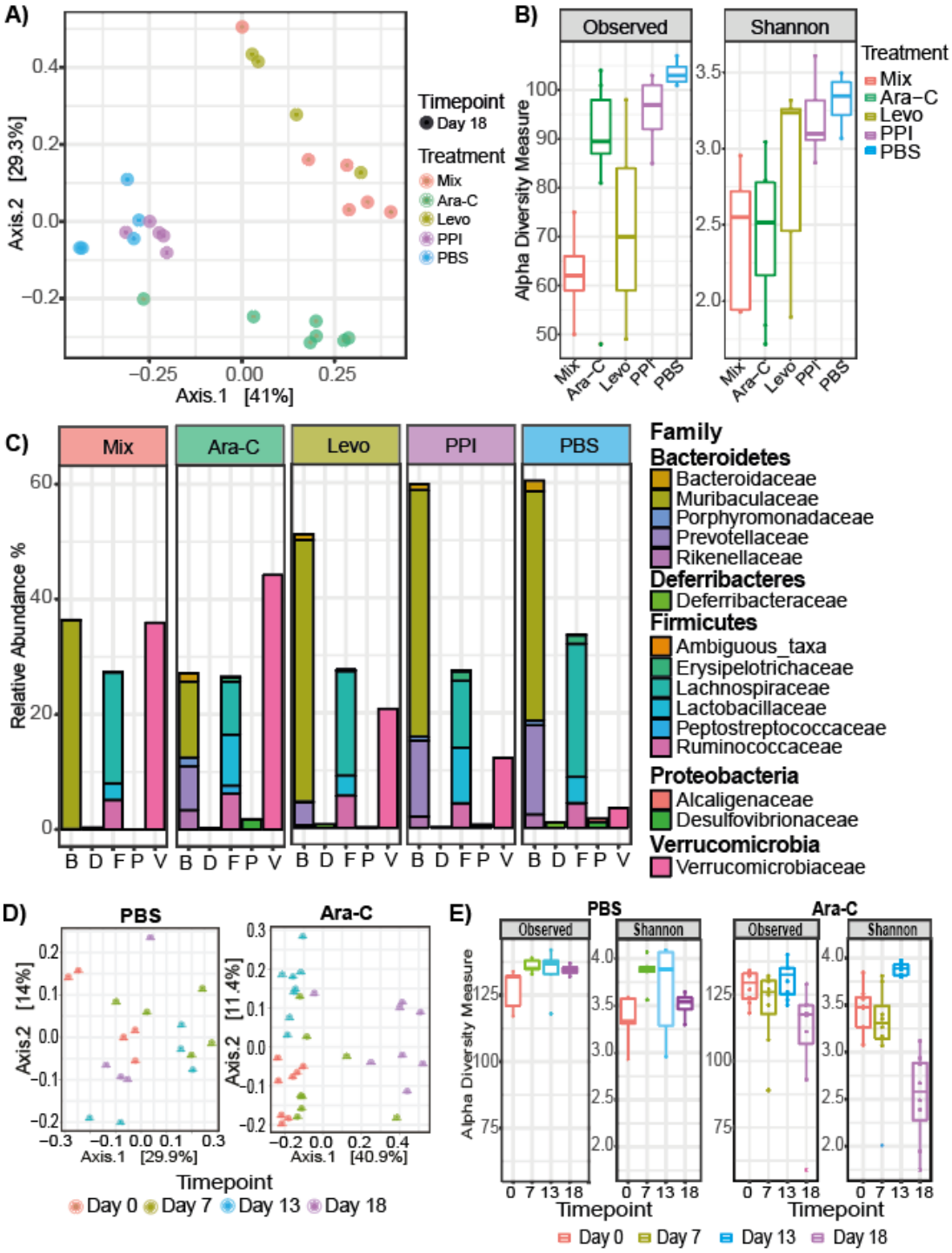

Figure 20: Each drug induces distinct changes on the microbiome of SPF-J mice. (A) Fecal bacterial microbiota composition on day 18 of SPF-J mice treated with Ara-C, Abx, PPI, a combination of all drugs or PBS as a control were evaluated using 16S rRNA gene sequencing. β-diversity was analyzed using a PCoA plot. (B) α-diversity after two consecutive cycles of chemotherapy in different groups of SPF-J mice was determined using Chao1 and Shannon index. (C) Average microbiome composition on day 18 from SPF-J mice treated with different drugs is displayed on family level. (D) β-diversity of fecal bacterial microbiota composition at day 0, 7, 13 and 18 of Ara-C treated and PBS treated SPF-J mice using a PCoA plot. (E) α-diversity in Ara-C and PBS treated SPF-J mice was determined on day 0, 7, 13 and 18 using Chao1 and Shannon index.

In the complex microbiome of SPF-J mice similar trends could be observed but different bacterial families were affected by Ara-C, Abx and PPI. Again, levofloxacin and combined treatment lead to similar changes in the overall composition, whereas PPI treatment induced only minor changes as samples clustered close to the PBS samples. In contrast, Ara-C treated mice clustered apart from all other groups (Fig 20A). In terms of species richness, antibiotics and combined treatment lead to strongest reduction in observed species numbers, whereas Ara-C and combined treatment lead to the strongest shift in Shannon diversity indicating that Ara-C changed the relation of species to each other (Fig 20B). Ara-C treatment strongly increased amounts of Verrucomicrobia especially the genus *Akkermansia* after two consecutive cycles of chemotherapy (Fig 20C). In contrast, taxa of the Bacteroides and Firmicutes phylum were reduced compared to the PBS group including *Muribaculaceae*, *Rikenellaceae* and *Lachnospiraceae*. PPI treatment did not lead to major changes in the microbiome composition with moderate increase of *Akkermansia* within the family of *Verrocomicrobiaceae* and minor decrease of *Lachnospiraceae*. levofloxacin eradicated or reduced Gram-negative Proteobacteria as well as other Gram-negative bacterial groups from the Bacteroidetes phylum including *Rikenellaceae*, *Porphyromonadaceae* and *Prevotellaceae,* whereas *Akkermansia* strongly increased compared to the PBS group. Mice receiving the combined therapy showed a strong increase of *Akkermansia* and eradication of Gram-negative Proteobacteria and Bacteroidetes except *Muribaculaceae* similar to the antibiotics group. Similar to what was observed in SPF-H mice, Ara-C alone was responsible to induce the fluctuating microbiome response with strong shifts in community structure (Fig 20D-E).

3.2.5 Chemotherapeutically-induced dysbiotic microbiome compositions likely elevate the risk for colonization with multi-drug resistant bacteria.

To test whether chemotherapeutic drugs, especially Ara-C elevate the risk for colonization with MDR-E, I performed different approaches *in vitro* and *in vivo*. First, SPF-H and SPF-J mice were treated with two consecutive cycles of chemotherapy before mice were sacrificed and isolated cecal content was spiked with a K. pn MDR1 strain. After 24 h of anaerobic incubation, colonies were recovered on selective agar plates (Fig 21A). Interestingly, K. pn MDR1 could grow better in PBS treated SPF-J cecal content compared to SPF-H cecal content, indicating that these mice are more susceptible for colonization with a this strain. Further, I could not find major difference in the colonization levels of Ara-C, PPI or Abx treated cecal content between the mouse lines or compared to the PBS control groups (Fig 21B). Next, more resistant SPF-H mice were treated with two consecutive cycles of Ara-C and were subsequently colonized with 10^8 CFUs K. pn MDR1 to test whether Ara-C pretreatment elevates the risk for MDR-E colonization.

Resulting CFUs showed a tendency of elevated CFUs in Ara-C treated mice at day 1 and day 3 (Fig 21C). Overall, SPF-H mice showed a relatively high degree of colonization resistance, as 5 out of 6 PBS treated mice cleared K. pn MDR1 already after 3 days post colonization (Fig 21D). Based on these observations in two pilot experiments in mice, I concluded that differences in initial microbiota composition predetermine the level of natural susceptibility towards colonization and Ara-C treatment leads to shifts in the community structure contributing to transiently elevated susceptibility against K. pn MDR1. Further experiments are required to validate this hypothesis.

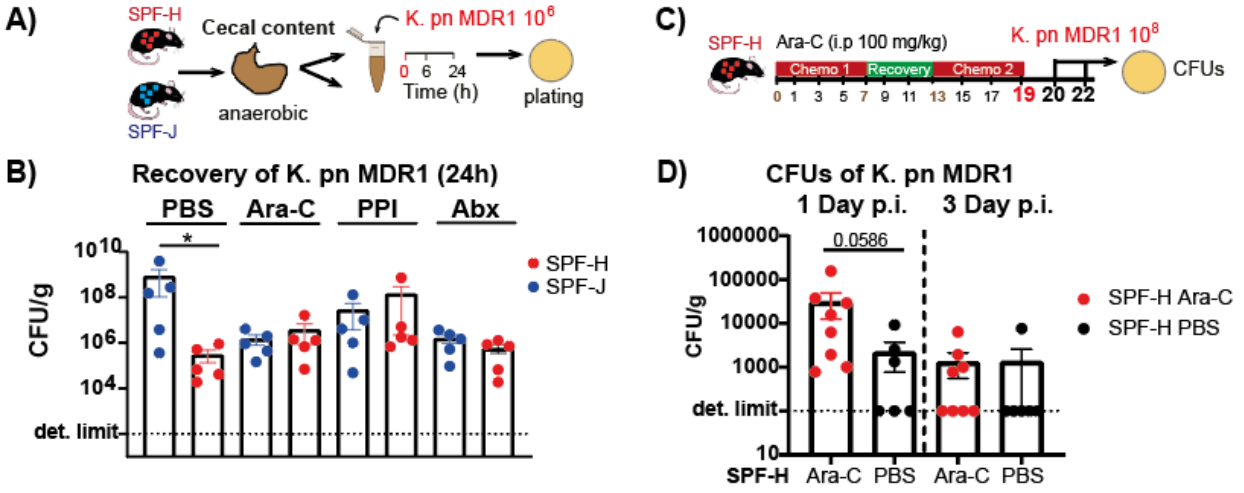

Figure 21: Induction chemotherapy-induced changes in the microbiome promote colonization with MDR-E. (A) SPF-H and SPF-J mice were treated with two consecutive cycles of Ara-C, levofloxacin (Abx), Pantoprazole (PPI) or PBS as a control. Mice were sacrificed and isolated cecal content was spiked with 10^6 CFU of K.pn MDR1 and incubated anaerobically for 24 h before plating on selective agar plates. (B) Recovered CFUs of K.pn MDR1 in isolated cecal content of PBS, Ara-C, PPI and Abx treated SPF-H and SPF-J mice. (C) SPF-H were treated with two consecutive cycles of Ara-C before colonization with 10^6 CFU of K.pn MDR1. After 24h, mice were sacrificed and feces were plated on selective agar plates. (D) Resulting CFUs of K.pn MDR1 after 1 day of colonization. Results represent one experiment with n = 5-7 mice/group as mean ± SEM. P values indicated represent a nonparametric Kruskal-Wallis test with *p<0.05.

Taken together I could show in this chapter that isogenic mouse lines with distinct microbiota profiles and distinct differences in species richness significantly differ in their susceptibility to develop SI mucositis when treated with two consecutive cycles of chemotherapy. I defined Ara-C as main driver for shifts in community structure and development of inflammation. Further, I demonstrated that the microbiota dynamically respond to the different phases of the chemotherapy and each drug induced selective changes on the individual microbiota composition, likely contributing to colonization susceptibility or resistance in different mouse lines. Further experiments are required to evaluate the direct impact of the microbiota composition regarding the colonization susceptibility caused by Ara-C.

3.3 The variability of the microbiota composition influences the susceptibility towards the intestinal pathogen *Citrobacter rodentium* via short chain fatty acid production

The following chapter has been published in the article entitled “Variations in microbiota composition of laboratory mice influence Citrobacter rodentium infection via variable short-chain fatty acid production”, PLoS Pathog. 2020 Mar 24;16(3):e1008448. doi: 10.1371/journal.ppat.1008448. [Epub ahead of print] by Osbelt L[1,2], Thiemann S[1], Smit N[1], Lesker TR[1], Schröter M[1], Gálvez EJC[1,3] et al. Figures and text from this publication have been adapted and partially modified for this chapter.

3.3.1 Isogenic mouse lines feature distinct microbiota compositions and varying disease kinetics after *Citrobacter rodentium* infection

Previous experiments in our group have shown that variations in microbiota composition in laboratory mice influence the susceptibility to *C. rodentium* infection independent of variation in diet and prior exposure to antibiotics. Initially, isogenic mouse lines on a highly related genetic background (C57Bl6/N, sublines Crl, Tac, Hsd and RJ) were infected with with 10^8 CFU *C. rodentium* by oral gavage (Figure 5B). Kinetics of *C. rodentium* colonization was noted to be significantly different between the different mouse lines (Figure 5C and D). Since SPF-1 (SPF-S) and SPF-2 (SPF-R) mice showed the highest difference in disease kinetics, I decided to further focus on the differences between these two mouse lines in this thesis.

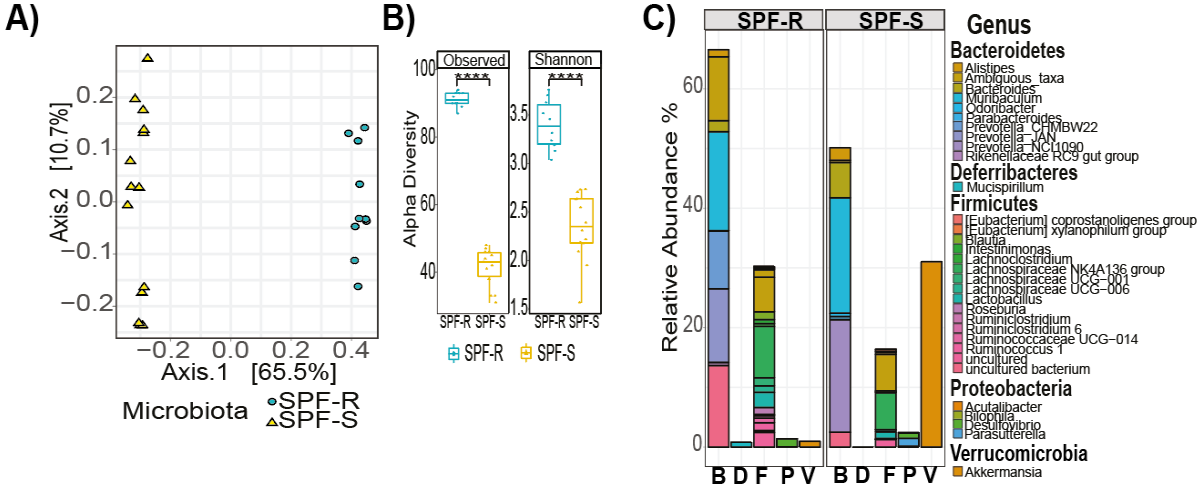

Figure 22: Microbiome differences between SPF-S and SPF-R mice. (A) Fecal microbiota of resistant SPF-R and susceptible SPF-S mice was analyzed using 16S rRNA gene sequencing using a PCoA plot. (B) α-diversity was determined using Chao1 and Shannon index. P values indicated represent a non-parametric Wilcoxon signed rank test ****p<0.0001. (C) Relative abundances are displayed at genus level. (Adapted and modified from Osbelt et al., 2020).

In general, the microbiome of both mouse-lines featured pronounced differences in term of beta-diversity (Fig 22A), alpha diversity (Fig 22B) and species composition (Fig 22C). The microbiota of SPF-R was more complex compared to SPF-S mice and harbored more and more divers bacteria in the Firmicutes phylum, whereas SPF-S mice were characterized by high portion of the genus *Akkermansia* within the phylum of Verrucomicrobia (Fig 22C).

3.3.2 Variations in microbiota composition are correlated with lethal outcome of infections with Shiga toxin expressing *C. rodentium* strains

Shiga toxin (Stx) is a virulence factor of EHEC contributing to its strong pathogenicity. Recombinant expression of Stx in *C. rodentium* has been demonstrated to cause lethal infection accompanied by intestinal inflammation and kidney damage (Mallick et al., 2012). To test whether microbiota-dependent differences in *C. rodentium* colonization would also affect infection with a more pathogenic *C. rodentium* strain, SPF-S and SPF-R mice were infected with a Stx-producing *C. rodentium* strain and fecal colonization as well as BWL and survival were analyzed. In line with the previous results using the less-pathogenic *C. rodentium* strain, the Stx-expressing *C. rodentium* strain also displayed delayed colonization in SPF-R mice during the first days of infection (Fig 23A). As likely direct consequence of higher colonization, SPF-S mice started to lose weight rapidly already after 3 days of infection, whereas SPF-R mice began to lose weight only at day 10 post infection (p.i.) (Fig 23B). Moreover, SPF-R mice displayed prolonged survival as SPF-S mice had a mean survival of 7 days, whereas SPF-R mice survived significantly longer with a median survival of 11.5 days (Fig 23C). These findings demonstrate that delayed colonization of SPF-R mice lead to reduced BWL and prolonged survival even when infected with a lethal *C. rodentium* strain.

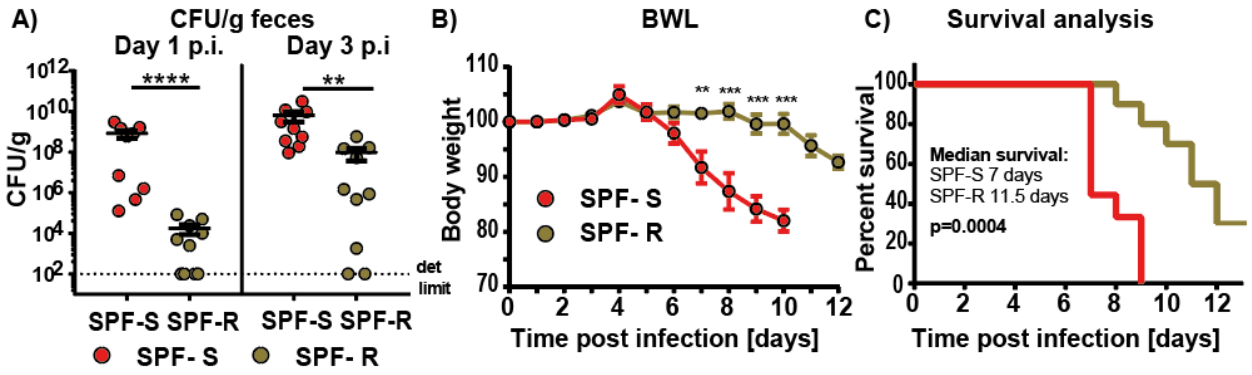

Figure 23: Variations in microbiota composition are correlated with lethal outcome of infections with a Shiga toxin-expressing *C. rodentium* strains. (A-C) SPF-S and SPF-R mice were infected orally with 10^8 CFU *C. rodentium* DBS 770 and fecal colonization, BWL and survival were determined. Dashed lines indicate the limit of detection. Results represent two independent experiments with n = 4-5 mice/group as mean ± SEM. P values indicated represent a nonparametric Kruskal-Wallis test, **p<0.01, ***p<0.001, ****p<0.0001 (adapted from Osbelt et al., 2020).

3.3.3 Delayed colonization in SPF-R mice is visible in all intestinal organs and tissues but most prominent in the cecum

To study the infection process further, the characterization of the infection dynamic was extended. First, viable fecal CFUs were determined six hours after infection to quantify whether similar numbers of viable *C. rodentium* pass the gastrointestinal tract of both mouse lines (Fig 24A). At this time-point, no differences in *C. rodentium* CFU were detected in the stool of both mouse lines suggesting that *C. rodentium* was not immediately killed during early gastro-intestinal passage. To test if observed differences in the fecal colonization are also visible in the intestinal organs, I infected both mouse lines with a bioluminescent *C. rodentium* strain and imaged the infection using an *in vivo* imaging system (IVIS) (Fig 24B). Again, SPF-S mice showed a higher colonization at the early time points (day 1 to 5) of infection, whereas the SPF-R mice were more highly colonized at later time points (day 8 to 12) of infection (Fig 24B).

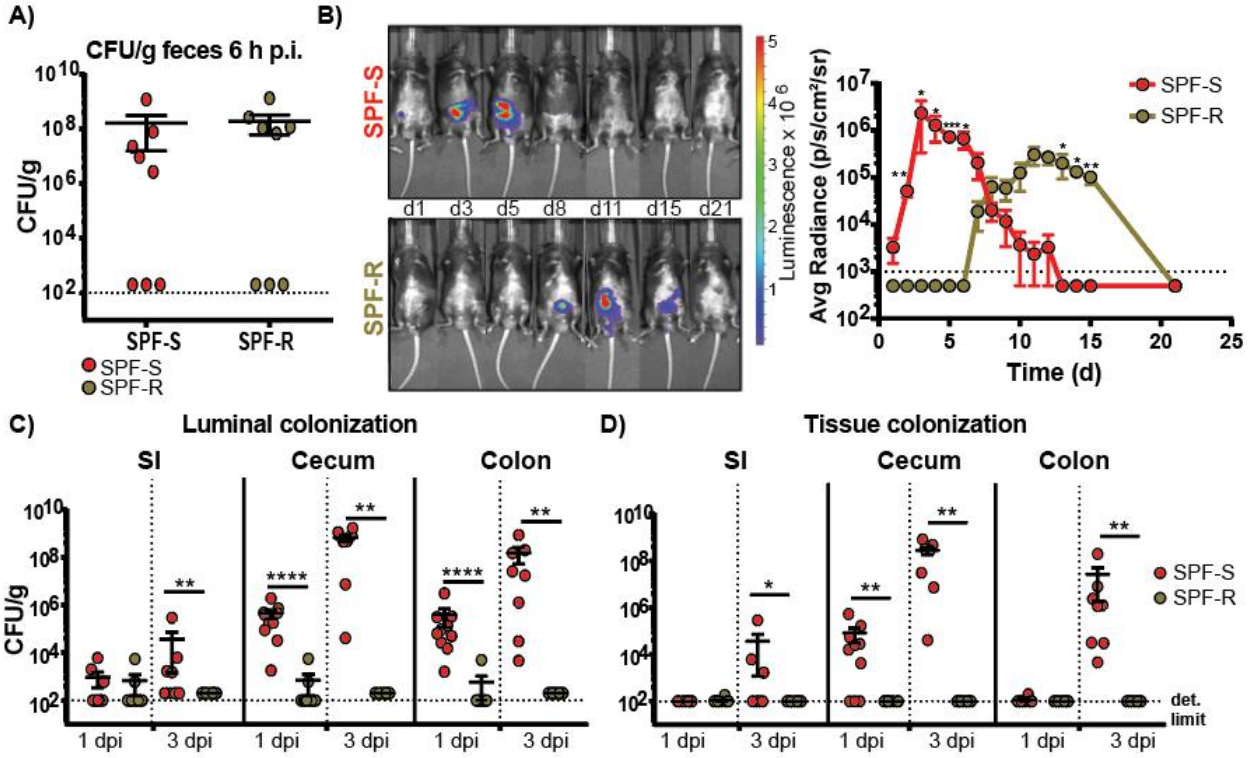

Figure 24: Delayed colonization in SPF-R mice is visible in all intestinal organs and tissues but most prominent in the cecum. (A) SPF-S and SPF-R mice were infected orally with 10^8 CFU *C. rodentium* and fecal colonization was determined after 6 hours p.i.. (B) SPF-S and SPF-R mice were infected orally with 10^8 CFU *C. rodentium* and infection was imaged *in vivo* using an IVIS imaging system. Average radiance (p/s/cm^3/sr) was determined at day 1, 3, 5, 8, 11, 15 and 21 p.i. (C-D) SPF-S and SPF-R mice were infected orally with 10^8 CFU *C. rodentium* and sacrificed after 1 day or 3 days p.i. CFU/g organ content and tissue was determined. Dashed lines indicate the limit of detection. Results represent two independent experiment with n = 5-7 mice/group as mean ± SEM. P values indicated represent a nonparametric Kruskal-Wallis test *p<0.05, **p<0.01, ***p<0.001, ****p<0.0001.

To test, whether the differences at the early time point of infection occur in the luminal content or in the intestinal organs, mice were sacrificed either 1 day or 3 days p.i.. Correlating with the other results, SPF-S mice displayed a significant higher pathogen burden in the intestinal content of the cecum and the colon, as well as in the cecal tissue already after one day and in the SI lumen and tissue after 3 days (Fig 24C-D).

3.3.4 Differences in colonization could be recovered *in vitro* indicating that mechanism mediated directly by resident microbes in the cecum

As differences in colonization between SPF-S and SPF-R mice occur mainly in the cecal lumen, I next assessed colonization *in vitro* to exclude influences of immune cells infiltrating after the infection. For this purpose, 10^6 CFU of *C. rodentium* was incubated under anaerobic and aerobic conditions in cecal content of SPF-S and SPF-R mice for 6 and 24 hours (Fig 25A). Strikingly, the cecal content of SPF-S mice enabled a significant higher pathogen burden compared to the cecal content of SPF-R mice in both conditions only after 24 but not 6 hours Fig 25B). This demonstrates that competition with the microbiota or extended presence of their products in the cecum is sufficient to inhibit the growth of *C. rodentium*. Furthermore, the inhibitory effect was only present in 1:1 or 1:2 diluted cecal content indicating that bacteria and or produces substances need to be present in higher concentrations to allow growth inhibition (Fig 25C). To determine, if the bacteria in the cecum itself or the presence of toxic substances or produced bacterial metabolites inhibit growth of *C. rodentium*, I separated the cecal content into bacterial pellet and supernatant before inoculation with *C. rodentium* (Fig 25D). Interestingly, growth was significantly reduced in the supernatant and in the pellet of SPF-R mice indicating that produced substances by distinct bacteria are responsible for the growth inhibition. Overall, levels of *C. rodentium* were more strongly reduced in the pellet and whole content compared to the supernatant alone, suggesting that cooperative mechanisms of distinct bacteria and produced metabolites in the cecum of SPF-R mice synergistically reduce CFUs of *C. rodentium* at the early stage of infection.

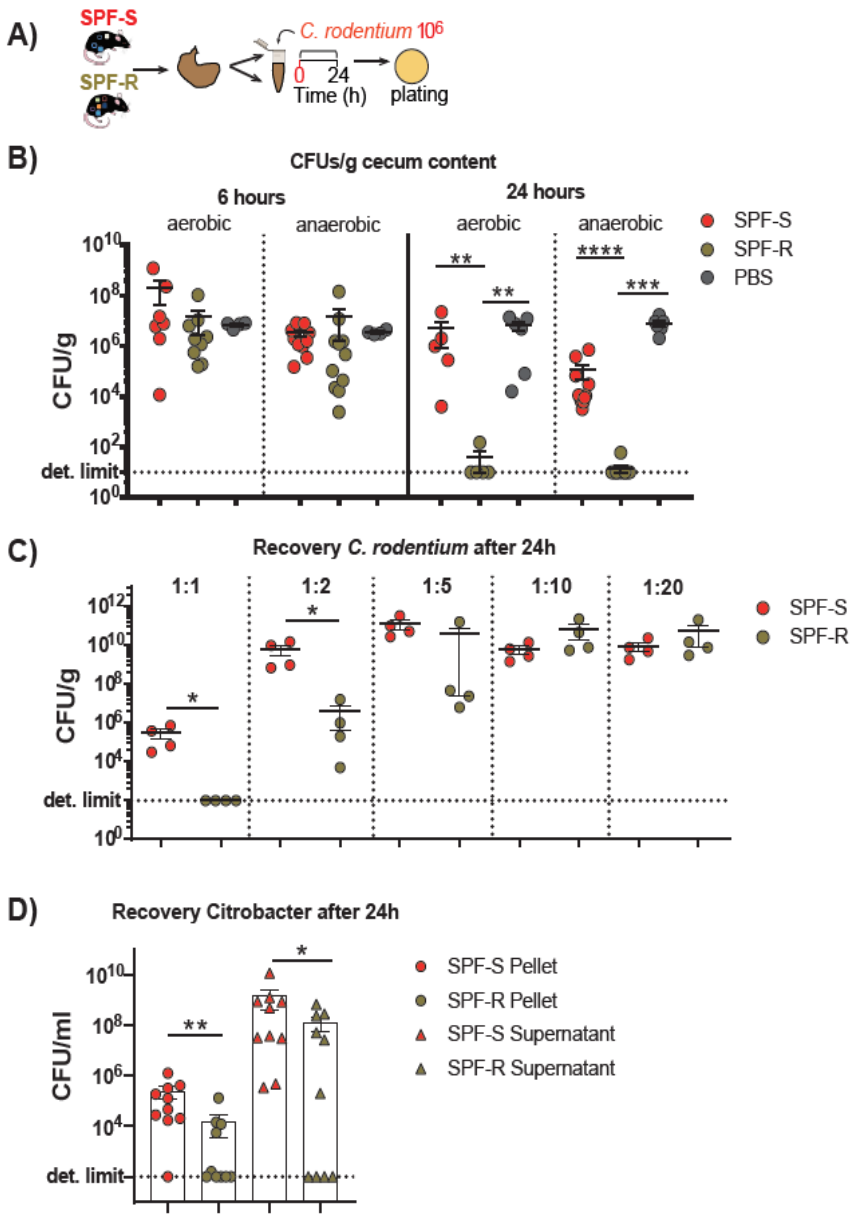

Figure 25 Different *in vitro* approaches could recover the observed phenotype. (A) Isolated cecal content of SPF-S and SPF-R mice was diluted 1:1 in PBS, inoculated with 10^6 CFU *C. rodentium* and cultivated under aerobic and anaerobic conditions for 24 hours before plating on selective agar plates. (B) Recovery of *C. rodentium* in isolated cecal content after 24 h of aerobic and anaerobic cultivation. (C) Recovered CFUs of *C. rodentium* after 24 h of anaerobic cultivation in isolated cecal content of SPF mice diluted 1:1, 1:2, 1:5, 1:10 or 1:20 in PBS. (D) Recovered CFUs of *C. rodentium* after 24 h of anaerobic cultivation in isolated cecal content (D) Recovered CFUs of *C. rodentium* after 24 h of anaerobic cultivation in isolated cecal content of SPF mice separated into bacterial pellet and supernatant by centrifugation, diluted 1:1 in PBS. Results represent one representative experiment with n=4-6 mice per group or multiple pooled experiments with up to 11 mice per group as Mean with SEM. P values indicated represent a nonparametric Mann-Whitney test *p<0.05, **p<0.01, ***p<0.001, ****p<0.0001.

3.3.5 Cohousing and transfer of cultivable bacteria from resistant SPF-R mice leads to variable protective outcome in SPF-S mice

To identify if bacteria linked to susceptibility or resistance can be transferred and alter susceptibility *in vivo*, SPF-S and SPF-R mice were either cohoused for 3 weeks to potentially transfer all bacteria, or received the cultivable fractions of aerobic and anaerobic bacteria isolated from the cecal content of SPF-R mice by oral gavage (Fig 26A). Subsequently, mice were infected with *C. rodentium* after 3 weeks of microbiota transfer and sacrificed at 3 days p.i. to determine CFUs in the intestinal organs and content. Strikingly, the protective phenotype did not show full penetrance and in all groups.

Some recipient SPF-S mice showed a fully protected phenotype, whereas other showed no or only minor reduction in the intestinal CFUs (Fig 26B-E). Of note, the cohousing and transfer experiments were repeated several times (n= 3 with 4-6 mice per group) with similar outcomes. In each experiment, some mice were fully protected, whereas others had similar CFUs as the untreated SPF-S mice (Fig 26D-E). Based on these observations, I hypothesized that the causative bacteria may only be transferred to some mice resulting in the variable protective effect.

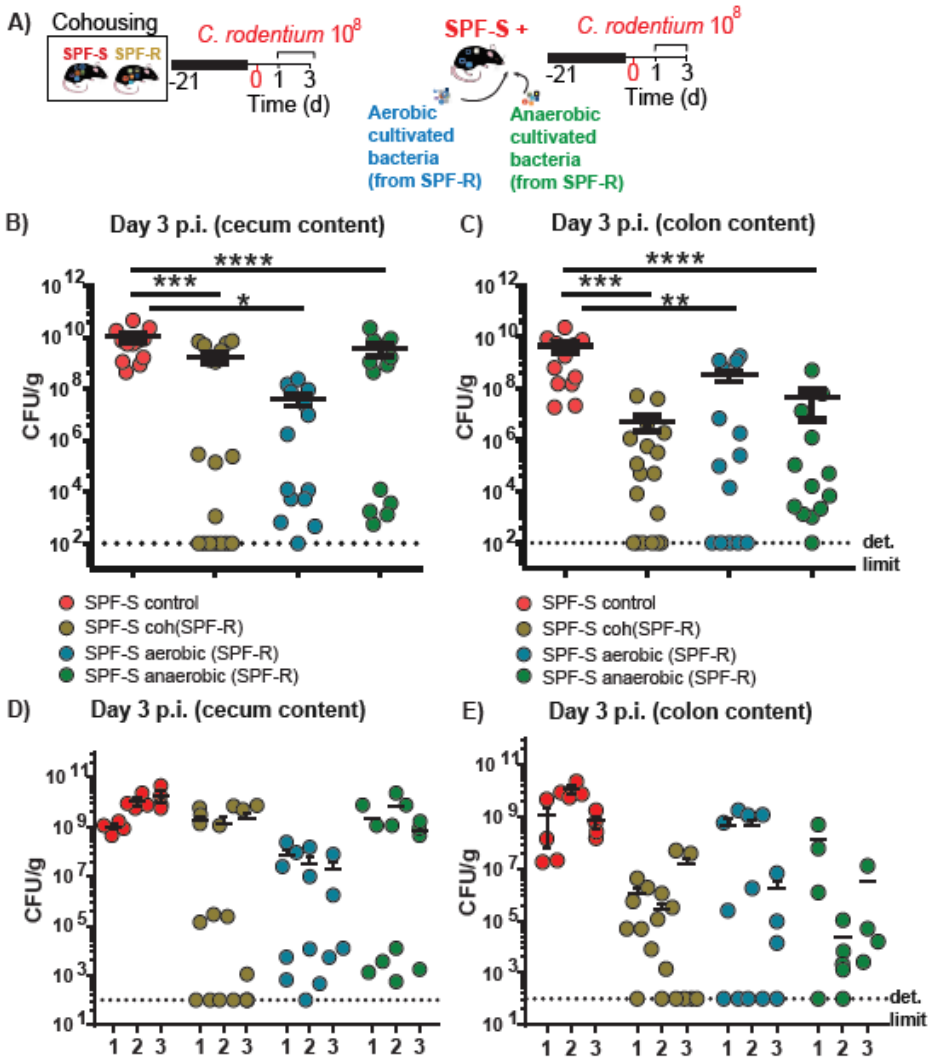

Figure 26: Cohousing and transfer of cultivable bacteria from resistant mice leads to variable protective outcome in SPF-S mice. (A) Groups of susceptible SPF-S mice were pretreated with different bacteria. One group was cohoused with SPF-R mice for 3 weeks before infection. One group received a mixture of all cultivable aerobic bacteria isolated from cecal content of SPF-R mice. One group received all cultivable anaerobic bacteria isolated from cecal content of SPF-R mice. The last group was left untreated. All mice were infected with 10^8 CFU *C. rodentium* after 3 weeks and CFUs/g feces and organ content and tissue were assessed after day 1 and 3 p.i. (B-C) Pooled CFUs of *C. rodentium* in the cecal and colon content at day 3 p.i. are displayed. (D-E) CFUs of *C. rodentium* in the cecal and colon content at day 3 p.i. are for each single experiment are displayed. Results represent three independent experiments with n = 4-6 mice per group as mean with SEM. *P* values indicated represent a Mann-Whitney U test comparison between groups with *p<0.05, **p<0.01, ***p<0.001, ****p<0.0001 (adapted from Osbelt et al., 2020).

3.3.6 Resistance of SPF-R mice is associated with higher diversity and abundance of bacteria in the Firmicutes phylum

To identify bacteria associated with the protective phenotype after microbiota transfer, all recipient animals were assigned to the classes “susceptible” or “resistant” according to the CFU/g cecal content after 3 days p.i. in the cecum (Fig 27A). All mice below the threshold value of 10^6 CFU/g cecal content were considered to be “resistant” whereas all animals above the threshold were considered to be “susceptible”. Analysis of the beta-diversity from SPF-S mice receiving anaerobic and aerobic bacteria from SPF-R mice revealed a clustering according to susceptibility (Fig 27B). Moreover, analysis of α-diversity showed significantly elevated species richness in terms of total observed species and in terms of numbers in relation to evenness in the resistant SPF-S mice (Fig 27C) indicating that more bacteria were transferred from the SPF-R microbiota, which harbor a more complex microbiota than the initial SPF-S microbiota (Fig 22A-C). The comparison of relative abundances on the genus level revealed striking differences according to the “susceptible” and “resistant” phenotypes regarding the abundance and diversity of bacteria within the Firmicutes phylum of both groups (anaerobic and aerobic bacteria transfer) (Fig 27D-E). A frequent trait of bacteria originating from this phylum is their involvement in the generation of SCFAs such as acetate, propionate and specifically butyrate. I hypothesized that resistance might be associated with a higher ratio of SCFA producing bacteria in the microbiota of SPF-R mice. To support this hypothesis the abundance of bacteria annotated to be involved in the production of butyrate was compared between the groups (Vital, Karch and Pieper 2017). Indeed, I found significantly elevated levels of bacteria of the genera *Lachnospiraceae, Ruminiclostridium, Butyricicoccus, Intestinimonas, Lachnoclostridium, Roseburia* and *Ruminicoccaceae* (Fig 27F-G; Fig 28F) in the cohoused mice or SPF-S mice receiving anaerobic or aerobic bacteria from SPF-R mice, whereas levels of *Coprococcus* were only elevated in mice receiving anaerobic cultivated bacteria (Fig 27F). The presence of distinct, putatively spore-forming, anaerobes in protected SPF-S mice receiving aerobically cultivated bacteria suggests that viable spores were transmitted. Furthermore, susceptible mice remained a high abundance of *Akkermansia* (Phylum Verrucomicrobia) in their microbiome (Fig 27D-E, Fig 28E), but *Akkermansia* abundance did not correlate with the phenotype change in SPF-S mice from susceptible to resistant (Fig 28G-H). Taken together, 16S rRNA gene sequencing supported the role of obligate anaerobic bacteria to be involved in the observed phenotype.

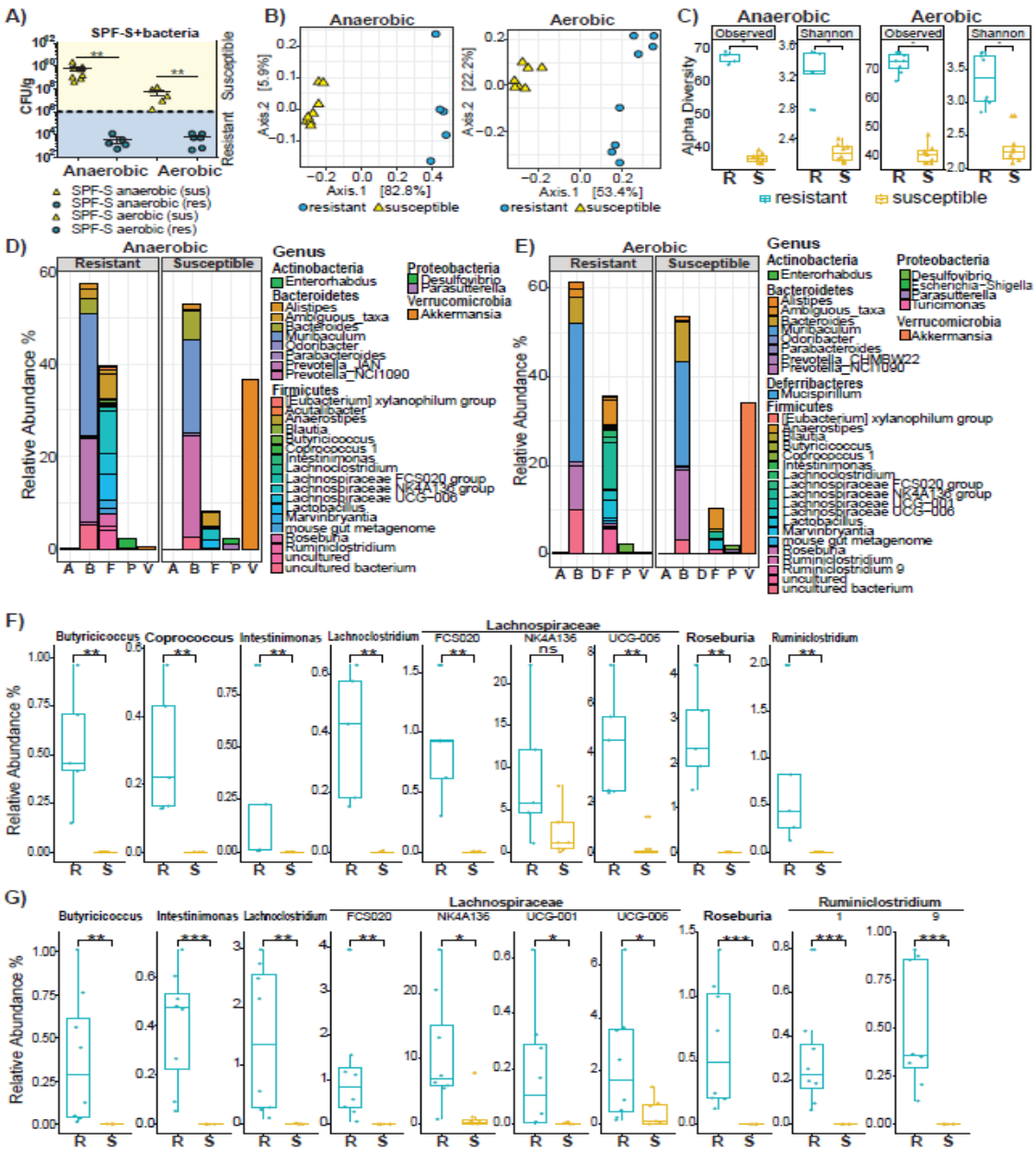

Figure 27: Resistance of SPF-R mice is associated with higher diversity and abundance of bacteria in the Firmicutes phylum. (A) Assignment of SPF-S mice receiving a cultivated fraction of anaerobically or aerobically cultivated bacteria from the SPF-R mice to the class "resistant" and "susceptible" according to the cecal CFUs of *C. rodentium* after day 3 p.i.. A threshold of 10^6 was used for discrimination of both groups. (B) Fecal microbiota of resistant and susceptible SPF-S mice of the "anaerobically treated" and "aerobically treated" group was analyzed using 16S rRNA gene sequencing after cohousing using a PCoA plot (C) α-diversity was determined using Chao1 and Shannon index. P values indicated represent a non-parametric Wilcoxon signed rank test *p<0.05, **p<0.01, ***p<0.001, ****p<0.0001. (D-E) Fecal microbiota of resistant and susceptible "anaerobically treated" and "aerobically treated" SPF-S mice were analyzed using 16S rRNA gene sequencing. Relative abundances of bacterial genera are shown and grouped according to their phylum. Bars represent the mean of all mice within the group. Representative data derived from three independent experiments are shown. (F-G) Relative abundance of significantly different SCFA producing members of treated SPF-S mice of the genera *Butyricicoccus*, *Coprococccus*, *Intestinimonas*, *Lachnoclostridium*, *Lachnospiraceae*, *Roseburia* and *Ruminoclostridium* are shown. P values indicated represent a non-parametric Wilcoxon signed rank test *p<0.05, **p<0.01, ***p<0.001 (adapted from Osbelt et al., 2020).

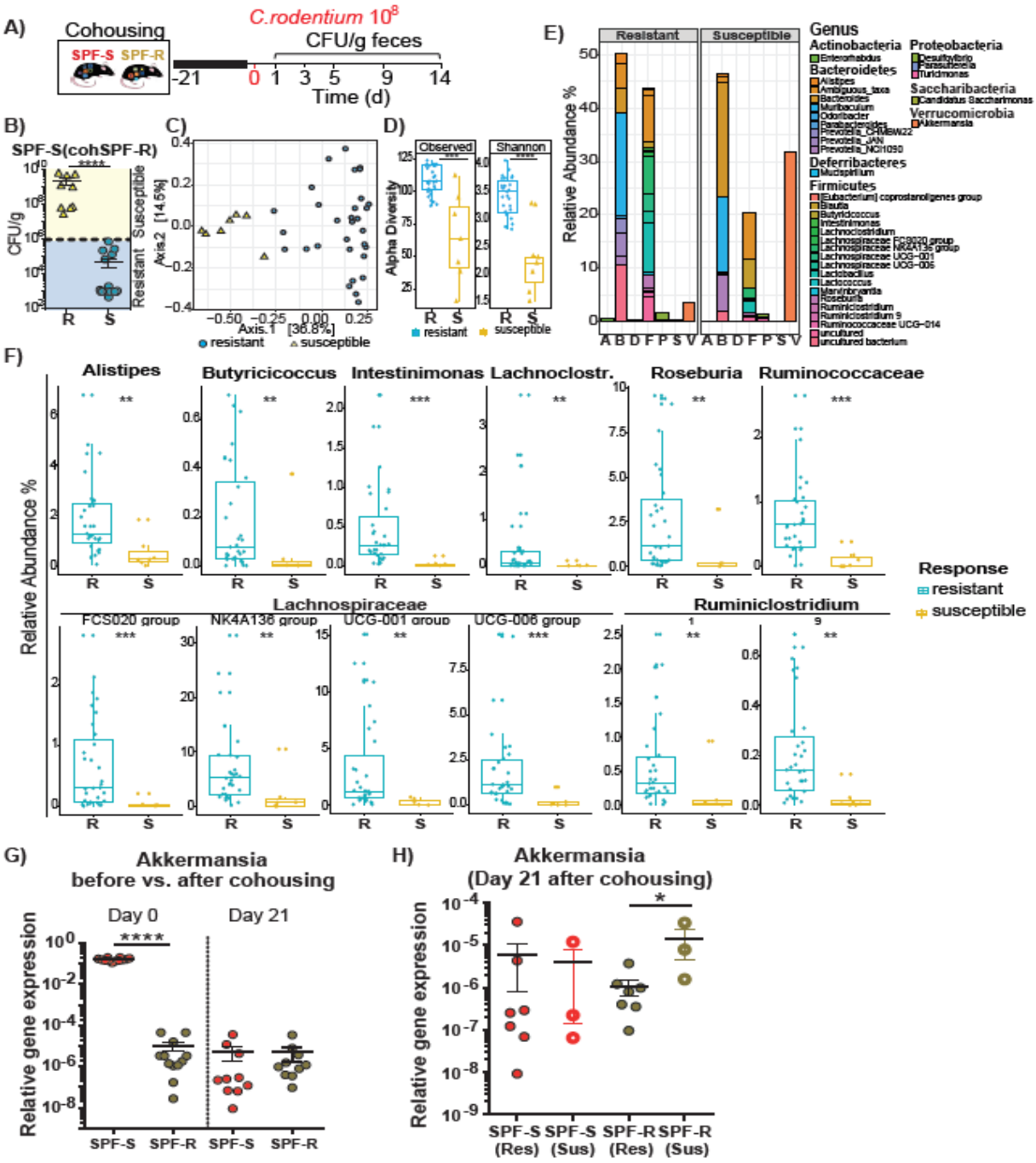

Figure 28: Cohousing experiments lead to various outcome in the phenotype with high abundance of SCFA producing bacteria in resistant mice. Cohousing experiments lead to various outcome in the phenotype with high abundance of SCFA producing bacteria in resistant mice. (A) SPF-S and SPF-R mice were cohoused for 4 weeks and infected with 10^8 CFU *C. rodentium*. (B) Assignment of cohoused SPF-S and SPF-R mice to the class "resistant" and "susceptible" according to the cecal CFUs of *C. rodentium* after day 3 p.i.. A threshold of 10^6 was used for discrimination of both groups. (C) Fecal microbiota was analyzed using 16S rRNA gene sequencing after cohousing using a PCoA plot. (D) α-diversity was determined using Chao1 and Shannon index. (E) Fecal microbiota of resistant and susceptible cohoused SPF-S and SPF-R mice was analyzed using 16S rRNA gene sequencing. Relative abundances of bacterial families are shown and grouped according to their phylum.

Bars represent the mean of all mice within the group. Representative data derived from three independent experiment are pooled. (F) Relative abundance of significantly different SCFA producing members between resistant and susceptible mice of the genus *Alistipes*, *Butyricicoccus*, *Intestinimonas*, *Lachnoclostridium*, *Lachnospiraceae*, *Roseburia*, *Ruminococcaceae* and *Ruminoclostridium* are shown. P values indicated represent a non-parametric Wilcoxon signed rank test *p<0.05, **p<0.01, ***p<0.001, ****p<0.0001. (G) Relative gene expression levels of *Akkermansia* in SPF-S and SPF-R animals before and after three weeks of cohousing. Values are normalized to total 16S. (H) Relative gene expression levels of *Akkermansia* cohoused SPF-S and SPF-R mice that changed or maintained the initial phenotype. Values are normalized to total 16S. P values indicated represent a non-parametric Wilcoxon signed rank test *p<0.05 (adapted from Osbelt et al., 2020).

Since the transfer of aerobic cultivated bacteria did also lead to reduced susceptibility, I hypothesized that a higher abundance and diversity of low abundance taxa such as endogenous *Enterobacteriaceae* and other facultative anaerobic bacteria may also impact the disease susceptibility in this context. Therefore, I first indirectly assessed oxygen availability in the intestinal tissue by measuring the protein levels of HIF1α, a marker for tissue hypoxia (Kelly et al., 2015). These analysis demonstrate that HIF1α was equally expressed in both mouse lines in the cecal tissue at steady state and 3 days p.i. (Fig 29A-B) confirming that hypoxic conditions and oxygen availability in the gut were comparable between both mouse lines. In a second approach, I cultivated fecal and cecal material of both mouse lines on Mac-Conkey agar plates as these taxa are below the detection limit of sequencing based approaches (Fig 29C-E). Indeed, I could recover significantly more facultative anaerobe bacteria from the cecum and feces of SPF-R mice (Fig 29C). Nevertheless, transfer of these bacteria into SPF-S mice did not lead to significantly reduced CFUs in the cecum and colon after 3 days p.i. (Fig 29G-H), suggesting that low abundance taxa and the availability of oxygen close to the mucosa do not play a major role in the protected phenotype. Overall, all 16S rRNA gene sequencing data and transfer experiments strongly suggest that transfer of different butyrate-producing species from the resistant SPF-R mouse line to SPF-S mice could contribute to resistance against *C. rodentium* infection.

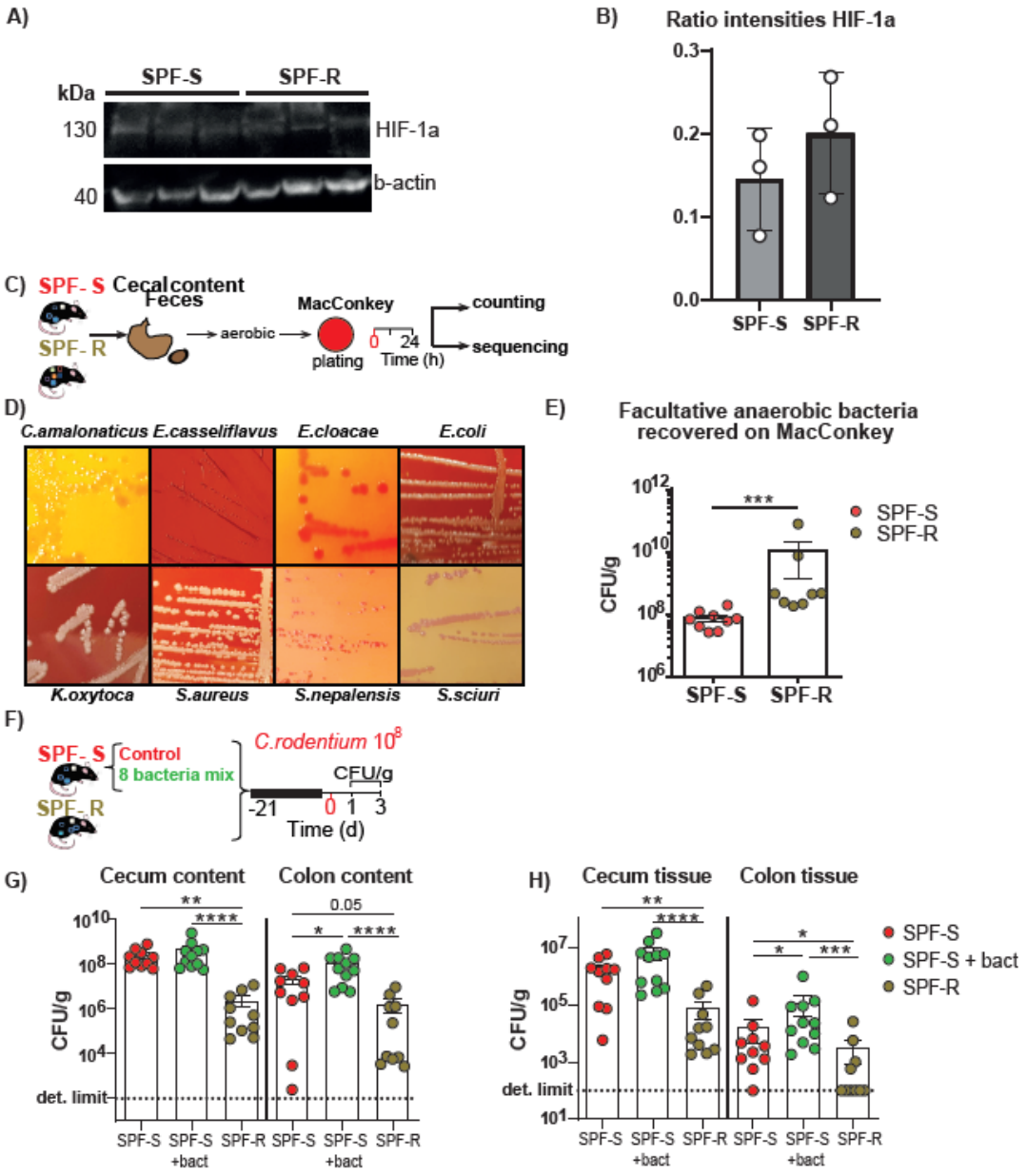

Figure 29: Isolated facultative anaerobic bacterial species do not contribute to inhibition of *C. rodentium in vivo*. (A) HIF-1 α protein from cecum tissue at steady state in SPF-R and SPF-S mice (B) Quantification of HIF-1 α protein compared to β-actin protein levels (loading control) (C) Serial dilutions of isolated cecal content and feces of SPF-S and SPF-R mice were plated on MacConkey agar plates without crystal violet and cultivated for 24 hours under aerobic conditions. Morphological different colonies were picked and streaked out again to obtain a pure culture. Single colonies were sent for sequencing. All aerobic colonies were counted for quantification (D) Isolated bacteria grown on Mac Conkey agar plates. (E) Quantification of cultivable aerobic bacteria in the feces of SPF-1 and SPF-2 mice growing on Mac Conkey agar plates media. Data represent two independent experiments with n=5-8 mice per group. (F) Groups of susceptible SPF-S mice were pretreated with isolated facultative anaerobic bacteria. All mice were infected with 10^8 CFU *C. rodentium* after 3 weeks of precolonization and CFUs/g organ content and tissue were assessed after 3 days p.i. (G-H) CFUs of *C. rodentium* in intestinal organ tissues and contents after 3 days p.i.. Results represent Mean and SEM of two independent experiments with n=6-10 mice per group. P values indicated represent a nonparametric Kruskal-Wallis test *p<0.05, **p<0.01, ***p<0.001, ****p<0.0001 (adapted from Osbelt et al., 2020).

3.3.7 The metabolomics profile of resistant SPF-R is characterized by elevated SCFA levels, which strongly impair the growth of *C. rodentium in vitro* at pH 6.0

Based on the microbial signatures in the resistant mice linking SCFA producing bacteria to the resistant phenotype, I next analyzed metabolome profiles in both mouse lines, particularly the levels of SCFAs. To characterize differences in the cecal metabolome in SPF-S and SPF-R mice at steady state and after infection, targeted (for SCFA) and non-targeted metabolomics (Fig 30A and Fig 31) were performed. Strikingly, SPF-R mice showed significantly elevated levels of butyrate in the cecum with an average concentration of 80 nmol/mg cecal content in contrast to levels around 20 nmol/mg cecal content in SPF-S mice at steady state and after infection. In addition, acetate was elevated in SPF-R mice at both time points, but the fold-difference was smaller as for butyrate. Propionate levels were also slightly increased in resistant SPF-R mice before and after infection (Fig 30A). Using non-targeted metabolomics, 70 out of 247 compounds could be successfully identified. A non-supervised cluster analysis revealed a strong separation of both mouse lines based on the intestinal metabolome profiles. The levels of 26 metabolites were already significantly different at steady state prior infection (Fig 31A and C). From these, 20 metabolite levels were significantly elevated in SPF-S mice compared to SPF-R mice, including different citric acid cycle intermediates or fermentation products such as succinate, fumarate and malate, urea-cycle and poly amine metabolism intermediates such as urea, putrescine and ornithine as well as the amino alcohol ethanolamine and the flavone apigenin (Fig 31A and C).

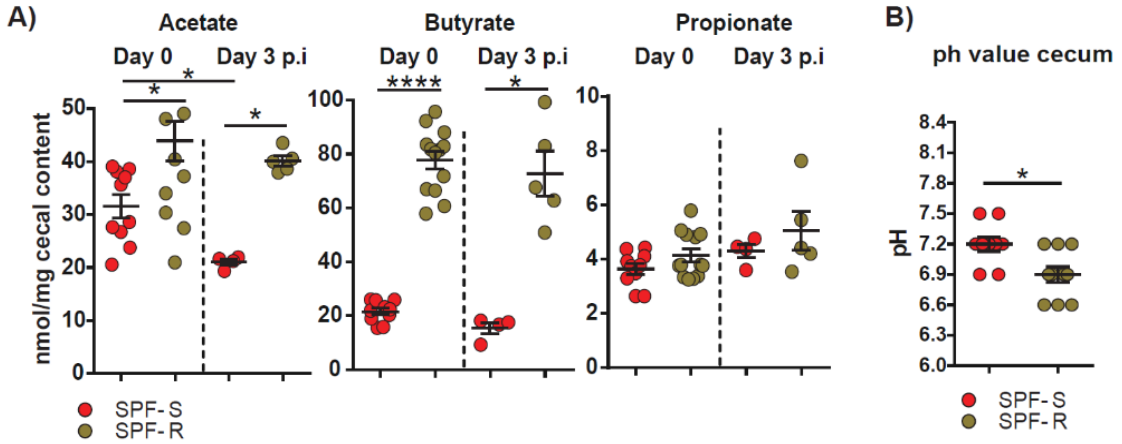

Figure 30: The metabolome of resistant SPF-R is characterized by elevated SCFA levels. (A) Cecal SCFA levels of butyrate, acetate and propionate for SPF-S and SPF-R mice at steady state and day 3 p.i. are displayed in nmol/mg cecal content. (B) Cecal pH in SPF-S and SPF-R mice at steady state. Pooled results of two independent experiments as mean ± SEM are shown. *P* values indicated represent a Mann-Whitney U test comparison between groups with *p<0.05, ****p<0.0001 (adapted and modified from Osbelt et al., 2020).

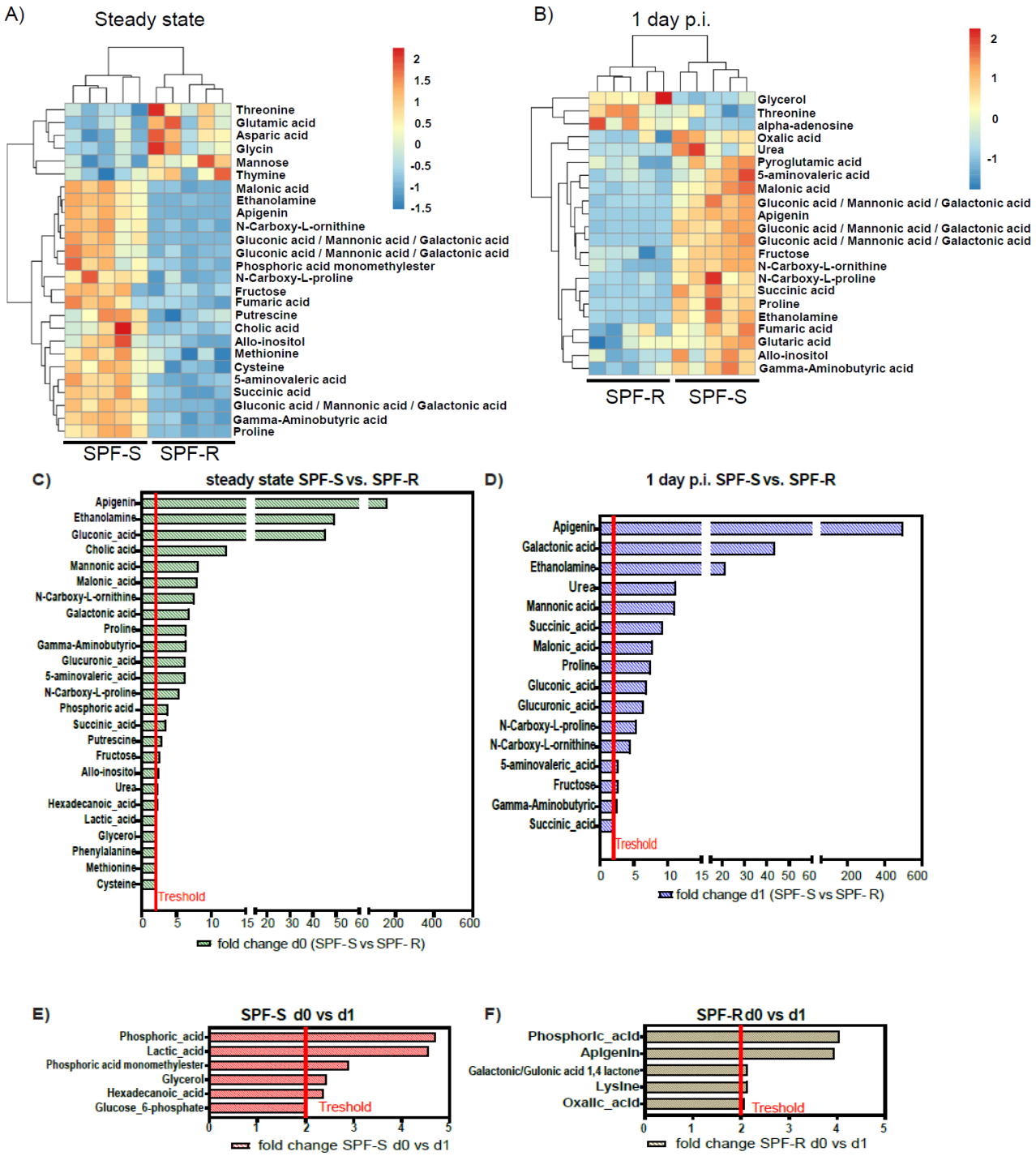

Figure 31: Untargeted metabolomics data of SPF-S and SPF-R mice before and after infection reveal strong differences between isogenic mouse lines. Heat maps of successfully annotated and significantly different metabolites between SPF-S and SPF-R mice at different time points: steady state (A) and day 1 p.i. (B). The two dendrograms for the heat map were calculated using Euclidean distance and ward linkage. *t*-tests with *p<0.05 were performed pairwise and significantly different metabolites between two extraction solvents are indicated. Fold changes of successfully annotated and significantly different metabolites between SPF-S and SPF-R at steady state (C) or at day 1 p.i. (D) are displayed. Fold changes of successfully annotated and significantly different metabolites within a mouse lines at different time points: SPF-S (E) and SPF-R (F). More than 2-fold changes between the indicated groups were set as a threshold (adapted from Osbelt et al., 2020).

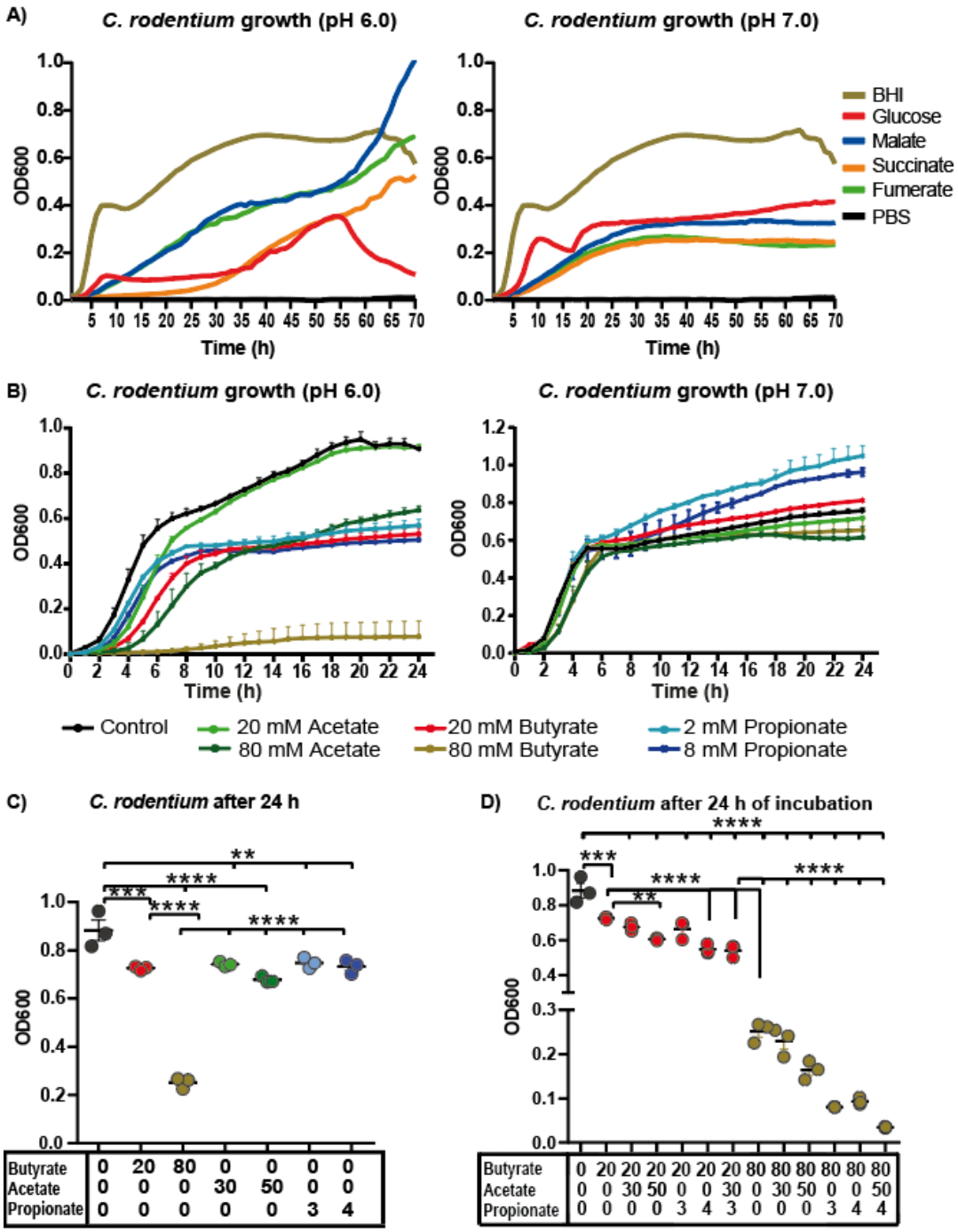

Figure 32: SPF-R SCFA levels strongly impair the growth of *C. rodentium in vitro* at pH 6.0. (A) *C. rodentium* growth over 70 h in Minimal medium supplemented with different carbon sources (20 w/v) at pH 6 or 7 compared to BHI and minimal medium with PBS. (B) *C. rodentium* growth displayed as optical density (OD) over time at pH 6.0 (left) or pH (7.0) in BHI medium supplemented with different concentrations of acetate, butyrate or propionate or without any SCFA added. (C-D) *Citrobacter* growth displayed as optical density (OD) over time at pH 6.0 in BHI medium supplemented with different mixtures of acetate, butyrate and propionate or without any SCFA added. (C-D) One data point represents mean value of three replicates. Values out of three independent experiments are displayed. *P* values indicated represent a One-way ANOVA between groups with **p<0.01, ***p<0.001, ****p<0.0001 (adapted and modified from Osbelt et al., 2020).

In contrast, only six metabolites, mostly amino acids were elevated in SPF-R mice. Several metabolites enriched in susceptible SPF-S mice (i.e. succinate, fumarate and malate) were sufficient to enable *in vitro* growth of *C. rodentium* as sole carbon sources in minimal media suggesting they could support *C. rodentium* growth early on *in vivo* (Fig 32A). Of note, at one day p.i. only minor changes in microbiome metabolite levels in both mouse lines were observed indicating that the early time point of infection did not change the metabolic landscape dramatically in both mouse lines compared to the steady state conditions (Fig 31E and F).

Based on the strongly altered SCFA concentrations and their previous association to growth inhibition of *Enterobacteriaceae* such as *Salmonella* Typhimurium (Jacobson et al., 2018), *E. coli* and *K. pneumoniae* (Sorbara et al., 2018), the inhibitory properties of different SCFAs were tested against *C. rodentium in vitro*. To do so, different concentrations of butyrate and acetate ranging from 10 mM to 100 mM and for propionate ranging from 1 mM to 8 mM were added to BHI medium. The pH values were normalized to a slightly acidic pH of 6.0 and a neutral pH of 7.0. Concentrations of SCFAs and pH approximately represent biological conditions measured in the mouse lines at steady state *in vivo* (Fig 30A and B). Measuring the optical density (OD) of *C. rodentium* over time, I noticed significantly impaired growth at higher concentrations of butyrate at a pH value of 6.0, whereas acetate and propionate did only partially reduce the growth of *C. rodentium* at pH 6.0 at high physiological concentrations. No significant effect for any SCFA was visible at neutral pH in line with findings on other *Enterobacteriaceae* (Sorbara et al. 2018) (Fig 32B-D). These results indicated that higher concentrations of SCFAs, especially butyrate, as seen in the SPF-R mice are able to abrogate growth of *C. rodentium in vitro*. Since SCFAs are present as a mixture under *in vivo* conditions, I tested different concentrations and combinations of the SCFAs as well approximately matching mixtures of all three SCFAs found in SPF-S and SPF-R mice against *C. rodentium in vitro*. First, butyrate was defined to be the main factor responsible for inhibition of *C. rodentium* growth when administered in concentrations higher than 50 mM (Fig 32C). Moreover, butyrate was even more effective when administered with 4 mM propionate or concentrations of acetate (30 mM and higher), whereas acetate and propionate alone were not sufficient to inhibit growth of *C. rodentium* completely even at the highest concentration tested (Fig 32B-D, Fig 33A-B). Finally, when all three SCFAs were tested together, the SPF-R mice related mixture of SCFAs lead to nearly complete abrogation of *C. rodentium* growth at pH of 6 but not 7, whereas the SPF-S related mixture of SCFAs did only have a minor impact on growth (Fig 32D, Fig 33B-D).

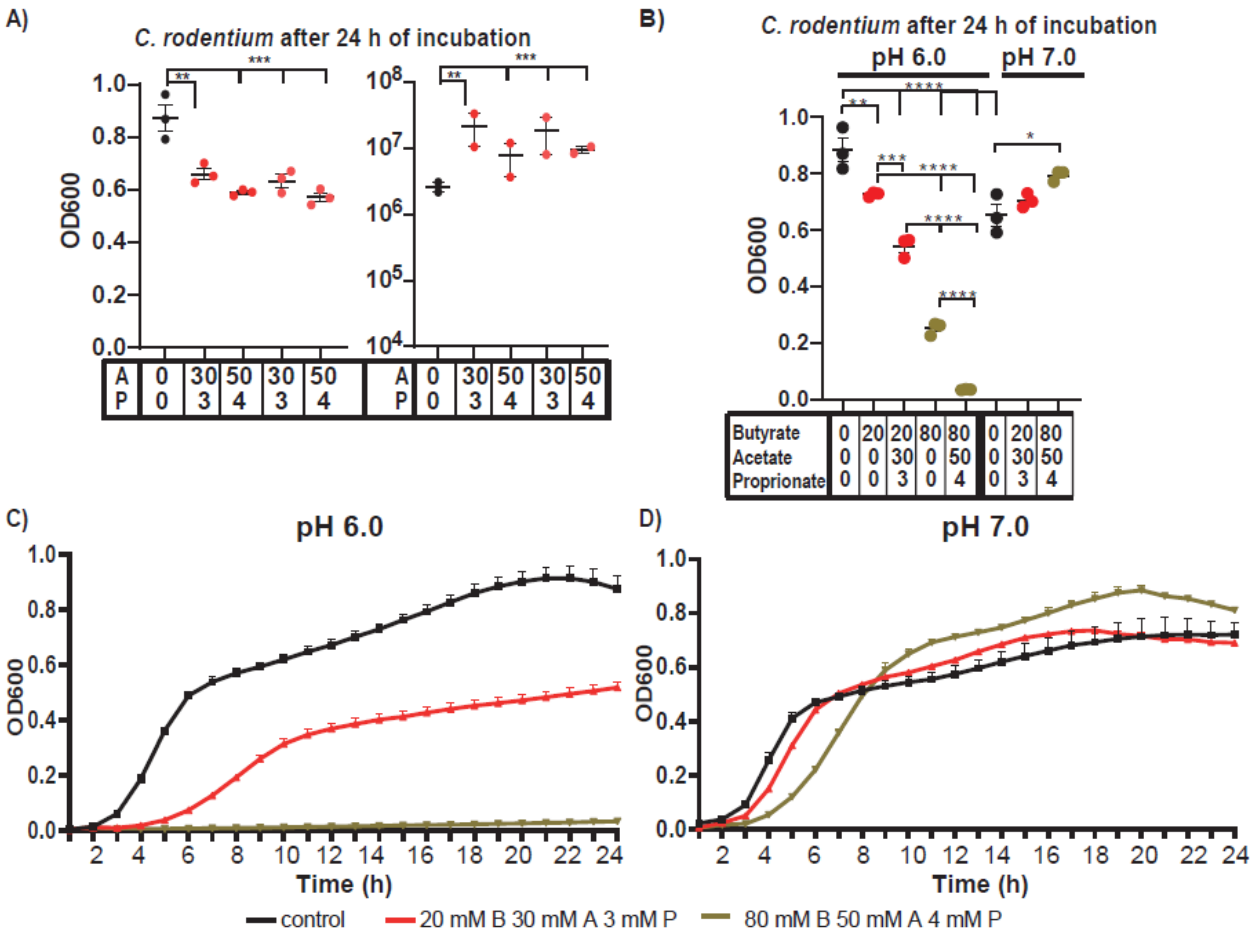

Figure 33: The metabolomics profile of resistant SPF-R is characterized by elevated SCFA levels, which strongly impair the growth of *C. rodentium in vitro* at pH 6.0. (A) *C. rodentium* growth displayed as optical density (OD) after 24 hours at pH 6.0 in BHI medium supplemented with different concentrations of acetate and propionate or without any SCFA added. (B) *C. rodentium* growth displayed as OD after 24 hours at pH 6.0 (left) or pH (7.0) in BHI medium supplemented with different concentrations of acetate, butyrate and propionate or without any SCFA added. One data point represents mean value of three replicates. Values out of three independent experiments are displayed. *P* values indicated represent a one-way ANOVA between groups with **p<0.01, ***p<0.001, ****p<0.0001. (C-D) *C. rodentium* growth displayed as OD over time at pH 6.0 (left) or pH (7.0) in BHI medium supplemented with different concentrations of acetate, butyrate and propionate or without any SCFA added. OD was measured every 60 min. Mean values ± SEM out of three independent experiments are displayed (adapted from Osbelt et al., 2020).

3.3.8 Supplementation of SPF-S mice with SCFA is sufficient to reduce *C. rodentium* growth *in vitro* as well as *in vivo*

Next, I wanted to test, whether an increase of the SCFA concentration in the SPF-S cecal content similar to the levels found in the SPF-R cecal content would be sufficient to achieve the protected phenotype *in vitro* and *in vivo*. First, isolated cecal content of SPF-S mice was supplemented with 80 mM of butyrate and adjusted to a pH of 6.0 and inoculated with 10^6 CFUs of *C. rodentium* and incubated for 24h at 37°C. As a comparison, untreated SPF-S and SPF-R cecal content was spiked with the same number of bacteria.

Recovery of viable *C. rodentium* colonies after 24 hours revealed that the butyrate supplementation of the cecal content was sufficient to achieve an inhibitory effect comparable to the one observed in SPF-R cecal content, indicating that the total amount of butyrate is as effective as the presence of specific bacteria for the protection (Fig 34A-B).

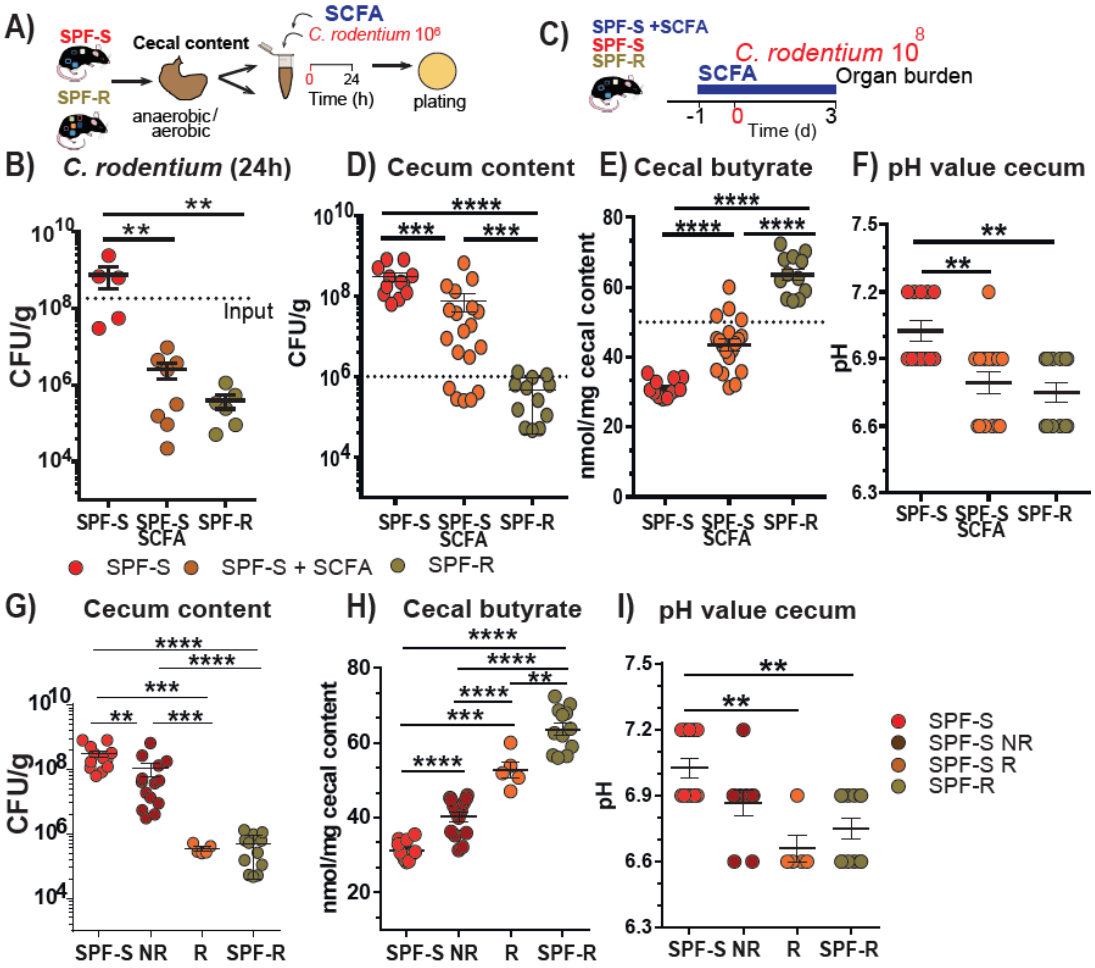

Figure 34: Supplementation of susceptible SPF-S mice with SCFA lead to reduced *C. rodentium* burden *in vitro* and *in vivo*. (A-B) Recovery of *Citrobacter* after 24 h anaerobic incubation in cecal content of SPF-S mice, SPF-S mice supplemented with 80 mM of butyrate, 50 mM acetate and 4 mM Propionate and SPF-R mice content. *P* values indicated represent a Mann-Whitney U test comparison between groups with **p<0.01. Dashed line indicates input level of *C. rodentium* (C-D) SPF-S mice were supplemented with 150 mM butyrate, 150 mM acetate and 30 mM propionate in the drinking water one day before infection until three days post infection. Untreated SPF-S and SPF-R as well as SCFA supplemented SPF-S mice were infected orally with 10^8 CFU *C. rodentium* and sacrificed three days p.i. to assess colonization. (D) *C. rodentium* CFUs in cecal lumen of individual mice of each group are displayed after day 3 p.i. Dashed line represents threshold level for resistant animals. (E) Cecal butyrate level of each group is displayed after day 3 p.i.. Dashed line represents threshold level for resistant animals. (F) Cecal butyrate level of each group is displayed after day 3 p.i. (G-I) Cecal CFUs, cecal butyrate level as well as cecal pH values are displayed for all groups. SCFA supplemented animals are grouped based on the CFU level for *C. rodentium* in the cecum after day 3 p.i.. Results represent three pooled experiments with n = 4-7 mice/group as mean ± SEM. *P* values indicated represent a Mann-Whitney U test comparison between groups with **p<0.01, ***p<0.001, ****p<0.0001 (adapted and modified from Osbelt et al., 2020).

Next, to verify these findings *in vivo*, susceptible SPF-S mice were supplemented with a SCFA mixture consisting of 150 mM butyrate, 150 mM acetate and 30 mM propionate in the drinking water (Fig 34C). Mice received SCFAs one day before infection until 3 days p.i.. Comparison of the CFUs in the cecum revealed significantly decreased CFUs in the SCFA supplemented SPF-S mice compared to untreated SPF-S mice (Fig 34D). Yet, in contrast to the SPF-R mice, mean CFUs were still significantly elevated. This coincided with only a partial restoration of protective SCFA concentration in the cecum after oral SCFA supplementation of SPF-S mice, indicating that sufficiently high concentrations of SCFAs have to be reached *in vivo* for the protection (Fig 34E). Of note, only 5 out of 19 animals reached the threshold of 50 nmol/mg butyrate which was required to abrogate *C. rodentium* growth *in vitro*. Those five responding animals achieved a fully protected phenotype similar to the SPF-R mice (Fig 34G). To exclude that those 5 animals had a different microbiota composition compared to the other animals tested, I assessed the microbiome composition before SCFA supplementation and at the end of the experiment at 3 days p.i. (Fig 35). The responding animals did not show pronounced microbiota differences before the start of SCFA supplementation in terms of species composition (Fig 35A and C) or species richness and evenness (Fig 35B). After 3 days p.i. similar microbiome compositions were observed in all three groups of SPF-S mice, except the abundance of *Enterobacteriaceae* (Fig 35C). Responder animals show significantly less *Citrobacter* compared to non-responding animals and control animals. Microbiome data supported the hypothesis that variations in the butyrate concentrations lead to changes in *Citrobacter* abundances rather than variability in the microbiota composition of the susceptible SPF microbiota. Furthermore, SCFA supplementation was sufficient to reduce the pH value to similar levels as found in resistant SPF-R mice (Fig 35F and I).

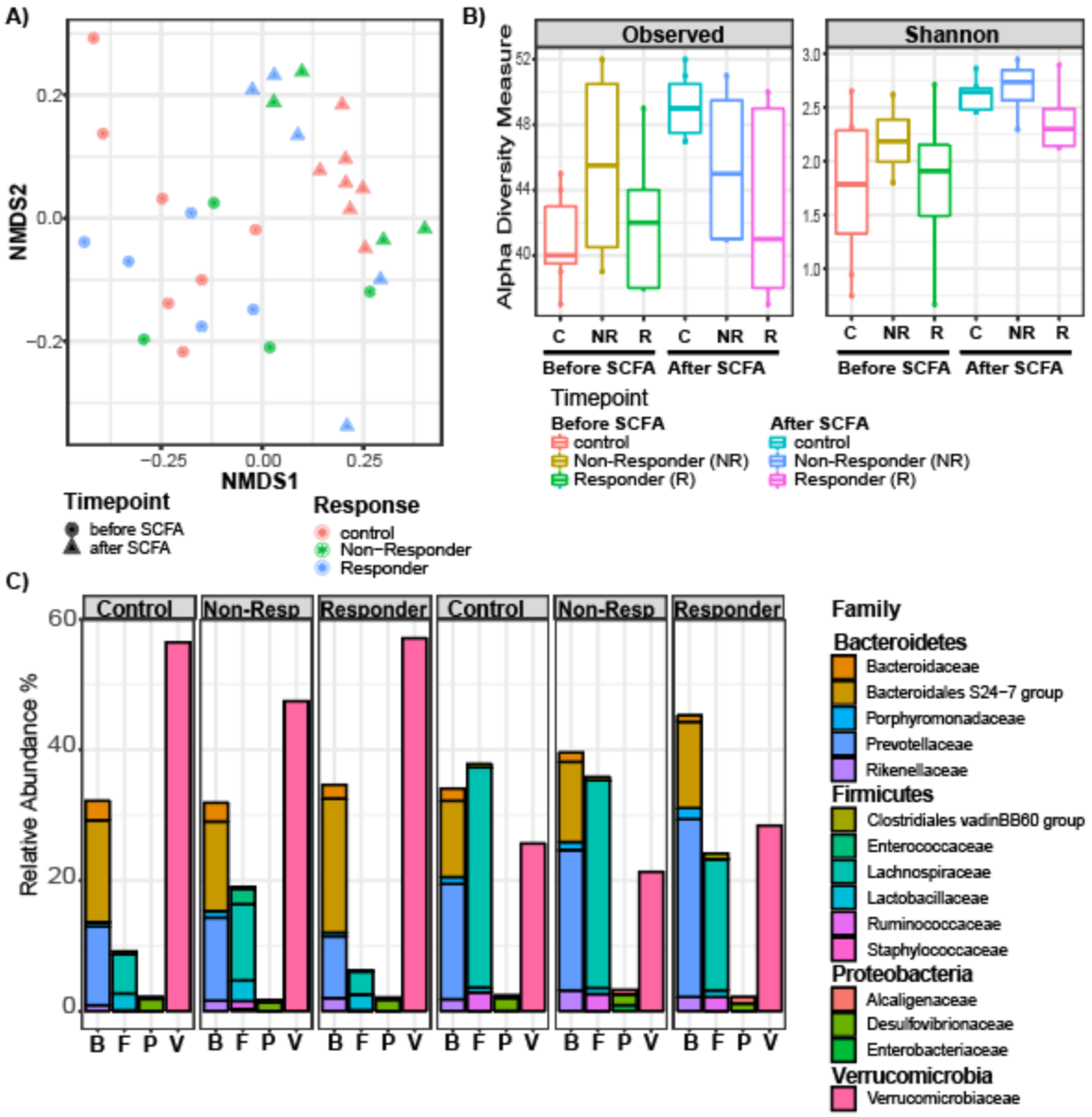

Figure 35: Short-term butyrate supplementation did not lead to major differences in the microbiome of SPF-S mice. (A) Fecal bacterial microbiota composition of butyrate supplemented animals were evaluated using 16S rRNA gene sequencing regarding to their response against *C. rodentium* infection. β-diversity was analyzed using Bray-Curtis dissimilarity matrix and NMDS. (B) α-diversity before and after SCFA supplementation in different groups of SPF-S mice was determined using Chao1 and Shannon index $p>0.05$. (C) Average microbiome level from different SPF-S mice displayed on family level (adapted and modified from Osbelt et al., 2020).

To assess the effects of butyrate specifically in the absence of the present bacteria in the SPF-S microbiota, I performed the *in vivo* butyrate supplementation in GF and antibiotic-treated SPF-S mice (Fig 36A and E). In both setups, mice received butyrate one day before infection until 3 days p.i.. In both experiments, CFUs in the cecum were partially reduced in the SCFA supplemented animals (Fig 36B and F). Corresponding SCFA values in the cecum were significantly elevated in both setups, but were overall low compared to naïve SPF-S conditions (Fig 36C and G). The cecal pH value was comparable between the untreated and treated animals but tended to be reduced in SCFA supplemented mice (Fig 36D and H). These experiments support the key role of butyrate to reduce the CFUs of *C. rodentium* under *in vitro* and *in vivo* conditions without other resident microbes.

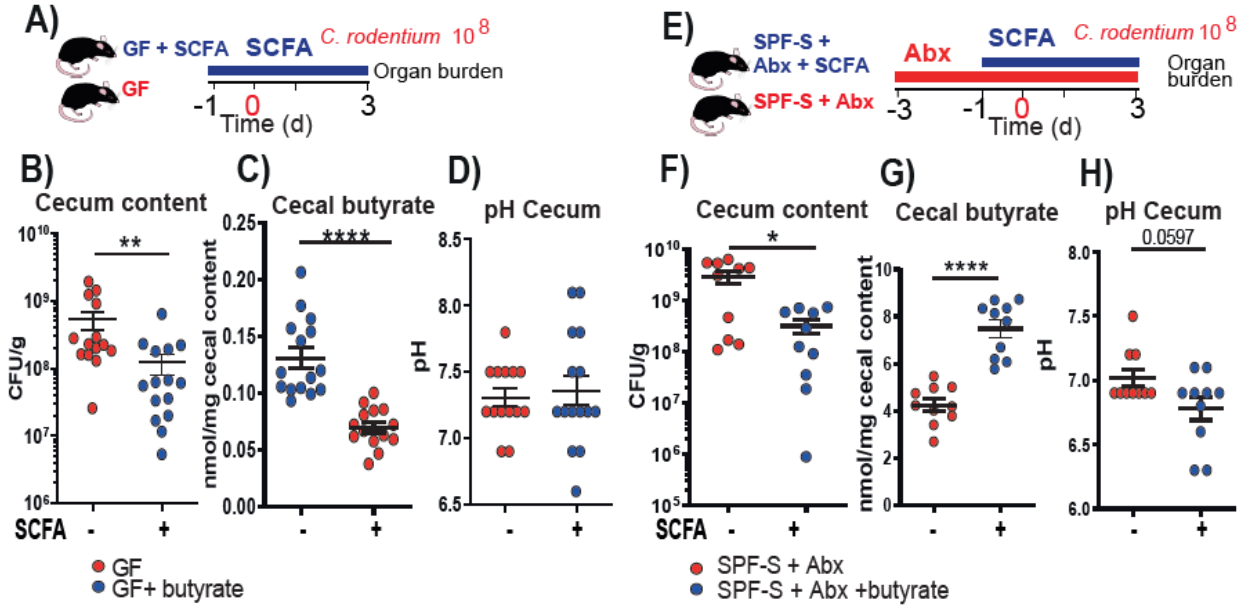

Figure 36: Supplementation of GF and antibiotic treated SPF-S mice significantly reduces *C. rodentium* CFUs. (A) C57BL6/N GF mice were supplemented with 150 mM butyrate in the drinking water one day before infection until three days post infection. (B) Cecal CFUs are displayed after day 3 p.i. (C-D) Cecal butyrate level and cecal pH of C57BL6/N GF mice supplemented with 150 mM in the drinking water at 3 days p.i. (E) Antibiotic treated SPF-S mice were supplemented with 150 mM butyrate in the drinking water one day before infection until three days post infection. (F) Cecal CFUs are displayed after day 3 p.i. (G-H) Cecal butyrate level and cecal pH at 3 days p.i. Mean and SEM of two independent experiments with n=5-9 mice per group. P values indicated represent a nonparametric Kruskal-Wallis test *p<0.05, **p<0.01, ***p<0.001, ****p<0.0001 (adapted and modified from Osbelt et al., 2020).

Taken together, these results validate that higher abundance and diversity of SCFA-producing bacteria in the cecum of SPF-R mice lead to elevated butyrate levels and reduced pH value in the lumen of the cecum, thereby efficiently reducing growth of *C. rodentium* at the early phase of infection.

3.4 Commensal *Klebsiella oxytoca* strains protect against colonization with multi-drug resistant *Klebsiella pneumoniae*

3.4.1 Pretreatment with ampicillin destroys natural colonization resistance in SPF-H mice and establishes a long term colonization of the pathogen

Due to the global spread and limited treatment options against MDR-E the fight against those pathogens has been declared as a critical priority (Cassini et al., 2019). AS FMT is an innovative tool to eradicate MDR-E without causing severe side effect but is undefined and largely uncontrollable, a growing interest in using distinct commensal species to selectively decolonize the microbiota from its MDR strains has been developed. Recently, Sorbara and colleagues proposed a gut colonization model for *K. pneumoniae* in mice (Sorbara et al., 2018). As differences in the microbiota composition strongly affect infection susceptibility, I first verified if this animal model was also suitable to model long term colonization of MDR *K. pneumoniae* in SPF and gnotobiotic animals in our facility. To do so, SPF mice with our in house microbiota (SPF-H) were treated for 6 consecutive days with ampicillin and colonized on day 3 of treatment with 10^8 CFUs K. pn MDR1, a clinical isolate belonging to ST395 previously described and used in the human *in vitro* assays (see chapter 3.1.1). Untreated SPF-H mice were taken as a control. Mice were monitored over 6 weeks for BWL and fecal colonization. Fecal samples were also used for 16S rRNA gene sequencing at the indicated time points (Fig 37A). Antibiotic- naïve SPF mice showed a high degree of colonization resistance and could clear out K. pn MDR1 in most of the cases after 14 days. Ampicillin treated mice showed a significant higher pathogen burden especially at the beginning with CFUs reaching up to 10^9 CFUs/ml compared to 10^3 to 10^4 CFUs/ml in control mice. In addition, these mice were unable to clear K. pn MDR1 even after 6 weeks of colonization suggesting a stable long-term integration of *K. pneumoniae* in the microbiome of amp-treated mice (Fig 37B). Weight loss or any sign of infection was absent in both groups, indicating that *K. pneumoniae* is an asymptomatic colonizer in healthy mice (Fig 37C). Next, changes in the microbiota during the six weeks of K. pn MDR1 colonization were assessed. Regarding species richness, no changes could be observed in the microbiota of control mice, whereas richness of the amp-treated animals was almost reduced to zero after 1 day post colonization (p.c.). After the end of amp treatment, species richness recovered over time almost reaching levels similar to control animals after six weeks. Nevertheless, species evenness in this animals was still lower after 6 weeks of colonization indicating that some long-term effects were still visible due to the antibiotics treatment (Fig 37D).

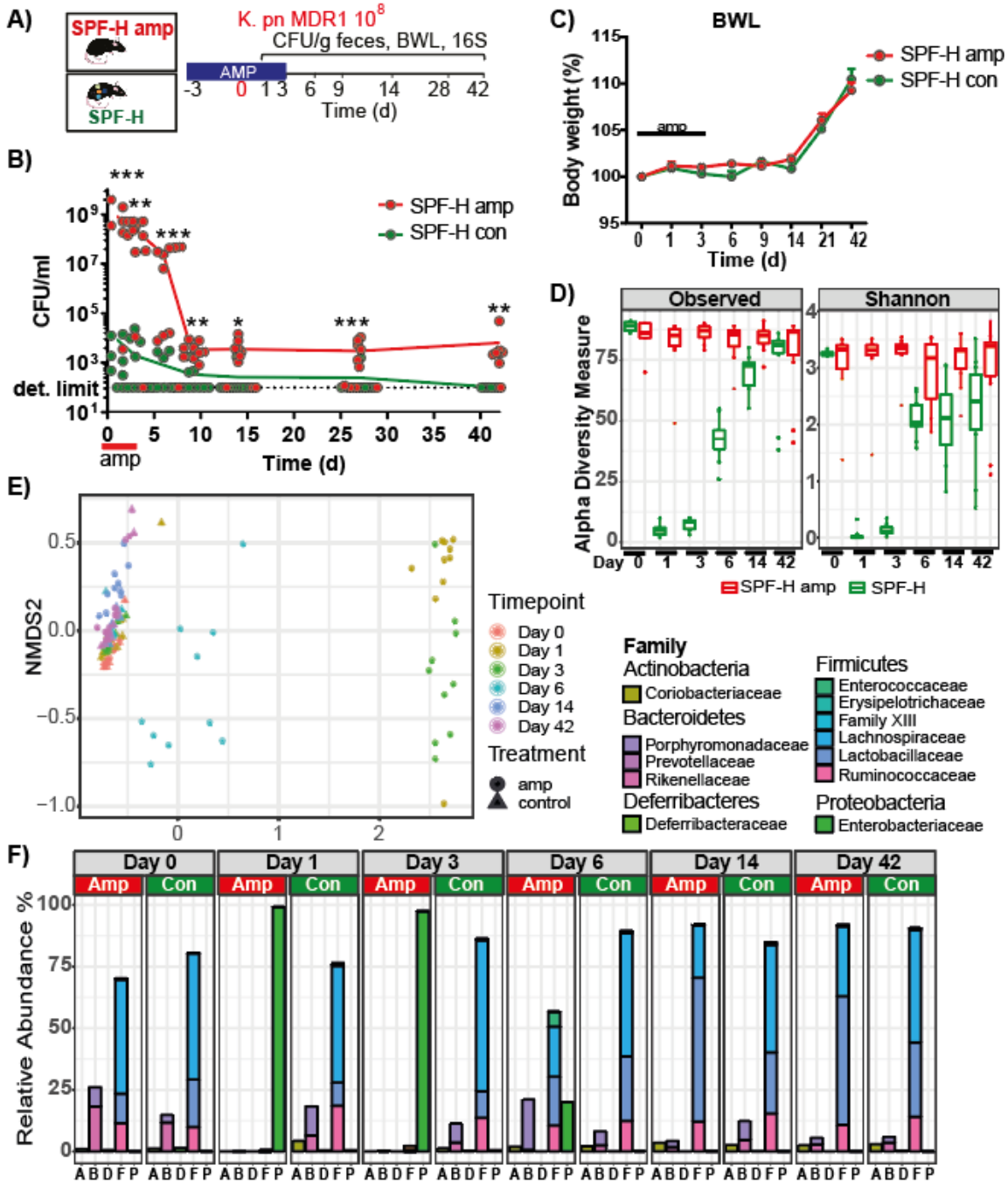

Figure 37: Ampicillin treatment renders SPF-H mice long-term susceptible to *K. pneumoniae* colonization. (A) SPF-H were pretreated with ampicillin in the drinking water for six consecutive days or left untreated as a control. After 3 days of treatment mice were colonized with 10^8 CFU/g K. pn MDR1 and feces were collected at indicated time points for determination of pathogen burden and 16S rRNA gene sequencing. (B) Resulting fecal burden of K. pn MDR1 after different time points of colonization. (C) Body weight was monitored during the course of the experiment. (D) α-diversity after different time points of colonization in amp treated and control mice was determined using Chao1 and Shannon index. (E) β-diversity was analyzed using Bray-Curtis dissimilarity matrix and NMDS. (F) Average microbiome composition after different time points of colonization from amp- treated SPF-H mice and control animals are displayed on family level. Mean and SEM of two independent experiments with n=5-9 mice per group. P values indicated represent a nonparametric Kruskal-Wallis test *p<0.05, **p<0.01, ***p<0.001.

Similarly beta diversity and species composition was severely affected during the early time points (day 1 and 3) clustering apart from all other samples and showing almost no other species beside *K. pneumoniae* in these animals (Fig 37E-F). After the end of the ampicillin treatment, species composition almost completely recovered, but levels of Lactobacilli remained higher compared to control animals (Fig 37F). Taken together, this colonization model established a stable long-term colonization in healthy mice without body weight loss or other signs of infection thereby making it a useful model to study the impact of specific commensal regarding their potential to prevent or decolonize MDR K. pn from the dysbiotic mouse gut and to reestablish homeostatic microbiome conditions.

3.4.2 The ampicillin mouse model induces reproducible and robust colonization with different *Klebsiella pneumoniae* strains

To test whether the established colonization model is also working for other relevant *Klebsiella* strains, SPF-H mice were colonized with another MDR strain from the highly relevant ST258 (K. pn MDR2) which is a major spread in the US and a hypervirulent strain belonging to the ST66 (K.pn HV) (Fig 38A). As a control amp-treated SPF-H mice were colonized with K. pn MDR1. Both strains achieved similar CFUs as the initially tested K. pn MDR1 (Fig 38B) Of note, MDR1 strain achieved significantly higher colonization at the early time points compared to HV, whereas MDR2 achieved higher colonization compared to MDR1 at later time point of colonization.

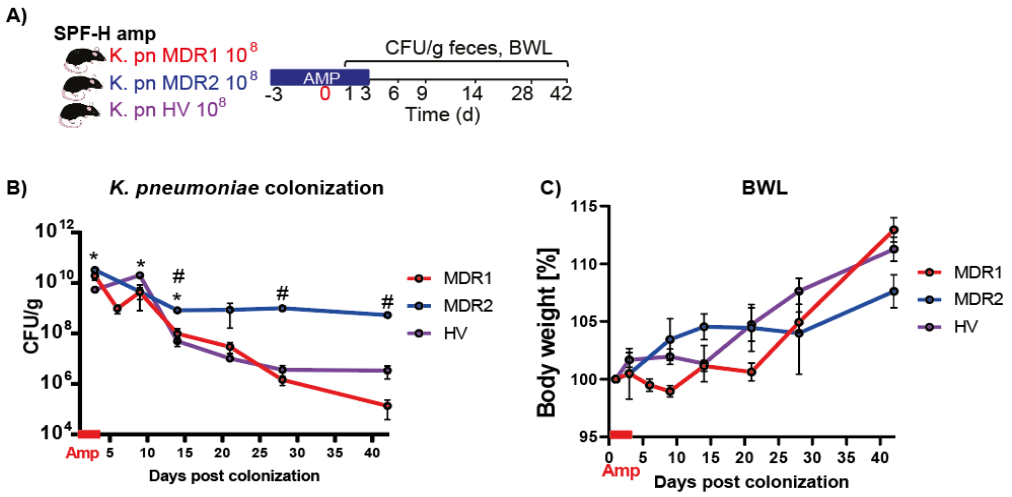

Figure 38: Colonization of SPF-H mice with different pathogenic *K. pneumoniae* strains. (A) SPF-H were pretreated with ampicillin in the drinking water for six consecutive days or left untreated as a control. After 3 days of treatment mice were colonized with 10^8 CFU/g of MDR or HV *K. pneumoniae* strains (MDR1, MDR2 and HV) and feces were collected at indicated time points for determination of pathogen burden. (B) Resulting fecal burden of *K. pneumoniae* after different time points of colonization. (C) Body weight was monitored during the course of the experiment. Mean and SEM of two independent experiments with n=5-9 mice per group. P values indicated represent a nonparametric Kruskal-Wallis test *p<0.05 (MDR1 vs. HV) or #p<0.05 (MDR1 vs. MDR2).

None of the mice cleared any of the strains tested even after six weeks of colonization indicating that the ampicillin mouse model works for *Klebsiella* strains in general. Similarly to what was observed with K.pn MDR1, mice did not lose any weight for the other strains tested indicating that immunocompetent mice did not suffer from infection with those strains. Taken together, the established model will be ideal to study the impact of commensal strains on the protection and decolonization against pathogenic MDR *Klebsiella* strains.

3.4.3 Gnotobiotic Oligo-MM^{12} mice and GF mice are naturally susceptible to MDR *K. pneumoniae* and are unable to clear the pathogen.

As a parallel approach, I wanted to establish a colonization model in naturally susceptible mice without antibiotic intervention and in more defined microbiota settings. To do so, Oligo-MM^{12} mice, which harbor 12 specific bacterial strains and no other γ-Proteobacteria as well as GF mice, which are devoid of any bacteria in the gut, were colonized with the K. pn MDR1 and fecal CFUs, body weight as well as the microbiota composition was assessed during 6 weeks of colonization (Fig 39A). As expected, Oligo-MM^{12} and GF mice were highly susceptible to *K. pneumoniae* colonization reaching high CFUs of almost 10^{10} CFU/g feces in GF mice and 10^{8} CFU/g after 1 day in Oligo-MM^{12} mice. Colonization remained stable over the whole time course of six weeks in both mouse lines and none of the mice was able to clear the pathogen from the gut (Fig 39B).

Similarly, to what was observed in SPF-mice, Oligo-MM^{12} mice did not lose any weight during the colonization (Fig 39C). In contrast, GF mice approximately lose 5% of body weight after challenge with K.pn MDR1 but recovered to 100% of body weight after 14 days. In total, Oligo-MM^{12} mice and GF did not gain as much weight as SPF- mice suggesting that *K. pneumoniae* challenge induced potentially some mild infection in these mice. This was supported by mild diarrhea in these mice, which was completely absent in SPF-mice supporting the role of a more complex microbiome in colonization resistance against *K. pneumoniae*. No major changes could be observed in the microbiome of Oligo-MM^{12} mice upon introduction of *K. pneumoniae* and no real clustering could be observed over the different time points (Fig 39D). Analysis of the species composition on genus level could not reveal any changes in the proportion of different species except for increasing abundance of *K. pneumoniae* until day 14 from where the ratio of K.pn MDR1 remained stable until day 42 (Fig 39E). Taken together, these colonization models are suitable to study the impact of selected species in defined microbiota settings for Oligo-MM^{12} mice or in a direct competition model of a defined bacterium against *K. pneumoniae* in GF animals.

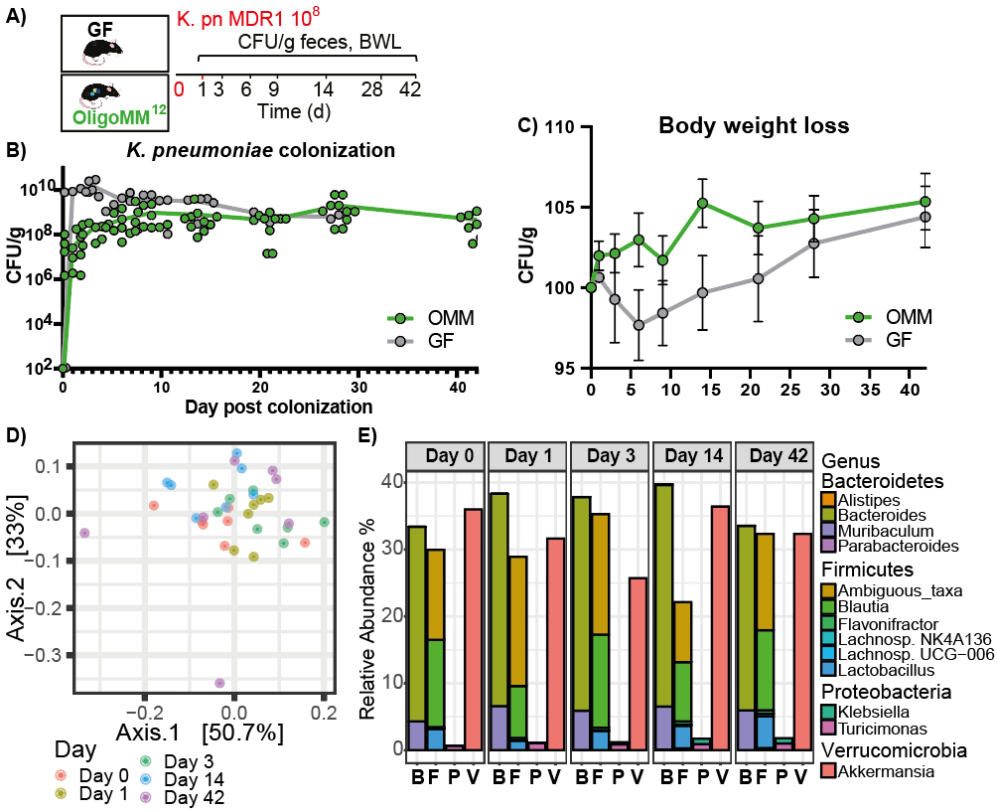

Figure 39: Oligo-MM[12] mice and GF mice are naturally susceptible to *K. pneumoniae*. (A) Oligo-MM[12] mice and GF animals were colonized with 10^8 CFU/g of K.pn MDR1 and feces were collected at indicated time points for determination of pathogen burden. (B) Resulting fecal burden of K.pn MDR1 after different time points of colonization. (C) Body weight was monitored during the course of the experiment. (D) β-diversity was analyzed using a PCoA plot. (E) Average microbiome composition after different time points of colonization of Oligo-MM[12] mice are displayed on family level. Results represents Mean and SEM of two independent experiments with n=4-5 mice per group. P values indicated represent a nonparametric Kruskal-Wallis test ns p>0.05.

3.4.4 Screening of human stool samples for commensal *Klebsiella* strains revealed high prevalence of *K. oxytoca* in protected stool samples.

After establishment of different animal models, I next aimed to isolate promising candidates to compete with MDR *K. pneumoniae* strains. For this purpose, different age groups of healthy volunteers were screened for commensal *Klebsiella* strains as we expected higher abundances of facultative anaerobes in the developing microbiome of children (Sekirov et al., 2010). In total, 59 healthy adults (MikroResist) and 54 healthy children (MikroKids) were recruited. For selection, fecal samples were streaked out on MacConkey agar plates with amp (MC+amp) as ampicillin resistance is present in 98% of all *Klebsiella* strains through presence of a chromosomal beta- lactamase (Livermore et al., 1995) and MacConkey agar is selective for enterobacteria. Grown colonies were picked and screened using a specific PCR and positive clones were subsequently send for sequencing (Fig 40A).

In addition, an aliquot was used to perform the *in vitro* growth assay with K. pn MDR1 to simultaneously define the colonization susceptibility of each individual. In total, 32 *Klebsiella* strains could be isolated from 29 healthy individuals. 16 species from 13 healthy adult volunteers and 16 species from 15 healthy children. The strain collection included 11 strains of *K. pneumoniae*, one strain of *K. quasipneumoniae*, one strain of *K. variicola* and 19 strains of *K. oxytoca* (Tab 28). From 59 healthy adults, 13 individuals were positive for commensal *Klebsiella* strains, which equals a prevalence of 22%. In children, the occurrence was slightly higher with 27.8 % as 15 out of 54 screened children were positive for *Klebsiella*. In both populations, occurrence of *Klebsiella* strains was rather associated with reduced CFUs as strains could only be isolated from resistant or intermediate individuals (Fig 40B-C). Of note, PCR based screening was only performed in the children cohort, thereby giving a trustable quantitative read-out only for this cohort. Interestingly, children showed overall reduced CFUs compared to the adult cohort and harbored significantly more *K. oxytoca* strains with two particularly resistant samples (MK1901 and MK1903) harboring high levels of a commensal *K. oxytoca* strain indicating that this species might be an interesting target for further analysis of protective capacities against *K. pneumoniae* (Fig 40B-C).

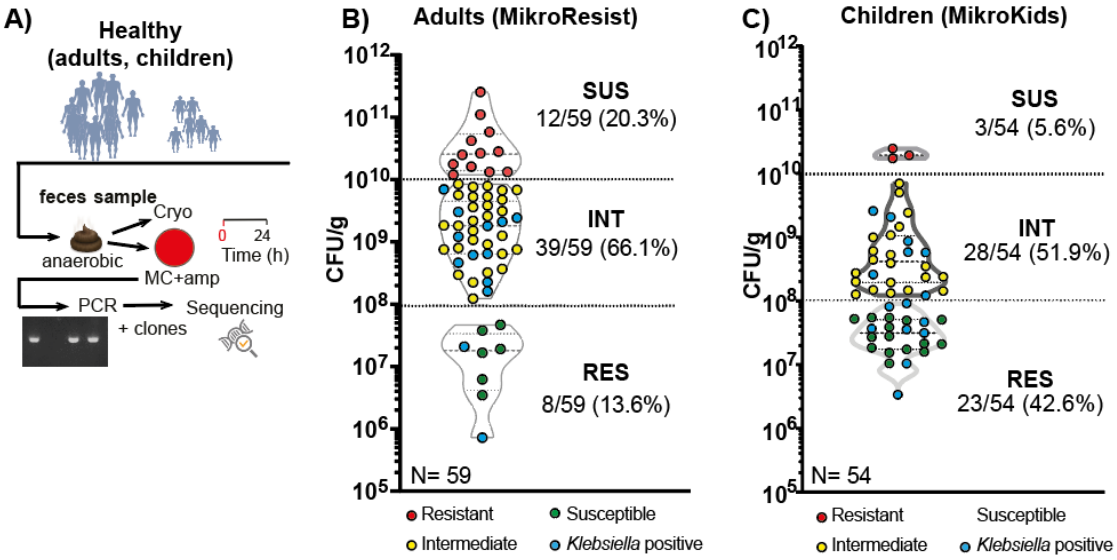

Figure 40: Occurrence of *Klebsiella* species in healthy human cohorts. (A) Workflow of *Klebsiella* isolation. Feces samples were plated on MacConkey agar plates containing ampicillin (MC+amp) as a selection marker. Grown colonies were screened with *Klebsiella* specific PCR and positive clones were send for sequencing and cryopreserved for further testing. (B) Prevalence of commensal *Klebsiella* species in adult MikroResist cohort (blue dots) in resistant (RES= green dots), intermediate (INT=yellow) and susceptible (SUS=red dots) stool samples inoculated with K. pn MDR1. (C) Prevalence of commensal *Klebsiella* species in MikroKids cohort (blue dots) in resistant (RES= green dots), intermediate (INT=yellow) and susceptible (SUS=red dots) stool samples inoculated with K. pn MDR1. Results represents mean of two replicates for n= 113 individuals.

Table 28: Commensal *Klebsiella* strain isolated from healthy volunteers

No	Donor	Species	Origin	Colony No.	Age-group	Sequence-type	Resistance phenotype[1]
1	MR1906	*K.variicola*	Stool	135	adult	ST697	ampicillin
2	MR1954	*K.quasipneumoniae*	Stool	145	elderly	ST144	ampicillin, chloramphenicol
3	MK1901	*K. pneumoniae*	Stool	78	infant	ST200	ampicillin, fosfomycin, chloramphenicol
4	MK1950	*K. pneumoniae*	Stool	100	adult	ST1764	ampicillin, ceftriaxone, fosfomycin, chloramphenicol
5	MK1949	*K. pneumoniae*	Stool	111	adult	ST86	ampicillin, chloramphenicol
4	MK1950	*K. pneumoniae*	Stool	112	adult	ST1764	ampicillin, ceftriaxone, fosfomycin, chloramphenicol
6	MR1906	*K. pneumoniae*	Stool	133	adult	ST1693	ampicillin, fosfomycin, chloramphenicol
7	MK1907	*K. pneumoniae*	Stool	147	youth	ST2097	ampicillin, chloramphenicol
8	MK1908	*K. pneumoniae*	Stool	149	youth	ST86	ampicillin
9	MR1909	*K. pneumoniae*	Stool	151	adult	ST23	ampicillin, fosfomycin, chloramphenicol
10	MR1919	*K. pneumoniae*	Stool	156	adult	ST395	ciprofloxacin I/R, gentamicin, streptomycin, ampicillin, ceftriaxone, amoxicillin/clavulanic acid, cefoxitin, meropenem, chloramphenicol, fosfomycin, amikacin, kanamycin, sulfisoxazole
11	MR1910	*K. pneumoniae*	Stool	157	adult	ST395	gentamicin, ciprofloxacin I/R, streptomycin, ampicillin, ceftriaxone, amoxicillin/clavulanic acid, cefoxitin, meropenem, chloramphenicol, fosfomycin, amikacin, kanamycin, sulfisoxazole
12	MR2001	*K. oxytoca*	Stool	1	adult	none	ampicillin (P)
13	MR2002	*K. oxytoca*	Stool	2	adult	none	ampicillin (P)
14	MR2003	*K. oxytoca*	Stool	3	adult	none	ampicillin (P)
15	MR2004	*K. oxytoca*	Stool	4	adult	none	ampicillin (P)
16	MK2005	*K. oxytoca*	Stool	5	toddler	none	ampicillin (P)
17	MK2009	*K. oxytoca*	Stool	9	child	none	ampicillin (P)
18	MK2012	*K. oxytoca*	Stool	12	child	none	ampicillin (P)
19	MK2013	*K. oxytoca*	Stool	13	toddler	none	ampicillin (P)
20	MK2014	*K. oxytoca*	Stool	14	toddler	none	ampicillin (P)
21	MK2016	*K. oxytoca*	Stool	16	child	none	ampicillin (P)
22	MK2018	*K. oxytoca*	Stool	18	toddler	none	ampicillin (P)
23	MK1903	*K. oxytoca*	Stool	17	infant	none	ampicillin
24	MK2019	*K. oxytoca*	Stool	19	child	none	ampicillin (P)
25	MK2020	*K. oxytoca*	Stool	20	child	none	ampicillin (P)
26	MK2021	*K. oxytoca*	Stool	21	toddler	none	ampicillin (P)
27	MK1901	*K. oxytoca*	Stool	22	toddler	none	ampicillin
28	MK2035	*K. oxytoca*	Stool	35	toddler	none	ampicillin (P)
29	MK2036	*K. oxytoca*	Stool	36	toddler	none	ampicillin (P)
30	MK2050	*K. oxytoca*	Stool	50	infant	none	ampicillin (P)

[1] Resitance phenotype was predicted by bioinformatical analysis and phenotypical screening, if not indicated otherwise. Strains marked with (P) were only phenotypically screened for resistance.

To analyze spread of antibiotic resistance in the *Klebsiella* isolates, genomes were sequenced using Illumina sequencing and analyzed regarding resistance genes to predict the resistance phenotype (Tab 28). In addition, strains were screened using antibiotics susceptibility testing kits to verify the predicted phenotypes. As expected, all of the isolates were resistant against ampicillin, confirming the occurrence of natural resistance against the antibiotics class of penicillins in *Klebsiella*. Of note, all *K. oxytoca* strains, the *K. variicola* strain and *K. pneumoniae* (MR1908) did not exhibit any further resistance genes, whereas all other commensal *K. pneumoniae* strains showed at least one additional resistance with some of the strains belonging to ST395 showing even multi-drug resistance. Microbiological resistance testing verified the bioinformatics prediction. Of note, whole genome sequencing data from 17 *K. oxytoca* strains have not yet been investigated, but the bioinformatics prediction of the first two *K. oxytoca* isolates verifying the microbiological screening results of antibiotics resistances.

Taken together, *K. oxytoca* exhibited far less wide-spread of antibiotics resistance as commensal *K. pneumoniae* strains. This analysis further supports the idea to focus on *K. oxytoca* strains as a potential target to fight MDR *K. pneumoniae* as transfer of resistance may be less common as for the exact same species but metabolically and ecologically behavior of this related strain should be still relatively similar.

3.4.5 Addition of *K. oxytoca* to amp treated cecal content efficiently reduces CFUs of recovered *K. pneumoniae*

To test whether commensal *K. oxytoca* strain isolated from protected individuals affect growth of MDR *K. pneumoniae in vitro,* SPF-H mice were treated with ampicillin for six consecutive days to diminish their natural colonization resistance. One day before sacrifice, mice were treated with *K. oxytoca* strain isolated from donor MK1903 (K. oxy A), MK1901 (K. oxy B) or left untreated as a control (Fig 41A). Precolonization was assessed the next day by plating the isolated cecal content on selective agar plates. Cecal content was spiked with 10^6 CFUs of K. pn MDR1 and incubated for 24h under anaerobic conditions before content was plated on LB-chloramp plates to recover viable amounts of K. pn MDR1. All animals were successfully colonized with *K. oxytoca* but amounts of recovered CFUs varied strongly between the mice (Fig 41B). Ampicillin treatment eradicates most microbes from the SPF-H microbiota resulting in a significant increase of pH value in all treated groups compared to the untreated control group, which was not affected by the precolonization with *K. oxytoca* (Fig 41C). Strikingly, recovered CFUs of K. pn MDR1 were significantly reduced upon precolonization with *K. oxytoca* (Fig 41D), but only some animals reached the same level of protection as the control animals with an intact microbiota.

I observed a strong anti-correlation between the level of precolonization with *K. oxytoca* and the resulting CFUs of MDR *K. pneumoniae* with a coefficient of determination $R^2 = 0.59$ for K. oxy A and $R^2 = 0.68$ for K. oxy B indicating that *K. oxytoca* has the potential to reduce MDR *K. pneumoniae* but the amounts of protective bacteria needs to overcome a certain threshold to achieve a protective effect under *in vitro* conditions.

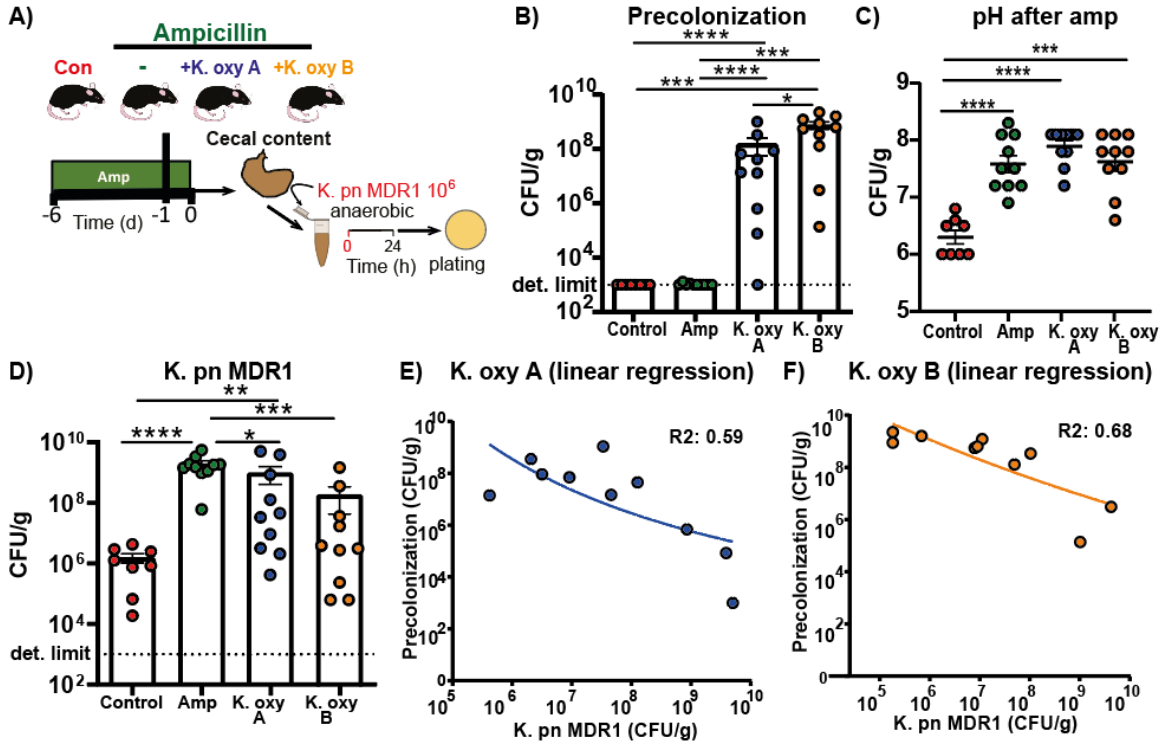

Figure 41: Addition of *K. oxytoca* to susceptible cecal content reduces CFUs of MDR *K. pneumoniae*. (A) SPF-H mice were treated with ampicillin for 6 consecutive days or left untreated as a control. At day 5 of treatment mice were colonized with 10^8 CFUs K. oxy A or K. oxy B overnight. The next day mice were sacrificed, cecal content was isolated, aliquoted and diluted 1:1 with BHI. Aliquots were spiked with 10^6 CFUs K. pn MDR1 and incubated for 24 h anaerobically before streaking on selective agar plates. (B) Rates of *K. oxytoca* precolonization in the different groups recovered on LB-amp plates. (C) pH values measured in the cecum of the differentially treated SPF-H mice. (D) Recovered CFUs of K. pn MDR1 in differentially treated SPF-H mice. (E-F) Linear regression curves of *K. oxytoca* precolonization levels plotted against resulting CFUs of K. pn MDR1. Mean and SEM of two independent experiments with n=4-5 mice per group. P values indicated represent a nonparametric Kruskal-Wallis test *p<0.05, **p<0.01, ***p<0.001, ****p<0.0001.

3.4.6 Pretreatment of antibiotic-treated mice with probiotic *K. oxytoca* facilitates clearance of MDR *K. pneumoniae* from the feces

Next, I wanted to test whether *K. oxytoca* could also help to clear MDR *K. pneumoniae* in antibiotic disturbed microbiota situations *in vivo*. To do so, SPF-H mice were precolonized with K. oxy A or K. oxy B for two weeks before colonization with 10^8 CFUs of K. pn MDR1.

Mice received ampicillin for 6 consecutive days during each intervention three days before until three days after colonization. Feces were taken after different time points of precolonization and colonization to assess levels of *K. oxytoca* and MDR *K. pneumoniae* (Fig 42A). As observed before, none of the mice lost body weight upon colonization with *K. oxytoca* or MDR *K. pneumoniae* (Fig 42B). Precolonization levels were comparable between both groups of *K. oxytoca* colonized mice but some mice showed reduced levels of colonization in the K. oxy A group (Fig 42C). Colonization kinetics revealed that both groups colonized with *K. oxytoca* strains exhibit significantly reduced levels of K. pn MDR1 (Fig 42D).

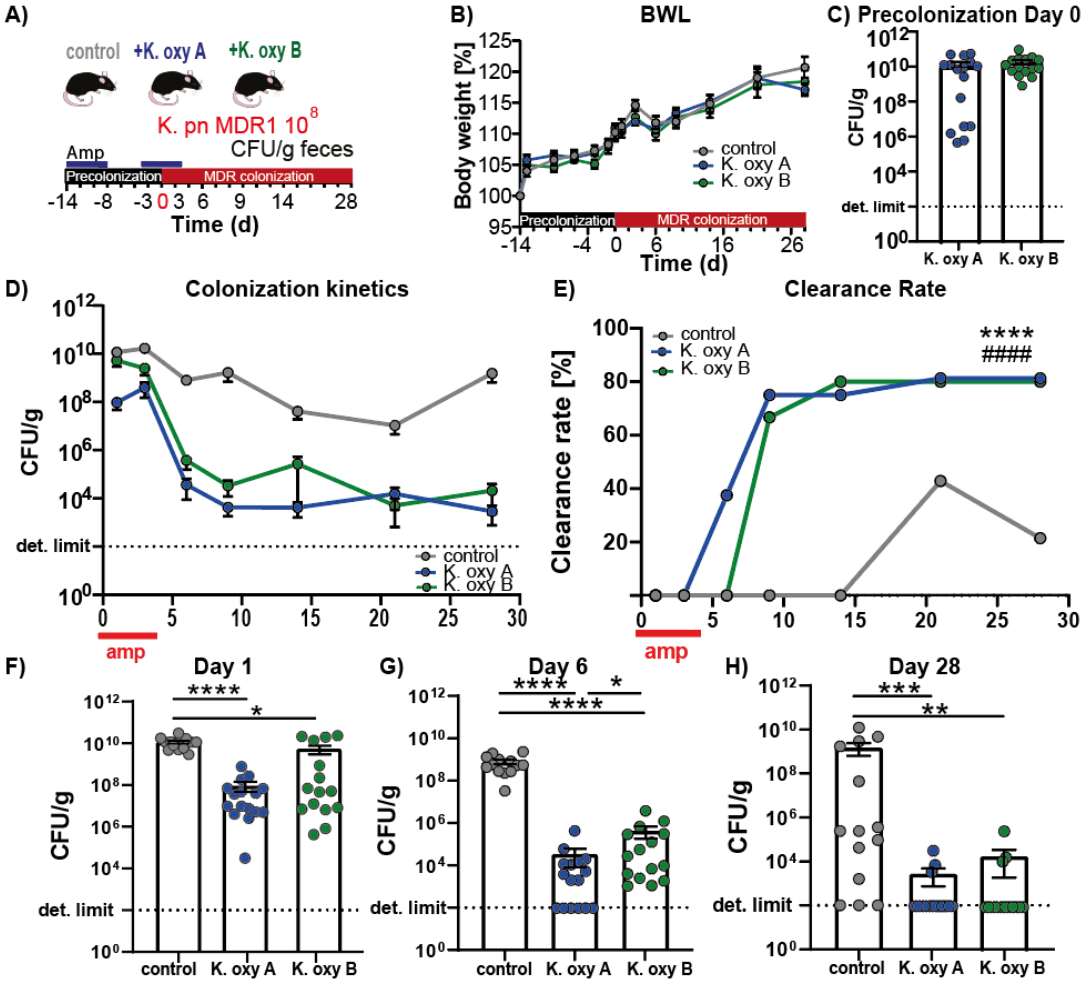

Figure 42: *K. oxytoca* increases clearance rates after antibiotic intervention in susceptible SPF-H mice. (A) SPF-H mice were treated with ampicillin for 6 consecutive days and precolonized with 10^8 CFUs K. oxy A or K. oxy B for two weeks before colonization. At day -3 of precolonization mice received a second cycle of ampicillin and were colonized with 10^8 CFUs K. pn MDR1 at day 0. CFUs were determined at indicated time points of colonization. (B) BWL over the course of the experiment. (C) Rates of *K. oxytoca* precolonization in the different groups recovered on LB-amp plates at day 0. (D) Colonization kinetics of CFUs of K. pn MDR1 in differentially treated SPF-H mice. (E) Clearance rates of K. pn MDR1 in differentially treated SPF-H mice. P values indicated represent a log-rank test ****p<0.0001 (control vs. K. oxy A), ####p<0.0001 (control vs. K. oxy B). (F-H) CFUs of K. pn MDR1 in the different groups after 1, 6 and 28 days p.c.. Mean and SEM of three independent experiments with n=4-7 mice per group. P values indicated represent a nonparametric Kruskal-Wallis test *p<0.05, **p<0.01, ***p<0.001, ****p<0.0001.

The effects were similar in both colonized groups but K. oxy A seems to reduce MDR *K. pneumoniae* faster than K. oxy B (Fig 42F-H). The clearance rates supported the observation of the CFU kinetics. *K. oxytoca* pretreated animals could clear MDR *K. pneumoniae* faster and up to 80% (13/16 animals for K. oxy A and 12/15 animals for K. oxy B) cleared the colonization after 28 days, whereas control animals could only clear the pathogen in 21.4 % of the cases (3/14 animals). Clearance in K. oxy A group was faster, as a high number of animals (6/16 = 37.5%) could clear the pathogen after 6 days already (Fig 42E). This experiments demonstrates that *K. oxytoca* efficiently reduces fecal CFUs of MDR *K. pneumoniae* and supports clearance from the microbiome of colonized animals.

3.4.7 Protective effect is specific for human *K. oxytoca* strains and generally effective against another MDR *K. pneumoniae* strain

To address the questions whether the protective effect is limited to a specific strain of *K. oxytoca*, is common for the species *K. oxytoca* in general or might also be present in other related species like *E. coli*, ampicillin treated SPF-H were colonized with different *K. oxytoca* strains isolated from humans (#21, #35, #36) or mice (CR) next to K. oxy A as a control and a commensal *E. coli* strain isolated from a healthy volunteer (#103) (Fig 43A).

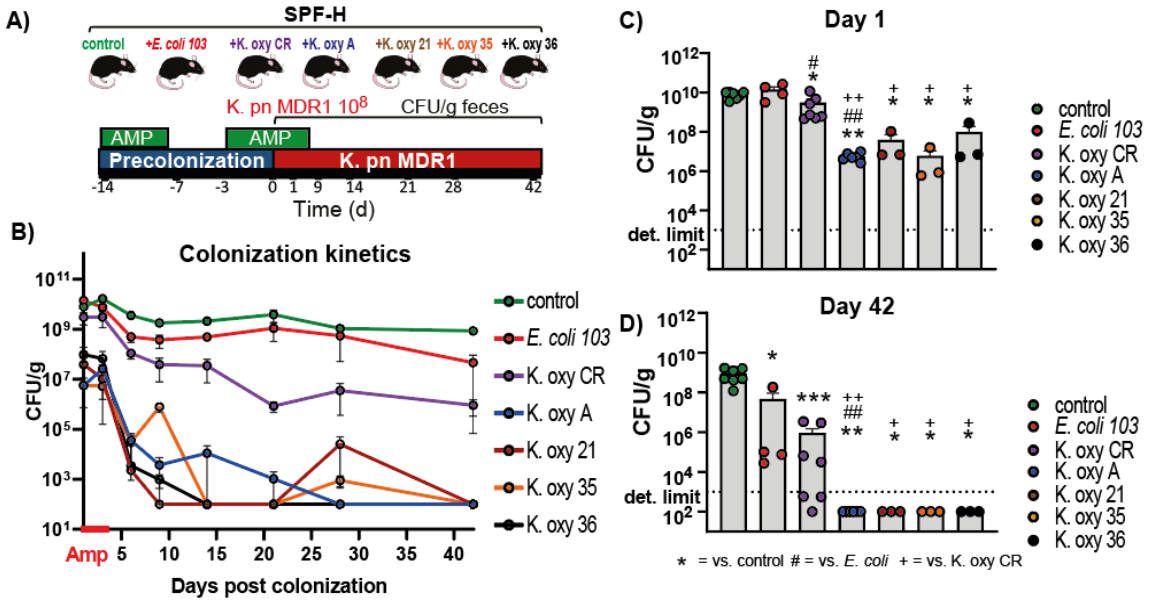

Figure 43: Protective effect of *K. oxytoca* is common for different isolates but species specific. (A) Ampicillin treated SPF-H mice were colonized with different *K. oxytoca* strains, *E. coli* or left uncolonized for 2 weeks prior colonization with K. pn MDR1. Fecal burden of the pathogen was assessed at different time points after the colonization. (B) Colonization kinetics of K. pn MDR1 in differentially colonized SPF-H mice. (C-D) Fecal colonization of K. pn MDR1 after 1 and 42 days p.c.. Mean and SEM of one or two independent experiments with n=3-4 mice per group. P values indicated represent a nonparametric Kruskal-Wallis test *p<0.05, **p<0.01 (strains vs. control), # p<0.05, ##p<0.01 (strains vs *E. coli*), +p<0.05, ++p<0.01 (strains vs. K. oxy CR).

I observed similar colonization kinetics in the other human *Klebsiella* isolates (#21, #35, #36) compared to K. oxy A with faster clearance rates and significantly reduces CFUs already after 1 day p.c.. The mouse commensal *K. oxytoca* strain isolated from SPF mice with Charles River microbiota exhibited a less pronounced protective effect regarding reduction of fecal CFUs and enhanced clearance (Fig 43B-D). Nevertheless, CFUs were still significantly reduced and remained stable at a reduced level until the end of the experiment (Fig 43B and D). In contrast, commensal human *E.coli* did not lead to significant reduction in the beginning and did not lead to total clearance of K. pn MDR1 after 6 weeks of colonization indicating that the protective effect is specific to the species *K. oxytoca*, occurs most strongly in human isolates but is less pronounced in a mouse-commensal *K. oxytoca* isolate.

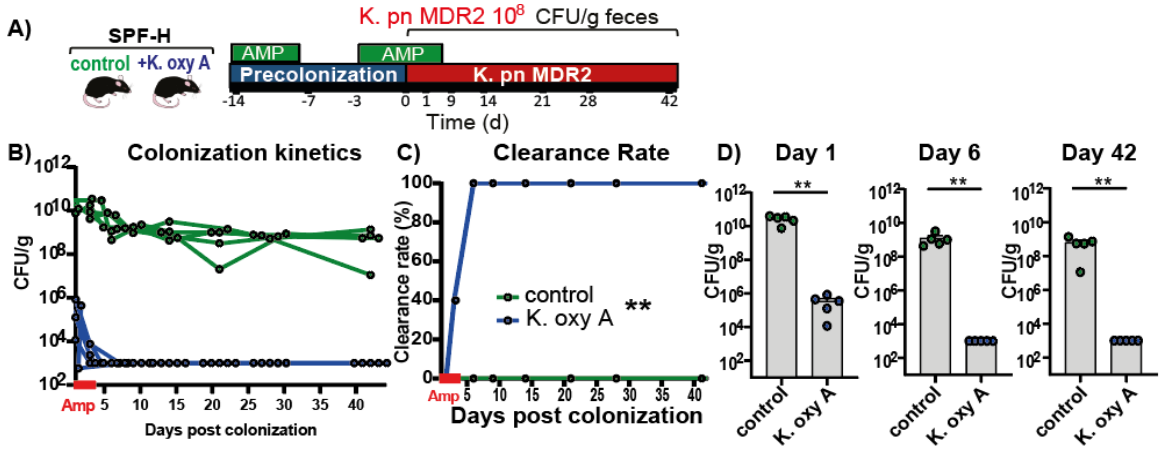

Figure 44: *K. oxytoca* protects against another common MDR *K. pneumoniae* strain. (A) SPF-H mice were treated with ampicillin and precolonized with K. oxy A prior colonization with K. pn MDR2. Fecal colonization was assessed at indicated time points of the colonization (B) Colonization kinetics of K. pn MDR2 in precolonized and control animals. (C) Clearance rates of K. pn MDR2 in precolonized and control animals. P value indicated represent a log-rank test **p<0.01. (D) Fecal burden of K. pn MDR2 on day 1, 6 and 42 after colonization. Mean and SEM of one independent experiment with n=5 mice per group. P values indicated represent a nonparametric Kruskal-Wallis test **p<0.01.

To investigate if the effect of *K. oxytoca* would also lead to the same level of protection against other MDR *K. pneumoniae* strains, ampicillin treated mice were colonized with K. oxy A or left uncolonized as a control. After two weeks, mice were colonized with K. pn MDR2 and fecal colonization was assessed after different time points of colonization (Fig 44A). K. oxy A efficiently reduced fecal CFUs of colonized mice already by day 1 by a factor of 10,000 (Fig 44B and D). After 6 days, precolonized mice completely cleared K. pn MDR2 from the feces (Fig 44 B and D), resulting in a clearance rate of 100 %, which was even more efficient than initially observed for K. pn MDR1 with rates above 80% (Fig 42E, Fig 44C). Taken together, these experiments revealed that human *K. oxytoca* strains exhibit a specific effect which is not observed with other commensal related enterobacteria such as *E. coli* and seem to have a broad-spectrum activity against different MDR *K. pneumoniae* strains.

3.4.8 Probiotic *K. oxytoca* protects naturally susceptible Oligo-MM^{12} mice from colonization and is able to directly compete with MDR *K. pneumoniae* at the early phase of colonization in GF mice

Next, I aimed to address the question whether *K. oxytoca* could also prevent colonization of MDR *K. pneumoniae* in gnotobiotic and GF mice which are naturally susceptible to colonization. First, Oligo-MM^{12} mice were colonized with K. oxy A, K. oxy B or *E.coli* 103 two weeks prior colonization with MDR *K. pneumoniae* and fecal colonization was monitored over 28 days (Fig 45A). Similar effects could be observed as initially seen in ampicillin treated SPF-H mice.

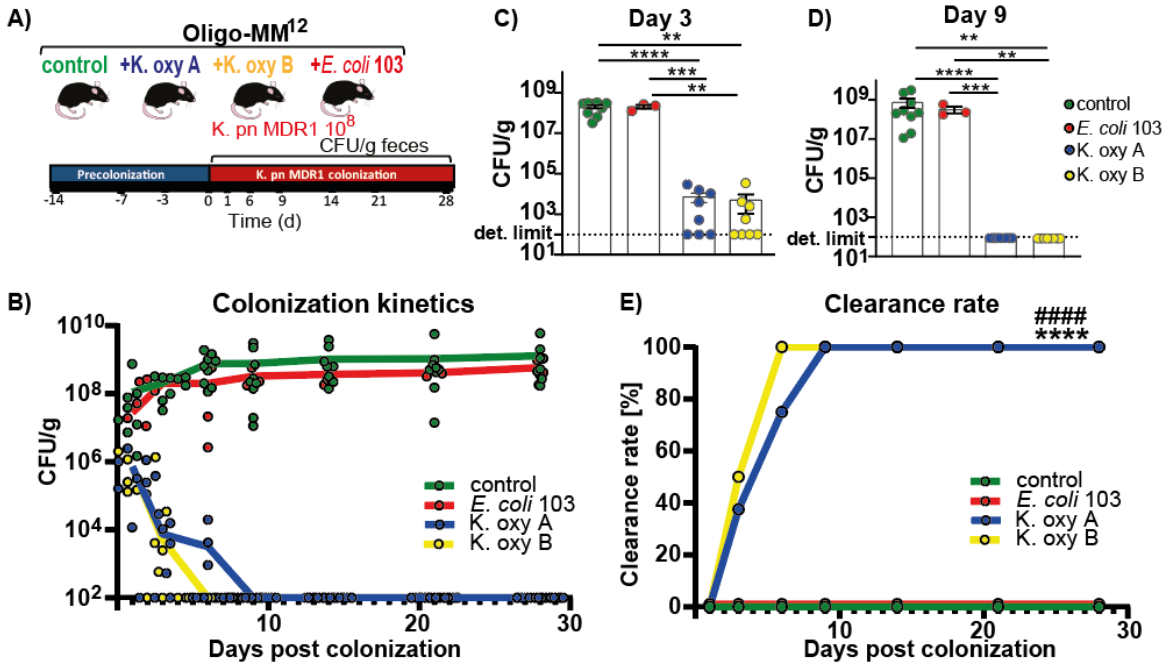

Figure 45: *K. oxytoca* protects Oligo-MM^{12} mice against MDR *K. pneumoniae*. (A) Oligo-MM^{12} mice were precolonized with K. oxy A, K.oxy B or *E. coli* 103 prior colonization with K. pn MDR1. Fecal colonization was assessed at indicated time points of the colonization (B) Colonization kinetics of K. pn MDR1 in precolonized and control animals. (C-D) Fecal burden of K. pn MDR1 after 3 and 9 days p.c. in different treated groups. Mean and SEM of two independent experiments with n= 3-5 mice per group. P values indicated represent a nonparametric Kruskal-Wallis test **p<0.01, ***p<0.001, ****p<0.0001. (E) Clearance rates of K. pn MDR1 in precolonized and control animals. P values indicated represent a log-rank test ****p<0.0001 (con/*E.coli* 103 vs K. oxy A), ####p<0.0001 (con/*E.coli* 103 vs K. oxy B).

Both *K. oxytoca* strains efficiently reduced fecal CFUs of MDR *K. pneumoniae* and achieved total clearance after 6 (K. oxy B) or 9 days (K. oxy A) post colonization (Fig 45B-E). In contrast, control group and *E. coli* 103 colonized mice exhibited similar high amount of *K. pneumoniae* during the whole course of colonization without any reduction or clearance (Fig 45B-E). This experiment highlighted that *K. oxytoca* is also capable to protect gnotobiotic mice with a defined microbiome composition from colonization with MDR *K. pneumoniae* indicating that the protection might occur via a direct competitive mechanism between the related *Klebsiella* species.

To further test the hypothesis that *K. oxytoca* actively reduces *K. pneumoniae*, I colonized GF animals with K. oxy A and *E. coli* 103 prior to colonization with MDR *K. pneumoniae* or left the mice untreated (Fig 46A). Body weight loss and fecal burden was assessed over 4 weeks. No significant body weight loss was detected upon colonization with MDR *K. pneumoniae* but mice did only gain fewer weight over the course of experiment. In contrast, all colonized mice gained up to 20% of weight during the course of experiment (Fig 46B) indicating that colonization with other enterobacteria supported the proper development of the animals. In terms of fecal colonization with MDR *K. pneumoniae* I found significantly reduced CFUs in the K. oxy A treated animals and to a lower extend also in the *E. coli* 103 colonized mice (Fig 46C-F). The protective effect of *E. coli* was only visible in the first three days of colonization. Afterwards, mice exhibited as high CFUs as untreated control mice (Fig 46D-F). Similarly, *K. oxytoca* could reduce the CFUs efficiently until day 3, but afterwards the protective effect was lost in some animals. Nevertheless, some animals remained reduced CFUs until day 21 accompanied with partial clearance (Fig 46C-F). Taken together, this experiment shows that *K. oxytoca* has the potential to directly inhibit the growth of MDR *K. pneumoniae* in the beginning of the colonization but need assisting microbiota to maintain the protective phenotype over a longer period of time to effectively clear the colonization.

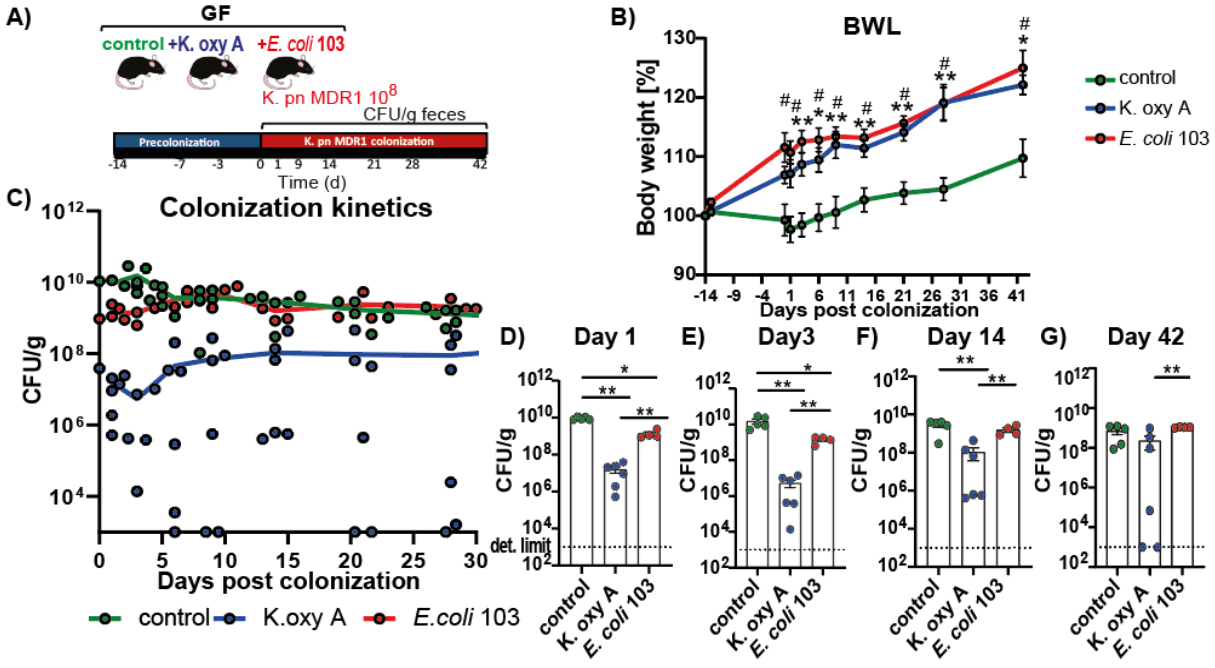

Figure 46: *K. oxytoca* partially protects GF mice against MDR *K. pneumoniae*. (A) GF mice were precolonized with K. oxy A, *E. coli* 103 or left untreated prior colonization with K. pn MDR1. Fecal colonization was assessed at indicated time points of the colonization (B) Body weight loss in control and colonized animals. P values indicated represent a nonparametric Kruskal-Wallis test *p<0.05, **p<0.01 (K. oxy A vs control) or #p<0.05 (*E. coli* 103 vs control). (C) Colonization kinetics of K. pn MDR1 in precolonized and control animals. (D-G) Fecal burden of K. pn MDR1 after 1, 3, 14 and 42 days p.c. in different treated groups. Mean and SEM of two independent experiments with n=2-3 mice per group. P values indicated represent a nonparametric Kruskal-Wallis test *p<0.05, **p<0.01.

3.4.9 Probiotic *K. oxytoca* protects susceptible animals from luminal and tissue invasion and systemic dissemination of the pathogen

To study the protective effect further, the characterization of the colonization dynamics was extended. To test if observed differences in the fecal colonization are also visible in the intestinal organs, SPF-H mice were precolonized with K. oxy A, K. oxy B or left uncolonized as a control prior to colonization with K. pn MDR1. Luminal and tissue invasion of K. pn MDR1 was assessed in the gastrointestinal organs including small intestine, cecum and colon as well as in the liver, and lymphatic organs including spleen and mesenteric lymph nodes (MLN) on day 6 p.c. as strongest differences in the fecal colonization were observed at this time point before (Fig 47A).

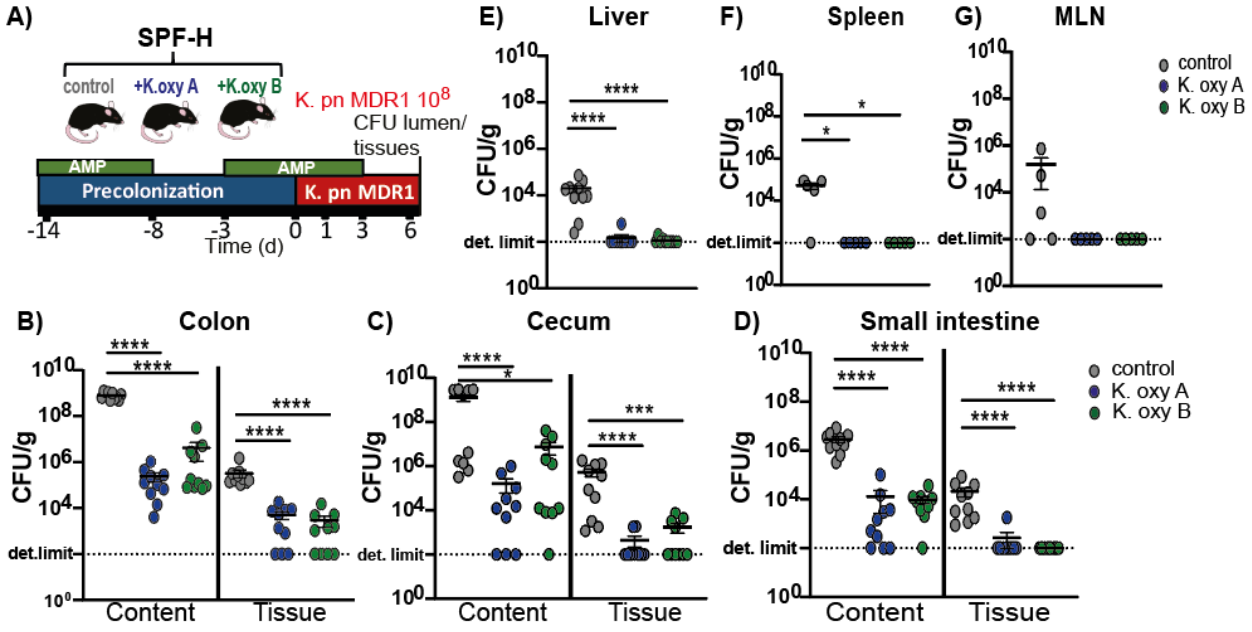

Figure 47: Probiotic *K. oxytoca* strain protects susceptible animals from luminal and tissue invasion and systemic spread. (A) SPF-H mice were treated with ampicillin and precolonized with K. oxy A or K. oxy B prior colonization with K. pn MDR1. Tissue and luminal colonization was assessed after 6 days p.c. (B-D) Luminal and tissue colonization of K. pn MDR1 in the colon, cecum and small intestine (E-G) Tissue invasion of K. pn MDR1 in liver, spleen and MLN. Mean and SEM of two independent experiments with n=5 mice per group. P values indicated represent a nonparametric Kruskal-Wallis test *p<0.05, ***p<0.001, ****p<0.0001.

I observed strong reduction in the gastrointestinal organ content as well as in the tissues in both precolonized groups compared to the control groups (Fig 47B-D). In addition, *K. oxytoca* colonized groups did not have any bacteria in the liver, spleen or MLN in contrast to the control animals, suggesting a systemic spread of the pathogen in control mice elevating the risk for blood stream infections (Fig 47E-G).

This experiment demonstrated a broad-spectrum activity of *K. oxytoca* in all gastrointestinal organs including reduction of pathogenic bacteria in the lumen and tissue and preventing the systemic spread into the liver and lymphatic tissues such as spleen and MLN. Two potential hypotheses could be drawn from these findings: First, protection might occur directly, via occupation of the same metabolic niche or production of inhibitory compounds, or indirectly via priming of the immune system due to the precolonization with *K. oxytoca*.

3.4.10 The adaptive immune-system is dispensable for the observed phenotype supporting the hypothesis of a direct competitive effect

To exclude the hypothesis that adaptive immunity plays a major role in the protective phenotype, I performed the same organ burden experiment using *Rag2*$^{-/-}$ SPF-H animals, which are devoid of any B- and T-cell population thereby having an impaired adaptive immune system (Fig 48A). The data were highly similar with the phenotype initially overserved in WT SPF-H mice. Similarly, CFUs in the gastrointestinal organs including cecum, colon and small intestine were significantly reduced in the lumen and the tissue in K. oxy A precolonized animals (Fig 48B-D).

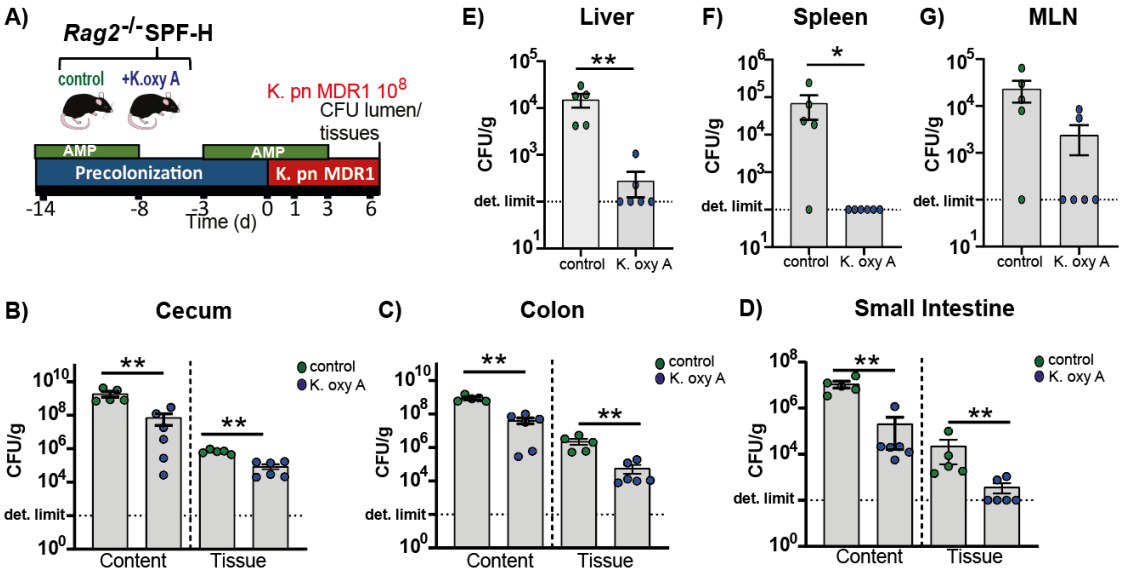

Figure 48: Organ burden results in *Rag2*$^{-/-}$ SPF-H mice show the same phenotype. (A) *Rag2*$^{-/-}$ deficient SPF-H mice were treated with ampicillin and precolonized with K. oxy A prior colonization with K. pn MDR1. Tissue and luminal colonization was assessed after 6 days p.c. (B-D) Luminal and tissue colonization of K. pn MDR1 in the colon, cecum and small intestine (E-G) Tissue invasion of K. pn MDR1 in liver, spleen and MLN. Mean and SEM of one independent experimen with n=5-6 mice per group. P values indicated represent a nonparametric Kruskal-Wallis test *p<0.05, **p<0.01.

In addition, bacterial burden in the liver and spleen was significantly reduced in precolonized mice (Fig 48E-F) and also tend to be lower in MLN (Fig 48G) indicating that K. oxy A could prevent the systemic spread of the pathogen without a sufficient adaptive immune response. Taken together, this experiment supported the hypothesis that the mechanism of *K. oxytoca* mediated protection against MDR *K. pneumoniae* is mediated by a direct mechanism of the commensal itself rather than an immune-mediated protection.

3.4.11 *K. oxytoca* helps anaerobic SCFA producers to recover faster after antibiotic dysbiosis thereby reestablishing colonization resistance.

As an immune-mediated mechanism was rather unlikely to explain the protective effect of *K. oxytoca*, I analyzed how *K. oxytoca* colonization might change the microbiome composition in the mice. To do so, cecal samples from the organ burden (day 6 p.c.) were sequenced, as strongest differences could be observed at this time point regarding species composition, species richness and general composition. In addition, cecal SCFA levels of these mice were measured. Interestingly, a strong clustering regarding the beta-diversity in precolonized animal on day 6 p.c. in the cecal content could be observed (Fig 49A). The "group affiliation" meaning if the mice were colonized with *K. oxytoca* or not was a main factor to explain observed differences between the groups with more than 75% attributed to this factor. In terms of alpha-diversity *K. oxytoca* treated animals displayed significantly higher species richness and evenness (Fig 49B) indicating major differences in species composition. Indeed, I could observe a highly divers microbiome in *K. oxytoca* precolonized animals in comparison to control animals which showed a dysbiotic species composition mainly consisting of *Klebsiella* in the phylum of Proteobacteria and *Enterococcaceae* in the phylum of Firmicutes (Fig 49C). Surprisingly, the microbiome of *K. oxytoca* treated animals had almost recovered full species diversity as found in untreated SPF-H mice with regard to species present and species richness (Fig 49D-F). Especially anaerobic species of the Bacteroidetes and Firmicutes phylum including *Rikenellaceae*, *Ruminococcaceae* and *Lachnospiraceae* were almost completely absent in the control animals but recovered fast in the *K. oxytoca* colonized mice (Fig 49C). One major trait of these bacterial families is the production of SCFA. As a proof, concentration of SCFA was determined in the cecal content of the organ burden samples. Indeed, I found significantly elevated levels of butyrate and propionate in SPF-H WT and *Rag2*$^{-/-}$ mice further supporting that *K. oxytoca* helps to reestablish colonization resistance by facilitating the recovery of anaerobic SCFA producers.

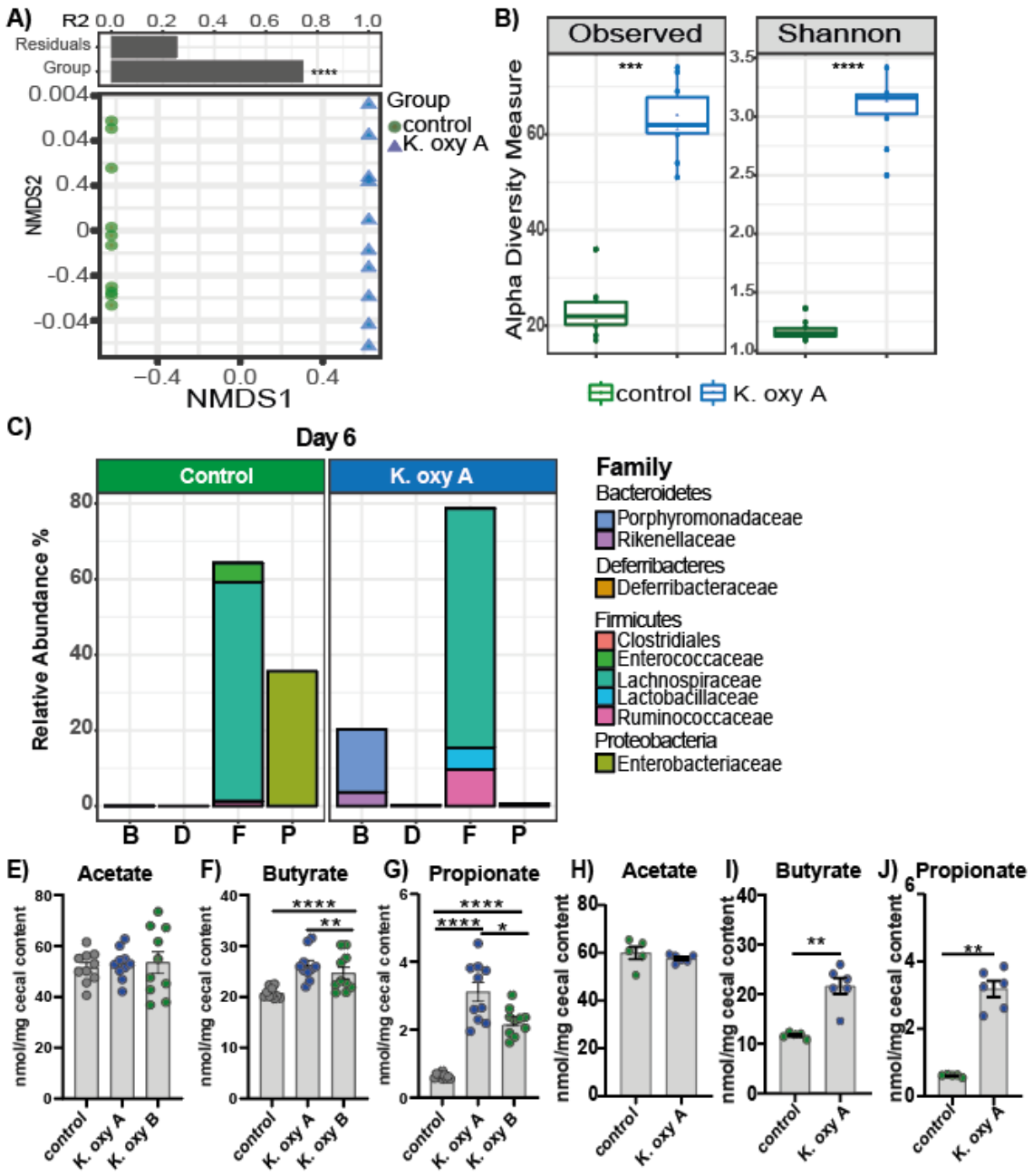

Figure 49: *K. oxytoca* reestablishes colonization resistance after antibiotic intervention. 16S rRNA gene sequencing data were performed using the cecal content of ampicillin treated SPF-H mice on day 6 p.c. with 10^8 CFU/g K. pn MDR1 (A) β-diversity of SPF-H mice on day 6 p.c. was analyzed using Bray-Curtis dissimilarity matrix and NMDS. To calculate the variance explained by individual factors such as colonization with *K. oxytoca* a permutational multivariate analysis of variance (ADONIS) was used. A significant effect was dedicated when $p < 0.05$ and $R^2 > 0.10$ (equivalent to 10% of explained variance) ****$p < 0.0001$. (B) α-diversity on day 6 p.c. in the control and K. oxy A colonized group was determined using Chao1 and Shannon index. (C) Average microbiome composition on day 6 p.c. displayed on family level. (D) Average microbiome composition over time in the feces displayed on family level. (E-J) SCFA measurements of acetate, butyrate and propionate in the cecum content of control and *K. oxytoca* colonized SPF-H WT (E-G) and *Rag2*$^{-/-}$ (H-J) mice. Mean and SEM of two independent experiments with n=5-6 mice per group. P values indicated represent a nonparametric Kruskal-Wallis test *p<0.05, **p<0.01, ****p<0.0001.

3.4.12 *K. oxytoca* colonization reduces MDR K. pn in humanized SUS donor mice

To verify if addition of *K. oxytoca* would help to reestablish colonization in humanized mice that received susceptible donor microbiotas I chose the same 2 SUS donors as previously described in chapter 3.1.2 and humanized two mice per donor. The same 4 INT donors were taken as a comparison (see 3.1.2). In addition, one out of the 2 SUS animals received *K. oxytoca* to analyze the impact on the colonization kinetics. Mice were precolonized for two weeks and were subsequently treated with ampicillin and colonized with K. pn MDR1 (Fig 50A). Indeed, addition of *K. oxytoca* to the susceptible donor microbiomes could efficiently lower the susceptibility in both donor mice with one mouse being able to completely clear the colonization (Fig 50B).

These preliminary data are a promising starting point for the development of new probiotics and validate the reproducibility and efficacy of *K. oxytoca* in a humanized model with multiple donors. Even though further screening of susceptible donors is required to prove the potency in various donor microbiota conditions, this experiments further substantiate the translational value.

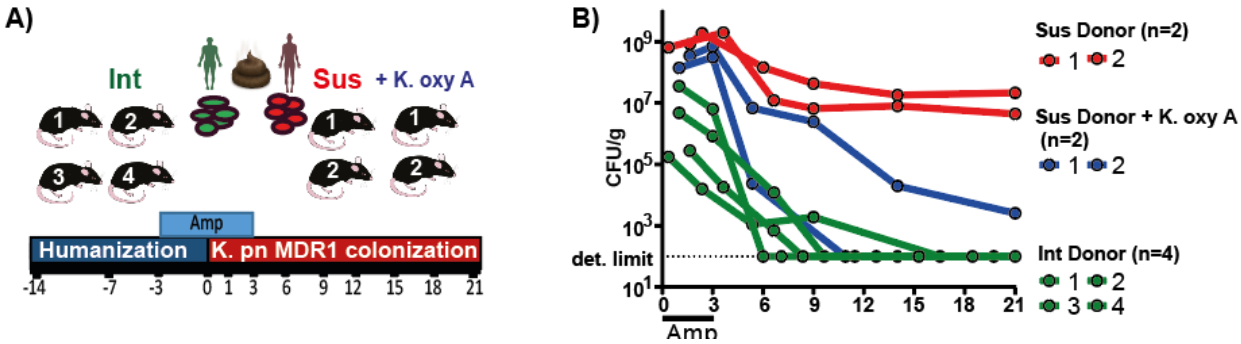

Figure 50: Humanization of GF mice transfers phenotype from donors. (A) Single GF mice received FT from different donors from the SUS or INT groups. Two mice received in addition K. oxy A prior to colonization with K. pn MDR1. Fecal burden was assessed after different time points after the colonization. (B) Resulting colonization kinetics of single GF mice receiving FT from different human donors. Means of one independent experiments with n=1 mice per group. P values indicated represent a nonparametric Kruskal-Wallis test p>0.05. (INT and SUS mice are the same as initially used in 3.1.2).

3.4.13 *K. oxytoca* has the therapeutic potential to interfere with already established MDR *K. pneumoniae* colonization

As I proofed that *K. oxytoca* has probiotic potential by efficiently blocking colonization and permanent establishment of MDR *K. pneumoniae* in the microbiome of antibiotic-treated and gnotobiotic animals, I wanted to test whether *K. oxytoca* could also lower or replace MDR *K. pneumoniae* after an already established colonization. To do so, mice were treated with ampicillin and colonized with K. pn MDR1. After three days of colonization, mice were subsequently colonized with K. oxy A or K. oxy B and fecal burden of K. pn MDR1 was assessed after different time points (Fig 51A). Indeed, mice treated with K. oxy A or K. oxy B cleared the colonization with K. pn MDR1 significantly faster compared to the control mice (Fig 51B-E). Comparing both *K. oxytoca* strains, clearance rate was faster with K. oxy A starting from day 9, 14 until day 28. After 42 days both strains were reaching similar levels as high as 80% (8/10) clearance, whereas only one animal (11.11%) of the control group could clear the colonization (Fig 51G). In addition, to verify if the mice also cleared *K. oxytoca* from the microbiome or if the bacterium was still detectable, feces were plated on amp plates. In the K. oxy A group, 5 out of 10 mice (50%) cleared the bacterium, whereas only 3/10 (30%) cleared K. oxy B. This observation indicated that in most of the cases K. pn MDR1 was successfully replaced by *K. oxytoca.*

Taken together, this pilot experiment supports the potential of *K. oxytoca* to act as both a potential probiotic strain but may also have therapeutic potential to cure MDR carriers who are already colonized with MDR *K. pneumoniae* strains. Further studies are required to unequivocally dissect the mechanism of action by which *K. oxytoca* reestablishes colonization resistance in the microbiome and if the bacterium has also potential to cure colonization and infection with other MDR bacteria.

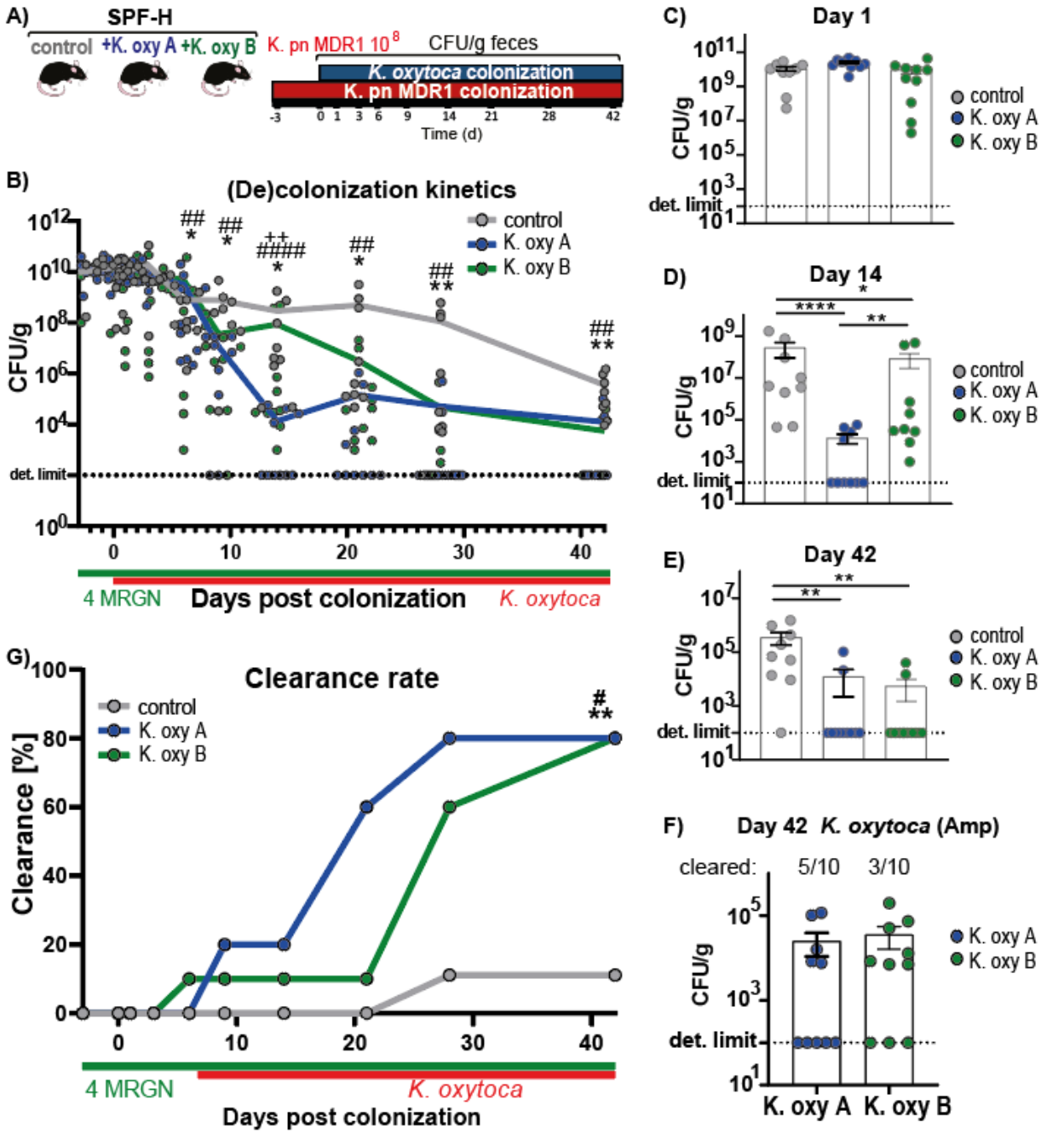

Figure 51: Decolonisation of MDR *K. pneumoniae* trough *K. oxytoca* treatment. (A) SPF-H mice were treated with ampicillin and colonized with K.pn MDR1. After three days, mice were colonized with K. oxy A, B or left untreated as a control. Fecal burden of the pathogen was assessed at indicated time points. (B) Resulting (de)colonization kinetics of K.pn MDR1 in the different groups. (C-E) Fecal burden of K.pn MDR1 at selected time point after 1, 14 and 42 days p.c. (F) Fecal levels of *K. oxytoca* in colonized mice after 42 days p.c. P values indicated represent a nonparametric Kruskal-Wallis test *p<0.05, **p<0.01 (K. oxy A vs. control), ##p<0.01, ####p<0.0001 (K. oxy B vs control), +p<0.05 (K. oxy A vs K. oxy B). (G) Resulting clearance rates of K. pn MDR1. Mean and SEM of two independent experiments with n=5 mice per group. P values indicated represent a log-rank test **p<0.01 (control vs. K. oxy A), #p<0.05 (control vs K. oxy B).

4. General Discussion

4.1 Individual infection susceptibility in healthy study populations is influences by multiple factors

The global spread of multi-drug resistant *Enterobacteriaceae* (MDR-E) has become one of the greatest health concerns worldwide. Initially considered as a healthcare-associated problem, growing evidence has rising that digestive carriage of MDR-E in the healthy population facilitates global spread (Kader, Kumar and Kamath 2007). The healthy intestinal microbiota has undoubted extensive impact in maintaining colonization resistance against invading pathogen via various direct and immune-mediated mechanisms (Libertucci and Young, 2019), but nevertheless, a large variability among healthy individuals regarding the susceptibility to different infection diseases even when experimentally exposed to a standardized infection inoculum is observed (Tacket et al., 2000).

Simplified *in vitro* systems would be valuable to understand factors in the healthy human microbiome, which might help to predict the risk for infection and serve as biomarkers to predict patient outcome. Hence, stool samples of 59 healthy volunteers were colonized in situ with an emerging MDR *K. pneumoniae* strain and CFUs of the pathogen were recovered after 24 h. This *in vitro* assay revealed large inter-individual differences with up to 100,000- fold differences in colonization levels when comparing the most susceptible and the most protected individuals. To better understand how the community protects the host from invading microorganisms, three community ecology principles can be applied to determine whether or not a pathogen can grow and ultimately survive in an established community: the availability of resources, presence of natural enemies and physical environment (Maldonado-Gómez et al., 2016; Shea and Chesson, 2002). In this work, numerous factors could be correlated with elevated protection including higher levels of SCFA, lower pH, the presence of specific bacterial species such as low abundant facultative anaerobes, SCFA producing genera *Ruminococcus* and *Coprococcus* and higher species richness which can be explained by at least one of the previously mentioned principles (Fig 52). The availability of resources meaning available nutrients is strongly influenced by the diet. Dietary fiber can strongly alter the community structure of the microbiota and subsequent function via the production of SCFA, such as acetate, propionate and butyrate (Den Besten et al., 2013). SCFAs are known to inhibit the growth of *Salmonella* (Jacobson et al., 2018) and other *Enterobacteriaceae* such as *Citrobacter* (Osbelt et al., 2020) and *Klebsiella* (Sorbara et al., 2018). SCFAs can induce intestinal epithelial cell production of AMPs by binding to the G-protein-coupled receptor GPR43 to stimulate reg3γ and β-defensins indirectly influencing microbiota homeostasis (Zhao et al., 2018).

In addition, SCFA can diffuse through the membrane, acidify the cytoplasm and thereby directly inhibit the growth of pathogens (Jacobson et al., 2018) (Fig 52A). The SCFA diffusion process and consequent toxicity are strongly influenced by the external pH, predicting the relative amount of non-ionized SCFA (Sun and Riordan, 2014). In turn, the inhibitory effect of SCFA is more prevalent or even only present under acidic conditions (Osbelt et al., 2020; Sorbara et al., 2018). Not only external pH mediates SCFA-toxicity but also the internal pH, which affects the transmembrane pH gradient that drives the influx of acid (Sun and O'Riordan, 2014). Although bacterial cytoplasm is relatively resistant to pH perturbation through its buffering capacity maintained by ionizable moieties such as amino acids side chains and its intrinsic membrane-impermeability to protons, different adaptive mechanisms such as proton transporters are actively involved to maintain the intracellular pH (Slonczewski et al., 2009). Subsequently, when external pH is low, organisms that require and maintain a neutral pH will face a higher transmembrane pH gradient leading to increased acid influx thereby being more susceptible to SCFA toxicity than those that can tolerate lower intracellular pH values (Sun and O'Riordan, 2014). Furthermore, pH might also influence the balance between Bacteroidetes and Firmicutes at least *in vitro* (Duncan et al., 2009), supporting the idea that changes in acetate, propionate, and butyrate ratios or levels along with pH might also influence the composition of the indigenous microbiota.

In line with these two important factors (pH and SCFA) who are likely cooperating to create a hostile physical environment for enteropathogens to grow, protection was further associated with higher levels of SCFA producing genera like *Ruminococcus* and *Coprococcus* (Fig 52A) and overall high species richness (Fig 52B) in the healthy adult cohort (MikroResist). The alpha- diversity is affected by many factors such as age, diet, geography and ethnic groups and in turn affects ecosystem functioning (Ma et al., 2019). Until now, alpha- diversity of the microbiota is often assumed to be an important factor but remains poorly studied and the appropriateness of general theories remain untested (Reese and Dunn, 2018). Generally, high species richness is seen as a beneficial factor, while low richness of gut microbiota has been associated with disturbed systems in patients with different diseases such as IBD, obesity or inflammatory morbidities (Le Chatelier et al., 2013; Ma et al., 2019). It is obvious that treatments with antibiotics reduce gut microbial community diversity and thereby making environmental niches vacant for foreign invaders (Robinson and Young, 2010). It remains still debatable if microbiota-associated diseases itself, which can trigger the use of antibiotics, is the cause or the consequence of "diversity loss" (Ma et al., 2019).

Observed differences in species richness in the healthy MikroResist cohort may be a characteristic feature of each individual, resulting from various factors such as repeated drug intake, fiber-rich or westernized diet. In addition, host genetics may be an influencing factor as westernized populations are generally facing a constant decrease of species richness in contrast to rural populations from developing countries (Koh et al., 2016; Martínez et al., 2015, Tyakht et al., 2014). One clear limitation of the MikroResist cohort is the lacking normalization of environmental influencing factors such as dietary fiber intake and the general huge variability of the human microbiota itself (Kim, Covington and Pamer, 2017). Even though all study participants claimed themselves as omnivorous, exact details about the consumed food before stool donation were missing. Further studies analyzing richness across broad cohorts from different regions in the world might help to determine causes of variations in healthy study populations.

Interestingly, I found a rare, novel cluster beside the reported *Bacteroides* and *Prevotella* enterotype who was formed by 22% of the individuals (13/59) tested, characterized by lower species richness and higher portion of *Akkermansia* and *Bifidobacteria* in their microbiotas (Fig 52B). Big human cohorts have initially distinguished three different enterotypes in humans named based on the bacteria who are found in high abundance in the respective microbiotas: *Bacteroides*, *Prevotella* and *Ruminococcus* (Arumugam et al., 2011). Studies suggested that enterotype affiliation is determined by dietary habits showing that protein and animal fat were associated with *Bacteroides* enterotype, whereas carbohydrates were associated with the *Prevotella* enterotype (Wu et al., 2011). Of note, also drastic short-term changes in diet are sufficient to alter the gut microbiota, indicating that also enterotype switches occur in individuals depending on the day when samples are taken (Bonder et al., 2016; David et al., 2014; Heinritz et al., 2016). In the MikroResist cohort, 6 out of 13 individuals belonging to the novel cluster were associated with the upper quartile of samples prone for colonization with MDR *K. pneumoniae*. Repeated sampling of protected and intermediate samples revealed relative stability of the observed phenotypes and enterotypes and also susceptible samples remained the highest CFUs over different repeats. Of note, recovered CFUs from one susceptible donors fluctuated stronger than the other samples indicating that specific changes in the microbiota may lead to some degree in colonization susceptibility variations but the general trend for low or high-risk groups may be more stable than initially expected.

To verify these associations in an *in vivo* colonization model, GF mice were colonized with susceptible and protected donor samples and colonized with MDR *K. pneumoniae.* These pilot experiments revealed that the different phenotypes (RES, INT and SUS) could successfully transferred into mice as those animals receiving feces from low or intermediately high-colonized donors could clear MDR *K. pneumoniae*

significantly faster than those animals receiving susceptible donor feces. Humanized mice are suitable tools for modeling infections and immunity in mice as the murine microbiota differs significantly from those in humans (Ernst, 2016, Wrzosek et al., 2018). Of note, these models face certain limitations such as the use of GF mice, which show several anomalies in their immune system due to the absence of microbes in their development (Macpherson and Harris, 2004; Round and Mazmanian, 2009). In addition, the used mice in this thesis harbored a native mouse gut, which differs from the gut physiology of humans and were feed regular mouse food, which may at least partially explain why some of the bacterial species found in the donor microbiota could not be transferred into the humanized mice. Nevertheless, these pilot experiments lead to promising results. These mice are thereby valuable tools to study the impact of human originating microbes and can facilitate the translational step from basic research to applied research and facilitate development of therapies.

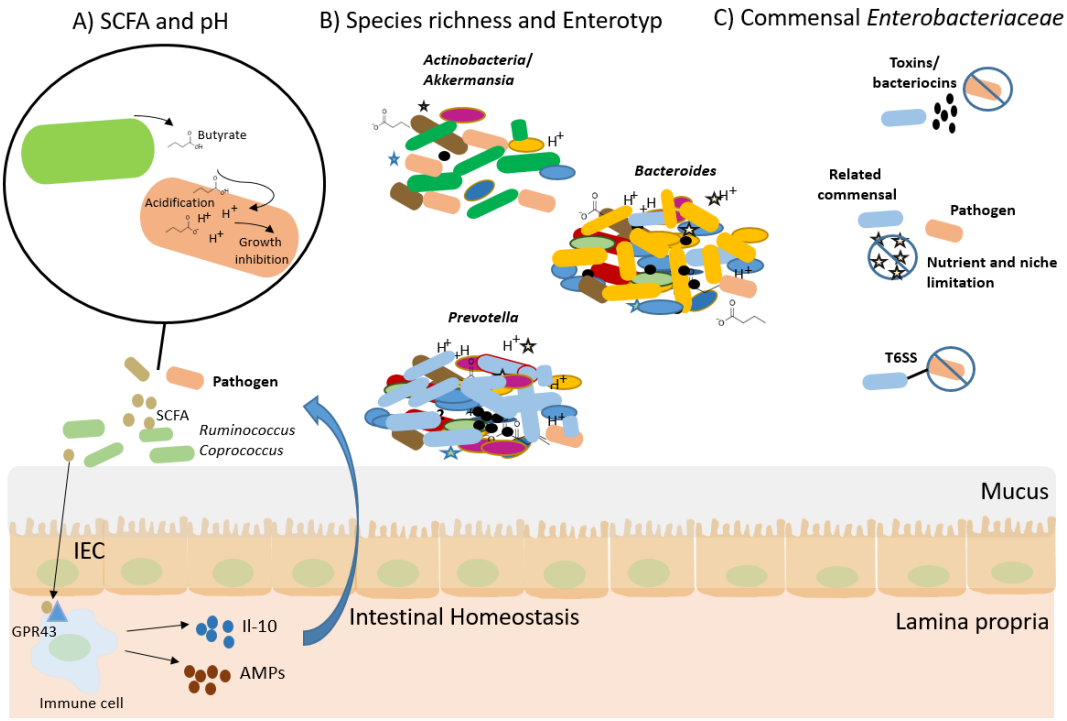

Figure 52: Factors influencing individual colonization susceptibility in this thesis. (A) Abundance of SCFA and SCFA-producing bacteria was positively correlated with protection. Butyrate can diffuse through the membrane and directly inhibit pathogen growth by intracellular acidification of SCFA trigger intestinal epithelial cell (IEC) production of AMPs and cytokines by binding to the G-protein-coupled receptor GPR43 indirectly influencing microbiota homeostasis. (B) Higher species richness was found in *Prevotella* and *Bacteroides* enterotype, whereas Act-Akk enterotype was correlated with reduced α- diversity and elevated colonization susceptibility. (C) Commensal *Enterobacteriaceae* were associated with protection. Reported mechanisms of protection include toxin or bacteriocin production, nutrient and niche competition and expression of T6SS, targeting related species.

The last factor who was associated with elevated resistance was higher portions and diversity of commensal *Enterobacteriaceae* (Fig 52C). This factor has to be clearly separated from the massive outgrowth of enterobacteria seen in the patient samples, which are associated with disturbed microbiota compositions. Of note, other studies observed the opposite correlation, linking the occurrence of related enterobacteria with elevated risk for infection (Stecher et al., 2013). The fact that related commensal species are competing for the same or similar essential and limited nutrients such as iron and zinc and the same environmental niches as pathogenic species are likely explanations for this protective association (Deriu et al., 2013; Gielda and DiRita, 2012). Another explanation is the specific targeting of related species by production of bacteriocins, antimicrobial peptides or T6SS (Duquesne et al., 2007; Cascales et al., 2007; Roelofs et al., 2016). Specifically, occurrence of other commensal *Klebsiella* strains was associated with resistance against MDR *K. pneumoniae* colonization in healthy volunteers.

The comparison of multiple human data sets further supported the hypothesis that antibiotic naive-microbiota suppresses growth of enterobacteria by acidification of the proximal colon and triggering SFCA mediated intracellular acidification (Sorbara et al., 2018). This hypothesis is further discussed in chapter 4.3. Another conclusion is that commensal related *Enterobacteriaceae* block the niche for incoming pathogens and compete for essential nutrients, oxygen or nitrate (Velazquez et al., 2019). This hypothesis is further reviewed in chapter 4.4.

In contrast to healthy individuals, I was further interested to analyze the microbiota of patients undergoing IC and HSCT as these patient populations are extremely vulnerable to infections (Taur et al., 2012; Taur et al., 2018). The primary clinical concern is not the colonization with *Enterobacteriaceae* itself but that expansion of these species in the gut increases the risk for subsequent BSI in these patients (Taur et al., 2012; Taur et al., 2015). The microbiota of leukemia patients was extremely variable and showed overall reduced colonization resistance in the *in vitro* assay with MDR *K. pneumoniae* compared to healthy controls. Similar principles applied for susceptible healthy individuals and were also found in the patients' microbiota including reduced alpha- diversity, especially in those patients facing a bloom with *Enterococcus* or *E. coli*, elevated levels of harmful bacteria and unusual shifts in beta- diversity, decrease in probiotic SCFA producers and decreased levels of SCFA as well as increased pH values. The microbiota profiles of patients from the MikroIntest cohort indicated that the natural microbiota composition is extremely unstable during the course of chemotherapy and is prone for infection as the high portions of samples that are dominated by *Enterobacteriaceae* (13/24 = 54.2%) or *Enterococcus* (6/24 = 25%) could reveal.

Studies focusing on the microbiota composition during chemotherapy and stem cell transplantation also reported marked shifts in bacterial populations inhabiting the gut with intestinal domination, defined as occupation of at least 30% of the microbiota by a single predominating bacterial taxon such as *Enterococcus* or various Proteobacteria (Taur et al., 2012; Galloway-Peña et al., 2016). In both studies, reduction in alpha diversity- during IC was significantly elevated in those individuals developing infections. In patients undergoing chemotherapy, direct correlation of higher colonization with advanced stages of chemotherapy could not be observed but in case of HSCT the susceptibility lowered in parallel with the time after stem cell transplantation defining the first two month as most critical period for infections. The excessive use of prophylactic and therapeutic antibiotics lowers the risk of bacterial infections but simultaneously disturbs the normal microbiome, i.e. colonization resistance, and leads to enteric domination with *Enterobacteriaceae* as resources and niches are vacant in response to reduced species richness. The impact of the single drugs are further discussed in chapter 4.2.

4.2 Cytarabine - driven mucositis severity is influenced by variations in microbiota composition in laboratory mice.

Research has intensified in the past years to investigate the impact of the microbiome during cancer, i.e. the initiation and the progression of the disease as well as complications during therapy. Of note, detailed analysis of the microbiome in infections during AML therapy are very limited (Galloway-Peña et al., 2016; Galloway-Peña et al., 2019). As the human data sets in this thesis and in other patients' populations reflect only a limited number of patients and the observed microbiota changes were highly variable between and within the patients, I decided to further investigate the impact of the chemotherapy drugs in isogenic mouse lines with variable microbiota compositions during IC. Two mouse lines with low divers (SPF-H) and complex (SPF-J) microbiota were treated with two repetitive cycles of high-dose Ara-C (100 mg/kg) combined with the antibiotic levofloxacin (40 mg/kg) and the PPI pantoprazole (40 mg/kg). Mice with less complex microbiota lost 10-15% of body weight during the course of the experiment, whereas SPF-J mice only lost 5-10% of body weight. Overall, BWL did not impact the survival rate of all treated animals and is comparable with body weight loss rates of 6% reported in patients undergoing IC, which did not impact survival (Keng et al., 2013).

One of the most common side effects during chemotherapy is development of mucositis in the oral cavity but also in the gastrointestinal tract (van Vliet et al., 2010). Mucositis is characterized by mucosal damage increasing intestinal permeability and facilitating bacterial translocation over the intestinal barrier increasing the risk for bacterial infection, inflammation and sepsis (Peterson and Artis, 2014).

In humans, symptoms include intestinal pain, vomiting, diarrhea and destruction of the intestinal epithelium that contributes to poor nutrient adsorption contributing consequently to weight loss (Keefe, 2007). In mice, histological scoring revealed pronounced mucositis in the SI of both mouse lines with changes most prominent in the last third of the SI. Interestingly, SPF-J mice exhibited a significantly more severe inflammation than SPF-H mice. Additional analysis of mice treated with individual drugs revealed that the inflammatory effect could be attributed to Ara-C alone. Until now, lacking selectivity of chemotherapeutics is the greatest drawback faced during treatment of cancer as these drugs barely distinguish between tumor cells and cells with high turnover found in the intestines promoting the development of mucositis (Keefe, 2007). Mucositis development can be divided into five phases (Corthésy, 2013; Sonis, 2004): In the initialization phase after administration of chemotherapy, cell injury occurs in response to DNA damage or generation of reactive oxygen species (ROS). During the second phase, several events may occur in parallel including activation of transcription factors such as NF- kB who is involved in regulation of cytokine expression and inflammatory adhesion molecules. These can in turn activate further signaling cascades influencing differentiation, proliferation of immune cells and activity of other cytokines. In this phase, immunoglobulin A (IgA) is essential to maintain intestinal homeostasis by commensal microbiota and prevention of interaction between pathogenic bacteria or toxins and the mucosa (Ferreira et al., 2012). In the third phase, increased presence of pro-inflammatory cytokines induces accelerated tissue damage, which in turn again amplifies the signal leading to increasing stress responses resulting in pronounced damage and apoptosis. In the fourth phase, known as ulceration, the epithelium begins to lose integrity visible as mucosal and tissue morphological changes. Ulceration weakens the intestinal barrier increasing the risk for bacterial translocation (Corthésy, 2013; Sonis, 2004). One of the most pronounced effect in this phase is villi shortening what can be observed in humans (Viana et al., 2013) and animals (Logan et al., 2007) in response to chemotherapy, which can be reversible as long as the underlying lamina propria is undamaged (Nolte, 2016). Villi shortening was also pronounced in both mouse lines used in this thesis with shortening up to over 75% compared to untreated control mice. Spontaneous healing occurs in the final healing phase after discontinuation of chemotherapy typically after one month (Sonis, 2004). According to the Sonis model, intestinal microbiota plays no role in the pathophysiology of mucositis. However, results observed in this thesis and literature support the hypothesis that the intestinal microbiota is an important factor contributing to inflammatory diseases and detrimental effects of chemotherapeutics and antibiotics eradicating probiotic anaerobic species facilitate mucositis development (van Vliet et al., 2010).

Van Vliet and colleagues proposed an extended model suggesting that the microbiota potentially influencing all steps of mucositis development (Fig 53): 1) Multiple intestinal bacteria are capable of decreasing NFκB activation, resulting in a diminished production of inflammatory cytokines or produce butyrate which has been shown to have profound anti-inflammatory effects (Den Besten et al., 2013). 2) Increased intestinal permeability can be attenuated by commensal bacteria directly and indirectly by induction of heat shock proteins (HSP) or SCFA production which can increase tight junction strength (Hamer et al., 2008). 3) The composition and thickness of the mucus layer is dependent on the intestinal microbiota as absence of microbes is associated with a decrease in goblet cells, and layer thickness (Round and Mazmanian, 2009). 4) The resistance to harmful stimuli and epithelial repair mechanisms is influenced by commensal via bacterial induction of NFκB through TLR, which controls physiological state of low-grade inflammation and stimulates tissue repair (Karrasch et al., 2006). Production of butyrate stimulates the migration of epithelial cells, thereby enhancing mucosal healing (Hamer et al., 2008). 5) The activation and release of immune effector molecules such as IgA is strongly regulated by resident microbes (Wang et al., 2006). Increased contact between microbiota and intestinal epithelium increases the expression of the C-type lectin reg3γ, which limits bacterial translocation and maintains intestinal integrity. (Fig 53). Taken together, the microbiota influences the expression and release of immune effector molecules, regulates itself and maintains homeostasis thereby positively influencing all phases in Sonis's mucositis model (Van Vliet et al., 2010).

Interestingly, mouse lines with complex microbiota developed more severe small intestinal mucositis characterized by stronger influx of inflammatory cells, degeneration of paneth cells and higher grades of damage to the morphology of the intestinal epithelium with regard to villi shortening and apoptosis of intestinal epithelial cells. As both mouse lines are genetically identical, it is likely that differences in their microbiota are responsible for observed differences in the inflammation severity. Diverse treatments have been shown to have beneficial effects in animal models after chemotherapy injury such as oral administration of IgA (Corthésy, 2013), amino acids (Beutheu et al., 2014; Posner and Haddad, 2007), fatty acids and butyrate (Ferreira et al., 2014), antioxidants and vitamins (Bodiga et al., 2012) as well as probiotics (Whitford et al., 2009). To understand the impact of chemotherapeutics on the host microbiota fecal samples were sequenced before and after each chemotherapy cycle in mice receiving single or combined treatment with Ara-C, levofloxacin and pantoprazole. In both mouse lines, a fluctuating pattern with changes in beta-diversity and alpha-diversity in response to chemotherapy was observed, underlining the dynamic and fast response of the microbiota and the ability to recover reduced or lost species after perturbations.

Comparing both mouse lines, SPF-J mice exhibited a more pronounced decrease of species after chemotherapy with almost 50% reduction of alpha –diversity. Especially obligate anaerobic bacteria were affected including *Lachnospiraceae* and *Rikenellaceae* as well as *Muribaculaceae,* which were not present in the low complexity SPF-H microbiota. In contrast, facultative anaerobic families such as *Lactobacillaceae* were elevated in both mouse lines and the genus *Akkermansia* was specifically increased in SPF-J mice upon treatment. *Akkermansia muciniphila* is a bacterium that scavenges mucins as a carbon and nitrogen source.

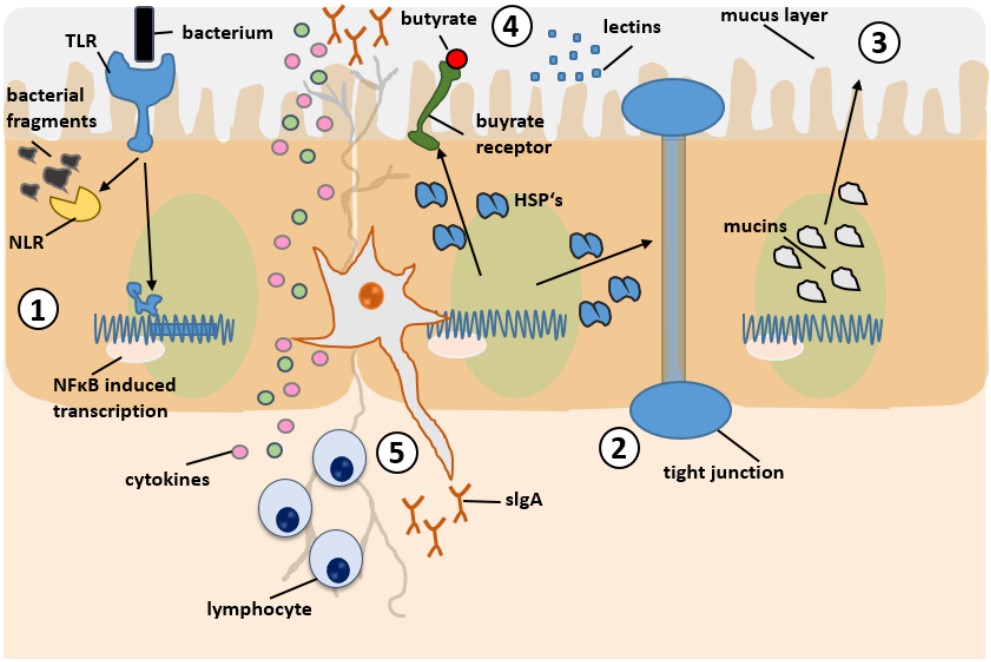

Figure 53: Potential pathways of the resident microbiota interfering in the development of mucositis. Depicted are five pathways in which intestinal bacteria can attenuate or aggravate mucositis: 1) influencing the inflammatory process, 2) influencing intestinal permeability, 3) influencing the composition of the mucus layer, 4) influencing resistance to harmful stimuli and enhancing epithelial repair, and finally, 5) the activation and release of immune effector molecules (adapted from Van Vliet et al., 2010).

It has been inversely associated with obesity and diabetes, and oral application of *A. muciniphila* protected mice from DSS-induced IBD phenotypes (Kang et al., 2013). On the other hand, *A. muciniphila* was also identified to be present in high relative abundance after 5-fluorouracil (5-FU) induced mucositis (Carvalho et al., 2018). Other studies even suggest that *A. muciniphila* which were actively involved in the pathological process of 5-FU induced intestinal mucositis (Li et al., 2017). The fact that *A. muciniphila* is only present in the microbiota of SPF-J but not SPF-H mice and was especially increased in the mice receiving Ara-C further supports the hypothesis that this bacterium might contribute to increased severity of mucositis.

Experimental transfer of *A. muciniphila* into SPF-H mice could test this hypothesis. Nevertheless, also SPF-H mice displayed mucositis in the small intestine. Here, Ara-C alone induced specific shifts to the overall community structure leading to a strong increase of *Erysipelotrichaceae* in SPF-H mice, especially the genus *Turicibacter* accompanied by reduction of *Lachnospiraceae* Family XIII in the Firmicutes phylum. Interestingly, human studies found significantly higher abundance of Erysipelotrichaceae and V*eillonella* in fecal samples collected prior to chemotherapy in patients that subsequently developed BSI compared to patients who did not develop subsequent BSI (Montassier et al., 2016). In summary, *Turicibacter* spp. as well as *A. muciniphila* are promising candidates for subsequent follow-up studies.

Besides mucositis, susceptibility to infections is another big health concern during chemotherapy and stem cell transplantation. *In vitro* inoculation of cecal content of SPF-J and SPF-H mice with MDR *K. pneumoniae* revealed higher colonization ability of PBS treated SPF-J mice suggesting that these mice may be naturally more susceptible to colonization with this pathogen. The content of Ara-C, PPI and Abx treated mice did not reveal major differences in terms of *in vitro* colonization levels between both mouse lines. In *in vivo* experiments, Ara-C treated mice tended to have elevated levels of *K. pneumoniae* in their feces compared to PBS treated control mice. Based on these pilot experiments, initial microbiota composition may predetermine level of natural colonization susceptibility against *Enterobacteriaceae* and Ara-C treatment potentially exacerbated the susceptibility for colonization and subsequent infection. Further experiments are required to assess the influence of Ara-C during infections more in detail. A detailed analysis of natural infection susceptibility in undisturbed microbiota setting is described in section 4.3.

4.3 The variability of the microbiota composition influences the susceptibility towards the intestinal pathogen *Citrobacter rodentium* via short chain fatty acid production

It is widely acknowledged that the intestinal microbiota has a significant impact on the individual susceptibility against invading pathogens and the severity of intestinal inflammation via direct and immune-mediated mechanisms (Buffie and Pamer, 2013). Especially reduction of the colonization resistance against certain *Enterobacteriaceae* such as *Salmonella* (Jacobson et al., 2018), *E. coli* or *K. pneumoniae* (Sorbara et al., 2018) after antibiotic treatment has been linked with a reduction of SCFA-producing bacteria. The *C. rodentium* model has been used intensively to model human infections with EHEC and EPEC and to dissect direct and immune-mediated mechanisms of the microbiota influencing susceptibility and severity. For example, it has been shown that antibiotic treatment renders mice more susceptible to *C. rodentium* infections (Wlodarska et al., 2011).

Also, the presence or absence of bacteria on a general level such as elevated Bacteroidetes over Firmicutes level (Willing et al., 2011) or the presence of a single kind of bacterium such as segmented-filamentous bacteria (SFB) (Ivanov et al., 2009) or higher ratios of Clostridia (Wlodarska et al., 2015) have been associated with elevated resistance toward *C. rodentium* via immune-mediated mechanisms. In contrast, the overall absence of microbes leads to enhanced susceptibility and persistence of *C. rodentium* GF mice (Kamada et al., 2012). Also direct mechanisms of commensal bacteria such as expansion of commensal *E. coli* are able to inhibit *C. rodentium* colonization by competition for monosaccharides as a nutrient source (Kamada et al., 2012). Following up on the observation that mice from different breeding facilities show different susceptibility in related gastrointestinal disease models such as *Salmonella* Typhimurium (Thiemann et al., 2017; Velazquez et al., 2019) or DSS-induced colitis (Roy et al., 2017) due to presence or absence of specific members of the microbiota, we decided to characterize the impact of the microbiota composition during *C. rodentium* infection, since knowledge about specific species and pathogen-commensal interactions that contribute to protection against colonization of *C. rodentium* remains elusive.

Initial experiments by a former co-worker (S. Thiemann) identified striking differences in the colonization with *C. rodentium* betweem genetically similar C57BL6/N sub-lines already at 1 day p.i.. Yet, the underlying mechanism was unknown. To exclude any influence of genetic differences or spontaneous mutations reported in C57BL/6N sublines (Kayagaki et al., 2011; Vande Walle et al., 2016), one susceptible (SPF-S) and one resistant (SPF-R) microbiota was transferred to genetically identical GF recipient mice. Fecal microbiota composition as well as disease progression was highly similar between formerly GF mice and their respective cohousing partners, further supporting that the phenotype is fully dependent on the microbiota. In this chapter, I aimed to explore the underlying mechanism in order to explain the observed differences in colonization.

Since *C. rodentium* causes mild inflammation in immunocompetent mice, I was interested to characterize using a more pathogenic *C. rodentium* strain whether delay in colonization would also translate into altered survival. To do so, a strain that is able to express Stx (Mallick et al., 2012), which is responsible for intestinal damage and life-threatening systemic diseases such as renal failure in EHEC infections was used (Nataro and Kaper, 1998). Again, SPF-S mice were less colonized after one and three days post infection and in line with these results showed significantly reduced body weight loss and prolonged survival.

In all infection experiments, differences in colonization were initially and most strongly detected in the cecal lumen at the early phase of infection. Furthermore, I was able to recover the phenotype by *in vitro* inoculation of isolated cecal content with *C. rodentium* indicating that cultivable bacteria are responsible for delaying colonization in protected mice without requiring the immune system of the host. In addition, the effect was present in the bacterial pellet as well as in the supernatant supporting the hypothesis that bacteria produce soluble products that may inhibit the growth of *C. rodentium* in the susceptible microbiota. The effect was only present in undiluted and 1:2 cecal content but not at higher dilutions tested, indicating that the bacterial products needed to present in a higher amount to exhibit their bactericidal effects. Direct competition can occur via multiple ways such as competition for essential nutrients and environmental niches (Pereira and Berry, 2017), production of toxic or inhibitory compounds including bacteriocins, microcins, SCFA or bile salts (Urdaneta and Casadesus, 2017; Flint et al., 2015; Sorbara and Pamer, 2019) or contact-mediated killing by expression of specific Type 6 secretion systems (Silverman et al., 2012).

As certain bacterial groups are more-or less likely to perform one of the above-mentioned strategies, I tried to identify the causative bacteria by analyzing the 16S rRNA gene profiles of cohoused and non-cohoused resistant and susceptible mice in order to identify and evaluate distinct bacterial biomarkers associated with susceptibility and protection towards *C. rodentium*. I identified that distinct features of the intestinal microbiota are associated with lower *C. rodentium* colonization in early phase of infection. Specifically, SCFA producing bacteria (Vital, Karch and Pieper, 2017) within the Firmicutes phylum such as *Intestinimonas, Lachnoclostridium, Roseburia* and *Ruminiclostridium* were significantly elevated, whereas the mucin-degrading bacterium *A. muciniphila* was only present in higher amounts in SPF-S mice. The presence of *A. muciniphila* has mostly been associated with beneficial properties and has been inversely correlated with several diseases including IBD, acute appendicitis, obesity and diabetes (Geerlings et al., 2018). Of note, these diseases may affect integrity or thickness of the mucus layer, thereby influencing abundances of *A. muciniphila*. In this thesis, comparison of the mucus layer and integrity could not reveal significant differences between both mouse lines. In addition, the abundance of *A. muciniphila* after cohousing did not correlate with changes in the phenotype of the mice suggesting that differences of *A. muciniphila* abundances may not sufficiently explain differences in susceptibility against *C. rodentium* in this work.

Further analysis of the 16S rRNA gene profiles of resistant SPF-S animals showed a clear clustering apart from the microbiome of susceptible mice characterized by overall increased species richness most pronounced in the abundance and diversity within the Firmicutes phylum indicating that indeed the presence of specific SCFA producing bacteria is responsible for resistance against *C. rodentium* infection (Fig 54). Further comparison of the metabolomics landscape revealed striking differences between SPF-S and SPF-R mice with a strong increase of succinate, malate and fumarate as well as urea cycle associated metabolites ornithine, putrescine and urea in the susceptible mice. Of note, SPF-R mice harbored significantly more and more divers *Enterobacteriaceae* in the cecum, which might consume metabolites that were elevated in the SPF-S environment thereby decreasing possible carbon sources for *C. rodentium* in the resistant SPF-R mice (Fig 54). Recently, a higher ratio of endogenous *Enterobacteriaceae* naturally occurring in the microbiota of laboratory animals have been associated with reduced susceptibility towards *Salmonella* Typhimurium (Velazquez et al., 2019). 16S rRNA gene sequencing and isolation experiments revealed higher level and more divers *Enterobacteriaceae* in the SPF-R microbiota but transfer of those bacteria isolated from the SPF-R to SPF-S mice did not significantly reduce CFUs in the cecum, suggesting that those bacteria did not play a major role in protection in this setting. Furthermore, susceptible SPF-S mice harbored significantly higher levels of *Bacteroides* species in the microbiome, which are known to increase metabolites involved in gluconeogenesis (Curtis et al., 2014). This modulation of the metabolite environment has been linked with enhanced EHEC virulence gene expression by an increase of A/E lesion formation through the transcription factor Cra, tightly regulated by sugar concentrations (Curtis et al., 2014). In addition, the compound ethanolamine was significantly elevated in susceptible mice known to serve as a carbon source for many related bacterial pathogens including *Salmonella*, *Escherichia* or *Klebsiella* (Garsin, 2010). In the case of *Salmonella* Typhimurium, decrease in luminal butyrate levels by eradication of butyrate producing bacteria through streptomycin treatment increased epithelial oxygenation and aerobic expansion of the pathogen (Rivera-Chávez et al., 2016). Similarly, increased oxygenation has also been shown to enhance mucosal *Citrobacter* colonization (Lopez et al., 2016). Furthermore, *Salmonella* can take growth advantage from consumption of non-fermentable carbon sources such as succinate (Spiga et al., 2017) or 1,2-propane-diol (Faber et al., 2017), whereas growth can be inhibited by microbiota derived SCFAs by acidification of the intracellular cytoplasm (Jacobson et al., 2018).

To exclude that oxygen availability plays a key role in the observed phenotype I assessed hypoxia inducible factor (HIF1-α) expression in the gut tissues of both mouse lines at steady state and 3 days p.i., which did not reveal significant differences between both mouse lines. HIF1-α is a transcription factor coordinating barrier protection, which is dependent on the bacteria-derived butyrate (Kelly et al., 2015).

The findings in this chapter suggest that natural occurring variations in the microbiota without any antibiotic intervention directly change the susceptibility response to gastrointestinal pathogens. These preexisting differences in the microbial environment such as presence and abundance of butyrate and succinate producers explain strongly differing disease susceptibility towards *C. rodentium* in isogenic mice, which might also be true for occurring variations in humans infected with a standardized EPEC inoculum (Pop et al. 2014; Tacket et al. 2000). Further focusing on the mechanism of suppression, I tested the inhibitory properties of butyrate on *C. rodentium* by supplementing BHI medium with different concentrations of butyrate, acetate and propionate individually and combined in physiological concentrations as in the cecum of the different mouse lines. Strikingly, only butyrate as well as the mixture of SCFAs found in the SPF-R mice was able to nearly completely abrogate the growth of *C. rodentium* at pH 6.0, but not at pH 7.0, indicating that not only the amount of SCFAs found in the cecum of SPF-R mice but also the reduced cecal pH is responsible for inhibition of *C. rodentium*.

In contrast to the inhibitory effects of SCFAs on *C. rodentium* observed in this thesis, SCFAs have been shown to specifically promote the adherence and motility of EHEC *in vitro* by activation of the expression of locus of enterocyte effacement (Yang et al., 2018), or intimate attachment and type III secretion (Tobe, Nakanishi and Sugimoto, 2011). Taken together, the role of SCFAs seems to be multifactorial and differential to the bacterial species present in the gut. Finally, I could demonstrate that supplementation of isolated cecal content of SPF-S mice *in vitro* as well as butyrate supplementation of SPF-S mice *in vivo* effectively reduced the colonization of *C. rodentium* accompanied by a reduction of the cecal pH value to the same extend as found in the resistant SPF-R mice when reaching a critical value of more than 50 nmol/mg in the cecum. Furthermore, butyrate supplementation in antibiotic depleted and GF animals also led to significantly reduced cecal CFUs highlighting the impact of SCFAs in this setting. Nevertheless, overall butyrate levels could not be restored by SCFA supplementation alone highlighting the importance of resident microbes to achieve fully protective SCFA levels. Based on these findings SCFA concentrations may serve as a biomarker to predict disease outcome after infection with certain *Enterobacteriaceae*.

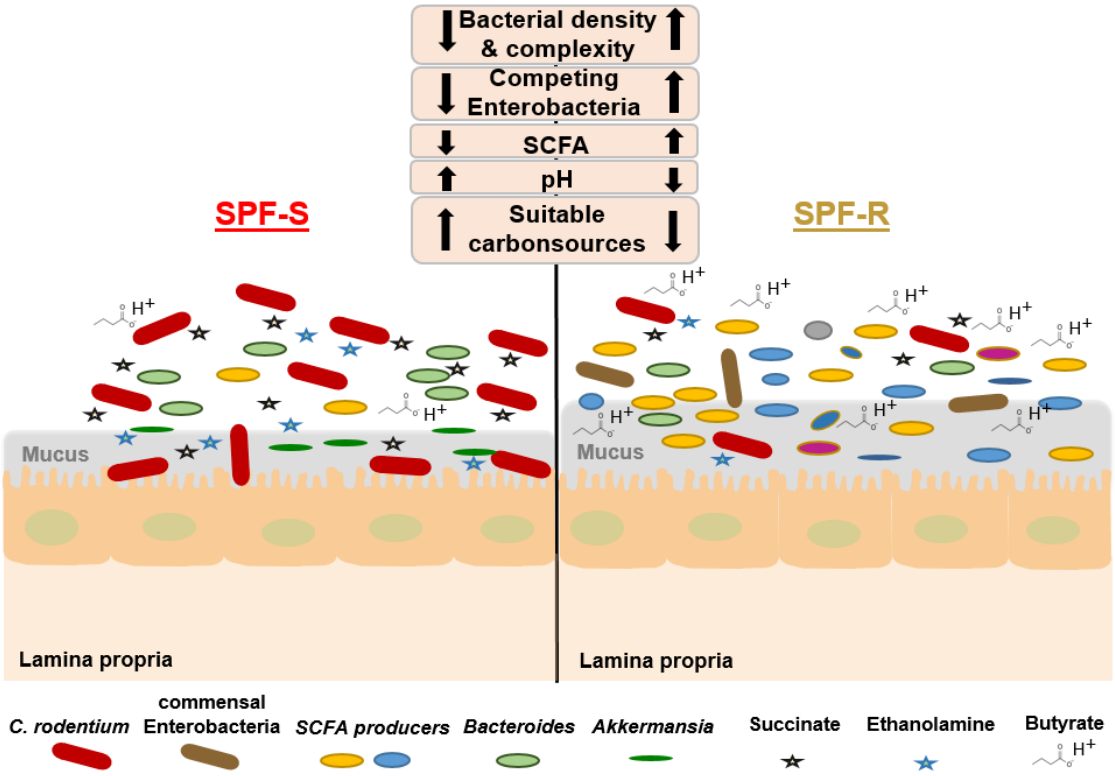

Figure 54: Microbiota related differences between SPF-S and SPF-R mice. Numerous differences regarding the microbiota composition and ecology could be identifies in both mouse lines. The microbiota of SPF-S mice is characterized by lower species richness, higher ratios of *Akkermansia* and *Bacteroides*, no competing enterobacteria, higher abundances of succinate and ethanolamine, lower levels of SCFA (especially butyrate) and higher pH values. The SPF-S microbiota is more susceptible to *Citrobacter* infection. In contrast, SPF-R mice harbor a complex microbiota with enterobacteria and high abundances of SCFA producing Firmicutes, lower pH value, less available carbon sources for *Citrobacter*, high levels of butyrate leading to a higher natural level of protection.

In summary, this chapter demonstrated that presence, abundance and diversity of SCFA producing bacteria strongly influenced disease kinetics and severity of *Citrobacter*-mediated disease (Fig 54). Furthermore, I could identify butyrate as a key metabolite for protection against *C. rodentium*. As previous studies have largely focused on immune-mediated mechanisms, however, these experiments demonstrated that natural variations in the microbiota strongly shape the metabolite environment and intestinal pH value, thereby contributing to naturally occurring variations in the susceptibility against enteropathogens such as *C. rodentium*. These findings highlight the need for microbiota normalization across laboratory mouse lines for infection experiments with the model-pathogen *C. rodentium* independent of investigations of diet and antibiotic usage.

4.4 Commensal *Klebsiella oxytoca* strains protect against colonization with multi-drug resistant *Klebsiella pneumoniae*

Multi-drug resistance in the family of Enterobacteriaceae is a great health-care associated problem worldwide (WHO, 2017). Especially the incidence of infections as well as the mortality rates linked to carbapenem-resistant *K. pneumoniae* is constantly increasing and has reached alarming rates in Europe (Cassini et al., 2019). The search for alternative intervention strategies new therapeutics is therefore urgently required. In this chapter, I aimed to investigate the potential of commensal related species to compete with carbapenem- resistant *K. pneumoniae* and to selectively decolonize MDR carrying mice with commensal *Klebsiella* strains.

At the moment there is no established mouse model for *Klebsiella* colonization in the gut (Bengoechea and Sa Pessoa, 2019). To find a suitable model to modulate long-term colonization with MDR *K. pneumoniae* in mice, different mouse strains including antibiotic naïve and antibiotic treated SPF-H mice, as well as gnotobiotic Oligo-MM^{12} which harbor 12 defined microbes in their gut (Brugiroux et al., 2016) mice and GF mice were colonized with a NDM-1 encoding *K. pneumoniae* clinical isolate representing an emerging MDR strain from the sequence type ST395. The antibiotic treated SPF-H mice as well as the gnotobiotic and GF animals could be easily and stably colonized whereas antibiotic naïve mice were either completely resistant or cleared the pathogen already after several days, whereas all other mouse strains remained high CFUs until the end of the experiments after six weeks. None of the mice showed any sign of local or systemic inflammation such as body weight loss or diarrhea, which indicated that MDR *K. pneumoniae* is an asymptomatic colonizer in immunocompetent mice. This observation is also common in humans as hospital-associated *Enterobacteriaceae* strains often expand in the gut without triggering overt inflammatory responses (Sorbara et al., 2018). The main problem of expansion of these species in the gut is the increased risk for subsequent development of a BSI in vulnerable patient populations and the global spread of antibiotic resistance (Taur et al., 2012). The observation that ampicillin-mediated destruction of the microbiota is associated with expansion of *Enterobacteriaceae* (van der Waaij et al., 1971) and the expansion in naturally susceptible Oligo-MM^{12} and GF mice indicates that the healthy and species-rich microbiota has the capacity to prevent the expansion of these strains. Even though previous colitis facilitates blooming of enterobacteria in the gut (Stecher, Maier and Hardt, 2013) enteric expansion of MDR strains occurs mostly asymptomatic suggesting that these strains are capable to inactivate microbiota-mediated inhibitory mechanisms that remain incompletely defined (Sorbara et al., 2018).

Thus, I next examined the changes in the microbiota during six weeks of *K. pneumoniae* colonization in ampicillin treated SPF mice. As expected, antibiotic treatment rendered the mice almost completely germ-free with reduction of species richness and diversity to almost zero. Even though the microbiota almost recovered completely after ending ampicillin treatment, species evenness was still lower after 6 weeks of colonization compared to antibiotic naïve infected control mice indicating that some long-term effects were still visible due to the *K. pneumoniae* and antibiotics treatment. In humans, antibiotic treatment has been reported to exhibit long-lasting effects on the microbiota. Some commensals have been eradicated from all hosts therefore being lost for recolonization (Jernberg et al., 2010). This species extinction is further exacerbated especially in westernized countries through fiber-poor diet, laxatives and hygiene leading to significant reduction of species richness in microbiotas of industrialized populations compared to individuals of rural countries (Mosca et al., 2016).

After establishment of different animal models, I next aimed to isolate promising candidates to compete with MDR *K. pneumoniae* strains. As direct competition for environmental niches in the gut is a fundamental requirement for invading species to successfully establish in the host, which is facilitated after antibiotic perturbation of the resident microbiota (Lam and Monack, 2014). I hypothesized that related commensal species might be promising candidates to compete with MDR *K. pneumoniae* strains as they might also exploit similar nutrient sources and grow in an oxygen-containing environment. To identify and isolate commensal *Klebsiella* strains, feces of 59 healthy adults and 54 healthy children were screened and assessed in an *in vitro* growth assay for colonization ability with MDR *K. pneumoniae* strains to identify particularly resistant individuals. In total, 16 *Klebsiella* strains were isolated from 13 healthy adult individuals and 16 strains from 15 healthy children. From 32 *Klebsiella* isolates in total, 11 strains belonged to the species *K. pneumoniae*, one strain each was identified as *K. quasipneumoniae* and *K. variicola* and 19 strains belonged to *K. oxytoca*. Currently, the genus *Klebsiella* includes 18 species from which five (*K. pneumoniae, K. quasipneumoniae, K. variicola, K. michiganensis* and *K. oxytoca*) are frequently found in the gut (Holt et al., 2015). Prevalence of *Klebsiella* strains in the gut reached 22 % in adults (13/59 positive) and 27.8 % in healthy children (15/54 positive). These data fit to reported prevalence in the literature with colonization rates ranging from 23% (Martin et al., 2016) up to 35 % in older studies (Matsen, Spindler and Blosser, 1974). Fecal carriage of multi-drug resistant *Enterobacteriaceae* has been described as important risk factor for colonization and subsequent infection especially in intensive care unit (ICU) patients (Feldman et al., 2013; Gorrie et al., 2017). To analyze how many of the isolated strains carry major resistance genes, genomes were sequenced by Illumina sequencing and resistance genes were used to predict resistance phenotypes.

Furthermore, the strains were screened by antibiotics susceptibility testing to verify the predicted phenotypes. Except for the naturally occurring resistance against ampicillin due to expression of chromosomally encoded class A gamma-lactamases in all species (Stock and Wiedemann, 2001) at least one additional resistance was found in all commensal *K. pneumoniae* strains except for isolate number #149. Two isolates belonged to the emerging sequence type ST395 and exhibited a carbapenem-resistance pattern. ST395 is frequently associated with nosocomial spread and MDR in Europe (Fasciana et al., 2019; Muggeo et al., 2018). Another two isolates belonged to ST1764, which was reported in 2019 to cause an outbreak of nosocomial infection caused by NDM-1 producing hypervirulent (hypermucoviscous) *K. pneumoniae* strain in China (Liu et al., 2019). Genomic sequencing revealed predicted resistance pattern for ampicillin, ceftriaxone, fosfomycin, and chloramphenicol. Another strain belonged to ST23 which has been also reported as an emerging MDR strain carrying a rare hybrid plasmid harboring virulence gene (Shen et al., 2019). Two strains belonged to ST86, which was reported in 2015 as a newly emerging HV strain with serotype K2 causing life-threatening infections (Zhang et al., 2015). It is commonly reported that hypervirulent strains exhibit less resistance genes but are more virulent than classical *K. pneumoniae* strains (Shen et al., 2019). In contrast to MDR *K. pneumoniae,* who are often associated with nosocomial infections, HV *K. pneumoniae* strains occur in the healthy community (Russo and Marr, 2019). In this work, one strain exhibited no further resistances except for ampicillin. The second strain was additionally resistant against chloramphenicol. Infections are more common in the Asian Pacific Rim but are increasingly occurring globally. Emergence of MDR HV *K. pneumoniae* strains is a constantly rising problem (Shen et al., 2019). The remaining strains belonged to ST1693, ST2097 and ST200. It is obvious how widespread resistance in *K. pneumoniae* in the healthy populations already is and as resistance is mostly plasmid encoded, it can be easily transmitted between different strains. Because of that, commensal *K. pneumoniae* strains might not be good candidates to fight MDR *K. pneumoniae.*

Nevertheless, in both cohorts (MikroKids and MikroResist) we found that occurrence of *Klebsiella* species was rather associated with reduced CFUs with particularly resistant individuals carrying strains of commensal *K. oxytoca.* In total, 19 strains were isolated from healthy individuals, with 4 strains (21.1%) found in healthy adults and 15 strains (78.9%) isolated from healthy children. These ratios are not surprising, as the portions of facultative anaerobic species is especially high in the developing microbiome below the age of three (Bäckhed et al., 2015; Dominguez-Bello, 2010). Two to ten percent of humans harbor *K. oxytoca* in their intestines (Herzog et al., 2014). Normally, *K. oxytoca* has been reported as an opportunistic pathogen implicated in various clinical diseases especially in infants (Chen et al., 2020; Darby et al., 2014; Reyman et al., 2019).

Studies suggest that *K. oxytoca* exerts its pathogenicity in part through a cytotoxine called tillivaline causing antibiotic-associated hemorrhagic colitis (AAHC) (Schneditz et al., 2014). In the last years, *K. oxytoca* has gained more clinical significance through acquisition of multiple resistances (Singh, Cariappa and Kaur, 2016). However, neither the identity of the toxin nor a complete repertoire of genes involved in *K. oxytoca* pathogenesis have been fully elucidated. On the other hand, more recent studies highlighted the potential of certain *Klebsiella* strains to act as a probiotic commensal. The ability of mice to retain or share the commensal *K. michiganensis,* a closely related species to *K. oxytoca* has been shown to sufficiently maintain colonization resistance after treatment with antibiotics against an *E. coli* by competition for essential nutrients (Oliveira et al., 2020). Interestingly, children harbored significantly more *K. oxytoca* strains compared to adults and exhibited overall reduced CFUs in the colonization assay with *K. pneumoniae.* Therefore, *K. pneumoniae* is a promising target for further analysis as we found this species also in the most protected sample and none of the strains exhibited further antibiotic resistance genes besides ampicillin indicating that MDR is far less widespread compared to *K. pneumoniae* isolates. Similar to *E. coli* Nissle, also some *K. oxytoca* strains could exhibit probiotic properties while other strains of the same species such as EHEC or EPEC are known pathogens (Fang, Jin and Hong, 2018).

Indeed, *K. oxytoca* isolated from protected individuals was capable to reduce growth of MDR *K. pneumoniae in vitro* and *in vivo* significantly, when added to ampicillin treated cecal content of mice before challenge with MDR *K. pneumoniae* or to Oligo-MM^{12} mice without antibiotic intervention. The effect was strong and reproducible in all animals, when reaching a certain threshold of precolonization. *In vitro* assays revealed that amounts of *K. oxytoca* present in the samples and the resulting CFUs of MDR *K. pneumoniae* were strongly anti-correlated suggesting direct effects are required to exhibit the protective properties. Furthermore, kinetics experiments revealed that clearance rates were significantly accelerated and improved with rates over 80% clearance after 6-9 days of MDR colonization, which were maintained until the end of experiment after 6 weeks. The effect was present in all tested (n=5) human isolates of *K. oxytoca*, but less pronounced in a mouse-commensal *K. oxytoca* strain and not present in a human commensal *E. coli* isolate indicating that the effect is generally present in *K. oxytoca* but is not common in other related *Enterobacteriaceae*. In addition, the protective properties of *K. oxytoca* could also be proven in another MDR *K. pneumoniae* strain belonging to ST258 who is an emerging strain in the US but also worldwide (Chen et al., 2014) suggesting broad-spectrum activity against a range of emerging *K. pneumoniae* strains. Lastly, *K. oxytoca* significantly reduced luminal and tissue associated *K. pneumoniae* in all gastrointestinal organs and inhibited systemic spread into liver and spleen in organ burden experiments (Fig 55).

Based on these findings, different hypotheses were constructed. Recent studies have demonstrated that *K. oxytoca* has the potential to stimulate specific immune cell subsets during early-life microbial colonization. Constantinides and colleagues could show that Mucosal-associated invariant T cells (MAIT cells) were induced during a specific early-life window in response to riboflavin-synthesizing commensals including *K. oxytoca*. MAIT cells display characteristics of innate and adaptive immunity boosting inflammation and microbial defense (Godfrey et al., 2019). This phenomenon permanently imprinted the abundance of this subset in tissues, controlling tissue repair and homeostasis thereby exhibiting long-term effects on the composition of the immune system (Constantinides et al., 2019). In the upper airways, Proteobacteria are key modulators of neonatal immune development by priming immunity through induction of IL17A (Sequeira et al., 2020) and induction of regulatory T cells promoting tolerance to allergens (Gollwitzer et al., 2014). In this work, it is rather unlikely that *K. oxytoca* elicits its protective properties via an immune-mediated mechanism due to multiple reasons. First, the phenotype was visible in isolated cecal content with short-term presence of *K. oxytoca* for 24h before *K. pneumoniae* was added. Second, the same protective effect was observed in organ burden experiments using *Rag2*$^{-/-}$ SPF-H mice, who are devoid of B- and T-cells thereby not having a proper adaptive immunity. However, to totally exclude any impact of innate immunity, experiments should be performed using knock-out mice without specific aspects of innate immunity and assessing cytokine profiles upon *K. oxytoca* colonization.

The fact that *K. oxytoca* could partially reduce MDR *K. pneumoniae* in isolated cecal content and in GF animals *in vivo,* rather supports the hypothesis that the protection is mediated by a direct competitive effect. A promising hypothesis is nutrient competition between related species, which have the capacity to grow on structurally similar and essential carbohydrates (Fig 55). This effect has been already demonstrated for multiple pathogens such as *C. rodentium* who is outcompeted by a commensal *E. coli* strain (Kamada et al., 2012). Similarly, Velazquez and colleagues proposed a mechanism by which probiotic *E. coli* or related *Enterobacteriaceae* conferred resistance by using its aerobic metabolism (Velazquez et al., 2019) or specialized iron transporters to compete with Salmonella for resources (Deriu et al., 2013). Besides *E. coli*, also the transfer of *K. michiganensis* between cohoused mice has been recently shown to outcompete *E. coli* by nutrient competition (Oliveira et al., 2020). Ongoing pilot experiments showed a big overlap in the ability of *K. oxytoca* and *K. pneumoniae* to use similar carbon sources and a tendency of *K. oxytoca* to grow faster on some mucus-derived carbon sources (data not shown). Further competition experiments and generation of different knock-out mutants are required to proof the influence of nutrient competition in the observed phenotype directly.

Another hypothesis is a direct antagonistic effect of *K. oxytoca* against *K. pneumoniae* such as production of inhibitory substances or contact-mediated killing through expression of T6SS. *Enterobacteriaceae* are common producers of specific short ribosomally synthesized bacteriocins called microcines, which are especially active against related species (Baquero et al., 2019). Microcins are promising antibacterial agents mediating the inhibition of the target cell via pore formation in bacterial membranes, inhibition of the DNA gyrase GyrB, impairment of transcription or action on cytochromes (Baquero et al., 2019). Bioinformatical analysis did not reveal presence of gene clusters such as MccE492 encoding for known microcins in any of the isolated *K. oxytoca* strains. Further experiments under *in vitro* conditions using trans-well plates could unravel if direct contact would be required to reduce *K. pneumoniae* or other inhibitory compounds are produced.

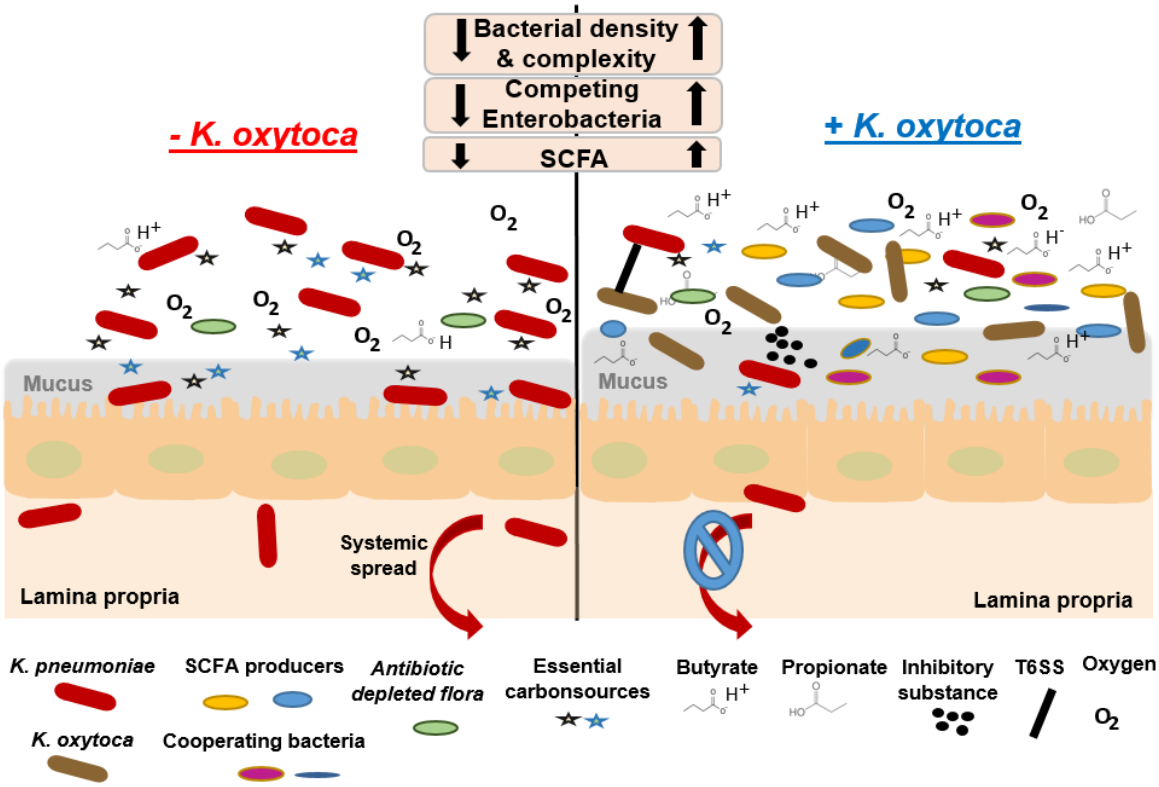

Figure 55: Potential mechanisms of *K. oxytoca* mediated protection. Multiple direct mechanisms might explain protective effect of *K. oxytoca* against MDR *K. pneumoniae*. *K. oxytoca* helps to reestablish a complex, species rich and SCFA producing microbiota after antibiotic depletion either by competition for oxygen or key nutrients. Eventually, *K. oxytoca* is able to produce any inhibitory substance or directly kill *K. pneumoniae* by expression of T6SS.

The fact that *K. oxytoca* could only partially reduce MDR *K. pneumoniae* in GF mice makes it likely that the protection occurs via a direct mechanism who involves other commensal species potentially reestablishing colonization resistance. Microbiota analysis revealed, that antibiotic treated, *K. oxytoca* precolonized mice recovered their anaerobic species and species richness faster than those without *K. oxytoca*. Especially the reoccurrence of SCFA promoting anaerobic species within the Firmicutes and Bacteroidetes phylum was significantly accelerated, which was accompanied by elevated SCFA levels already after 6 days after MDR colonization (Fig 55). This cooperating commensal hypothesis has been already demonstrated for VRE by Caballero and colleagues in which defined consortia containing *Blautia producta* and *Clostridium bolteae* restored colonization resistance against VRE and cleared VRE from the intestines of mice (Caballero et al., 2017). As the protective effect is also visible in Oligo-MM^{12} mice, further experiments should examine the potential of each of these twelve bacteria to establish long-term protection together with *K. oxytoca* by single transfer of bacteria into GF mice.

The therapeutic potential was further supported by experiments proving the ability of *K. oxytoca* to lower the CFUs and to improve clearance of mice who were initially colonized with MDR *K. pneumoniae*. In addition, *K. oxytoca* was also capable to improve clearance in mice who were humanized with susceptible donor microbiota to the same levels of mice who received more resistant donor feces. These findings support the therapeutic or prophylactic administration of a commensal bacterium to individuals with compromised microbiota composition, which may has the potential to reduce inter-patient transmission and intra-patient dissemination of highly antibiotic-resistant pathogens.

5. Outlook and future directions

In this thesis, global aspects regarding the interplay between microbiota composition and infection susceptibility during health and disease were investigated. Even though several interesting observations were made, e.g. key factors such as butyrate, an acidic pH value and presence of key species such as *K. oxytoca* were identified as relevant determinants; the understanding of many basic, conserved functions of these diverse, health-promoting microbial communities is incomplete. In line with other studies, we confirmed that patients undergoing treatment against hematological malignancies have a disturbed microbiota that favors pathogen colonization. Future studies are warranted to identify additional factors that are responsible for providing colonization resistance and/or pathogen displacement. It will be of high importance to consider the safety profile of any pre- or probiotic intervention, as many of the relevant patient populations are immunocompromised.

A particularly fascinating observation in this thesis was the case of *K. oxytoca*, which is part of the microbiota of healthy individuals and who protected against the colonization with MDR *K. pneumoniae*. While the exact mechanism of how *K. oxytoca* provides colonization resistance against *K. pneumoniae* is still unknown, experiments suggested that *K. oxytoca* could be used in a preventive manner to lower the risk for MDR colonization during antibiotic intervention but also has curative potential to selectively decolonize the host from its MDR pathogens after established colonization. Protective effects against two different clinically relevant *K. pneumoniae* strains was demonstrated, but additional experiments will be required to exactly determine the spectrum of protective activity. Finally, *K. oxytoca* treatment was associated with the faster recovery of obligate anaerobic species in mice and could in the future be potentially be explored for patients after chemotherapy or other diseases requiring treatment with broad-spectrum antibiotics and immunosuppressive drugs.

In principle, *K. oxytoca* meets the criteria established by the WHO defining a probiotic as “a live organism, which provides a benefit to the host when provided in adequate quantities” (FAO/WHO 2002). However, not all probiotics are beneficial in all circumstances. The careful testing of *K. oxytoca* especially the impact of tillivaline under *in vitro* and *in vivo* conditions is a prerequisite to minimize potential side effects especially with regard to the application in vulnerable patient cohorts. Further development of a novel probiotic requires detailed knowledge about the mechanism of action by which *K. oxytoca* prevents MDR colonization.

Ongoing experiments are therefore focusing on the generation of gene-deficient strains, which are deficient in potential key factors for protection, e.g. unable to utilize oxygen and different carbon sources, or are impaired in the production of tillivaline. Determination whether the live organism, secreted products (such as surface-layer proteins), or probiotic-derived products (such as bacteriocins) are sufficient to mediate the beneficial effect requires further study. In case one of the latter are indeed responsible for the effect, safety concerns could be reduced as live organisms may mutate over time or may have contraindicated effects in certain patient populations. Once, the underlying mechanism has been identified, the knowledge could be a starting point to design strategies for the reacquisition of natural commensals and to routinely restore microbiota composition after chemotherapy or antibiotics intervention with defined consortia of health promoting bacteria and metabolites. In the future, carefully selected and fully tested probiotics could provide alternative treatment options if conventional therapies have failed or may even serve as a fist-line choice of therapy for some patients.

6. References

1. Al-Dasooqi N, Sonis ST, Bowen JM, et al. Emerging evidence on the pathobiology of mucositis. *Support Care Cancer*. 2013;21(11):3233-3241. doi:10.1007/s00520-013-1900-x
2. Alexander JL, Wilson ID, Teare J, Marchesi JR, Nicholson JK, Kinross JM. Gut microbiota modulation of chemotherapy efficacy and toxicity. *Nat Rev Gastroenterol Hepatol*. 2017;14(6):356-365. doi:10.1038/nrgastro.2017.20
3. Arpaia N, Campbell C, Fan X, et al. Metabolites produced by commensal bacteria promote peripheral regulatory T-cell generation. *Nature*. 2013;504(7480):451-455. doi:10.1038/nature12726
4. Arslan N. Obesity, fatty liver disease and intestinal microbiota. *World J Gastroenterol*. 2014;20(44):16452-16463. doi:10.3748/wjg.v20.i44.16452
5. Arumugam M, Raes J, Pelletier E, et al. Enterotypes of the human gut microbiome. *Nature*. 2011;473(7346):174-180. doi:10.1038/nature09944
6. Asaduzzaman SM, Sonomoto K. Lantibiotics: Diverse activities and unique modes of action. *J Biosci Bioeng*. 2009;107(5):475-487. doi:10.1016/j.jbiosc.2009.01.003
7. Bäckhed F, Fraser CM, Ringel Y, et al. Defining a healthy human gut microbiome: Current concepts, future directions, and clinical applications. *Cell Host Microbe*. 2012;12(5):611-622. doi:10.1016/j.chom.2012.10.012
8. Bäckhed F, Roswall J, Peng Y, et al. Dynamics and stabilization of the human gut microbiome during the first year of life. *Cell Host Microbe*. 2015;17(5):690-703. doi:10.1016/j.chom.2015.04.004
9. Bäumler AJ, Sperandio V. Interactions between the microbiota and pathogenic bacteria in the gut. *Nature*. 2016;535(7610):85-93. doi:10.1038/nature18849
10. Becattini S, Littmann ER, Carter RA, et al. Commensal microbes provide first line defense against Listeria monocytogenes infection. *J Exp Med*. 2017;214(7):1973-1989. doi:10.1084/jem.20170495
11. Beck JA, Lloyd S, Hafezparast M, et al. Genealogies of mouse inbred strains. *Nat Genet*. 2000;24(1):23-25. doi:10.1038/71641
12. Bengoechea JA, Sa Pessoa J. *Klebsiella pneumoniae* infection biology: living to counteract host defences. *FEMS Microbiol Rev*. 2019;43(2):123-144. doi:10.1093/femsre/fuy043
13. Beutheu S, Ouelaa W, Guérin C, et al. Glutamine supplementation, but not combined glutamine and arginine supplementation, improves gut barrier function during chemotherapy-induced intestinal mucositis in rats. *Clin Nutr*. 2014;33(4):694-701. doi:10.1016/j.clnu.2013.09.003
14. Bhinder G, Sham HP, Chan JM, Morampudi V, Jacobson K, Vallance BA. The Citrobacter rodentium Mouse Model: Studying Pathogen and Host Contributions to Infectious Colitis. *J Vis Exp*. 2013;(72). doi:10.3791/50222
15. Bodiga VL, Bodiga S, Surampudi S, et al. Effect of vitamin supplementation on cisplatin-induced intestinal epithelial cell apoptosis in Wistar/NIN rats. *Nutrition*. 2012;28(5):572-580. doi:10.1016/j.nut.2011.09.007
16. Bohnhoff M, Miller CP, Martin WR. Resistance of the mouse's intestinal tract to experimental Salmonella infection. I. Factors which interfere with the initiation of infection by oral inoculation. *J Exp Med*. 1964;120:805-816. doi:10.1084/jem.120.5.805
17. Bonder MJ, Tigchelaar EF, Cai X, et al. The influence of a short-term gluten-free diet on the human gut microbiome. *Genome Med*. 2016;8(1):45. doi:10.1186/s13073-016-0295-y
18. Bouskra D, Brézillon C, Bérard M, et al. Lymphoid tissue genesis induced by commensals through NOD1 regulates intestinal homeostasis. *Nature*. 2008;456(7221):507-510. doi:10.1038/nature07450
19. Brandi G, Dabard J, Raibaud P, et al. Intestinal Microflora and Digestive Toxicity of Irinotecan in Mice. *Clin Cancer Res*. 2006;12(4):1299-1307. doi:10.1158/1078-0432.CCR-05-0750
20. Broberg CA, Palacios M, Miller VL. Klebsiella: A long way to go towards understanding this enigmatic jet-setter. *F1000Prime Rep*. 2014;6:64. doi:10.12703/P6-64
21. Brugiroux S, Beutler M, Pfann C, et al. Genome-guided design of a defined mouse microbiota that confers colonization resistance against Salmonella enterica serovar Typhimurium. *Nat Microbiol*. 2016;2:16215. doi:10.1038/nmicrobiol.2016.215
22. Buffie CG, Bucci V, Stein RR, et al. Precision microbiome reconstitution restores bile acid mediated resistance to Clostridium difficile. *Nature*. 2015;517(7533):205-208. doi:10.1038/nature13828

23. Buffie CG, Pamer EG. Microbiota-mediated colonization resistance against intestinal pathogens. *Nat Rev Immunol*. 2013;13(11):790-801. doi:10.1038/nri3535
24. Caballero S, Carter R, Ke X, et al. Distinct but Spatially Overlapping Intestinal Niches for Vancomycin-Resistant Enterococcus faecium and Carbapenem-Resistant Klebsiella pneumoniae. Baumler AJ, ed. *PLOS Pathog*. 2015;11(9):e1005132. doi:10.1371/journal.ppat.1005132
25. Caballero S, Kim S, Carter RA, et al. Cooperating Commensals Restore Colonization Resistance to Vancomycin-Resistant Enterococcus faecium. *Cell Host Microbe*. 2017;21(5):592-602.e4. doi:10.1016/j.chom.2017.04.002
26. Caballero S, Pamer EG. Microbiota-Mediated Inflammation and Antimicrobial Defense in the Intestine. *Annu Rev Immunol*. 2015;33(1):227-256. doi:10.1146/annurev-immunol-032713-120238
27. Caporaso JG, Lauber CL, Walters WA, et al. Global patterns of 16S rRNA diversity at a depth of millions of sequences per sample. *Proc Natl Acad Sci*. 2011;108(Supplement_1):4516-4522. doi:10.1073/pnas.1000080107
28. Caporaso JG, Kuczynski J, Stombaugh J, et al. QIIME allows analysis of high-throughput community sequencing data. *Nat Methods*. 2010;7(5):335-336. doi:10.1038/nmeth.f.303
29. Carvalho R, Vaz A, Pereira FL, et al. Gut microbiome modulation during treatment of mucositis with the dairy bacterium Lactococcus lactis and recombinant strain secreting human antimicrobial PAP. *Sci Rep*. 2018;8(1):1-10. doi:10.1038/s41598-018-33469-w
30. Cascales E, Buchanan SK, Duche D, et al. Colicin Biology. *Microbiol Mol Biol Rev*. 2007;71(1):158-229. doi:10.1128/mmbr.00036-06
31. Cassini A, Högberg LD, Plachouras D, et al. Attributable deaths and disability-adjusted life-years caused by infections with antibiotic-resistant bacteria in the EU and the European Economic Area in 2015: a population-level modelling analysis. *Lancet Infect Dis*. 2019;19(1):56-66. doi:10.1016/S1473-3099(18)30605-4
32. Centre. Centre for disease control. https://www.cdc.gov/drugresistance/about.html. Accessed March 13, 2020.
33. Chang S, Chen W, Yang J. Another formula for calculating the gene change rate in real-time RT-PCR. *Mol Biol Rep*. 2009;36(8):2165-2168. doi:10.1007/s11033-008-9430-1
34. Chen L, Mathema B, Pitout JDD, DeLeo FR, Kreiswirth BN. Epidemic Klebsiella pneumoniae ST258 is a hybrid strain. *MBio*. 2014;5(3). doi:10.1128/mBio.01355-14
35. Chen Y, Brook TC, Soe CZ, et al. Preterm infants harbour diverse Klebsiella populations, including atypical species that encode and produce an array of antimicrobial resistance- and virulence-associated factors. *Microb Genomics*. May 2020:mgen000377. doi:10.1099/mgen.0.000377
36. Cho I, Yamanishi S, Cox L, et al. Antibiotics in early life alter the murine colonic microbiome and adiposity. *Nature*. 2012;488(7413):621-626. doi:10.1038/nature11400
37. Chung H, Pamp SJ, Hill JA, et al. Gut immune maturation depends on colonization with a host-specific microbiota. *Cell*. 2012;149(7):1578-1593. doi:10.1016/j.cell.2012.04.037
38. Claesson MJ, Jeffery IB, Conde S, et al. Gut microbiota composition correlates with diet and health in the elderly. *Nature*. 2012;488(7410):178-184. doi:10.1038/nature11319
39. Clarke SF, Murphy EF, O'Sullivan O, et al. Exercise and associated dietary extremes impact on gut microbial diversity. *Gut*. 2014;63(12):1913-1920. doi:10.1136/gutjnl-2013-306541
40. Codjoe F, Donkor E. Carbapenem Resistance: A Review. *Med Sci*. 2017;6(1):1. doi:10.3390/medsci6010001
41. Collins JW, Keeney KM, Crepin VF, et al. Citrobacter rodentium: infection, inflammation and the microbiota. *Nat Rev Microbiol*. 2014;12(9):612-623. doi:10.1038/nrmicro3315
42. Constantinides MG, Link VM, Tamoutounour S, et al. MAIT cells are imprinted by the microbiota in early life and promote tissue repair. *Science (80-)*. 2019;366(6464). doi:10.1126/science.aax6624
43. Corr SC, Li Y, Riedel CU, O'Toole PW, Hill C, Gahan CGM. Bacteriocin production as a mechanism for the antiinfective activity of Lactobacillus salivarius UCC118. *Proc Natl Acad Sci U S A*. 2007;104(18):7617-7621. doi:10.1073/pnas.0700440104
44. Corthésy B. Role of secretory IgA in infection and maintenance of homeostasis. *Autoimmun Rev*. 2013;12(6):661-665. doi:10.1016/j.autrev.2012.10.012

45. Curtis MM, Hu Z, Klimko C, Narayanan S, Deberardinis R, Sperandio V. The gut commensal Bacteroides thetaiotaomicron exacerbates enteric infection through modification of the metabolic landscape. *Cell Host Microbe*. 2014;16(6):759-769. doi:10.1016/j.chom.2014.11.005
46. Daharsh L, Ramer-Tait AE, Li Q. Stable Engraftment of a Human Gut Bacterial Microbiome in Double Humanized BLT-mice. *bioRxiv*. August 2019:749093. doi:10.1101/749093
47. Darby A, Lertpiriyapong K, Sarkar U, et al. Cytotoxic and Pathogenic Properties of Klebsiella oxytoca Isolated from Laboratory Animals. Bereswill S, ed. *PLoS One*. 2014;9(7):e100542. doi:10.1371/journal.pone.0100542
48. David LA, Maurice CF, Carmody RN, et al. Diet rapidly and reproducibly alters the human gut microbiome. *Nature*. 2014;505(7484):559-563. doi:10.1038/nature12820
49. Degruttola AK, Low D, Mizoguchi A, Mizoguchi E. Current understanding of dysbiosis in disease in human and animal models. *Inflamm Bowel Dis*. 2016;22(5):1137-1150. doi:10.1097/MIB.0000000000000750
50. Den Besten G, Van Eunen K, Groen AK, Venema K, Reijngoud DJ, Bakker BM. The role of short-chain fatty acids in the interplay between diet, gut microbiota, and host energy metabolism. *J Lipid Res*. 2013;54(9):2325-2340. doi:10.1194/jlr.R036012
51. Deriu E, Liu JZ, Pezeshki M, et al. Probiotic bacteria reduce salmonella typhimurium intestinal colonization by competing for iron. *Cell Host Microbe*. 2013;14(1):26-37. doi:10.1016/j.chom.2013.06.007
52. Dethlefsen L, Huse S, Sogin ML, Relman DA. The pervasive effects of an antibiotic on the human gut microbiota, as revealed by deep 16s rRNA sequencing. *PLoS Biol*. 2008;6(11):2383-2400. doi:10.1371/journal.pbio.0060280
53. Devkota S. Prescription drugs obscure microbiome analyses. *Science (80-)*. 2016;351(6272):452-453. doi:10.1126/science.aaf1353
54. Diancourt L, Passet V, Verhoef J, Grimont PAD, Brisse S. Multilocus sequence typing of Klebsiella pneumoniae nosocomial isolates. *J Clin Microbiol*. 2005;43(8):4178-4182. doi:10.1128/JCM.43.8.4178-4182.2005
55. Dobson GP, Letson HL, Biros E, Morris J. Specific pathogen-free (SPF) animal status as a variable in biomedical research: Have we come full circle? *EBioMedicine*. 2019;41:42-43. doi:10.1016/j.ebiom.2019.02.038
56. Dominguez-Bello MG, Costello EK, Contreras M, et al. Delivery mode shapes the acquisition and structure of the initial microbiota across multiple body habitats in newborns. *Proc Natl Acad Sci U S A*. 2010;107(26):11971-11975. doi:10.1073/pnas.1002601107
57. Dong N, Lin D, Zhang R, Chan EW-C, Chen S. Carriage of blaKPC-2 by a virulence plasmid in hypervirulent Klebsiella pneumoniae. *J Antimicrob Chemother*. 2018;73(12):3317-3321. doi:10.1093/jac/dky358
58. Donia MS, Cimermancic P, Schulze CJ, et al. A systematic analysis of biosynthetic gene clusters in the human microbiome reveals a common family of antibiotics. *Cell*. 2014;158(6):1402-1414. doi:10.1016/j.cell.2014.08.032
59. Duncan SH, Louis P, Thomson JM, Flint HJ. The role of pH in determining the species composition of the human colonic microbiota. *Environ Microbiol*. 2009;11(8):2112-2122. doi:10.1111/j.1462-2920.2009.01931.x
60. Duquesne S, Destoumieux-Garzón D, Peduzzi J, Rebuffat S. Microcins, gene-encoded antibacterial peptides from enterobacteria. *Nat Prod Rep*. 2007;24(4):708-734. doi:10.1039/b516237h
61. Durant JA, Corrier DE, Ricke SC. Short-chain volatile fatty acids modulate the expression of the hilA and invF genes of Salmonella Typhimurium. *J Food Prot*. 2000;63(5):573-578. doi:10.4315/0362-028X-63.5.573
62. Edgar RC. Search and clustering orders of magnitude faster than BLAST. *Bioinformatics*. 2010;26(19):2460-2461. doi:10.1093/bioinformatics/btq461
63. Ernst W. Humanized mice in infectious diseases. *Comp Immunol Microbiol Infect Dis*. 2016;49:29-38. doi:10.1016/j.cimid.2016.08.006
64. Faber F, Thiennimitr P, Spiga L, et al. Respiration of Microbiota-Derived 1,2-propanediol Drives Salmonella Expansion during Colitis. *PLoS Pathog*. 2017;13(1). doi:10.1371/journal.ppat.1006129
65. Faber F, Tran L, Byndloss MX, et al. Host-mediated sugar oxidation promotes post-antibiotic pathogen expansion. *Nature*. 2016;534(7609):697-699. doi:10.1038/nature18597

66. Fabich AJ, Jones SA, Chowdhury FZ, et al. Comparison of carbon nutrition for pathogenic and commensal Escherichia coli strains in the mouse intestine. *Infect Immun*. 2008;76(3):1143-1152. doi:10.1128/IAI.01386-07
67. Fang K, Jin X, Hong SH. Probiotic Escherichia coli inhibits biofilm formation of pathogenic E. coli via extracellular activity of DegP. *Sci Rep*. 2018;8(1):1-12. doi:10.1038/s41598-018-23180-1
68. FAO, WHO. Guidelines for the Evaluation of Probiotics in Food. *WHO Work Rep*. 2002:1-11.
69. Farmer AD, Mohammed SD, Dukes GE, Mark Scott S, Hobson AR. Caecal pH is a biomarker of excessive colonic fermentation. *World J Gastroenterol*. 2014;20(17):5000-5007. doi:10.3748/wjg.v20.i17.5000
70. Fasciana T, Gentile B, Aquilina M, et al. Co-existence of virulence factors and antibiotic resistance in new Klebsiella pneumoniae clones emerging in south of Italy. *BMC Infect Dis*. 2019;19(1):928. doi:10.1186/s12879-019-4565-3
71. Feldman N, Adler A, Molshatzki N, et al. Gastrointestinal colonization by KPC-producing Klebsiella pneumoniae following hospital discharge: Duration of carriage and risk factors for persistent carriage. *Clin Microbiol Infect*. 2013;19(4). doi:10.1111/1469-0691.12099
72. Feng Y, Lu Y, Yao Z, Zong Z. Carbapenem-resistant hypervirulent klebsiella pneumoniae of sequence type 36. *Antimicrob Agents Chemother*. 2018;62(7). doi:10.1128/AAC.02644-17
73. Ferreira TM, Leonel AJ, Melo MA, et al. Oral supplementation of butyrate reduces mucositis and intestinal permeability associated with 5-fluorouracil administration. *Lipids*. 2012;47(7):669-678. doi:10.1007/s11745-012-3680-3
74. Ferreyra JA, Wu KJ, Hryckowian AJ, Bouley DM, Weimer BC, Sonnenburg JL. Gut microbiota-produced succinate promotes C. Difficile infection after antibiotic treatment or motility disturbance. *Cell Host Microbe*. 2014;16(6):770-777. doi:10.1016/j.chom.2014.11.003
75. Flint H. Links between diet, gut microbiota composition and gut metabolism. *Proc Nutr Soc*. 2015;74:13-22.
76. Galloway-Peña JR, Smith DP, Sahasrabhojane P, et al. The role of the gastrointestinal microbiome in infectious complications during induction chemotherapy for acute myeloid leukemia. *Cancer*. 2016;122(14):2186-2196. doi:10.1002/cncr.30039
77. Galloway-Peña JR, Peterson CB, Malik F, et al. Fecal Microbiome, Metabolites, and Stem Cell Transplant Outcomes: A Single-Center Pilot Study. *Open forum Infect Dis*. 2019;6(5):ofz173-ofz173. doi:10.1093/ofid/ofz173
78. Gantois I, Ducatelle R, Pasmans F, et al. Butyrate specifically down-regulates Salmonella pathogenicity island 1 gene expression. *Appl Environ Microbiol*. 2006;72(1):946-949. doi:10.1128/AEM.72.1.946-949.2006
79. Garrett WS. Cancer and the microbiota. *Science*. 2015;348(6230):80-86. doi:10.1126/science.aaa4972
80. Garsin DA. Ethanolamine utilization in bacterial pathogens: roles and regulation. *Nat Rev Microbiol*. 2010;8(4):290-295. doi:10.1038/nrmicro2334
81. Geerlings SY, Kostopoulos I, de Vos WM, Belzer C. Akkermansia muciniphila in the Human Gastrointestinal Tract: When, Where, and How? *Microorganisms*. 2018;6(3). doi:10.3390/microorganisms6030075
82. Generoso S V., Martins FS, Cartelle CT, et al. Evaluation of mucositis induced by irinotecan after microbial colonization in germ-free mice. *Microbiology*. 2015;161(10):1950-1960. doi:10.1099/mic.0.000149
83. Gielda L, DiRita V. Zinc competition among the intestinal microbiota. *MBio*. 2012;3:e00171-12.
84. Gifford AH, Kirkland KB. Risk factors for Clostridium difficile-associated diarrhea on an adult hematology-oncology ward. *Eur J Clin Microbiol Infect Dis*. 2006;25(12):751-755. doi:10.1007/s10096-006-0220-1
85. Gill SR, Pop M, Deboy RT, et al. Metagenomic analysis of the human distal gut microbiome. *Science*. 2006;312(5778):1355-1359. doi:10.1126/science.1124234
86. Godfrey DI, Koay HF, McCluskey J, Gherardin NA. The biology and functional importance of MAIT cells. *Nat Immunol*. 2019;20(9):1110-1128. doi:10.1038/s41590-019-0444-8
87. Gollwitzer ES, Saglani S, Trompette A, et al. Lung microbiota promotes tolerance to allergens in neonates via PD-L1. *Nat Med*. 2014;20(6):642-647. doi:10.1038/nm.3568
88. Goodrich JK, Waters JL, Poole AC, et al. Human genetics shape the gut microbiome. *Cell*. 2014;159(4):789-799. doi:10.1016/j.cell.2014.09.053
89. Gorrie CL, Mirčeta M, Wick RR, et al. Gastrointestinal Carriage Is a Major Reservoir of Klebsiella pneumoniae Infection in Intensive Care Patients. Clin Infect Dis. https://www.ncbi.nlm.nih.gov/pmc/articles/PMC5850561/. Published 2017. Accessed May 10, 2020.

90. Gough EK, Moodie EEM, Prendergast AJ, et al. The impact of antibiotics on growth in children in low and middle income countries: Systematic review and meta-analysis of randomised controlled trials. *BMJ*. 2014;348:g2267. doi:10.1136/bmj.g2267
91. Gu D, Dong N, Zheng Z, et al. A fatal outbreak of ST11 carbapenem-resistant hypervirulent Klebsiella pneumoniae in a Chinese hospital: a molecular epidemiological study. *Lancet Infect Dis*. 2018;18(1):37-46. doi:10.1016/S1473-3099(17)30489-9
92. Gupta V, Kumar R, Sood U, Singhvi N. Reconciling Hygiene and Cleanliness: A New Perspective from Human Microbiome. *Indian J Microbiol*. 2020;60(1):37-44. doi:10.1007/s12088-019-00839-5
93. Haidar G, Clancy CJ, Chen L, et al. Identifying Spectra of Activity and Therapeutic Niches for Ceftazidime-Avibactam and Imipenem-Relebactam against Carbapenem-Resistant Enterobacteriaceae. *Antimicrob Agents Chemother*. 2017;61(9). doi:10.1128/aac.00642-17
94. Hamer HM, Jonkers D, Venema K, Vanhoutvin S, Troost FJ, Brummer RJ. Review article: The role of butyrate on colonic function. *Aliment Pharmacol Ther*. 2008;27(2):104-119. doi:10.1111/j.1365-2036.2007.03562.x
95. Hayashi H, Takahashi R, Nishi T, Sakamoto M, Benno Y. Molecular analysis of jejunal, ileal, caecal and recto-sigmoidal human colonic microbiota using 16S rRNA gene libraries and terminal restriction fragment length polymorphism. *J Med Microbiol*. 2005;54(11):1093-1101. doi:10.1099/jmm.0.45935-0
96. Heinritz SN, Weiss E, Eklund M, et al. Intestinal microbiota and microbial metabolites are changed in a pig model fed a high-fat/low-fiber or a low-fat/high-fiber diet. *PLoS One*. 2016;11(4):e0154329. doi:10.1371/journal.pone.0154329
97. Herzog KAT, Schneditz G, Leitner E, et al. Genotypes of Klebsiella oxytoca isolates from patients with nosocomial pneumonia are distinct from those of isolates from patients with antibiotic-associated hemorrhagic colitis. *J Clin Microbiol*. 2014;52(5):1607-1616. doi:10.1128/JCM.03373-13
98. Hiller K, Hangebrauk J, Jäger C, Spura J, Schreiber K, Schomburg D. MetaboliteDetector: Comprehensive Analysis Tool for Targeted and Nontargeted GC/MS Based Metabolome Analysis. *Anal Chem*. 2009;81(9):3429-3439. doi:10.1021/ac802689c
99. Holt KE, Wertheim H, Zadoks RN, et al. Genomic analysis of diversity, population structure, virulence, and antimicrobial resistance in Klebsiella pneumoniae, an urgent threat to public health. *Proc Natl Acad Sci U S A*. 2015;112(27):E3574-E3581. doi:10.1073/pnas.1501049112
100. Hsiao EY, McBride SW, Hsien S, et al. Microbiota modulate behavioral and physiological abnormalities associated with neurodevelopmental disorders. *Cell*. 2013;155(7):1451-1463. doi:10.1016/j.cell.2013.11.024
101. Human Microbiome Project Consortium. Structure, function and diversity of the healthy human microbiome. *Nature*. 2012;486(7402):207-214. doi:10.1038/nature11234
102. Hung CC, Garner CD, Slauch JM, et al. The intestinal fatty acid propionate inhibits Salmonella invasion through the post-translational control of HilD. *Mol Microbiol*. 2013;87(5):1045-1060. doi:10.1111/mmi.12149
103. Imhann F, Bonder MJ, Vila AV, et al. Proton pump inhibitors affect the gut microbiome. *Gut*. 2016;65(5):740-748. doi:10.1136/gutjnl-2015-310376
104. Ivanov IIII, Atarashi K, Manel N, et al. Induction of Intestinal Th17 Cells by Segmented Filamentous Bacteria. *Cell*. 2009;139(3):485-498. doi:10.1016/j.cell.2009.09.033
105. Jacobson A, Lam L, Rajendram M, et al. A Gut Commensal-Produced Metabolite Mediates Colonization Resistance to Salmonella Infection. *Cell Host Microbe*. 2018;24(2):296-307.e7. doi:10.1016/j.chom.2018.07.002
106. Jakobsson HE, Abrahamsson TR, Jenmalm MC, et al. Decreased gut microbiota diversity, delayed Bacteroidetes colonisation and reduced Th1 responses in infants delivered by Caesarean section. *Gut*. 2014;63(4):559-566. doi:10.1136/gutjnl-2012-303249
107. Janda JM AS. The Enterobacteria, 2nd Edition. *Gut*. 2006;56(9):1330-1331. doi:10.1136/gut.2007.126417
108. Jernberg C, Löfmark S, Edlund C, Jansson JK. Long-term impacts of antibiotic exposure on the human intestinal microbiota. *Microbiology*. 2010;156(11):3216-3223. doi:10.1099/mic.0.040618-0
109. Jin M, Qian Z, Yin J, Xu W, Zhou X. The role of intestinal microbiota in cardiovascular disease. *J Cell Mol Med*. 2019;23(4):2343-2350. doi:10.1111/jcmm.14195
110. Journet L, Cascales E. The Type VI Secretion System in Escherichia coli and Related Species. *EcoSal Plus*. 2016;7(1). doi:10.1128/ecosalplus.ESP-0009-2015

111. Kader AA, Kumar A, Kamath KA. Fecal Carriage of Extended-Spectrum β-Lactamase–Producing Escherichia coli and Klebsiella pneumoniae in Patients and Asymptomatic Healthy Individuals . *Infect Control Hosp Epidemiol*. 2007;28(9):1114-1116. doi:10.1086/519865
112. Kamada N, Kim Y-G, Sham HP, et al. Regulated Virulence Controls the Ability of a Pathogen to Compete with the Gut Microbiota.*Science*.2012 doi:10.1126/science.1222195
113. Kang C, Ban M, Choi E-J, et al. Extracellular Vesicles Derived from Gut Microbiota, Especially Akkermansia muciniphila, Protect the Progression of Dextran Sulfate Sodium-Induced Colitis. Paredes-Sabja D, ed. *PLoS One*. 2013;8(10):e76520. doi:10.1371/journal.pone.0076520
114. Kang MJ, Kim HG, Kim JS, et al. The effect of gut microbiota on drug metabolism. *Expert Opin Drug Metab Toxicol*. 2013;9(10):1295-1308. doi:10.1517/17425255.2013.807798
115. Karrasch T, Steinbrecher KA, Allard B, Baldwin AS, Jobin C. Wound-induced p38MAPK-dependent histone H3 phosphorylation correlates with increased COX-2 expression in enterocytes. *J Cell Physiol*. 2006;207(3):809-815. doi:10.1002/jcp.20626
116. Kayagaki N, Warming S, Lamkanfi M, et al. Non-canonical inflammasome activation targets caspase-11. *Nature*. 2011;479(7371):117-121. doi:10.1038/nature10558
117. Keefe DM. Intestinal mucositis: mechanisms and management. *Curr Opin Oncol*. 2007;19(4):323-327. doi:10.1097/CCO.0b013e3281214412
118. Kelly CJ, Zheng L, Campbell EL, et al. Crosstalk between microbiota-derived short-chain fatty acids and intestinal epithelial HIF augments tissue barrier function. *Cell Host Microbe*. 2015;17(5):662-671. doi:10.1016/j.chom.2015.03.005
119. Kelly CR, Khoruts A, Staley C, et al. Effect of fecal microbiota transplantation on recurrence in multiply recurrent clostridium difficile infection a randomized trial. *Ann Intern Med*. 2016;165(9):609-616. doi:10.7326/M16-0271
120. Keng MK, Sidana S, Mukherjee S, et al. The Degree and Effect Of Weight Loss In Acute Myeloid Leukemia Patients Receiving Induction and Post-Remission Chemotherapy. *Blood*. 2013;122(21):3889-3889. doi:10.1182/BLOOD.V122.21.3889.3889
121. Kennedy EA, King KY, Baldridge MT. Mouse microbiota models: Comparing germ-free mice and antibiotics treatment as tools for modifying gut bacteria. *Front Physiol*. 2018;9(OCT):1534. doi:10.3389/fphys.2018.01534
122. Kim S, Covington A, Pamer EG. The intestinal microbiota: Antibiotics, colonization resistance, and enteric pathogens. *Immunol Rev*. 2017;279(1):90-105. doi:10.1111/imr.12563
123. Koh A, De Vadder F, Kovatcheva-Datchary P, Bäckhed F. From dietary fiber to host physiology: Short-chain fatty acids as key bacterial metabolites. *Cell*. 2016;165(6):1332-1345. doi:10.1016/j.cell.2016.05.041
124. Kommineni S, Bretl DJ, Lam V, et al. Bacteriocin production augments niche competition by enterococci in the mammalian gastrointestinal tract. *Nature*. 2015;526(7575):719-722. doi:10.1038/nature15524
125. Kozyrskyj AL, Ernst P, Becker AB. Increased risk of childhood asthma from antibiotic use in early life. *Chest*. 2007;131(6):1753-1759. doi:10.1378/chest.06-3008
126. Lam LH, Monack DM. Intraspecies Competition for Niches in the Distal Gut Dictate Transmission during Persistent Salmonella Infection. *PLoS Pathog*. 2014;10(12):e1004527. doi:10.1371/journal.ppat.1004527
127. Lawhon SD, Maurer R, Suyemoto M, Altier C. Intestinal short-chain fatty acids alter Salmonella typhimurium invasion gene expression and virulence through BarA/SirA. *Mol Microbiol*. 2002;46(5):1451-1464. doi:10.1046/j.1365-2958.2002.03268.x
128. Lawley TD, Walker AW. Intestinal colonization resistance. *Immunology*. 2013;138(1):1-11. doi:10.1111/j.1365-2567.2012.03616.x
129. Le Chatelier E, Nielsen T, Qin J, et al. Richness of human gut microbiome correlates with metabolic markers. *Nature*. 2013;500(7464):541-546. doi:10.1038/nature12506
130. Li HL, Lu L, Wang XS, et al. Alteration of gut microbiota and inflammatory cytokine/chemokine profiles in 5-fluorouracil induced intestinal mucositis. *Front Cell Infect Microbiol*. 2017;7(OCT). doi:10.3389/fcimb.2017.00455
131. Libertucci J, Young VB. The role of the microbiota in infectious diseases. *Nat Microbiol*. 2019;4(1):35-45. doi:10.1038/s41564-018-0278-4

132. Little AEF, Robinson CJ, Peterson SB, Raffa KF, Handelsman J. Rules of Engagement: Interspecies Interactions that Regulate Microbial Communities. *Annu Rev Microbiol*. 2008;62(1):375-401. doi:10.1146/annurev.micro.030608.101423
133. Litvak Y, Mon KKZ, Nguyen H, et al. Commensal Enterobacteriaceae Protect against Salmonella Colonization through Oxygen Competition. *Cell Host Microbe*. 2019;25(1):128-139.e5. doi:10.1016/j.chom.2018.12.003
134. Liu Z, Gu Y, Li X, et al. Identification and characterization of NDM-1-producing hypervirulent (Hypermucoviscous) Klebsiella pneumoniae in China. *Ann Lab Med*. 2019;39(2):167-175. doi:10.3343/alm.2019.39.2.167
135. Livermore D. beta-Lactamases in laboratory and clinical resistance.*Clin Microbiol Rev*.1995. doi:PMID: 8665470
136. Logan RM, Stringer AM, Bowen JM, et al. The role of pro-inflammatory cytokines in cancer treatment-induced alimentary tract mucositis: Pathobiology, animal models and cytotoxic drugs. *Cancer Treat Rev*. 2007;33(5):448-460. doi:10.1016/j.ctrv.2007.03.001
137. Lozupone CA, Stombaugh JI, Gordon JI, Jansson JK, Knight R. Diversity, stability and resilience of the human gut microbiota. *Nature*. 2012;489(7415):220-230. doi:10.1038/nature11550
138. Ma Z (Sam), Li L, Gotelli NJ. Diversity-disease relationships and shared species analyses for human microbiome-associated diseases. *ISME J*. 2019;13(8):1911-1919. doi:10.1038/s41396-019-0395-y
139. Macpherson AJ, Harris NL. Interactions between commensal intestinal bacteria and the immune system. *Nat Rev Immunol*. 2004;4(6):478-485. doi:10.1038/nri1373
140. Mähler M, Bristol IJ, Leiter EH, et al. Differential susceptibility of inbred mouse strainsto dextran sulfate sodium-induced colitis. *Am J Physiol*. 1998;274:544-551. moz-extension://e856aca9-cf72-4f84-81c8-922185c83562/enhanced-reader.html?openApp&pdf=https%3A%2F%2Fpdfs.semanticscholar.org%2F7f7e%2F435195df232d7a44b007d7e40eb832ccd315.pdf. Accessed March 20, 2020.
141. Maier L, Pruteanu M, Kuhn M, et al. Extensive impact of non-antibiotic drugs on human gut bacteria. *Nature*. 2018;555(7698):623-628. doi:10.1038/nature25979
142. Maier L, Vyas R, Cordova CD, et al. Microbiota-derived hydrogen fuels salmonella typhimurium invasion of the gut ecosystem. *Cell Host Microbe*. 2013;14(6):641-651. doi:10.1016/j.chom.2013.11.002
143. Maldonado-Gómez MX, Martínez I, Bottacini F, et al. Stable Engraftment of Bifidobacterium longum AH1206 in the Human Gut Depends on Individualized Features of the Resident Microbiome. *Cell Host Microbe*. 2016;20(4):515-526. doi:10.1016/j.chom.2016.09.001
144. Mallick EM, McBee ME, Vanguri VK, et al. A novel murine infection model for Shiga toxin–producing Escherichia coli. *J Clin Invest*. 2012;122(11):4012-4024. doi:10.1172/JCI62746
145. Marques TM, Wall R, Ross RP, Fitzgerald GF, Ryan CA, Stanton C. Programming infant gut microbiota: Influence of dietary and environmental factors. *Curr Opin Biotechnol*. 2010;21(2):149-156. doi:10.1016/j.copbio.2010.03.020
146. Martin RM, Bachman MA. Colonization, infection, and the accessory genome of Klebsiella pneumoniae. *Front Cell Infect Microbiol*. 2018;8(JAN). doi:10.3389/fcimb.2018.00004
147. Martin RM, Cao J, Brisse S, et al. Molecular Epidemiology of Colonizing and Infecting Isolates of Klebsiella pneumoniae. *mSphere*. 2016;1(5). doi:10.1128/msphere.00261-16
148. Martínez I, Stegen JC, Maldonado-Gómez MX, et al. The Gut Microbiota of Rural Papua New Guineans: Composition, Diversity Patterns, and Ecological Processes. *Cell Rep*. 2015;11(4):527-538. doi:10.1016/j.celrep.2015.03.049
149. Matsen JM, Spindler JA, Blosser RO. Characterization of Klebsiella Isolates from Natural Receiving Waters and Comparison with Human Isolates. *Appl Microbiol*. 1974;28(4):672.
150. Mayer EA. Gut feelings: The emerging biology of gut-"brain communication. *Nat Rev Neurosci*. 2011;12(8):453-466. doi:10.1038/nrn3071
151. McMurdie PJ, Holmes S. Phyloseq: An R Package for Reproducible Interactive Analysis and Graphics of Microbiome Census Data. *PLoS One*. 2013;8(4). doi:10.1371/journal.pone.0061217
152. Merla C, Rodrigues C, Passet V, et al. Description of Klebsiella spallanzanii sp. nov. and of Klebsiella pasteurii sp. nov. *Front Microbiol*. 2019;10(OCT):2360. doi:10.3389/fmicb.2019.02360

153. Montassier E, Gastinne T, Vangay P, et al. Chemotherapy-driven dysbiosis in the intestinal microbiome. *Aliment Pharmacol Ther*. 2015;42(5):515-528. doi:10.1111/apt.13302
154. Montassier E, Al-Ghalith GA, Ward T, et al. Pretreatment gut microbiome predicts chemotherapy-related bloodstream infection. *Genome Med*. 2016;8(1):49. doi:10.1186/s13073-016-0301-4
155. Moore RE, Townsend SD. Temporal development of the infant gut microbiome. *Open Biol*. 2019;9(9):190128. doi:10.1098/rsob.190128
156. Morgan XC, Tickle TL, Sokol H, et al. Dysfunction of the intestinal microbiome in inflammatory bowel disease and treatment. *Genome Biol*. 2012;13(9):R79. doi:10.1186/gb-2012-13-9-r79
157. Morrison DJ, Preston T. Formation of short chain fatty acids by the gut microbiota and their impact on human metabolism. *Gut Microbes*. 2016;7(3):189-200. doi:10.1080/19490976.2015.1134082
158. Mosca A, Leclerc M, Hugot JP. Gut microbiota diversity and human diseases: Should we reintroduce key predators in our ecosystem? *Front Microbiol*. 2016;7(MAR). doi:10.3389/fmicb.2016.00455
159. Muggeo A, Guillard T, Klein F, et al. Spread of Klebsiella pneumoniae ST395 non-susceptible to carbapenems and resistant to fluoroquinolones in North-Eastern France. *J Glob Antimicrob Resist*. 2018;13:98-103. doi:10.1016/j.jgar.2017.10.023
160. Nataro JP, Kaper JB. Diarrheagenic Escherichia coli. *Clin Microbiol Rev*. 1998;11:142-201. doi:file://Z:\References\Text Files\00000004469.txt
161. Nedialkova LP, Denzler R, Koeppel MB, et al. Inflammation Fuels Colicin Ib-Dependent Competition of Salmonella Serovar Typhimurium and E. coli in Enterobacterial Blooms. *PLoS Pathog*. 2014;10(1). doi:10.1371/journal.ppat.1003844
162. Neumann-Schaal M, Hofmann JD, Will SE, Schomburg D. Time-resolved amino acid uptake of Clostridium difficile 630Δerm and concomitant fermentation product and toxin formation. *BMC Microbiol*. 2015;15(1):281. doi:10.1186/s12866-015-0614-2
163. Ng KM, Ferreyra JA, Higginbottom SK, et al. Microbiota-liberated host sugars facilitate post-antibiotic expansion of enteric pathogens. *Nature*. 2013;502(7469):96-99. doi:10.1038/nature12503
164. Nguyen TLA, Vieira-Silva S, Liston A, Raes J. How informative is the mouse for human gut microbiota research? *DMM Dis Model Mech*. 2015;8(1):1-16. doi:10.1242/dmm.017400
165. Nicholson JK, Holmes E, Kinross J, et al. Host-gut microbiota metabolic interactions. *Science*. 2012;336(6086):1262-1267. doi:10.1126/science.1223813
166. Niscola P, Romani C, Cupelli L, et al. Mucositis in patients with hematologic malignancies: an overview. *Haematologica*. 2007;92(2).
167. Nolte T, Brander-Weber P, Dangler C, et al. Nonproliferative and proliferative lesions of the gastrointestinal tract, pancreas and salivary glands of the rat and mouse. *J Toxicol Pathol*. 2016;29(1):1S-124S. doi:10.1293/tox.29.1S
168. Oliveira RA, Ng KM, Correia MB, et al. Klebsiella michiganensis transmission enhances resistance to Enterobacteriaceae gut invasion by nutrition competition. *Nat Microbiol*. 2020;5(4):630-641. doi:10.1038/s41564-019-0658-4
169. Osbelt L, Thiemann S, Smit N, et al. Variations in microbiota composition of laboratory mice influence Citrobacter rodentium infection via variable short-chain fatty acid production. *PLoS Pathog*. 2020;16(3). doi:10.1371/journal.ppat.1008448
170. Panebianco C, Andriulli A, Pazienza V. Pharmacomicrobiomics: exploiting the drug-microbiota interactions in anticancer therapies. *Microbiome*. 2018;6(1):92. doi:10.1186/s40168-018-0483-7
171. Pédron T, Mulet C, Dauga C, et al. A crypt-specific core microbiota resides in the mouse colon. *MBio*. 2012;3(3). doi:10.1128/mBio.00116-12
172. Pereira FC, Berry D. Microbial nutrient niches in the gut. *Environ Microbiol*. 2017;19:1366-1378.
173. Perez-Muñoz ME, Arrieta MC, Ramer-Tait AE, Walter J. A critical assessment of the “sterile womb” and “in utero colonization” hypotheses: Implications for research on the pioneer infant microbiome. *Microbiome*. 2017;5(1):1-19. doi:10.1186/s40168-017-0268-4
174. Petersen C, Round JL. Defining dysbiosis and its influence on host immunity and disease. *Cell Microbiol*. 2014;16(7):1024-1033. doi:10.1111/cmi.12308
175. Peterson DE, Bensadoun R-J, Roila F, ESMO Guidelines Working Group O behalf of the EGW. Management of oral and gastrointestinal mucositis: ESMO Clinical Practice Guidelines. *Ann Oncol Off J Eur Soc Med Oncol*. 2011;22 Suppl 6(Suppl 6):vi78-84. doi:10.1093/annonc/mdr391

176. Peterson LW, Artis D. Intestinal epithelial cells: Regulators of barrier function and immune homeostasis. *Nat Rev Immunol*. 2014;14(3):141-153. doi:10.1038/nri3608
177. Picard C, Fioramonti J, Francois A, Robinson T, Neant F, Matuchansky C. Review article: bifidobacteria as probiotic agents - physiological effects and clinical benefits. *Aliment Pharmacol Ther*. 2005;22(6):495-512. doi:10.1111/j.1365-2036.2005.02615.x
178. Pickard JM, Maurice CF, Kinnebrew MA, et al. Rapid fucosylation of intestinal epithelium sustains host-commensal symbiosis in sickness. *Nature*. 2014;514(7524):638-641. doi:10.1038/nature13823
179. Pils MC, Pisano F, Fasnacht N, et al. Monocytes/macrophages and/or neutrophils are the target of IL-10 in the LPS endotoxemia model. *Eur J Immunol*. 2010;40(2):443-448. doi:10.1002/eji.200939592
180. Poirel L, Potron A, Nordmann P. OXA-48-like carbapenemases: the phantom menace. *J Antimicrob Chemother*. 2012;67(7):1597-1606. doi:10.1093/jac/dks121
181. Pop M, Walker AW, Paulson J, et al. Diarrhea in young children from low-income countries leads to large-scale alterations in intestinal microbiota composition. *Genome Biol*. 2014;15(6):R76. doi:10.1186/gb-2014-15-6-r76
182. Posner MR, Haddad RI. Novel agents for the treatment of mucositis. *J Support Oncol*. 2007;5(9 SUPPL. 4):33-39.
183. Pouncey AL, Scott AJ, Alexander JL, Marchesi J, Kinross J. Gut microbiota, chemotherapy and the host: the influence of the gut microbiota on cancer treatment. *Ecancermedicalscience*. 2018;12:868. doi:10.3332/ecancer.2018.868
184. Price MN, Dehal PS, Arkin AP. FastTree 2 - Approximately maximum-likelihood trees for large alignments. *PLoS One*. 2010;5(3). doi:10.1371/journal.pone.0009490
185. Quigley EMM. Gut microbiome as a clinical tool in gastrointestinal disease management: Are we there yet? *Nat Rev Gastroenterol Hepatol*. 2017;14(5):315-320. doi:10.1038/nrgastro.2017.29
186. Rajilić-Stojanović M, de Vos WM. The first 1000 cultured species of the human gastrointestinal microbiota. *FEMS Microbiol Rev*. 2014;38(5):996-1047. doi:10.1111/1574-6976.12075
187. Rea MC, Sit CS, Clayton E, et al. Thuricin CD, a posttranslationally modified bacteriocin with a narrow spectrum of activity against Clostridium difficile. *Proc Natl Acad Sci U S A*. 2010;107(20):9352-9357. doi:10.1073/pnas.0913554107
188. Reese AT, Dunn RR. Drivers of microbiome biodiversity: A review of general rules, feces, and ignorance. *MBio*. 2018;9(4). doi:10.1128/mBio.01294-18
189. Reyman M, van Houten MA, van Baarle D, et al. Impact of delivery mode-associated gut microbiota dynamics on health in the first year of life. *Nat Commun*. 2019;10(1):1-12. doi:10.1038/s41467-019-13014-7
190. Rigby RJ, Carr J, Orgel K, King SL, Lund PK, Dekaney CM. Intestinal bacteria are necessary for doxorubicin-induced intestinal damage but not for doxorubicin-induced apoptosis. *Gut Microbes*. 2016;7(5):414-423. doi:10.1080/19490976.2016.1215806
191. Rivera-Chávez F, Zhang LF, Faber F, et al. Depletion of Butyrate-Producing Clostridia from the Gut Microbiota Drives an Aerobic Luminal Expansion of Salmonella. *Cell Host Microbe*. 2016;19(4):443-454. doi:10.1016/j.chom.2016.03.004
192. Robinson CJ, Young VB. Antibiotic administration alters the community structure of the gastrointestinal microbiota. *Gut Microbes*. 2010;1(4):279-284. doi:10.4161/gmic.1.4.12614
193. Roe AJ, O'Byrne C, McLaggan D, Booth IR. Inhibition of Escherichia coli growth by acetic acid: A problem with methionine biosynthesis and homocysteine toxicity. *Microbiology*. 2002;148(7):2215-2222. doi:10.1099/00221287-148-7-2215
194. Roelofs KG, Coyne MJ, Gentyala RR, Chatzidaki-Livanis M, Comstock LE. Bacteroidales secreted antimicrobial proteins target surface molecules necessary for gut colonization and mediate competition in vivo. *MBio*. 2016;7(4). doi:10.1128/mBio.01055-16
195. Round JL, Mazmanian SK. The gut microbiota shapes intestinal immune responses during health and disease. *Nat Rev Immunol*. 2009;9(5):313-323. doi:10.1038/nri2515
196. Roy U, Gálvez EJC, Iljazovic A, et al. Distinct Microbial Communities Trigger Colitis Development upon Intestinal Barrier Damage via Innate or Adaptive Immune Cells. *Cell Rep*. 2017;21(4):994-1008. doi:10.1016/j.celrep.2017.09.097

197. Russell AB, Hood RD, Bui NK, Leroux M, Vollmer W, Mougous JD. Type VI secretion delivers bacteriolytic effectors to target cells. *Nature*. 2011;475(7356):343-349. doi:10.1038/nature10244
198. Russo TA, Marr CM. Hypervirulent Klebsiella pneumoniae. *Clin Microbiol Rev*. 2019;32(3). doi:10.1128/CMR.00001-19
199. Sadler R, Singh V, Benakis C, et al. Microbiota differences between commercial breeders impacts the post-stroke immune response. *Brain Behav Immun*. 2017;66:23-30. doi:10.1016/J.BBI.2017.03.011
200. Sana TG, Flaugnatti N, Lugo KA, et al. Salmonella Typhimurium utilizes a T6SS-mediated antibacterial weapon to establish in the host gut. *Proc Natl Acad Sci U S A*. 2016;113(34):E5044-E5051. doi:10.1073/pnas.1608858113
201. Sandhya P, Danda D, Sharma D, Scaria V. Does the buck stop with the bugs?: an overview of microbial dysbiosis in rheumatoid arthritis. *Int J Rheum Dis*. 2016;19(1):8-20. doi:10.1111/1756-185X.12728
202. Sartor RB. Microbial Influences in Inflammatory Bowel Diseases. *Gastroenterology*. 2008;134(2):577-594. doi:10.1053/J.GASTRO.2007.11.059
203. Sassone-Corsi M, Chairatana P, Zheng T, et al. Siderophore-based immunization strategy to inhibit growth of enteric pathogens. *Proc Natl Acad Sci U S A*. 2016;113(47):13462-13467. doi:10.1073/pnas.1606290113
204. Sassone-Corsi M, Nuccio SP, Liu H, et al. Microcins mediate competition among Enterobacteriaceae in the inflamed gut. *Nature*. 2016;540(7632):280-283. doi:10.1038/nature20557
205. Schaedler RW, Dubs R, Costello R. Association of germfree mice with bacteria isolated from normal mice. *J Exp Med*. 1965;122(2):77-82. doi:10.1084/jem.122.1.77
206. Schneditz G, Rentner J, Roier S, et al. Enterotoxicity of a nonribosomal peptide causes antibiotic-associated colitis. *Proc Natl Acad Sci U S A*. 2014;111(36):13181-13186. doi:10.1073/pnas.1403274111
207. Schulz MD, Atay Ç, Heringer J, et al. High-fat-diet-mediated dysbiosis promotes intestinal carcinogenesis independently of obesity. *Nature*. 2014;514(7253):508-512. doi:10.1038/nature13398
208. Sekirov I, Russell SL, Caetano M Antunes L, Finlay BB. Gut microbiota in health and disease. *Physiol Rev*. 2010;90(3):859-904. doi:10.1152/physrev.00045.2009
209. Sekirov I, Tam NM, Jogova M, et al. Antibiotic-induced perturbations of the intestinal microbiota alter host susceptibility to enteric infection. *Infect Immun*. 2008;76(10):4726-4736. doi:10.1128/IAI.00319-08
210. Sevelsted A, Stokholm J, Bønnelykke K, Bisgaard H. Cesarean section chronic immune disorders. *Pediatrics*. 2015;135(1):e92-e98. doi:10.1542/peds.2014-0596
211. Shea K, Chesson P. Community ecology theory as a framework for biological invasions. *Trends Ecol Evol*. 2002;17(4):170-176. doi:10.1016/S0169-5347(02)02495-3
212. Shen D, Ma G, Li C, et al. Emergence of a multidrug-resistant hypervirulent klebsiella pneumoniae sequence type 23 strain with a rare blaCTX-M-24-harboring virulence plasmid. *Antimicrob Agents Chemother*. 2019;63(3). doi:10.1128/AAC.02273-18
213. Sheu CC, Lin SY, Chang YT, Lee CY, Chen YH, Hsueh PR. Management of infections caused by extended-spectrum β–lactamase-producing Enterobacteriaceae: current evidence and future prospects. *Expert Rev Anti Infect Ther*. 2018;16(3):205-218. doi:10.1080/14787210.2018.1436966
214. Shin N-R, Whon TW, Bae J-W. Proteobacteria: microbial signature of dysbiosis in gut microbiota. *Trends Biotechnol*. 2015;33(9):496-503. doi:10.1016/j.tibtech.2015.06.011
215. Shreiner AB, Kao JY, Young VB. The gut microbiome in health and in disease. *Curr Opin Gastroenterol*. 2015;31(1):69-75. doi:10.1097/MOG.0000000000000139
216. Silverman JM, Brunet YR, Cascales E, Mougous JD. Structure and Regulation of the Type VI Secretion System. *Annu Rev Microbiol*. 2012;66(1):453-472. doi:10.1146/annurev-micro-121809-151619
217. Singh L, Cariappa MP, Kaur M. Klebsiella oxytoca: An emerging pathogen? *Med J Armed Forces India*. 2016;72(Suppl 1):S59-S61. doi:10.1016/j.mjafi.2016.05.002
218. Slonczewski JL, Fujisawa M, Dopson M, Krulwich TA. Cytoplasmic pH Measurement and Homeostasis in Bacteria and Archaea. *Adv Microb Physiol*. 2009;55:1-79, 317. doi:10.1016/S0065-2911(09)05501-5
219. Smajs D, Micenková L, Smarda J, et al. Bacteriocin synthesis in uropathogenic and commensal Escherichia coli: Colicin E1 is a potential virulence factor. *BMC Microbiol*. 2010;10:288. doi:10.1186/1471-2180-10-288
220. Sokolowska M, Frei R, Lunjani N, Akdis CA, O'Mahony L. Microbiome and asthma. *Asthma Res Pract*. 2018;4(1). doi:10.1186/s40733-017-0037-y
221. Sommer F, Bäckhed F. The gut microbiota — masters of host development and physiology. *Nat Rev Microbiol*. 2013;11(4):227-238. doi:10.1038/nrmicro2974

222. Sonis ST. A biological approach to mucositis. *J Support Oncol*. 2004;2(1):21-32.
223. Sonnenburg ED, Sonnenburg JL. Starving our microbial self: The deleterious consequences of a diet deficient in microbiota-accessible carbohydrates. *Cell Metab*. 2014;20(5):779-786. doi:10.1016/j.cmet.2014.07.003
224. Sorbara MT, Dubin K, Littmann ER, et al. Inhibiting antibiotic-resistant Enterobacteriaceae by microbiota-mediated intracellular acidification. *J Exp Med*. 2019;216(1):84-98. doi:10.1084/jem.20181639
225. Sorbara MT, Pamer EG. Interbacterial mechanisms of colonization resistance and the strategies pathogens use to overcome them. *Mucosal Immunol*. 2019;12(1):1-9. doi:10.1038/s41385-018-0053-0
226. Spiga L, Winter MG, Furtado de Carvalho T, et al. An Oxidative Central Metabolism Enables Salmonella to Utilize Microbiota-Derived Succinate. *Cell Host Microbe*. 2017;22(3):291-301.e6. doi:10.1016/j.chom.2017.07.018
227. Stecher B. Like will to like: abundances of closely related species can predict susceptibility to intestinal colonization by pathogenic and commensal bacteria. *PLoS Pathog*. 2010;6:e1000711.
228. Stecher B, Berry D, Loy A. Colonization resistance and microbial ecophysiology: Using gnotobiotic mouse models and single-cell technology to explore the intestinal jungle. *FEMS Microbiol Rev*. 2013;37(5):793-829. doi:10.1111/1574-6976.12024
229. Stecher B, Maier L, Hardt W-D. "Blooming" in the gut: how dysbiosis might contribute to pathogen evolution. *Nat Rev Microbiol*. 2013;11(4):277-284. doi:10.1038/nrmicro2989
230. Stehr M, Greweling MC, Tischer S, et al. Charles River altered Schaedler flora (CRASF) remained stable for four years in a mouse colony housed in individually ventilated cages. *Lab Anim*. 2009;43(4):362-370. doi:10.1258/la.2009.0080075
231. Stock I, Wiedemann B. Natural antibiotic susceptibility of Klebsiella pneumoniae, K. oxytoca, K. planticola, K. ornithinolytica and K. terrigena strains. *J Med Microbiol*. 2001;50(5):396-406. doi:10.1099/0022-1317-50-5-396
232. Stringer A, Gibson R, Bowen J, Keefe D. Chemotherapy-Induced Modifications to Gastrointestinal Microflora: Evidence and Implications of Change. *Curr Drug Metab*. 2009;10(1):79-83. doi:10.2174/138920009787048419
233. Suay-García B, Pérez-Gracia MT. Present and future of carbapenem-resistant Enterobacteriaceae (CRE) infections. *Antibiotics*. 2019;8(3). doi:10.3390/antibiotics8030122
234. Subramanian S, Huq S, Yatsunenko T, et al. Persistent gut microbiota immaturity in malnourished Bangladeshi children. *Nature*. 2014;510(7505):417-421. doi:10.1038/nature13421
235. Sun Y, O'Riordan MXD. Regulation of bacterial pathogenesis by intestinal short-chain fatty acids. In: *Advances in Applied Microbiology*. Vol 85. Academic Press Inc.; 2013:93-118. doi:10.1016/B978-0-12-407672-3.00003-4
236. Tacket CO, Sztein MB, Losonsky G, et al. Role of EspB in experimental human enteropathogenic Escherichia coli infection. *Infect Immun*. 2000;68(6):3689-3695. http://www.ncbi.nlm.nih.gov/pubmed/10816529. Accessed May 8, 2018.
237. Takasuna K, Hagiwara T, Hirohashi M, et al. Inhibition of intestinal microflora β-glucuronidase modifies the distribution of the active metabolite of the antitumor agent, irinotecan hydrochloride (CPT-11) in rats. *Cancer Chemother Pharmacol*. 1998;42(4):280-286. doi:10.1007/s002800050818
238. Taur Y, Coyte K, Schluter J, et al. Reconstitution of the gut microbiota of antibiotic-treated patients by autologous fecal microbiota transplant. *Sci Transl Med*. 2018;10(460). doi:10.1126/scitranslmed.aap9489
239. Taur Y, Jenq RR, Perales MA, et al. The effects of intestinal tract bacterial diversity on mortality following allogeneic hematopoietic stem cell transplantation. *Blood*. 2014;124(7):1174-1182. doi:10.1182/blood-2014-02-554725
240. Taur Y, Jenq RR, Ubeda C, Van Den Brink M, Pamer EG. Role of intestinal microbiota in transplantation outcomes. *Best Pract Res Clin Haematol*. 2015;28(2-3):155-161. doi:10.1016/j.beha.2015.10.013
241. Taur Y, Xavier JB, Lipuma L, et al. Intestinal Domination and the Risk of Bacteremia in Patients Undergoing Allogeneic Hematopoietic Stem Cell Transplantation. *Clin Infect Dis*. 2012;55(7):905-914. doi:10.1093/cid/cis580
242. Thiemann S, Smit N, Roy U, et al. Enhancement of IFNγ Production by Distinct Commensals Ameliorates Salmonella -Induced Disease. *Cell Host Microbe*. 2017;21(6):682-694.e5. doi:10.1016/j.chom.2017.05.005

243. Thiennimitr P, Winter SE, Winter MG, et al. Intestinal inflammation allows Salmonella to use ethanolamine to compete with the microbiota. *Proc Natl Acad Sci U S A*. 2011;108(42):17480-17485. doi:10.1073/pnas.1107857108
244. Tilg H, Moschen AR. Microbiota and diabetes: An evolving relationship. *Gut*. 2014;63(9):1513-1521. doi:10.1136/gutjnl-2014-306928
245. Tojo R, Suárez A, Clemente MG, et al. Intestinal microbiota in health and disease: Role of bifidobacteria in gut homeostasis. *World J Gastroenterol*. 2014;20(41):15163. doi:10.3748/wjg.v20.i41.15163
246. Tong M, Jacobs JP, McHardy IH, Braun J. Sampling of Intestinal Microbiota and Targeted Amplification of Bacterial 16S rRNA Genes for Microbial Ecologic Analysis. *Curr Protoc Immunol*. 2014;2014:7.41.1-7.41.11. doi:10.1002/0471142735.im0741s107
247. Topping DL, Clifton PM. Short-chain fatty acids and human colonic function: Roles of resistant starch and nonstarch polysaccharides. *Physiol Rev*. 2001;81(3):1031-1064. doi:10.1152/physrev.2001.81.3.1031
248. Trompette A, Gollwitzer ES, Yadava K, et al. Gut microbiota metabolism of dietary fiber influences allergic airway disease and hematopoiesis. *Nat Med*. 2014;20(2):159-166. doi:10.1038/nm.3444
249. Turnbaugh PJ, Hamady M, Yatsunenko T, et al. A core gut microbiome in obese and lean twins. *Nature*. 2009;457(7228):480-484. doi:10.1038/nature07540
250. Turnbaugh PJ, Ley RE, Mahowald MA, Magrini V, Mardis ER, Gordon JI. An obesity-associated gut microbiome with increased capacity for energy harvest. *Nature*. 2006;444(7122):1027-1031. doi:10.1038/nature05414
251. Tyakht A V., Alexeev DG, Popenko AS, Kostryukova ES, Govorun VM. Rural and urban microbiota: To be or not to be? *Gut Microbes*. 2014;5(3):351-356. doi:10.4161/gmic.28685
252. Urdaneta V, Casadesus J. Interactions between bacteria and bile salts in the gastrointestinal and hepatobiliary tracts. *Front Med*. 2017;4:163.
253. Van Der Waaij D, Berghuis-de Vries JM, Lekkerkerk-Van Der Wees JEC. Colonization resistance of the digestive tract in conventional and antibiotic-treated mice. *J Hyg (Lond)*. 1971;69(3):405-411. doi:10.1017/S0022172400021653
254. van Duin D, Doi Y. The global epidemiology of carbapenemase-producing Enterobacteriaceae. *Virulence*. 2017;8(4):460-469. doi:10.1080/21505594.2016.1222343
255. van Vliet MJ, Harmsen HJM, de Bont ESJM, Tissing WJE. The role of intestinal microbiota in the development and severity of chemotherapy-induced mucositis. *PLoS Pathog*. 2010;6(5):1-7. doi:10.1371/journal.ppat.1000879
256. Vande Walle L, Jiménez Fernández D, Demon D, et al. Does caspase-12 suppress inflammasome activation? *Nature*. 2016;534(7605):E1-E4. doi:10.1038/nature17649
257. Velazquez EM, Nguyen H, Heasley KT, et al. Endogenous Enterobacteriaceae underlie variation in susceptibility to Salmonella infection. *Nat Microbiol*. 2019;4(6):1057-1064. doi:10.1038/s41564-019-0407-8
258. Viana ML, Dos Santos RDGC, Generoso SDV, et al. The role of l-arginine-nitric oxide pathway in bacterial translocation. *Amino Acids*. 2013;45(5):1089-1096. doi:10.1007/s00726-013-1558-1
259. Viaud S, Daillère R, Boneca IG, et al. Harnessing the intestinal microbiome for optimal therapeutic immunomodulation. *Cancer Res*. 2014. doi:10.1158/0008-5472.CAN-14-0987
260. Villarino NF, LeCleir GR, Denny JE, et al. Composition of the gut microbiota modulates the severity of malaria. *Proc Natl Acad Sci U S A*. 2016;113(8):2235-2240. doi:10.1073/pnas.1504887113
261. Vimr ER, Kalivoda KA, Deszo EL, Steenbergen SM. Diversity of Microbial Sialic Acid Metabolism. *Microbiol Mol Biol Rev*. 2004;68(1):132-153. doi:10.1128/mmbr.68.1.132-153.2004
262. Vital M, Karch A, Pieper DH. Colonic Butyrate-Producing Communities in Humans: an Overview Using Omics Data. *mSystems*. 2017;2(6). doi:10.1128/mSystems.00130-17
263. Vlasova AN, Kandasamy S, Chattha KS, Rajashekara G, Saif LJ. Comparison of probiotic lactobacilli and bifidobacteria effects, immune responses and rotavirus vaccines and infection in different host species. *Vet Immunol Immunopathol*. 2016;172:72-84. doi:10.1016/j.vetimm.2016.01.003
264. Wang B, Yao M, Lv L, Ling Z, Li L. The Human Microbiota in Health and Disease. *Engineering*. 2017;3(1):71-82. doi:10.1016/J.ENG.2017.01.008
265. Wang Q, Garrity GM, Tiedje JM, Cole JR. Naïve Bayesian classifier for rapid assignment of rRNA sequences into the new bacterial taxonomy. *Appl Environ Microbiol*. 2007;73(16):5261-5267. doi:10.1128/AEM.00062-07

266. Wang Z, Xiao G, Yao Y, Guo S, Lu K, Sheng Z. The role of bifidobacteria in gut barrier function after thermal injury in rats. *J Trauma - Inj Infect Crit Care*. 2006;61(3):650-657. doi:10.1097/01.ta.0000196574.70614.27
267. Wannemuehler MJ, Overstreet AM, Ward D V., Phillips GJ. Draft genome sequences of the altered Schaedler flora, a defined bacterial community from gnotobiotic mice. *Genome Announc*. 2014;2(2). doi:10.1128/genomeA.00287-14
268. Whitford EJ, Cummins AG, Butler RN, et al. Effects of Streptococcus thermophilus TH-4 on intestinal mucositis induced by the chemotherapeutic agent 5-Fluorouracil (5-FU). *Cancer Biol Ther*. 2009;8(6):505-511. doi:10.4161/cbt.8.6.7594
269. Whitman WB, Coleman DC, Wiebe WJ. Prokaryotes: the unseen majority. *Proc Natl Acad Sci U S A*. 1998;95(12):6578-6583. doi:10.1073/pnas.95.12.6578
270. WHO. United Nations meeting on antimicrobial resistance. *Bull World Health Organ*. 2016;94(9):638-639. doi:10.2471/blt.16.020916
271. WHO. Diarrhoeal disease. https://www.who.int/news-room/fact-sheets/detail/diarrhoeal-disease. Published 2020. Accessed March 11, 2020.
272. Wiles S, Clare S, Harker J, et al. Organ specificity, colonization and clearance dynamics in vivo following oral challenges with the murine pathogen Citrobacter rodentium. *Cell Microbiol*. 2004;6(10):963-972. doi:10.1111/j.1462-5822.2004.00414.x
273. Willing BP, Vacharaksa A, Croxen M, Thanachayanont T, Finlay BB. Altering host resistance to infections through microbial transplantation. *PLoS One*. 2011;6(10). doi:10.1371/journal.pone.0026988
274. Wlodarska M, Willing B, Keeney KM, et al. Antibiotic treatment alters the colonic mucus layer and predisposes the host to exacerbated Citrobacter rodentium-induced colitis. *Infect Immun*. 2011;79(4):1536-1545. doi:10.1128/IAI.01104-10
275. Wlodarska M, Willing BP, Bravo DM, Finlay BB. Phytonutrient diet supplementation promotes beneficial Clostridia species and intestinal mucus secretion resulting in protection against enteric infection. *Sci Rep*. 2015;5. doi:10.1038/srep09253
276. Wrzosek L, Ciocan D, Borentain P, et al. Transplantation of human microbiota into conventional mice durably reshapes the gut microbiota. *Sci Rep*. 2018;8(1):1-9. doi:10.1038/s41598-018-25300-3
277. Wu GD, Chen J, Hoffmann C, et al. Linking long-term dietary patterns with gut microbial enterotypes. *Science (80-)*. 2011;334(6052):105-108. doi:10.1126/science.1208344
278. Xu X, Zhang X. Effects of cyclophosphamide on immune system and gut microbiota in mice. *Microbiol Res*. 2015;171:97-106. doi:10.1016/J.MICRES.2014.11.002
279. Yamazawa K, Kanno H, Seki K, Kuzuta T, Matsui H, Sekiya S. Life-threatening Clostridium difficile-associated diarrhea induced by paclitaxel-carboplatin combination chemotherapy. *Acta Obstet Gynecol Scand*. 2001;80(8):768-769. http://www.ncbi.nlm.nih.gov/pubmed/11531624. Accessed October 11, 2019.
280. Yang F, Yang L, Chang Z, Chang L, Yang B. Regulation of virulence and motility by acetate in enteropathogenic Escherichia coli. *Int J Med Microbiol*. 2018;308(7):840-847. doi:10.1016/j.ijmm.2018.07.010
281. Yasuda K, Oh K, Ren B, et al. Biogeography of the intestinal mucosal and lumenal microbiome in the rhesus macaque. *Cell Host Microbe*. 2015;17(3):385-391. doi:10.1016/j.chom.2015.01.015
282. Yatsunenko T, Rey FE, Manary MJ, et al. Human gut microbiome viewed across age and geography. *Nature*. 2012;486(7402):222-227. doi:10.1038/nature11053
283. Yoo DH, Kim IS, Van Le TK, Jung IH, Yoo HH, Kim DH. Gut microbiota-mediated drug interactions between lovastatin and antibiotics. *Drug Metab Dispos*. 2014;42(9):1508-1513. doi:10.1124/dmd.114.058354
284. Zhang R, Lin D, Chan EWC, Gu D, Chen GX, Chen S. Emergence of carbapenem-resistant serotype K1 hypervirulent Klebsiella pneumoniae strains in China. *Antimicrob Agents Chemother*. 2016;60(1):709-711. doi:10.1128/AAC.02173-15
285. Zhang Y, Sun J, Mi C, et al. First report of two rapid-onset fatal infections caused by a newly emerging hypervirulent K. Pneumonia ST86 strain of serotype K2 in China. *Front Microbiol*. 2015;6(JUL). doi:10.3389/fmicb.2015.00721
286. Zhao Y, Chen F, Wu W, et al. GPR43 mediates microbiota metabolite SCFA regulation of antimicrobial peptide expression in intestinal epithelial cells via activation of mTOR and STAT3. *Mucosal Immunol*. 2018;11(3):752-762. doi:10.1038/mi.2017.118

287. Zipperer A, Konnerth MC, Laux C, et al. Human commensals producing a novel antibiotic impair pathogen colonization. *Nature*. 2016;535(7613):511-516. doi:10.1038/nature18634
288. Zwielehner J, Lassl C, Hippe B, et al. Changes in Human Fecal Microbiota Due to Chemotherapy Analyzed by TaqMan-PCR, 454 Sequencing and PCR-DGGE Fingerprinting. doi:10.1371/journal.pone.0028654

Ehrenerklärung

Ich versichere hiermit, dass ich die vorliegende Arbeit ohne unzulässige Hilfe Dritter und ohne Benutzung anderer als der angegebenen Hilfsmittel angefertigt habe; verwendete fremde und eigene Quellen sind als solche kenntlich gemacht.

Ich habe insbesondere nicht wissentlich:

- Ergebnisse erfunden oder widersprüchliche Ergebnisse verschwiegen,
- statistische Verfahren absichtlich missbraucht, um Daten in ungerechtfertigter Weise zu interpretieren,
- fremde Ergebnisse oder Veröffentlichungen plagiiert,
- fremde Forschungsergebnisse verzerrt wiedergegeben.

Mir ist bekannt, dass Verstöße gegen das Urheberrecht Unterlassungs- und Schadensersatzansprüche des Urhebers sowie eine strafrechtliche Ahndung durch die Strafverfolgungsbehörden begründen kann.

Ich erkläre mich damit einverstanden, dass die Arbeit ggf. mit Mitteln der elektronischen Datenverarbeitung auf Plagiate überprüft werden kann.

Die Arbeit wurde bisher weder im Inland noch im Ausland in gleicher oder ähnlicher Form als Dissertation eingereicht und ist als Ganzes auch noch nicht veröffentlicht.

_____

Ort, Datum

_____

Unterschrift